

Quantum information and quantum computation

Vorlesung
summer semester 2020
Technische Universität Berlin



Dr. Gernot Schaller

November 9, 2020

Contents

1	A brief intro to classical computation	9
1.1	The circuit model of classical computation	9
1.2	Example: Binary addition	11
1.3	Going quantum?	12
2	Qubit(s)	13
2.1	One qubit	13
2.2	Qubit control	15
2.3	Single qubit gates	15
2.4	Multiple qubits	18
2.5	Quantum applications of two qubits	22
2.5.1	Bell inequalities	22
2.5.2	Superdense coding	24
2.5.3	No-cloning theorem	25
2.5.4	Quantum teleportation	25
2.6	The partial trace	27
3	The circuit model of quantum computation	29
3.1	Deutsch and Deutsch-Jozsa problems	29
3.2	Backward compatibility	33
3.3	Controlled operations	34
3.4	Universality of quantum computation	35
3.4.1	Decomposition of d -level unitaries into 2-level unitary matrices	36
3.4.2	Decomposition of 2-level unitaries into single qubit and CNOT	38
3.4.3	Approximating single-qubit and CNOT by discrete gates	39
3.5	Quantum Fourier Transform	41
3.6	Quantum search	45
3.7	Control errors	49
4	Open quantum systems	51
4.1	An exactly solvable model of decoherence	51
4.2	Lindblad master equation: Microscopic derivation	53
4.3	Lindblad master equation: General properties	60
5	Adiabatic quantum computation	63
5.1	The adiabatic theorem for closed systems	64
5.2	Adiabatic qubit control	65

5.3	Adiabatic control in presence of thermal dissipation	67
5.4	The adiabatic Grover search	68
5.5	Adiabatic approaches to an NP-complete problem	71
5.6	An adiabatic adder	74
5.7	An adiabatic multiplier	76
5.8	The 1d quantum Ising model in a transverse field	77
5.8.1	Exact Diagonalization	78
5.8.2	Adiabatic criterion	85
5.8.3	Non-straight interpolation	86
6	Information measures	91
6.1	Quantum operations	91
6.2	Comparing density matrices	92
6.2.1	Trace Distance	92
6.2.2	Fidelity	96
6.2.3	Quantum relative entropy	97
6.3	Entanglement	99
6.3.1	Entanglement entropy	99
6.3.2	Examples	101
6.3.3	Entanglement of mixed states	105
6.3.4	Concurrence	106
6.3.5	Examples	108
7	Quantum Thermodynamics	115
7.1	Nonequilibrium thermodynamics	115
7.1.1	Example: Two coupled qubits	119
7.1.2	Numeric example: Ising model	120
7.1.3	Example: Transient entropy production for pure-dephasing	121
7.1.4	Use of Spohn's inequality	123
7.2	Quantum Otto cycle	125
7.2.1	Modeling of closed (unitary) strokes	126
7.2.2	Modeling of open (dissipative) strokes	127
7.2.3	Strokes in the quantum Otto cycle	128
7.2.4	Harmonic oscillator working fluid with finite times	130
7.2.5	Collective spin working fluid with finite times	132
7.2.6	Analogous equilibrium cycle	135
7.3	Quantum-mechanical evolution towards equilibrium	136
8	Selected phenomena and applications	139
8.1	Reservoir models	139
8.1.1	Tight-binding chain	140
8.1.2	Example: Evolution under a 1d reservoir	142
8.1.3	Higher-dimensional tight-binding lattices	144
8.1.4	Reservoirs with periodic boundary conditions	145
8.1.5	Spin reservoir: Ising model	146
8.2	Topological single-particle pumping	149

Die Termine der Vorlesung sind Montags von 12:15–13:45 und Dienstags von 12:15–13:45. Die dazugehörige Übung wird von Dr. Ling Na Wu gehalten. Wegen der Corona-Krise werden Vorlesung und Übung voraussichtlich nur online stattfinden. Die Veranstaltung ist erweiterbar zu einem vollen Wahlpflichtfach (12 LP), indem zusätzlich an einem Seminar oder einer Spezialvorlesung aus der Theoretischen Physik teilgenommen wird (in Absprache mit dem Dozenten).

Voraussetzungen für die Teilnahme: Quantenmechanik, (wünschenswert: Quantenmechanik II), Spaß am Tüfteln, Internetzugang

Dieses Vorlesungsskript (Englisch) wird online verfügbar sein unter

<http://www1.itp.tu-berlin.de/schaller/lectures.html>.

Korrekturen und Vorschläge sollten an folgende email-Adresse gesendet werden:

gernot.schaller@tu-berlin.de.

Zuletzt noch ein Hinweis: Dieses Skript wird erst während der Vorlesung ausgebaut und verbessert werden. Es ist kein Originalwerk sondern basiert auf Büchern, Manuskripten, persönlichen Erfahrungen und nicht zuletzt vielen wertvollen Hinweisen, ich danke hier z.B. insbesondere Philipp Stammer. Es wird nach jeder Vorlesung in aktualisierter Fassung online gestellt, es empfiehlt sich daher, nicht gleich zu Anfang alles auszudrucken.

Literaturhinweise:

- M. A. Nielsen and I. L. Chuang, *Quantum Computation and Quantum Information*, Cambridge University Press, Cambridge (2000). [1]
- J. Preskill, *Quantum Computation*, lecture notes <http://www.theory.caltech.edu/~preskill/ph219/>.

Wir werden folgende Inhalte behandeln

- klassische und Quanten-gates
- Quanten-Algorithmen
- Realisierungen
- adiabatische Quantenrechner
- Dekohärenz

Prerequisites

This lecture builds upon basic knowledge of quantum mechanics. You should therefore be familiar with the following:

- Quantum systems are described by the Schrödinger equation

$$i\hbar\partial_t\Psi(\mathbf{r},t) = H(\mathbf{r},t)\Psi(\mathbf{r},t), \quad (1)$$

where $H(\mathbf{r},t)$ is known as Hamilton operator and may contain spatial derivatives acting to the right. The solution to this partial differential equation $\Psi(\mathbf{r},t)$ is called **wave function** and has a probability density interpretation $P(\mathbf{r},t) = |\Psi(\mathbf{r},t)|^2$.

- We will make use of the Dirac Bra-Ket notation, where, notationally, the state of a quantum system can be characterized by a "ket" $|\Psi(t)\rangle$, which is a vector in a Hilbert space. Scalar products between two kets are denoted by $\langle\Phi|\Psi\rangle$, and the wave function is then given by $\Psi(\mathbf{r},t) = \langle\mathbf{r}|\Psi(t)\rangle$, with $\hat{\mathbf{r}}|\mathbf{r}\rangle = \mathbf{r}|\mathbf{r}\rangle$ denoting the eigenstates of the position operator. Throughout the lecture, we will use units where $\hbar = 1$. In these units, energy has units of inverse time, such that $H \cdot t$ is manifestly dimensionless. The **Schrödinger equation** then reads for the state $|\Psi(t)\rangle$ simply

$$|\dot{\Psi}\rangle = -iH|\Psi\rangle. \quad (2)$$

Here, $H = H^\dagger$ is the Hamilton operator which can have different eigenstates.

- When H is time-independent, this equation is formally solved by

$$|\Psi(t)\rangle = U(t)|\Psi_0\rangle = e^{-iHt}|\Psi_0\rangle, \quad (3)$$

where $U(t)$ is known as **time evolution operator** and $|\Psi_0\rangle$ is the initial state. It is easy to show that it is unitary $U^\dagger = U^{-1}$.

- When H is time-dependent, we can likewise introduce a time evolution operator that obeys

$$|\Psi(t)\rangle = U(t)|\Psi_0\rangle. \quad (4)$$

Insertion into the Schrödinger equation shows that the time evolution operator in general obeys

$$\frac{d}{dt}U(t) = -iH(t)U(t). \quad (5)$$

Integrating this equation yields the expansion

$$\begin{aligned}
U(t) &= \mathbf{1} - i \int_0^t H(t_1) dt_1 - \int_0^t dt_1 \int_0^{t_1} dt_2 H(t_1) H(t_2) \pm \dots \\
&= \sum_{n=0}^{\infty} (-i)^n \int_0^t dt_1 \int_0^{t_1} dt_2 \dots \int_0^{t_{n-1}} dt_n H(t_1) \dots H(t_n) \\
&\equiv \mathcal{T} \sum_{n=0}^{\infty} \left(-i \int_0^t H(t') dt' \right)^n = \mathcal{T} \exp \left\{ -i \int_0^t H(t') dt' \right\}, \tag{6}
\end{aligned}$$

where \mathcal{T} is also known as time-ordering operator. By comparing the two expressions, one can see that $\mathcal{T}H(t_1)H(t_2) = H(t_1)H(t_2)\Theta(t_1 - t_2) + H(t_2)H(t_1)\Theta(t_2 - t_1)$, i.e., it sorts the operators by their time argument.

- The Hamiltonian of any two-level system (**qubit**) can be represented by **Pauli matrices**

$$\begin{aligned}
H &= h_x \sigma^x + h_y \sigma^y + h_z \sigma^z, \\
\sigma^x &= \begin{pmatrix} 0 & 1 \\ 1 & 0 \end{pmatrix}, \quad \sigma^y = \begin{pmatrix} 0 & -i \\ +i & 0 \end{pmatrix}, \quad \sigma^z = \begin{pmatrix} +1 & 0 \\ 0 & -1 \end{pmatrix}. \tag{7}
\end{aligned}$$

Since any Hamiltonian is hermitian $H = H^\dagger$, we have that $h_\alpha \in \mathbb{R}$. The Pauli matrices obey the relations

$$[\sigma^\alpha, \sigma^\beta] = 2i\epsilon_{\alpha\beta\gamma}\sigma^\gamma, \quad \{\sigma^\alpha, \sigma^\beta\} = 2\delta_{\alpha\beta}\mathbf{1}. \tag{8}$$

- The time evolution operator for any two-level system subject to a constant Hamiltonian may be explicitly computed

$$\begin{aligned}
U(t) &= e^{-iHt} = e^{-iht \left[\frac{h_x}{h} \sigma^x + \frac{h_y}{h} \sigma^y + \frac{h_z}{h} \sigma^z \right]} = \exp \{ -iht \mathbf{e}_h \cdot \boldsymbol{\sigma} \} \\
&= \cos(ht)\mathbf{1} - i \sin(ht) \mathbf{e}_h \cdot \boldsymbol{\sigma}, \tag{9}
\end{aligned}$$

where we used that $h = \sqrt{h_x^2 + h_y^2 + h_z^2}$. Thereby, if we let a constant Hamiltonian H act for a certain time t , we can implement an arbitrary unitary operation on a two-level system.

- Upon a projective measurement of an observable $O = O^\dagger$ with spectral decomposition

$$O = \sum_{\ell} \lambda_{\ell} |\ell\rangle \langle \ell|, \tag{10}$$

with eigenvalues λ_{ℓ} and eigenstates $|\ell\rangle$, we can only obtain measurement results λ_{ℓ} , i.e., the eigenvalues of the observable. Upon the outcome ℓ , the state of the system instantaneously collapses to

$$|\Psi\rangle \rightarrow |\Psi^{(\ell)}\rangle = \frac{|\ell\rangle \langle \ell|\Psi\rangle}{|\langle \ell|\Psi\rangle|}, \tag{11}$$

and the probability of this particular outcome is given by $P_{\ell} = |\langle \ell|\Psi\rangle|^2$. This means that the measurement collapses the state of the system onto eigenstates of the observable. If we do not allow the state to change after the measurement (which happens e.g. if we measure the energy of the system and thereby collapse into an energy eigenstate), a subsequent measurement of the same observable will thus always yield the same result.

Chapter 1

A brief intro to classical computation

Why should we study classical computation if we are interested in quantum computation? For the circuit model, the answer is three-fold

- Many techniques and concepts from classical computation can be transferred to quantum computation.
- Computer scientists have thought about the resources it takes to solve a particular problem. They have invented classification schemes of difficult and not-so-difficult problems, and these schemes are useful to classify quantum algorithms as well.
- From knowing classical computation, we know where quantum computers may outperform classical ones.

1.1 The circuit model of classical computation

Even classical computers are complicated structures (if not convinced, try to build one). They can be implemented based on different architectures, and computer scientists have found a language that allows to abstract from a given architecture. The **circuit model of computation** attempts to formalize computation on finite-size computers by circuits [1].

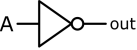
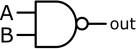
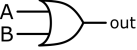
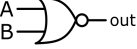
These circuits consist of **wires** and **gates** and process bitwise information. Wires simply pass information in terms of classical bits, that can take the values zero or one from one place to another. In a diagrammatic language, they are just represented by a straight line. In contrast, a gate performs a simple computational task. By combining simple gates and wires one can implement more gates that can perform more complicated tasks, as formalized below:

A **logic gate** is a function $f : \{0, 1\}^k \rightarrow \{0, 1\}^\ell$ that transforms k input bits into ℓ output bits.

- Both input and output bits may take all allowed values $\mathbf{b}^{\text{in}} = (b_1^{\text{in}}, b_2^{\text{in}}, \dots, b_k^{\text{in}})$ with $b_i^{\text{in}} \in \{0, 1\}$ and likewise $\mathbf{b}^{\text{out}} = (b_1^{\text{out}}, b_2^{\text{out}}, \dots, b_\ell^{\text{out}})$ with $b_i^{\text{out}} \in \{0, 1\}$.
- Since any configuration of input or output bits can be mapped to one of the 2^k input states or 2^ℓ output states, one can understand a logic gate also as a function on sets.
- A popular example of such sets is the binary representation of positive integers.

Some important gates are displayed in Tab. 1.1 From such simple gates, all the complex abilities of nowadays computers can be implemented. We can explore this at the example of adding numbers in binary representation.

Table 1.1: Simple logic gates and their graphical representation. Wires (lines) can carry one bit of information. Conventionally, the bits enter from the left and leave to the right. To avoid inconsistencies, loops are forbidden. Thus, 2^k different input states are mapped to 2^ℓ different output states. Figure source: Wikipedia.

gate	symbol	k	ℓ	bit truth table		
NOT		1	1	A	out	
				0	1	
				1	0	
AND		2	1	A	B	out
				0	0	0
				0	1	0
				1	0	0
				1	1	1
NAND		2	1	A	B	out
				0	0	1
				0	1	1
				1	0	1
				1	1	0
OR		2	1	A	B	out
				0	0	0
				0	1	1
				1	0	1
				1	1	1
NOR		2	1	A	B	out
				0	0	1
				0	1	0
				1	0	0
				1	1	0
XOR		2	1	A	B	out
				0	0	0
				0	1	1
				1	0	1
				1	1	0

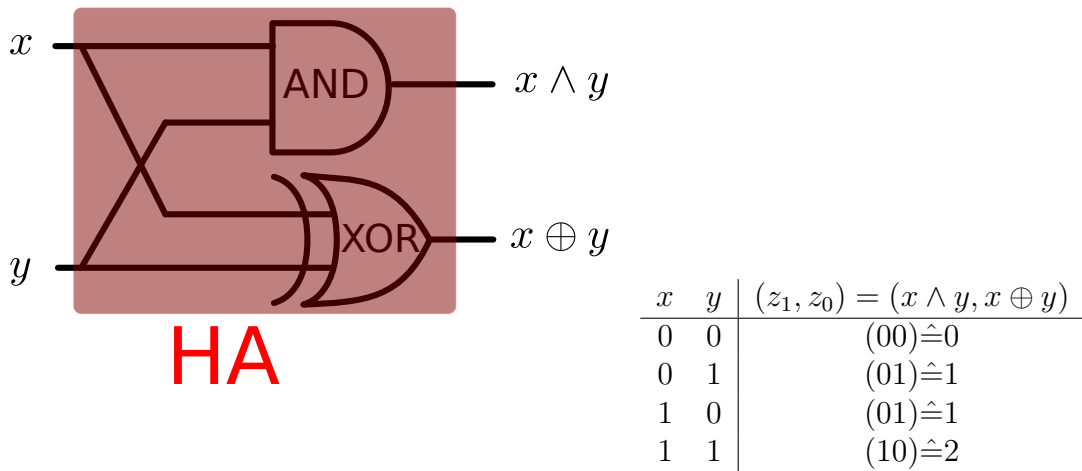


Figure 1.1: Left: Half-adder gate. The gate takes two bits x and y as input and computes via using a XOR and an AND gate from Tab. 1.1 their bitwise sum as $x \oplus y$ and a carry bit $x \wedge y$. A HA gate can be used as the first step of a bitwise adder.

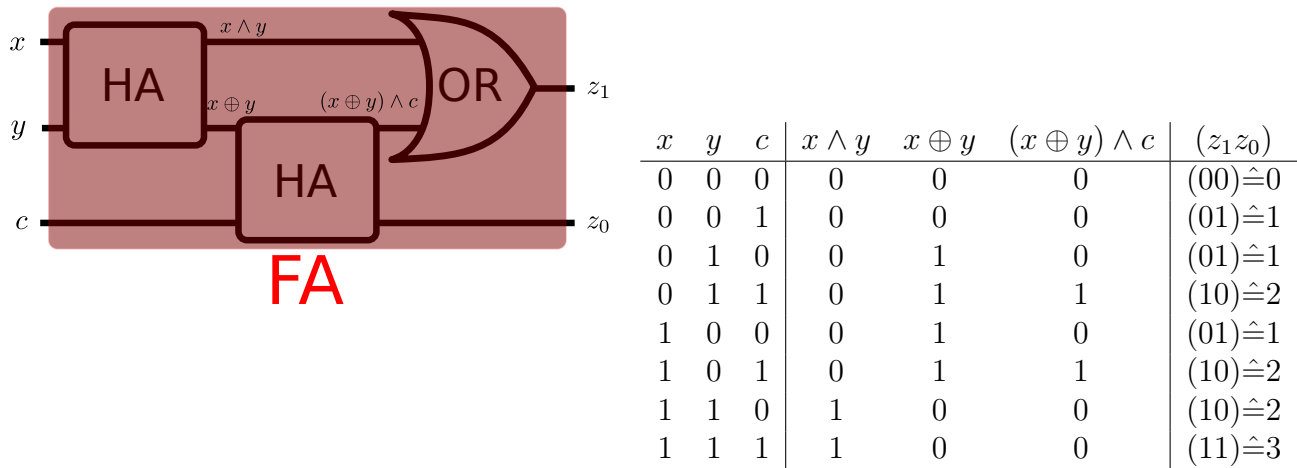


Figure 1.2: Full adder (FA) gate. The gate takes three input bits and outputs their sum by computing $z_1 = (x \wedge y) \vee ((x \oplus y) \wedge c)$ and $z_0 = x \oplus y \oplus c$. It can be constructed from two HA gates from Fig. 1.1 and an OR gate from Tab. 1.1.

1.2 Example: Binary addition

By combining an AND and a XOR gate, we can generate a so-called half-adder (HA), see Fig. 1.1. Mapping all possible inputs into a table, we see that the half-adder (HA) computes the sum of two single bits.

However, if we want to compute the sum of longer digit numbers, we need to compute the sum of three bits (convince yourself of this). If all bits are set, the maximum result of three bits is thus $3 \hat{=} 11$, such a full-adder will have to return two output bits, such that we are searching for a gate with three inputs and two outputs. It can be constructed from two HA gates and an OR gate, see Fig. 1.2.

Finally, to compute something useful, we can combine the initial HA and subsequent FA by appropriately passing the carry bits as inputs to the next FA gates, see Fig. 1.3.

The example should demonstrate the following

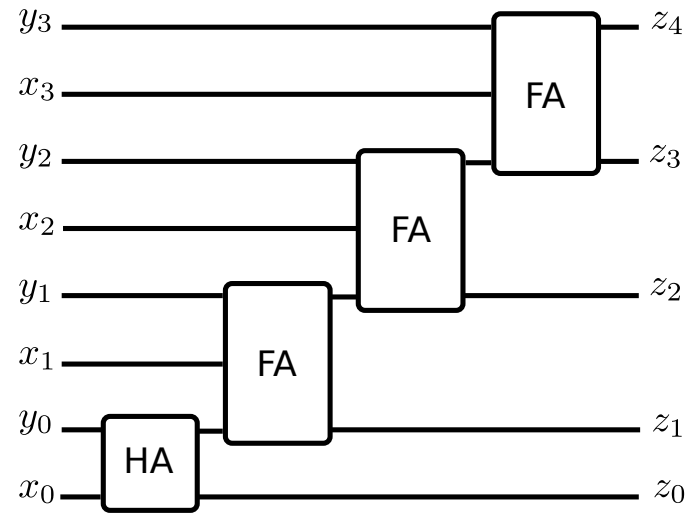


Figure 1.3: Adder circuit for adding two four-digit binary numbers $(x_3x_2x_1x_0)$ and $(y_3y_2y_1y_0)$ to generate a five-digit binary number $(z_4z_3z_2z_1z_0)$. The circuit combines the HA gate from Fig. 1.1 and the FA gate from Fig. 1.2 to implement addition the usual way it is taught in school. The generalization of the circuit to longer binaries is straightforward.

- complex circuits may be composed from a few elementary gates
- modularization into smaller gates helps to transfer algorithms into circuits
- classically, the number of output and input bits may be different (e.g. deletion of information)
- presupposing that implementation of every gate is associated with some cost, one gets an estimate of the algorithmic complexity simply by counting the number of elementary gates.

1.3 Going quantum?

This is unfortunately not so easy. We can surely perform quantum gates that are more powerful than their classical counterparts and constitute the quantum advantage, but unfortunately there are some classical operations that cannot be performed.

For example, looking at the Schrödinger equation, we noted that the time evolution operator is unitary. This means, it can always be inverted and *preserves the information of the initial state*. Quantum circuits therefore must have the same number of input and output (qu-)bits. If for a classical algorithm the number of input and output bits differ, this may require us to start a potential quantum algorithm with a number of so-called **ancilla qubits**.

Further, we cannot just copy a quantum bit into two as is e.g. done in the HA-gate in Fig. 1.1. Quantum-mechanically, this is forbidden by a no-cloning theorem.

These problems make the design of quantum algorithms difficult. Let us start with something simpler and consider the basic building block of computation.

Chapter 2

Qubit(s)

2.1 One qubit

A classical bit can only take the values $b_i \in \{0, 1\}$. In contrast, a **qubit** (or qbit) can be in any superposition state

$$|\Psi\rangle = \alpha |0\rangle + \beta |1\rangle \quad : \quad |\alpha|^2 + |\beta|^2 = 1, \quad (2.1)$$

since the Schrödinger equation allows for superposition of solutions.

- Any quantum-mechanical two-level system that allows for superpositions can implement a qubit. If transitions to other levels are strongly suppressed, we may also consider a many-level quantum system as an approximate qubit. Likewise, the two lowest levels of a harmonic oscillator (ground state and first excited state) can implement a qubit.
- Since any two-level system can be described by a Pauli matrix Hamiltonian, we have conventionally taken the eigenstates of the Pauli σ^z matrix as the basis states for our qubit

$$\sigma^z |0\rangle = + |0\rangle, \quad \sigma^z |1\rangle = - |1\rangle. \quad (2.2)$$

This basis is conventionally called **computational basis** and importantly, the states are orthogonal $\langle 0|1\rangle = 0$.

- The complex numbers α and β can be written in polar representation, which together with the normalization condition allows us to write a qubit state as

$$|\Psi\rangle = e^{+i\gamma} \left(\cos \frac{\theta}{2} |0\rangle + e^{+i\phi} \sin \frac{\theta}{2} |1\rangle \right) \hat{=} \cos \frac{\theta}{2} |0\rangle + e^{+i\phi} \sin \frac{\theta}{2} |1\rangle, \quad (2.3)$$

where we can neglect the global phase γ since it is not observable. Thus, we can fully characterize the state of a qubit by two angles or – alternatively – by a point on the unit sphere. The latter is known as **Bloch sphere representation**. On the poles of the Bloch sphere we have the computational basis states $|0\rangle$ and $|1\rangle$, which we could identify with classical bits. Any state on the surface of the Bloch sphere is called pure.

- While the evolution of the state under the Schrödinger equation is deterministic, the probabilistic quantum character kicks in when we want to measure the value of the qubit. This measurement corresponds conventionally to the expectation value of the Pauli σ^z matrix

$$\sigma^z = + |0\rangle \langle 0| - |1\rangle \langle 1|, \quad (2.4)$$

and from the measurement postulate we find that there will be the two measurement outcomes 0 and 1, which occur with probabilities $P_0 = \cos^2 \frac{\theta}{2}$ and $P_1 = \sin^2 \frac{\theta}{2}$, which add up to unity.

- Suppose we only know that our quantum system is in a particular state with a certain probability. This could be implemented by a situation where you get a two-level atom repeatedly, prepared in some state like the ground state or the first excited state (or other states) with a certain probability. Then, we can either solve the Schrödinger equation for every initial state separately and afterwards average over the initial states. A more elegant approach is to use a so-called **density matrix** or **statistical operator** representation, which already includes such averaging procedures. Such a density matrix can be written as

$$\rho = \sum_n P_n |\Psi_n\rangle \langle \Psi_n|, \quad (2.5)$$

where P_n are probabilities to be in the state $|\Psi_n\rangle$. Density matrices are

- self-adjoint $\rho = \rho^\dagger$
- trace-normalized $\text{Tr} \{\rho\} = 1$
- positive semidefinite $\langle \Psi | \rho | \Psi \rangle \geq 0 \quad \forall |\Psi\rangle$,

and any matrix fulfilling these conditions is a valid density matrix. Expectation values of observables are computed via the trace

$$\langle A \rangle = \text{Tr} \{A\rho\} = \text{Tr} \{\rho A\}, \quad (2.6)$$

and the time-dependent density matrix obeys the von-Neumann equation

$$\dot{\rho} = -i[H, \rho]. \quad (2.7)$$

Note that the states $|\Psi_n\rangle$ can be, but need not be orthogonal $\langle \Psi_n | \Psi_m \rangle \neq \delta_{nm}$. If they are, Eq. (2.5) is just the spectral decomposition, and the P_n are the eigenvalues. However, this is not true when $\langle \Psi_n | \Psi_m \rangle \neq \delta_{nm}$. Physically, this corresponds to a situation, where one is given the qubit e.g. with $P_0 = 1/3$ in the state $|0\rangle$, with $P_1 = 1/3$ in the state $|1\rangle$, and with $P_{\rightarrow} = 1/3$ in the state $|\rightarrow\rangle = \frac{1}{\sqrt{2}}[|0\rangle + |1\rangle]$. A state described by a density matrix ρ is then called **pure state**, if $\rho^2 = \rho$ or $\rho = |\Psi\rangle \langle \Psi|$.

Specifically for a qubit, its general state can be parametrized as a point inside or on the Bloch sphere

$$\rho = \frac{1}{2} [\mathbf{1} + \mathbf{n} \cdot \boldsymbol{\sigma}] \quad \mathbf{n} \cdot \mathbf{n} \leq 1 \quad n_i \in \mathbb{R}. \quad (2.8)$$

The pure states are on the surface of the Bloch sphere, and the others inside.

- The time-dependent expectation value of some observable σ^α is then given by

$$\langle \sigma^\alpha \rangle_t = \text{Tr} \{ \sigma^\alpha \rho(t) \} = \text{Tr} \left\{ \sigma^\alpha \frac{1}{2} [\mathbf{1} + \mathbf{n}(t) \cdot \boldsymbol{\sigma}] \right\} = n_\alpha(t), \quad (2.9)$$

where we have used that $(\sigma^\alpha)^2 = \mathbf{1}$ and that the Pauli matrices are traceless.

2.2 Qubit control

Let us consider a qubit in some (for simplicity) pure state. We can reach any other pure state on the Bloch sphere surface by acting with a constant Hamiltonian for a finite time. Using the Hamiltonian $H = \mathbf{h} \cdot \boldsymbol{\sigma}$ with identity ($h = \sqrt{h_x^2 + h_y^2 + h_z^2}$)

$$U(t) = e^{-i\mathbf{h} \cdot \boldsymbol{\sigma} t} = \cos(ht)\mathbf{1} - i \sin(ht)\mathbf{e}_{\mathbf{h}} \cdot \boldsymbol{\sigma}, \quad (2.10)$$

we can for example rotate the state $|0\rangle$ to any desired point on the Bloch sphere

$$U(t)|0\rangle = \left[\cos(ht) - i \sin(ht) \frac{h_z}{h} \right] |0\rangle + \left[-i \sin(ht) \frac{h_x}{h} + \sin(ht) \frac{h_y}{h} \right] |1\rangle. \quad (2.11)$$

However, to ensure that afterwards the qubit remains at the target state, we have to turn on and off the time-dependence of the Hamiltonian. If that switching process is to a good approximation instantaneous, we can write

$$U_{\text{gate}} = e^{-iH_{\text{control}}T_{\text{gate}}} \quad (2.12)$$

with a gate operation time T_{gate} . This means that our assumption of a time-independent Hamiltonian has to be violated at least in the beginning and in the end.

But this does not invalidate the analysis. The same gate can be implemented with a time-dependent dimensionless envelope function $g(t)$ fulfilling

$$g(t \leq 0) = 0, \quad g(t \geq T_{\text{gate}}) = 0, \quad \int_0^{T_{\text{gate}}} g(t) dt = T_{\text{gate}}, \quad (2.13)$$

when we have a control Hamiltonian of the form

$$H(t) = g(t)H_{\text{control}}. \quad (2.14)$$

Since this operator does commute with itself at different times $[H(t), H(t')] = 0$, the time-ordering has no effect and we can write the time evolution operator as

$$U(t) = \exp \left[-i \int_0^{T_{\text{gate}}} H(t) dt \right] = U_{\text{gate}}. \quad (2.15)$$

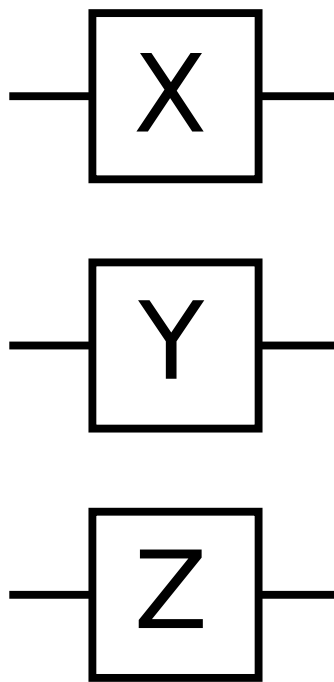
In fact, on the surface of the Bloch sphere this transformation can be understood as a simple rotation.

2.3 Single qubit gates

The Pauli matrices themselves are particular unitary gates that can be applied to a qubit. We can write them with (9) as exponentials of other matrices

$$\begin{aligned} X &= \sigma^x = ie^{-i\pi/2\sigma^x} = e^{i\pi/2}[\mathbf{1} - \sigma^x], \\ Y &= \sigma^y = ie^{-i\pi/2\sigma^y} = e^{i\pi/2}[\mathbf{1} - \sigma^y], \\ Z &= \sigma^z = ie^{-i\pi/2\sigma^z} = e^{i\pi/2}[\mathbf{1} - \sigma^z], \end{aligned} \quad (2.16)$$

Figure 2.1:
Diagrammatic representation of single qubit gates. The state of the input qubit (wire from the left) is transformed by applying the respective gate transformation, yielding the output qubit (wire to the right). In contrast to classical gates, quantum gates always have the same number of input and output qubits.



and in the exponent we could identify a Hamiltonian and a gate operation time, which we can also represent diagrammatically, see Fig. 2.1. Clearly, this is not unique, by multiplying a Hamiltonian with an arbitrary constant and dividing the gate operation time by the same constant, the gate action remains the same. Furthermore, since $X^2 = Y^2 = Z^2 = \mathbf{1}$, we could equivalently write these gates e.g. as

$$\begin{aligned} X &= e^{i3\pi/2[\mathbf{1}-\sigma^x]}, \\ Y &= e^{i3\pi/2[\mathbf{1}-\sigma^y]}, \\ Z &= e^{i3\pi/2[\mathbf{1}-\sigma^z]}, \end{aligned} \quad (2.17)$$

In the computational basis

$$|0\rangle \hat{=} \begin{pmatrix} 1 \\ 0 \end{pmatrix}, \quad |1\rangle \hat{=} \begin{pmatrix} 0 \\ 1 \end{pmatrix} \quad (2.18)$$

we can represent the Pauli matrices as

$$\sigma^x = |0\rangle\langle 1| + |1\rangle\langle 0|, \quad \sigma^y = -i|0\rangle\langle 1| + i|1\rangle\langle 0|, \quad \sigma^z = |0\rangle\langle 0| - |1\rangle\langle 1|. \quad (2.19)$$

In this basis, we see that the X gate flips the basis state, whereas the Y gate additionally equips it with a phase factor and the Z gate does not flip but only comes with a phase factor

$$\begin{aligned} X|0\rangle &= |1\rangle, & X|1\rangle &= |0\rangle, \\ Y|0\rangle &= i|1\rangle, & Y|1\rangle &= -i|0\rangle, \\ Z|0\rangle &= +|0\rangle, & Z|1\rangle &= -|1\rangle. \end{aligned} \quad (2.20)$$

In other words, the X gate is equivalent to a NOT gate. Beyond such gates, we will also consider the Hadamard gate

$$H = \frac{1}{\sqrt{2}} \begin{pmatrix} 1 & 1 \\ 1 & -1 \end{pmatrix}. \quad (2.21)$$

It transforms the computational basis states into superposition states

$$H|0\rangle = \frac{1}{\sqrt{2}} [|0\rangle + |1\rangle]. \quad (2.22)$$

We have already noted that the most general unitary transformation on a two-level system can be fully parametrized by three numbers

$$U = e^{-it\mathbf{h}\cdot\boldsymbol{\sigma}} = \cos(ht)\mathbf{1} - i\sin(ht)\frac{\mathbf{h}\cdot\boldsymbol{\sigma}}{h}. \quad (2.23)$$

Rewriting this slightly, we see that this actually corresponds to a rotation on the Bloch sphere

$$U = e^{-iht\mathbf{e}_h\cdot\boldsymbol{\sigma}} \quad (2.24)$$

around the axis defined by the unit vector

$$\mathbf{e}_h = \begin{pmatrix} \frac{h_x}{h} \\ \frac{h_y}{h} \\ \frac{h_z}{h} \end{pmatrix}, \quad h = \sqrt{h_x^2 + h_y^2 + h_z^2} \quad (2.25)$$

by an angle $\phi = 2ht$. Note however, that this only holds up to possible phase factors, consider e.g. the rotation around $\mathbf{e}_h = \mathbf{e}_y$ by an angle $\phi = 2ht = 2\pi$. This means that by changing the strength of the Hamiltonian h or the gate operation time t , we can in principle perform arbitrary rotations on the Bloch sphere. For a given experimental setup we may not be able to just provide a desired axis \mathbf{e}_h . Then, it is helpful to realize that – just as general rotations can be decomposed into rotations around the principal axes – an arbitrary unitary rotation can be written as

$$\begin{aligned} U &= e^{i\alpha} \begin{pmatrix} e^{-i\beta/2} & 0 \\ 0 & e^{+i\beta/2} \end{pmatrix} \begin{pmatrix} \cos(\gamma/2) & -\sin(\gamma/2) \\ +\sin(\gamma/2) & \cos(\gamma/2) \end{pmatrix} \begin{pmatrix} e^{-i\delta/2} & 0 \\ 0 & e^{+i\delta/2} \end{pmatrix} \\ &= e^{i\alpha} e^{-i\beta/2\sigma^z} e^{-i\gamma/2\sigma^y} e^{-i\delta/2\sigma^z} \end{aligned} \quad (2.26)$$

with $\alpha, \beta, \gamma, \delta \in \mathbb{R}$. This shows that by experimentally implementing only two different Hamiltonians (here something proportional to σ^z and σ^y), we can engineer arbitrary unitary transformations on a single qubit.

It seems that a qubit is much more powerful than a classical bit, since on the Bloch sphere we have more space available. In principle, initializing the qubit in the state $|0\rangle$, we can apply a single qubit rotation on it to generate a state

$$\begin{aligned} |\Psi(h, \theta, \phi)\rangle &= U(h, \theta, \phi) |0\rangle = e^{-ih(\sin\theta\cos\phi\sigma^x + \sin\theta\sin\phi\sigma^y + \cos\theta\sigma^z)} |0\rangle \\ &= [\cos(h) - i\sin(h)\cos(\theta)] |0\rangle + [-i\sin(h)\sin(\theta)\cos(\phi) + \sin(h)\sin(\theta)\sin(\phi)] |1\rangle \\ &\equiv \alpha |0\rangle + \beta |1\rangle \end{aligned} \quad (2.27)$$

on the Bloch sphere, which can be quantified by just two angles. Since these numbers may be represented by infinitely long binary sequences, we can in principle store an infinite amount of information in a single qubit, only limited by the resolution of the implementation of the unitary gate. The problem however is that we cannot get back this information, since the measurement postulate will prevent this. Suppose that we perform a final measurement of σ^z . Then, we can only get out the two outcomes 0 and 1. We will get outcome 0 with probability

$$P_0 = \cos^2(h) + \sin^2(h)\cos^2(\theta). \quad (2.28)$$

After this outcome, the qubit will be in the state $|0\rangle$, and the information is lost. Outcome 1 will occur with probability

$$P_1 = \sin^2(h) \sin^2(\theta) \sin^2(\phi) + \sin^2(h) \sin^2(\theta) \cos^2(\phi) = \sin^2(h) \sin^2(\theta), \quad (2.29)$$

and we can verify $P_0 + P_1 = 1$. After this outcome, the qubit is in state $|1\rangle$, and the information is lost. So while a qubit seems very powerful, readout is a problem.

2.4 Multiple qubits

As in the classical case, little can be achieved with one qubit. If you consider many identical qubits (actually, without necessarily letting them interact), each of the qubits can have their individual state on the Bloch sphere. So, the joint state of all e.g. two qubits altogether can be such that any basis state of the first qubit can be combined with any basis state of the second qubit.

This is not exclusive to qubits but can be applied to any quantum system. The way to define a basis for the Hilbert space of the composite system is formalized in the **tensor product**: Let $|v_i\rangle$ denote an orthonormal basis of Hilbert space V and $|w_j\rangle$ denote an orthonormal basis of Hilbert space W . Then, a basis of Hilbert space $U = V \otimes W$ is formed by all possible combinations of the individual basis vectors

$$|u_{ij}\rangle = |v_i\rangle \otimes |w_j\rangle. \quad (2.30)$$

It obeys a number of useful properties.

- Scalar factors $z \in \mathbb{C}$ can be multiplied to any of the basis states

$$z |v_i\rangle \otimes |w_j\rangle = (z |v_i\rangle) \otimes |w_j\rangle = |v_i\rangle \otimes (z |w_j\rangle). \quad (2.31)$$

- The tensor product is bilinear

$$\begin{aligned} (|v_1\rangle + |v_2\rangle) \otimes |w\rangle &= |v_1\rangle \otimes |w\rangle + |v_2\rangle \otimes |w\rangle, \\ |v\rangle \otimes (|w_1\rangle + |w_2\rangle) &= |v\rangle \otimes |w_1\rangle + |v\rangle \otimes |w_2\rangle. \end{aligned} \quad (2.32)$$

- In the composite Hilbert space, the scalar product is inherited from the local Hilbert spaces. Since we can expand an arbitrary state in the composite Hilbert space in the composite basis, it suffices to write the orthonormality condition for the joint basis states

$$\langle u_{ij} | u_{kl} \rangle = (\langle v_i | \otimes \langle w_j |) (|v_k\rangle \otimes |w_\ell\rangle) = \langle v_i | v_k \rangle \langle w_j | w_\ell \rangle = \delta_{ik} \delta_{j\ell}. \quad (2.33)$$

With this, the scalar product of arbitrary states $|\Psi\rangle = \sum_{ij} c_{ij} |u_{ij}\rangle$ and $|\Phi\rangle = \sum_{kl} \bar{c}_{kl} |u_{kl}\rangle$ can be expressed as

$$\langle \Psi | \Phi \rangle = \sum_{ij,kl} c_{ij}^* \bar{c}_{kl} \langle u_{ij} | u_{kl} \rangle = \sum_{ij} c_{ij}^* \bar{c}_{ij}. \quad (2.34)$$

- Arbitrary linear operators in U can be expressed as

$$C = \sum_{\alpha} c_{\alpha} A_{\alpha} \otimes B_{\alpha}, \quad (2.35)$$

where A_α and B_α only act in V and W , respectively. On an arbitrary state, an operator C acts as

$$C|\Psi\rangle = \sum_{ij} \sum_{\alpha} c_{ij} c_{\alpha} (A_{\alpha}|v_i\rangle) \otimes (B_{\alpha}|w_j\rangle), \quad (2.36)$$

such that it is fully defined once its decomposition into operators of the individual Hilbert spaces is known.

- Notationally, we note that the explicit writing of the symbol \otimes is often omitted when it can be guessed from the context. For example, for qubits we can follow the convention of always writing the value of the first qubit on the first position to denote the basis states as $|z_1\rangle \otimes |z_2\rangle = |z_1\rangle |z_2\rangle = |z_1, z_2\rangle = |z_1 z_2\rangle$. Similarly, operators acting on many qubits can be decomposed into tensor products of operators acting on individual qubits (which we know can be represented by Pauli matrices). Therefore, we denote the Pauli matrices acting on multiple qubits by two indices

$$\sigma^{\alpha} \rightarrow \sigma_i^{\alpha} \quad : \quad \alpha \in \{x, y, z\}, i \in \{1, \dots, n\}. \quad (2.37)$$

Since identity operators act trivially in their respective subspace, they are often omitted notationally. For example, for two qubits one could write $\sigma^x \otimes \mathbf{1} = \sigma_1^x$ or $\sigma^x \otimes \sigma^y = \sigma_1^x \sigma_2^y = \sigma_2^y \sigma_1^x$, which holds because operators acting on different Hilbert spaces do by construction commute. Summarizing this, we could also write the commutation relations of Pauli matrices as

$$[\sigma_a^{\alpha}, \sigma_b^{\beta}] = \delta_{ab} 2i \epsilon_{\alpha\beta\gamma} \sigma_a^{\gamma}. \quad (2.38)$$

- While the tensor product can be used to construct a basis in the composite Hilbert space, in general a basis of the composite Hilbert space need not be decomposable into single tensor products of the individual Hilbert spaces. A valid orthonormal basis for two qubits, for example is given by

$$\{|00\rangle, |01\rangle, |10\rangle, |11\rangle\}. \quad (2.39)$$

This is the one which follows from the tensor product (and we have omitted the tensor symbol for brevity). However, in quantum mechanics we can form superpositions, such that an alternative orthonormal basis is given by

$$\left\{ \frac{1}{\sqrt{2}}(|00\rangle + |11\rangle), \frac{1}{\sqrt{2}}(|00\rangle - |11\rangle), \frac{1}{\sqrt{2}}(|01\rangle + |10\rangle), \frac{1}{\sqrt{2}}(|01\rangle - |10\rangle) \right\}. \quad (2.40)$$

This basis is formed of the so-called **Bell states**. States that cannot be written as a single tensor product are called **entangled**. For example, the state $\frac{1}{\sqrt{2}}(|10\rangle + |11\rangle) = |1\rangle \otimes \frac{1}{\sqrt{2}}(|0\rangle + |1\rangle)$ is not entangled while the state $\frac{1}{\sqrt{2}}(|00\rangle + |11\rangle)$ is entangled.

- The construction can be applied recursively: By combining e.g. the 4 basis states for two qubits with the 2 basis states of another qubit, we find that there are 8 basis states for three qubits. In general, the Hilbert space dimension of n qubits will be exponentially large

$$d_n = 2^n. \quad (2.41)$$

When computing a wave function for n qubits, this means that in general 2^n complex coefficients have to be stored to characterize the wave function. This unfavorable scaling demonstrates that the simulation of a quantum computer on a classical one is futile. We will use the **computational basis** by using the eigenstates of the Pauli σ^z matrices for all the qubits, i.e., a basis state for n qubits is denoted as

$$|z_1 z_2 \dots z_n\rangle \quad : \quad z_i \in \{0, 1\}. \quad (2.42)$$

A convenient ordering of these basis states arises from the binary representation of the numbers $0 \dots (2^n - 1)$.

- The definition of the tensor product does not make any statement on the ordering of the basis states. A particular ordering of basis states allows to represent the tensor product by the **Kronecker product**: If \mathbf{A} is an $m \times n$ matrix and \mathbf{B} is a $p \times q$ matrix, the tensor product of $\mathbf{A} \otimes \mathbf{B}$ has in the lexicographic basis the representation (A_{ij} denote the matrix elements of \mathbf{A})

$$\mathbf{A} \otimes \mathbf{B} = \begin{pmatrix} A_{11}\mathbf{B} & A_{12}\mathbf{B} & \dots & A_{1n}\mathbf{B} \\ A_{21}\mathbf{B} & A_{22}\mathbf{B} & & A_{2n}\mathbf{B} \\ \vdots & \vdots & & \vdots \\ A_{m1}\mathbf{B} & A_{m2}\mathbf{B} & \dots & A_{mn}\mathbf{B} \end{pmatrix}. \quad (2.43)$$

The dimension of the resulting matrix is $mp \times nq$.

For example, the tensor products of basis vectors become for two qubits

$$\begin{aligned} |0\rangle \otimes |0\rangle &\hat{=} \begin{pmatrix} 1 \\ 0 \end{pmatrix} \otimes \begin{pmatrix} 1 \\ 0 \end{pmatrix} = \begin{pmatrix} 1 \begin{pmatrix} 1 \\ 0 \end{pmatrix} \\ 0 \begin{pmatrix} 1 \\ 0 \end{pmatrix} \end{pmatrix} = \begin{pmatrix} 1 \\ 0 \\ 0 \\ 0 \end{pmatrix} \hat{=} |00\rangle, \\ |0\rangle \otimes |1\rangle &\hat{=} \begin{pmatrix} 1 \\ 0 \end{pmatrix} \otimes \begin{pmatrix} 0 \\ 1 \end{pmatrix} = \begin{pmatrix} 1 \begin{pmatrix} 0 \\ 1 \end{pmatrix} \\ 0 \begin{pmatrix} 0 \\ 1 \end{pmatrix} \end{pmatrix} = \begin{pmatrix} 0 \\ 1 \\ 0 \\ 0 \end{pmatrix} \hat{=} |01\rangle, \\ |1\rangle \otimes |0\rangle &\hat{=} \begin{pmatrix} 0 \\ 1 \end{pmatrix} \otimes \begin{pmatrix} 1 \\ 0 \end{pmatrix} = \begin{pmatrix} 0 \begin{pmatrix} 1 \\ 0 \end{pmatrix} \\ 1 \begin{pmatrix} 1 \\ 0 \end{pmatrix} \end{pmatrix} = \begin{pmatrix} 0 \\ 0 \\ 1 \\ 0 \end{pmatrix} \hat{=} |10\rangle, \\ |1\rangle \otimes |1\rangle &\hat{=} \begin{pmatrix} 0 \\ 1 \end{pmatrix} \otimes \begin{pmatrix} 0 \\ 1 \end{pmatrix} = \begin{pmatrix} 0 \begin{pmatrix} 0 \\ 1 \end{pmatrix} \\ 1 \begin{pmatrix} 0 \\ 1 \end{pmatrix} \end{pmatrix} = \begin{pmatrix} 0 \\ 0 \\ 0 \\ 1 \end{pmatrix} \hat{=} |11\rangle. \end{aligned} \quad (2.44)$$

An important operator is the **CNOT gate**: It acts on two qubits. One of these is the control qubit (e.g. the first) and the gate performs a spin flip on the other qubit when the control qubit is set to $|1\rangle$ and does nothing to it when the control qubit is in the state $|0\rangle$, as depicted in Fig. 2.2. In the computational basis its matrix representation can be computed via the

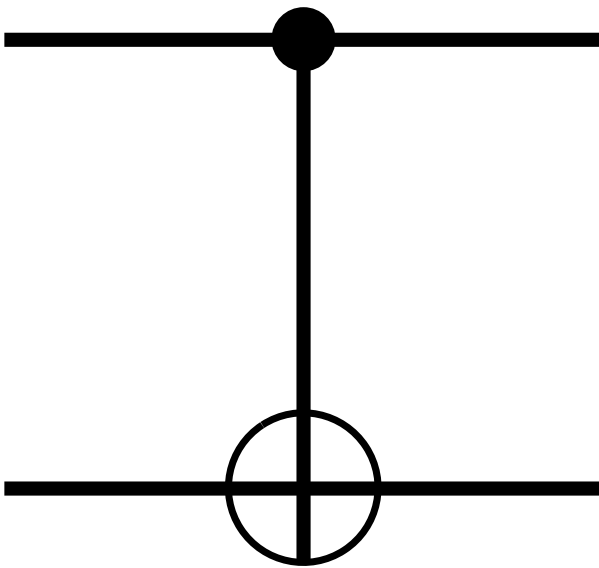


Figure 2.2: Quantum circuit symbol of a CNOT (controlled-not) gate. The filled dot symbolizes the control qubit, and the crossed circle the target qubit. Roles of control and target qubits may be interchanged.

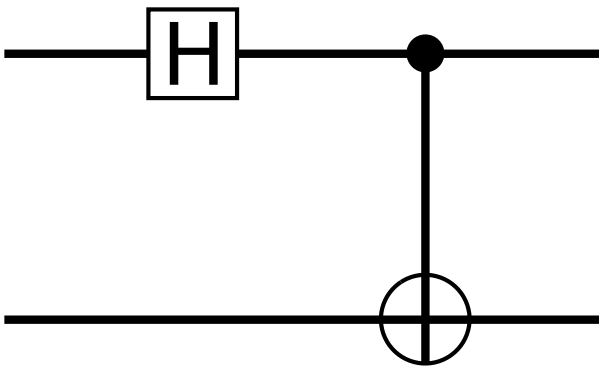


Figure 2.3: Quantum circuit to create Bell states from the computational basis states. When fed in $|00\rangle$, the application of the Hadamard gate first transforms the state into $\frac{1}{\sqrt{2}}[|00\rangle + |10\rangle]$. Acting afterwards with a CNOT gate, the state becomes $\frac{1}{\sqrt{2}}[|00\rangle + |11\rangle]$.

Kronecker product

$$\begin{aligned} \text{CNOT}_{12} &= \frac{1}{2} [\mathbf{1} + \sigma^z] \otimes \mathbf{1} + \frac{1}{2} [\mathbf{1} - \sigma^z] \otimes \sigma^x \\ &= \begin{pmatrix} 1 & \cdot & \mathbf{1} & 0 & \cdot & \mathbf{1} \\ 0 & \cdot & \mathbf{1} & 0 & \cdot & \mathbf{1} \end{pmatrix} + \begin{pmatrix} 0 & \cdot & \sigma^x & 0 & \cdot & \sigma^x \\ 0 & \cdot & \sigma^x & 1 & \cdot & \sigma^x \end{pmatrix} = \begin{pmatrix} 1 & 0 & 0 & 0 \\ 0 & 1 & 0 & 0 \\ 0 & 0 & 0 & 1 \\ 0 & 0 & 1 & 0 \end{pmatrix}. \end{aligned} \quad (2.45)$$

Note that even if the CNOT gate flips the target qubit, it does not copy the state of the control qubit. Even if we always feed in the target qubit as $|0\rangle$, the control qubit cannot be copied in general: Although the state of the control qubit is copied into the target qubit for the particular control qubit states $|0\rangle$ and $|1\rangle$, this does not hold for a general superposition. Rather, for a control qubit state $\alpha|0\rangle + \beta|1\rangle$, the joint qubits afterwards are in the entangled state $\alpha|00\rangle + \beta|11\rangle$. The CNOT gate is an entangling gate.

In fact, the CNOT gate together with a single-qubit Hadamard gate can be used to create the Bell states from the computational basis states as depicted in Fig. 2.3. This diagram is read from left to right, such that the resulting unitary can be obtained from the product of

a Hadamard gate on the first qubit

$$H_1 = H \otimes \mathbf{1} \hat{=} \frac{1}{\sqrt{2}} \begin{pmatrix} 1 \cdot \mathbf{1} & 1 \cdot \mathbf{1} \\ 1 \cdot \mathbf{1} & -1 \cdot \mathbf{1} \end{pmatrix} = \frac{1}{\sqrt{2}} \begin{pmatrix} 1 & 0 & 1 & 0 \\ 0 & 1 & 0 & 1 \\ 1 & 0 & -1 & 0 \\ 0 & 1 & 0 & -1 \end{pmatrix} \quad (2.46)$$

and a CNOT gate

$$\text{CNOT}_{12} H_1 = \frac{1}{\sqrt{2}} \begin{pmatrix} 1 & 0 & 1 & 0 \\ 0 & 1 & 0 & 1 \\ 0 & 1 & 0 & -1 \\ 1 & 0 & -1 & 0 \end{pmatrix}. \quad (2.47)$$

2.5 Quantum applications of two qubits

Entangled states are among the most intriguing features of quantum physics. Suppose we prepare a two-qubit system in the first of the Bell states (2.40)

$$|\Psi\rangle = \frac{1}{\sqrt{2}} [|00\rangle + |11\rangle]. \quad (2.48)$$

This state is evidently entangled. The two qubits are shared between two parties (conventionally called Alice and Bob). Ideally, we assume that in the separation process, the fragile quantum superposition is not harmed. The two parties can be extremely far apart. Now, Alice can locally measure her qubit in the computational basis. On the global system, this corresponds to a measurement of the observable σ_1^z . If she measures the outcome $+1$, the state is projected onto the post-measurement state $|\Psi'\rangle = |00\rangle$. In contrast, if she measures the outcome -1 , the post-measurement state is $|\Psi'\rangle = |11\rangle$. Thereby, Bob's qubit is immediately in the same state as Alice's state, independent of the distance between Alice and Bob. This *spooky action at a distance* led Einstein, Podolsky and Rosen to the conjecture that quantum mechanics might be incomplete [2]. Numerous experiments have however confirmed our view that quantum mechanics is complete.

2.5.1 Bell inequalities

In 1964 John Stewart Bell published a paper on expectation values of classical observables [3]. He derived an inequality that should be obeyed if classical common sense is correct (and accordingly, quantum mechanics is incomplete). So let us for a moment forget about quantum mechanics and non-commuting observables etc. The assumptions in the Bell inequalities are that

- particles have properties that exist objectively, i.e., these properties exist without the measurement, a condition that is known as *realism*
- a local measurement of the properties on one of the particles cannot influence the measurement result on the other particle, a condition that is termed *locality*

Together, these assumptions are known as *local realism*. Under these assumptions, Bell derived a simple inequality which has experimentally shown to be violated, disproving at least one of the assumptions.

To simplify further, we assume that the particles can have different properties (like color and charge) that can take two different values each, which we label ± 1 (like red vs. green or positive vs. negative). Then, the thought experiment goes as follows: A third party prepares two particles in some way that is repeatable. The first particle goes to Alice, the second particle is sent to Bob. Now, both Alice and Bob perform *randomly* one measurement of either the first property (e.g. color) or the second property (e.g. charge) of their respective particle. Here, the particles need not even be identical, such that the measured properties can in principle be different. What is important however is that these measurements are performed *causally disconnected* (let Alice and Bob be sufficiently far apart) and that Alice and Bob do not agree on a particular random protocol but decide independently and randomly what measurement to perform. Alice calls the first property $Q \in \{-1, +1\}$ and the second property $R \in \{-1, +1\}$ and Bob calls the first property $S \in \{-1, +1\}$ and the second $T \in \{-1, +1\}$. Then, no matter what the actual values are we find that the quantity

$$QS + RS + RT - QT = (Q + R)S + (R - Q)T \in \{-2, +2\}, \quad (2.49)$$

which simply follows by realizing that either $(Q + R = \pm 2$ and $Q - R = 0)$ or $(R - Q = \pm 2$ and $Q + R = 0)$. Now the experiment is repeated multiple times. Let $p(q, r, s, t)$ denote the probability that $Q = q$, $R = r$, $S = s$, and $T = t$ (due to experimental noise and the preparation procedure, the preparation process will in general be stochastic). Then, the expectation value of the above quantity can be upper-bounded via

$$E(QS + RS + RT - QT) = \sum_{qrst} p(q, r, s, t)(qs + rs + rt - qt) \leq +2 \sum_{qrst} p(q, r, s, t) = 2. \quad (2.50)$$

Likewise, we can lower-bound this via

$$E(QS + RS + RT - QT) = \sum_{qrst} p(q, r, s, t)(qs + rs + rt - qt) \geq -2 \sum_{qrst} p(q, r, s, t) = -2. \quad (2.51)$$

Summarizing, the **Bell inequalities** (or **CHSH inequalities** after Clauser, Horne, Shimony, Holt) read by linearity of the expectation value

$$-2 \leq E(QS) + E(RS) + E(RT) - E(QT) \leq +2. \quad (2.52)$$

Doing the experiment many times and recording their results together with the information what type of measurement was performed, Alice and Bob can meet again some time in the future and evaluate the l.h.s. of the above equation. For example $E(QS)$ is obtained by averaging the products of measurement results where both Alice and Bob measured their first property, and an estimate of $E(RS)$ can be obtained by averaging the products of measurement results where Alice measured her first and Bob his second property. If the underlying assumption of local realism is correct, the expectation value will lie inside the above bound. Corresponding experiments have been performed [4], which have confirmed the violation of the Bell inequalities.

We can convince ourselves that some (not all) quantum mechanical superposition states can break the Bell inequalities, thereby invalidating the assumption of local realism. To see this, consider the Bell state (we can take any but might need to use different observables)

$$|\Psi\rangle = \frac{1}{\sqrt{2}} [|01\rangle - |10\rangle] \quad (2.53)$$

with the observables for Alice

$$Q = Z_1 = \sigma^z \otimes \mathbf{1}, \quad R = X_1 = \sigma^x \otimes \mathbf{1} \quad (2.54)$$

and the observables for Bob

$$S = \frac{1}{\sqrt{2}}[X_2 + Z_2] = \mathbf{1} \otimes \frac{1}{\sqrt{2}}[\sigma^x + \sigma^z], \quad T = \frac{1}{\sqrt{2}}[X_2 - Z_2] = \mathbf{1} \otimes \frac{1}{\sqrt{2}}[\sigma^x - \sigma^z], \quad (2.55)$$

where the main point is simply that Bob measures in a Basis which is rotated in comparison to Alice basis. Note that all these observables have possible values ± 1 as assumed. We get the quantum-mechanical expectation values

$$\begin{aligned} \langle QS \rangle &= \langle \Psi | \sigma^z \otimes \frac{1}{\sqrt{2}}[\sigma^x + \sigma^z] | \Psi \rangle \\ &= \left(\frac{1}{\sqrt{2}} \right)^3 [\langle 01 | - \langle 10 |] [\sigma^z \otimes \sigma^x | 01 \rangle - \sigma^z \otimes \sigma^x | 10 \rangle + \sigma^z \otimes \sigma^z | 01 \rangle - \sigma^z \otimes \sigma^z | 10 \rangle] \\ &= \frac{1}{2} \frac{1}{\sqrt{2}} [\langle 01 | - \langle 10 |] [|00\rangle + |11\rangle - |01\rangle + |10\rangle] = -\frac{1}{\sqrt{2}}. \end{aligned} \quad (2.56)$$

In a similar fashion, the other expectation values become

$$\langle RS \rangle = -\frac{1}{\sqrt{2}}, \quad \langle RT \rangle = -\frac{1}{\sqrt{2}}, \quad \langle QT \rangle = +\frac{1}{\sqrt{2}}. \quad (2.57)$$

Altogether, this yields $\langle QS + RS + RT - QT \rangle = -4/\sqrt{2} = -2\sqrt{2}$ which clearly breaks the Bell inequality. Thereby, entangled states can carry stronger correlations than classically possible, and the assumptions of local realism are wrong.

2.5.2 Superdense coding

By using entanglement, Alice can send two classical bits of information with sending only one qubit. Suppose Alice and Bob are provided the Bell state $|\Psi\rangle = \frac{1}{\sqrt{2}}[|00\rangle + |11\rangle]$. Alice takes the first qubit and Bob the second. When Alice is alone, she performs local operations on her qubit – depending on the two classical bits she wants to transmit. With this, she creates all possible Bell states:

intended bitstring	applied operation by Alice	resulting state
00	$\mathbf{1}_1$	$\frac{1}{\sqrt{2}} [00\rangle + 11\rangle]$
01	Z_1	$\frac{1}{\sqrt{2}} [00\rangle - 11\rangle]$
10	X_1	$\frac{1}{\sqrt{2}} [10\rangle + 01\rangle]$
11	Y_1	$\frac{1}{\sqrt{2}} [10\rangle - 01\rangle]$

To do so, Alice only needs to act on the first of the qubits. Then, she sends her qubit to Bob.

Being in possession of both qubits, Bob may now perform suitable measurements to determine which state was sent. This is not straightforward but possible since the Bell states are all orthogonal and can therefore be faithfully distinguished. Formally, such a measurement could be performed by measuring a nonlocal observable such as e.g. $\hat{A} = \sum_i \lambda_i |\Psi_i\rangle \langle \Psi_i|$ with $|\Psi_i\rangle$ denoting the Bell states and λ_i arbitrary different eigenvalues. Alternatively, Bob could apply a two-qubit unitary to rotate the sent Bell state back to one of the computational basis states and afterwards measure these in the local $\sigma_{1/2}^z$ basis. Diagrammatically, this would correspond to the inverse gate of Fig. 2.3: Since

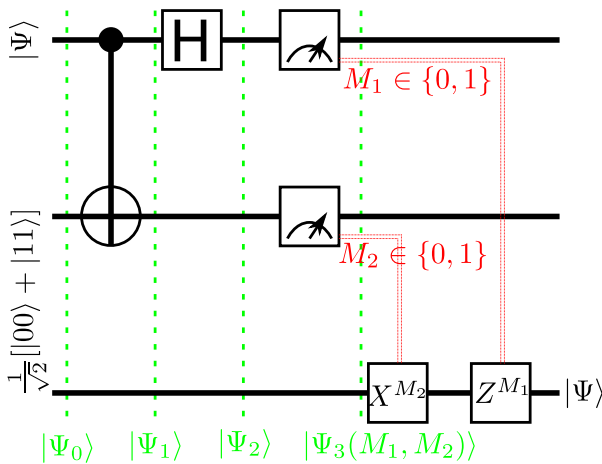


Figure 2.4: Circuit for the quantum teleportation of a qubit from the first qubit (upper wire) into the third qubit (lower wire). At the meter symbols, a classical measurement in the computational basis is performed, such that the quantum superposition is projected onto the basis states (double lines indicate classical communication). Depending on the measurement outcome, single qubit gates are finally performed ($M_i = 1$) or not ($M_i = 0$).

the Hadamard gate and CNOT gates are their own inverses, the corresponding quantum circuit simply has the order of the gates reversed. This allows Bob to extract the sent information and – having pre-shared an entangled state – Alice can transmit two classical bits by sending only a single qubit to Bob. In general, we can understand entangled state as a useful resource.

2.5.3 No-cloning theorem

Many classical algorithms make excessive use of copies of bits. Of course, we can just measure the state of a qubit, project it e.g. on the states $|0\rangle$ or $|1\rangle$ and then prepare a second qubit in the same state depending on the measurement outcome. This would yield two qubits in the same state $|00\rangle$ or $|11\rangle$, but this procedure would not work if we want to copy a general superposition state. Unfortunately, the laws of quantum mechanics forbid the direct copying of qubits with an unknown state. To see this in a bit more general fashion, let us assume that we have a unitary U that manages to copy two states $|\phi\rangle$ and $|\psi\rangle$ into an ancilla qubit that is initially prepared in some defined state $|s\rangle$

$$U|\psi\rangle \otimes |s\rangle = |\psi\rangle \otimes |\psi\rangle, \quad U|\phi\rangle \otimes |s\rangle = |\phi\rangle \otimes |\phi\rangle. \quad (2.58)$$

We can already see that the initial information of the ancilla state $|s\rangle$ is gone in the final result, such that we cannot go back with an inverse unitary, leading to a contradiction. Alternatively, we can however also look at the inner product

$$\langle\psi|\phi\rangle = [\langle\psi| \otimes \langle s|] U^\dagger U [|\phi\rangle \otimes |s\rangle] = [\langle\psi| \otimes \langle\psi|] [|\phi\rangle \otimes |\phi\rangle] = \langle\psi|\phi\rangle^2. \quad (2.59)$$

This means that a unitary operation can only clone 2 states that are orthogonal to each other $\langle\phi|\psi\rangle = 0$ or identical $\langle\phi|\psi\rangle = 1$, but not a general quantum state.

2.5.4 Quantum teleportation

Although we cannot copy a qubit, it is possible to teleport it by using classical communication of two bits. For this, one needs three qubits. The first qubit is the one that needs to be teleported and is prepared in an unknown state $|\Psi\rangle = \alpha|0\rangle + \beta|1\rangle$. The other two qubits are prepared in the entangled state $\frac{1}{\sqrt{2}}[|00\rangle + |11\rangle]$, see Fig. 2.4. The three-qubit gate is fed with the initial state

$$|\Psi_0\rangle = [\alpha|0\rangle + \beta|1\rangle] \frac{1}{\sqrt{2}}[|00\rangle + |11\rangle] = \frac{\alpha}{\sqrt{2}}|000\rangle + \frac{\alpha}{\sqrt{2}}|011\rangle + \frac{\beta}{\sqrt{2}}|100\rangle + \frac{\beta}{\sqrt{2}}|111\rangle. \quad (2.60)$$

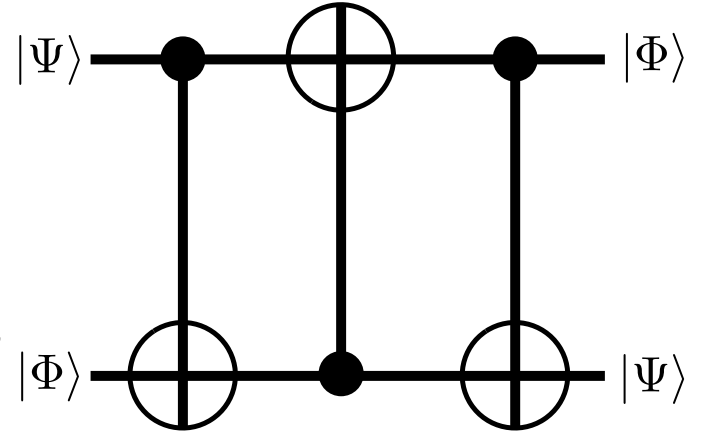


Figure 2.5: Three CNOT gates can implement a SWAP gate, interchanging arbitrary two states $|\Psi\rangle$ and $|\Phi\rangle$.

After a CNOT_{12} gate, the state becomes

$$|\Psi_1\rangle = \frac{\alpha}{\sqrt{2}}|000\rangle + \frac{\alpha}{\sqrt{2}}|011\rangle + \frac{\beta}{\sqrt{2}}|110\rangle + \frac{\beta}{\sqrt{2}}|101\rangle. \quad (2.61)$$

Subsequently, a Hadamard gate is applied to the first qubit

$$|\Psi_2\rangle = \frac{\alpha}{2}|000\rangle + \frac{\alpha}{2}|100\rangle + \frac{\alpha}{2}|011\rangle + \frac{\alpha}{2}|111\rangle + \frac{\beta}{2}|010\rangle - \frac{\beta}{2}|110\rangle + \frac{\beta}{2}|001\rangle - \frac{\beta}{2}|101\rangle. \quad (2.62)$$

The information α, β of the qubit is now distributed between the two parties. Now, the first two qubits are locally measured in the computational basis (that is, we measure σ_1^z and σ_2^z). Four different results can arise, for which the measurement postulate yields

$$\begin{aligned} |\Psi_3(0, 0)\rangle &= \alpha|000\rangle + \beta|001\rangle = |00\rangle \otimes [\alpha|0\rangle + \beta|1\rangle], \\ |\Psi_3(0, 1)\rangle &= |01\rangle \otimes [\alpha|1\rangle + \beta|0\rangle], \\ |\Psi_3(1, 0)\rangle &= |10\rangle \otimes [\alpha|0\rangle - \beta|1\rangle], \\ |\Psi_3(1, 1)\rangle &= |11\rangle \otimes [\alpha|1\rangle - \beta|0\rangle]. \end{aligned} \quad (2.63)$$

Now, the third qubit already carries the full information of the initial state. The final conditional single-qubit rotations merely serve to correct the relative phase or the bit flip, such that the final state of the third qubit is always $|\Psi\rangle$

$$\begin{aligned} |\Psi_4(0, 0)\rangle &= |00\rangle \otimes |\Psi\rangle, & |\Psi_4(0, 1)\rangle &= |01\rangle \otimes |\Psi\rangle, \\ |\Psi_4(1, 0)\rangle &= |10\rangle \otimes |\Psi\rangle, & |\Psi_4(1, 1)\rangle &= |11\rangle \otimes |\Psi\rangle. \end{aligned} \quad (2.64)$$

A SWAP gate can be seen as another way to transfer a state between two qubits. It is composed from alternating CNOT gates

$$\text{SWAP}_{12} = \text{CNOT}_{12}\text{CNOT}_{21}\text{CNOT}_{12}, \quad (2.65)$$

see also Fig. 2.5. To see this formally, consider that for $|\Psi\rangle = [\alpha_1|0\rangle + \beta_1|1\rangle]$ and $|\Phi\rangle = [\alpha_2|0\rangle + \beta_2|1\rangle]$

$$\begin{aligned} \text{SWAP}_{12}|\Psi\rangle \otimes |\Phi\rangle &= \text{SWAP}_{12}[\alpha_1\alpha_2|00\rangle + \alpha_1\beta_2|01\rangle + \beta_1\alpha_2|10\rangle + \beta_1\beta_2|11\rangle] \\ &= \text{CNOT}_{12}\text{CNOT}_{21}[\alpha_1\alpha_2|00\rangle + \alpha_1\beta_2|01\rangle + \beta_1\alpha_2|11\rangle + \beta_1\beta_2|10\rangle] \\ &= \text{CNOT}_{12}[\alpha_1\alpha_2|00\rangle + \alpha_1\beta_2|11\rangle + \beta_1\alpha_2|01\rangle + \beta_1\beta_2|10\rangle] \\ &= [\alpha_1\alpha_2|00\rangle + \alpha_1\beta_2|10\rangle + \beta_1\alpha_2|01\rangle + \beta_1\beta_2|11\rangle] \\ &= [\alpha_2|0\rangle + \beta_2|1\rangle] \otimes [\alpha_1|0\rangle + \beta_1|1\rangle]. \end{aligned} \quad (2.66)$$

However, the difference to teleportation is that in order to implement this gate, the CNOT gates have to bridge the physical distance between the qubits, whereas in teleportation we just use entanglement and classical communication.

2.6 The partial trace

For a given pure bipartite state $|\Psi_{AB}\rangle$ (e.g. defined on the Hilbert space of two qubits) on the Hilbert space $A \otimes B$, we can compute local observables O of the Hilbert space A (e.g. only referring to the first qubit) by expectation values

$$\langle O_A \rangle = \langle O_A \mathbf{1}_B \rangle = \langle \Psi_{AB} | O \otimes \mathbf{1} | \Psi_{AB} \rangle . \quad (2.67)$$

If the state is a product state (i.e., a non-entangled state) $|\Psi_{AB}\rangle = |\Psi_A\rangle \otimes |\Psi_B\rangle$, this can be easily shown to be $\langle O_A \rangle = \langle \Psi_A | O | \Psi_A \rangle$, i.e., in case of qubits it only depends on the state of the first qubit. By contrast, if the state is entangled, the evaluation of a local observable can be more involved, since all the components have to be taken into account. For example, with $|\Psi\rangle = \frac{1}{\sqrt{2}}[|00\rangle + |11\rangle]$ we get

$$\langle \Psi | \sigma_1^\alpha | \Psi \rangle = \langle \Psi | \sigma^\alpha \otimes \mathbf{1} | \Psi \rangle = \frac{1}{2} [\langle 0 | \sigma^\alpha | 0 \rangle + \langle 1 | \sigma^\alpha | 1 \rangle] = 0 . \quad (2.68)$$

For many qubits, this leads to significantly (exponentially) more terms as we have more and more basis states to consider. The density matrix can also be used as a convenient tool to evaluate local (that act only in a part of the full Hilbert space as e.g. only few of all the qubits) observables. We know that for the pure state

$$\rho_{AB} = |\Psi_{AB}\rangle \langle \Psi_{AB}| \quad (2.69)$$

we can likewise compute the local observable as $\langle O_A \rangle = \text{Tr}_{AB} \{ O \otimes \mathbf{1} \rho_{AB} \}$, which does not buy us anything in terms of complexity. However, we can define a so-called reduced density matrix that fully describes the statistics of subsystem A only. This works via the **partial trace**. Whereas a full trace maps an operator to a number, the partial trace merely reduces the dimension of the operator. So if $|a_i\rangle$ are states in Hilbert space A and $|b_i\rangle$ are states in Hilbert space B , the partial trace over B reduces an operator from $A \otimes B$ into an operator only acting on A

$$\text{Tr}_B \{ |a_1\rangle \langle a_2| \otimes |b_1\rangle \langle b_2| \} \equiv |a_1\rangle \langle a_2| \text{Tr} \{ |b_1\rangle \langle b_2| \} . \quad (2.70)$$

For example, for two qubits we would have $\text{Tr}_2 \{ \sigma_1^x \} = \text{Tr}_2 \{ \sigma^x \otimes \mathbf{1} \} = \sigma^x \text{Tr} \{ \mathbf{1} \} = 2\sigma^x$, which only acts on the Hilbert space of the first qubit.

The **reduced density matrix** is defined via the partial trace

$$\rho_A = \text{Tr}_B \{ \rho_{AB} \} . \quad (2.71)$$

It has the following properties

- If ρ_{AB} is a valid density matrix in $A \otimes B$, ρ_A is a valid density matrix in A .
- Specifically, if $\rho_{AB} = \rho_A \otimes \rho_B$ with valid density matrices ρ_A and ρ_B , then $\rho_A = \text{Tr}_B \{ \rho_A \otimes \rho_B \}$.

- Expectation values of local observables can be computed with the reduced density matrix

$$\langle O_A \rangle = \text{Tr} \{ O \otimes \mathbf{1} \rho_{AB} \} = \text{Tr} \{ O \rho_A \} , \quad (2.72)$$

which is now the whole point of the procedure.

- Pure entangled states in $A \otimes B$ become mixed under the partial trace, whereas non-entangled states remain pure. For example, we have for $\Psi_{AB} = |01\rangle$

$$\rho_A = \text{Tr}_B \{ |01\rangle \langle 01| \} = \text{Tr}_2 \{ |0\rangle \otimes |1\rangle \langle 0| \otimes \langle 1| \} = |0\rangle \langle 0| \text{Tr} \{ |1\rangle \langle 1| \} = |0\rangle \langle 0| , \quad (2.73)$$

which evidently is just a pure state. Alternatively, for $\Psi_{AB} = \frac{1}{\sqrt{2}}[|00\rangle + |11\rangle]$ we get

$$\rho_A = \frac{1}{2} \text{Tr}_B \{ |00\rangle \langle 00| + |00\rangle \langle 11| + |11\rangle \langle 00| + |11\rangle \langle 11| \} = \frac{1}{2} [|0\rangle \langle 0| + |1\rangle \langle 1|] , \quad (2.74)$$

which is a mixed (non-pure) state.

- One can show that the partial trace is the unique mapping that preserves the measurement statistics of local observables.

Chapter 3

The circuit model of quantum computation

3.1 Deutsch and Deutsch-Jozsa problems

Quantum and classical computers are different in many aspects. A most prominent one is that for a quantum computer we are able to feed in (complex-valued) superposition states, whereas for a classical computer we could at best feed in a statistical mixture. Loosely speaking, this allows one to evaluate many possible input states in parallel. Technically challenging, we will need entanglement to generate some quantum speedup and unfortunately, one has to think deeply on how to utilize measurement.

A simple example that demonstrates quantum supremacy via the parallel evaluation of many inputs goes as follows: Let $f(x)$ denote a function that maps $\{0, 1\} \rightarrow \{0, 1\}$. There are four possibilities for such a function

function	values	
a.)	$f_a(0) = 0$	$f_a(1) = 0$
b.)	$f_b(0) = 0$	$f_b(1) = 1$
c.)	$f_c(0) = 1$	$f_c(1) = 0$
d.)	$f_d(0) = 1$	$f_d(1) = 1$

For each of these functions one can show that the operation

$$U_f |x, y\rangle = |x, y \oplus f(x)\rangle, \quad (3.1)$$

where \oplus indicates addition modulo 2, can be implemented by a unitary operation U_f depending on the function chosen. This is summarized in this table

xy	$x(y \oplus f_a(x))$	$x(y \oplus f_b(x))$	$x(y \oplus f_c(x))$	$x(y \oplus f_d(x))$
00	00	00	01	01
01	01	01	00	00
10	10	11	10	11
11	11	10	11	10

For example, we can write the case *a.*) in the table above simply as the identity and the second column as a CNOT gate

$$U_{f_a} = \mathbf{1}, \quad U_{f_b} = \text{CNOT}_{12}, \quad U_{f_c} = X_2 \text{CNOT}_{12}, \quad U_{f_d} = X_2. \quad (3.2)$$

Instead of feeding in a computational basis state to the unitary U_f , we can also feed in a superpo-

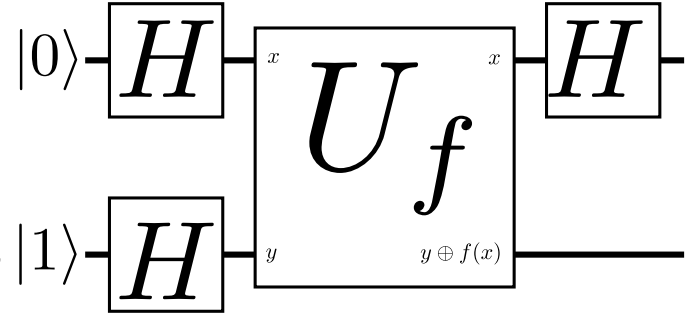


Figure 3.1: Quantum circuit for the Deutsch problem. Upon evaluation of the first qubit at the end of the algorithm, one can determine whether the function $f(x)$ is balanced or not with only a single application of the quantum circuit.

sition in the first qubit and the state $|0\rangle$ in the second

$$U_f H_1 |00\rangle = U_f \frac{1}{\sqrt{2}} [|0\rangle + |1\rangle] \otimes |0\rangle = \frac{1}{\sqrt{2}} [|0, 0 \oplus f(0)\rangle + |1, 0 \oplus f(1)\rangle] = \frac{1}{\sqrt{2}} [|0, f(0)\rangle + |1, f(1)\rangle]. \quad (3.3)$$

Thus, with only using one evaluation, the resulting state has computed the function f at two values. Unfortunately, this is not yet useful as a classical measurement of the first qubit would either yield $f(0)$ or $f(1)$, such that we would have to run the above circuit at least twice and there would be rather a disadvantage in comparison to the classical case, where two evaluations suffice with certainty. To turn this into something with a quantum computation advantage, we have to slightly generalize this picture.

We note that $f_a(x)$ and $f_d(x)$ always give the same value (they are not balanced), whereas $f_b(x)$ and $f_c(x)$ give different values on different inputs (they are called balanced). To classically determine whether a function is balanced or not, we require two function evaluations. The **Deutsch algorithm** corresponds to a quantum circuit depicted in Fig. 3.1. It demonstrates that this global feature of the function $f(x)$ (is it balanced or not) can be revealed with just one evaluation of the quantum circuit [5]. The initial Hadamard gates yield the state

$$H_1 H_2 |01\rangle = \frac{1}{2} [|0\rangle + |1\rangle] \otimes [|0\rangle - |1\rangle] = \frac{1}{2} [|00\rangle - |01\rangle + |10\rangle - |11\rangle]. \quad (3.4)$$

Afterwards, application of the unitary implies

$$\begin{aligned} U_f H_1 H_2 |01\rangle &= \frac{1}{2} [|0, f(0)\rangle - |0, 1 \oplus f(0)\rangle + |1, f(1)\rangle - |1, 1 \oplus f(1)\rangle] \\ &= \begin{cases} \frac{1}{\sqrt{2}} [|0\rangle + |1\rangle] \otimes \frac{1}{\sqrt{2}} [|f\rangle - |1 \oplus f\rangle] & : f(0) = f(1) = f \\ \frac{1}{\sqrt{2}} [|0\rangle - |1\rangle] \otimes \frac{1}{\sqrt{2}} [|f(0)\rangle - |1 \oplus f(0)\rangle] & : f(1) = 1 \oplus f(0) \end{cases} \\ &= \begin{cases} \pm \frac{1}{\sqrt{2}} [|0\rangle + |1\rangle] \otimes \frac{1}{\sqrt{2}} [|0\rangle - |1\rangle] & : f(0) = f(1) = f \\ \pm \frac{1}{\sqrt{2}} [|0\rangle - |1\rangle] \otimes \frac{1}{\sqrt{2}} [|0\rangle - |1\rangle] & : f(1) = 1 \oplus f(0) \end{cases}, \end{aligned} \quad (3.5)$$

where in the last line we have used that $1 \oplus f$ is always just the other state for $f \in \{0, 1\}$, just that we may at most get a sign factor. Importantly, the two possible states of the first qubit are orthogonal and depend on the global property whether the function is balanced $f(1) = 1 \oplus f(0) = 1 - f(0)$ or not $f(0) = f(1) = f \in \{0, 1\}$. The purpose of the final Hadamard gate is simply to rotate back to the computational basis

$$H_1 U_f H_1 H_2 |01\rangle = \begin{cases} \pm |0\rangle \otimes \frac{1}{\sqrt{2}} [|0\rangle - |1\rangle] & : f(0) = f(1) = f \\ \pm |1\rangle \otimes \frac{1}{\sqrt{2}} [|0\rangle - |1\rangle] & : f(1) = 1 \oplus f(0) \end{cases}. \quad (3.6)$$

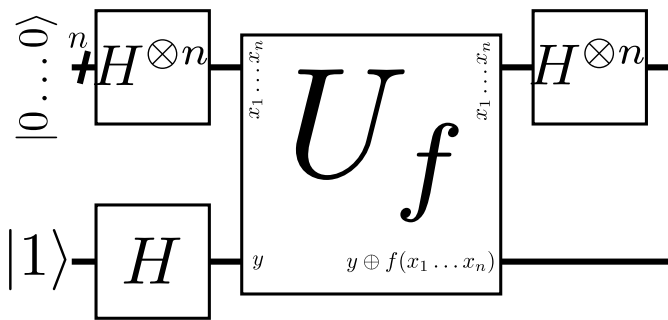


Figure 3.2: The Deutsch-Jozsa quantum circuit is a generalization of the Deutsch quantum circuit from Fig. 3.1 to many input qubits. The upper wire marks n qubits with parallel identical actions performed on.

Now, measurement of the first qubit yields with certainty the global property of the function f (balanced or not) with a single run of the circuit only. A corresponding classical circuit would have to be run twice.

The previous example serves as a proof of principle but is not very impressive. There is only a speedup of a factor of two, which is beaten by the additional effort to implement a quantum computer by orders of magnitude. However, the Deutsch problem can be generalized to many qubits, where one can see that the scaling of the computational complexity is different on a classical and on a quantum computer.

In the **Deutsch-Jozsa problem**, one considers the problem of a function of many bits $f : \{0, 1\}^n \rightarrow \{0, 1\}$. Additionally, one is given the promise that the function $f(\mathbf{x}) = f(x_1, \dots, x_n)$ is either constant $f(\mathbf{x}) = \text{const}$ for all 2^n different values of \mathbf{x} or balanced, that is for 2^{n-1} values of \mathbf{x} it yields 0 and for the other 2^{n-1} values it yields 1. An example for a balanced function could be whether the number of ones in the input \mathbf{x} is even (assign 0) or odd (assign 1)

$$f(\mathbf{x}) = (-1)^{x_1+x_2+\dots+x_n}. \quad (3.7)$$

Given that the function is either balanced or constant, to find out whether the function f is actually balanced or constant, one would classically have to sample it at least 2 times and at most $2^{n-1} + 1$ times: If we get two different values as the first two results, we know that the function is balanced. If we get equal values until the $(2^{n-1} + 1)$ st result we know that the function must be constant. Clearly, by sampling stochastically, one would pretty soon know whether the function is balanced or not, but in the worst case, one could get 2^{n-1} similar results although the function is actually balanced, which would be revealed by the next measurement then. So the worst-case classical complexity is $2^{n-1} + 1$ function evaluations.

A corresponding quantum circuit could actually achieve this in a single run, i.e., with an **exponential speedup**, which is exemplified by the **Deutsch-Jozsa problem** [6]. Given a unitary acting on $n + 1$ qubits

$$U_f |x_1, \dots, x_n, y\rangle = U_f |\mathbf{x}, y\rangle = |\mathbf{x}, y \oplus f(\mathbf{x})\rangle, \quad (3.8)$$

which leaves the first n qubits invariant and imprints the result of the function $f(\mathbf{x})$ on the $n + 1$ st qubit, the Deutsch algorithm from Fig. 3.1 can be generalized in a straightforward way, see Fig. 3.2. After the application of the initial $n + 1$ Hadamard gates the state is

$$\begin{aligned}
H_1 \dots H_{n+1} |0 \dots 0, 1\rangle &= \frac{1}{\sqrt{2}}[|0\rangle + |1\rangle] \otimes \dots \otimes \frac{1}{\sqrt{2}}[|0\rangle + |1\rangle] \otimes \frac{1}{\sqrt{2}}[|0\rangle - |1\rangle] \\
&= \frac{1}{2^{n/2}} \sum_{x_1=0}^1 \dots \sum_{x_n=0}^1 |x_1 \dots x_n\rangle \otimes \frac{1}{\sqrt{2}}[|0\rangle - |1\rangle] \\
&= \frac{1}{2^{n/2}} \sum_{\mathbf{x}=0}^{2^n-1} |\mathbf{x}\rangle \otimes \frac{1}{\sqrt{2}}[|0\rangle - |1\rangle]. \tag{3.9}
\end{aligned}$$

Here, we have simply used that the Hadamard transform on the state $|0 \dots 0\rangle$ of the first n qubits simply yields all computational basis states for n qubits. After applying the unitary that computes the function, we obtain

$$\begin{aligned}
U_f H^{\otimes(n+1)} |\mathbf{0}, 1\rangle &= \frac{1}{2^{n/2}} \sum_{\mathbf{x}=0}^{2^n-1} |\mathbf{x}\rangle \otimes \frac{1}{\sqrt{2}} [|f(\mathbf{x})\rangle - |1 \oplus f(\mathbf{x})\rangle] \\
&= \frac{1}{2^{n/2}} \sum_{\mathbf{x}=0}^{2^n-1} (-1)^{f(\mathbf{x})} |\mathbf{x}\rangle \otimes \frac{1}{\sqrt{2}} [|0\rangle - |1\rangle], \tag{3.10}
\end{aligned}$$

such that now the information of the function is stored in the first n qubits. Here, we have simply used that a sign occurs only if $f(\mathbf{x}) = 1$. Now, we only have to apply the final n Hadamard gates. For a single qubit, we have

$$H|x\rangle = \frac{1}{\sqrt{2}} \sum_{z=0}^1 (-1)^{x \cdot z} |z\rangle, \tag{3.11}$$

which we can generalize for n qubits as

$$H^{\otimes n} |x_1 \dots x_n\rangle = \frac{1}{2^{n/2}} \sum_{z_1=0}^1 \dots \sum_{z_n=0}^1 (-1)^{x_1 z_1 + \dots + x_n z_n} |z_1 \dots z_n\rangle \equiv \frac{1}{2^{n/2}} \sum_{\mathbf{z}=0}^{2^n-1} (-1)^{\mathbf{x} \cdot \mathbf{z}} |\mathbf{z}\rangle. \tag{3.12}$$

Applying this for the first n qubits of our state, we eventually get

$$H^{\otimes n} U_f H^{\otimes(n+1)} |\mathbf{0}, 1\rangle = \frac{1}{2^n} \sum_{\mathbf{z}=0}^{2^n-1} \left[\sum_{\mathbf{x}=0}^{2^n-1} (-1)^{\mathbf{x} \cdot \mathbf{z} + f(\mathbf{x})} \right] |\mathbf{z}\rangle \otimes \frac{1}{\sqrt{2}} [|0\rangle - |1\rangle]. \tag{3.13}$$

Now, the prefactor in square brackets can be analyzed depending on $f(\mathbf{x})$. To determine whether the function is balanced or not, we measure the first n qubits. Particularly, the amplitude for the state $|0 \dots 0\rangle$ is $\sum_{\mathbf{x}} (-1)^{f(\mathbf{x})} / 2^n$. When now $f(\mathbf{x})$ is constant, this amounts to a phase of ± 1 , whereas all other amplitudes have to vanish – the state needs to remain normalized. In contrast, when $f(\mathbf{x})$ is balanced, the amplitude of $|0 \dots 0\rangle$ will vanish. Therefore, measurements of the first n qubits will

- yield always 0 when $f(\mathbf{x})$ is constant
- yield 1 in at least one case when \mathbf{x} is balanced.

Summarizing, the algorithm shows that one can obtain an exponential speedup in comparison to the classical case provided the function U_f can be implemented with polynomial effort in the problem size. Unfortunately, the Deutsch-Jozsa problem has no known applications except quite constructed problems. However, it poses the question which unitaries on a quantum computer can actually be implemented and what the associated cost is.

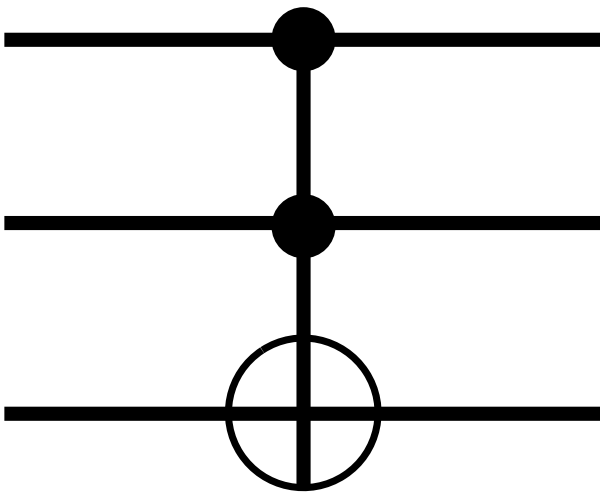


Figure 3.3: Circuit symbol for the CCNOT (Toffoli) gate. The control qubits (upper two wires) are not affected, but the target qubit (lower wire) is flipped when both control qubits are set. The gate is its own inverse.

3.2 Backward compatibility

We have stated that the NAND gate is universal for classical computation. Provided we have a quantum computer, one may wonder whether it is possible to implement classical circuits on it. Of course, some adaptations may be necessary since quantum circuits must have as many output qubits as they have input qubits. Therefore, one will generally need to make use of ancilla qubits that are initially set to a defined state. Then, one can think of gates that can implement e.g. a classically universal NAND gate for certain inputs. The simplest of these gates is the **Toffoli gate**. It acts on three qubits, leaves the first two invariant and flips the third if the first two are both in the state $|1\rangle$

$$\begin{aligned}
 \text{Toffoli}_{123} &= \frac{1}{2}[\mathbf{1} - \sigma^z] \otimes \frac{1}{2}[\mathbf{1} - \sigma^z] \otimes \sigma^x + \frac{1}{2}[\mathbf{1} + \sigma^z] \otimes \frac{1}{2}[\mathbf{1} - \sigma^z] \otimes \mathbf{1} \\
 &\quad + \frac{1}{2}[\mathbf{1} - \sigma^z] \otimes \frac{1}{2}[\mathbf{1} + \sigma^z] \otimes \mathbf{1} + \frac{1}{2}[\mathbf{1} + \sigma^z] \otimes \frac{1}{2}[\mathbf{1} + \sigma^z] \otimes \mathbf{1} \\
 &= \frac{1}{4}[\mathbf{1} - Z_1 - Z_2 + Z_1 Z_2] X_3 + \frac{1}{4}[3 \cdot \mathbf{1} + Z_1 + Z_2 - Z_1 Z_2].
 \end{aligned} \tag{3.14}$$

It can also be seen as a controlled-controlled-NOT (CCNOT) gate, see Fig. 3.3. The truth table of the Toffoli gate

input	output
000	000
001	001
010	010
011	011
100	100
101	101
110	111
111	110

reveals by its matrix representation that the gate is a unitary transformation and in particular that if the third input qubit is in the state $|1\rangle$, the third output qubit will encode the NAND gate on the first two qubits (bold symbols in the table above)

$$\text{Toffoli}_{123} |z_1 z_2\rangle \otimes |1\rangle = |z_1 z_2\rangle \otimes |\text{NAND}(z_1, z_2)\rangle. \tag{3.15}$$

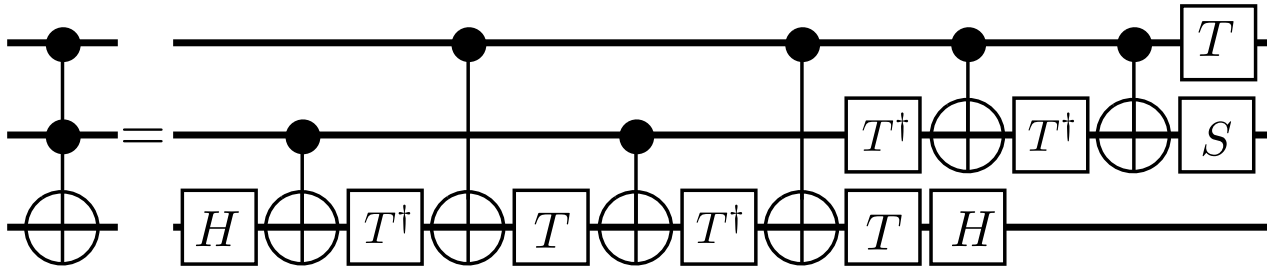


Figure 3.4: Replacement circuit for the Toffoli (CCNOT) gate from Fig. 3.3. CNOT operations and single-qubit gates like Hadamard, phase gate and $\pi/8$ -gate suffice to implement the Toffoli gate.

Likewise, we can argue that by setting the first input qubit in state $|1\rangle$ and the last input qubit in state $|0\rangle$, the third output qubit will become a copy of the second (red numbers in the table above). Note that this can only copy classical bits but not a qubit, compare Sec. 2.5.3. So in effect, universal quantum computers are backward compatible, provided one can work with a sufficient number of ancilla qubits.

The Toffoli gate can be implemented with a sequence of particular single-qubit gates like the Hadamard gate (2.21), the phase gate

$$S = \begin{pmatrix} 1 & 0 \\ 0 & i \end{pmatrix} \quad (3.16)$$

and the $\pi/8$ gate

$$T = \begin{pmatrix} 1 & 0 \\ 0 & e^{i\pi/4} \end{pmatrix} = \begin{pmatrix} 1 & 0 \\ 0 & \frac{1}{\sqrt{2}}[1+i] \end{pmatrix} = e^{i\pi/8} \begin{pmatrix} e^{-i\pi/8} & 0 \\ 0 & e^{+i\pi/8} \end{pmatrix} \quad (3.17)$$

and CNOT gates (2.45), as exemplified in Fig. 3.4.

3.3 Controlled operations

We have introduced the CNOT gate as a particular controlled operation that is performed if the control qubit is in state $|1\rangle$. Alternatively, we could imagine to perform a general controlled unitary operation

$$C(U)_{12} = \frac{1}{2}[\mathbf{1} + \sigma^z] \otimes \mathbf{1} + \frac{1}{2}[\mathbf{1} - \sigma^z] \otimes U, \quad (3.18)$$

which applies a general single qubit unitary to the target qubit when the control qubit is in state $|1\rangle$ and does nothing if it is in the state $|0\rangle$. One can understand that any single qubit unitary can be decomposed as

$$U = e^{i\alpha}AXBXC \quad : \quad ABC = \mathbf{1}, \quad (3.19)$$

with other single-qubit unitaries A , B , C , a global phase α and the bitflip gate $X = \sigma^x$. We can always choose $C = B^{-1}A^{-1}$, and $\bar{B} = XBX$ can be understood as just another unitary, such that there is actually nothing to prove but only to accept that we express the unitary U by a sequence of rotations. From this decomposition one can deduce that the circuit in Fig. 3.5

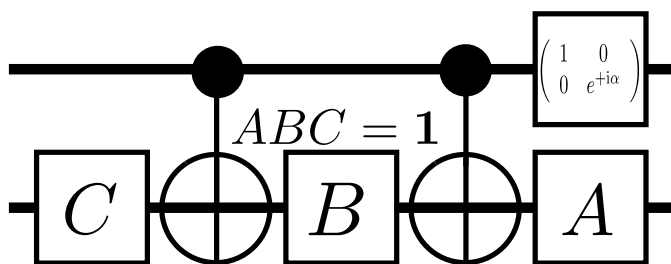


Figure 3.5: A controlled unitary operation can be implemented by CNOT gates and single qubit gates. If the control qubit is in $|0\rangle$, nothing happens due to $ABC = 1$. To the contrary, for a set control qubit, the circuit maps $|1\rangle \otimes |\Psi\rangle$ to $e^{i\alpha} |1\rangle \otimes AXBXC |\Psi\rangle = |1\rangle \otimes U\Psi$.

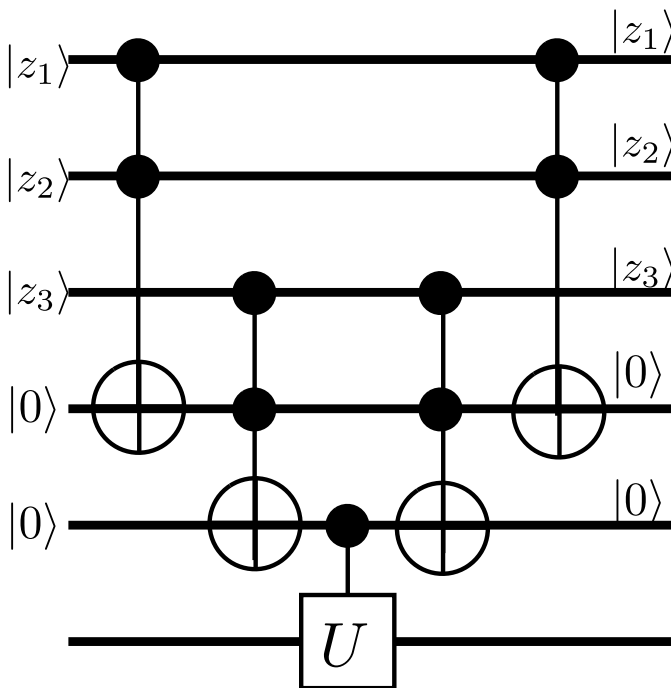


Figure 3.6: Multi-qubit controlled unitaries can be implemented from single-qubit controlled unitaries and Toffoli gates – both can be implemented with CNOT and single qubit gates as depicted in Fig. 3.5 and Fig. 3.4. The example shows a $C^3(U)$ operation and requires two ancillas. The final Toffoli gates just serve to bring back the two ancilla qubits back to their initial state.

implements a controlled unitary operation by means of CNOT gates and single qubit unitaries. If the control qubit is in state $|0\rangle$, the X gates are not applied and the target qubit is left untouched due to $ABC = 1$. By contrast, if the control qubit is in the state $|1\rangle$ the circuit by construction implements the desired unitary operation on the target qubit.

Now, a multi-qubit controlled operation $C^n(U)$ is executed iff all n control qubits are in the state $|1\rangle$ and it is not executed when just one of them is in the state $|0\rangle$, see Fig. 3.6. They can be implemented with Toffoli gates and a single controlled unitary operation, which means that with some ancilla qubits, multi-qubit controlled unitaries can be implemented with a number of CNOT gates and single-qubit rotations (for the Toffoli gates) and a controlled unitary operation.

Sometimes, it may be required to execute a controlled operation not conditioned on the state $|1\rangle$ but conditioned on the state $|0\rangle$. In quantum circuits, this is just symbolized with a white dot instead of a black one, see Fig. 3.7 This way, controlled single qubit operations may be applied to two individual computational basis states only.

3.4 Universality of quantum computation

One may wonder about the necessary building blocks to implement universal quantum computation, i.e., what are the necessary building blocks to implement the most general unitary. The reasoning is split into three steps.

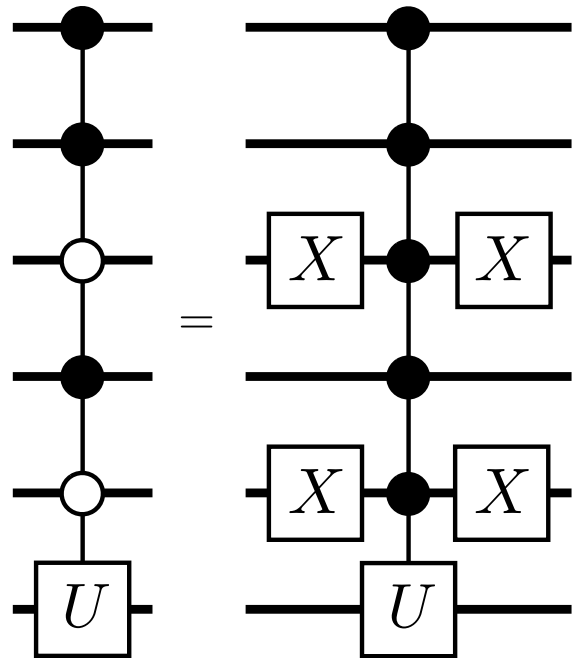


Figure 3.7: Controlled (multi-qubit) unitaries conditioned on the state $|0\rangle$ rather than on the state $|1\rangle$ – symbolized by white circles – can be implemented with bitflip gates X .

- First, we show that a general $d \times d$ unitary matrix can be exactly expressed by products of $d \times d$ unitary matrices that act non-trivially only on two components.
- Second, we show that these unitary matrices with two non-trivial components can be exactly represented by the CNOT gate and continuous single-qubit rotations.
- Finally, we show that with using a discrete set of single-qubit gates, one can approximate arbitrary continuous single-qubit unitaries to arbitrary precision.

These constructions do not fix the efficiency of the implementation, they altogether just state that it is possible to implement arbitrary unitaries by using a discrete set of gates only, of which only one (CNOT) is entangling.

3.4.1 Decomposition of d -level unitaries into 2-level unitary matrices

A general $d \times d$ unitary matrix U can be multiplicatively decomposed into products of $d \times d$ two-level unitary matrices

$$U = V_1 \cdot \dots \cdot V_k \quad : \quad k \leq d(d-1)/2. \quad (3.20)$$

For example, the most general 4×4 unitary for two qubits can be decomposed into products of at most 6 two-level unitaries.

So see this, we first consider the case $d = 3$ as an example and write the most general 3-level unitary as

$$U = \begin{pmatrix} u_{11} & u_{12} & u_{13} \\ u_{21} & u_{22} & u_{23} \\ u_{31} & u_{32} & u_{33} \end{pmatrix}. \quad (3.21)$$

The first step is now to find a two-level unitary U_1 , such that the product U_1U has a vanishing (2,1) component (we assume that $u_{21} \neq 0$ from the beginning, otherwise we can just skip this and choose U_1 as identity). In fact, this can be achieved by

$$U_1 = \frac{1}{\sqrt{|u_{11}|^2 + |u_{21}|^2}} \begin{pmatrix} u_{11}^* & u_{21}^* & 0 \\ u_{21} & -u_{11} & 0 \\ 0 & 0 & 1 \end{pmatrix}. \quad (3.22)$$

The matrix U_1 is evidently unitary and exemplifies what is meant by a 3×3 two-level matrix: It acts non-trivially only on the first two components. Explicit evaluation of the product yields

$$U_1U = \begin{pmatrix} u'_{11} & u'_{12} & u'_{13} \\ 0 & u'_{22} & u'_{23} \\ u'_{31} & u'_{32} & u'_{33} \end{pmatrix} \quad (3.23)$$

where we have just not written the primed values explicitly. In the second step, we seek for another two-level unitary such that U_2U_1U has a vanishing (3,1) component (again, if $u'_{31} = 0$, we may choose an even simpler U_2). In full analogy, we choose

$$U_2 = \frac{1}{\sqrt{|u'_{11}|^2 + |u'_{31}|^2}} \begin{pmatrix} u'_{11}{}^* & 0 & u'_{31}{}^* \\ 0 & 1 & 0 \\ u'_{31} & 0 & -u'_{11} \end{pmatrix}, \quad (3.24)$$

which is yet another 3×3 two-level unitary matrix. Explicit evaluation yields now that both the (2,1) and (3,1) components vanish, and in fact even more

$$U_2U_1U = \begin{pmatrix} 1 & u''_{12} & u''_{13} \\ 0 & u''_{22} & u''_{23} \\ 0 & u''_{32} & u''_{33} \end{pmatrix} = \begin{pmatrix} 1 & 0 & 0 \\ 0 & u''_{22} & u''_{23} \\ 0 & u''_{32} & u''_{33} \end{pmatrix}, \quad (3.25)$$

where the second equality follows by reasoning that products of unitaries remain unitary, and columns as well as rows of unitary matrices must be normalized. Finally, we choose to find a two-level unitary such that in $U_3U_2U_1U$ the (3,2) component vanishes

$$U_3 = \frac{1}{\sqrt{|u''_{22}|^2 + |u''_{32}|^2}} \begin{pmatrix} 1 & 0 & 0 \\ 0 & u''_{22}{}^* & u''_{32}{}^* \\ 0 & u''_{32} & -u''_{22} \end{pmatrix}. \quad (3.26)$$

Possibly equipping the last column with a phase, we eventually obtain

$$U_3U_2U_1U = \mathbf{1}, \quad (3.27)$$

or – alternatively $U = U_1^\dagger U_2^\dagger U_3^\dagger$, such that we can identify $V_i = U_i^\dagger$. Altogether, the recursive building of the procedure is quite analogous to Householder or Givens rotations [7] – the difference is that here the unitary only acts from the left.

The generalization to $d \times d$ unitary matrices is analogous: For the elimination of the first column off-diagonals we need $d - 1$ unitaries, for the next $d - 2$, then $d - 3$ and so on until only one off-diagonal is left. The total number of unitaries is thus

$$k = \sum_{j=1}^{d-1} j = \frac{d(d-1)}{2}. \quad (3.28)$$

One should keep in mind however that for n qubits, $d = 2^n$, such that an exponential number of two-level matrices may be needed in the worst case, so this is actually the most expensive step in the implementation of a general unitary. Fortunately, for many specific unitaries there exist much more efficient decompositions.

3.4.2 Decomposition of 2-level unitaries into single qubit and CNOT

Knowing that every unitary can be written as a product of two-level unitaries, we want to show that any two-level unitary can be implemented with single qubit rotations and CNOT gates. So let us assume that we have a two-level unitary U , such that there are two states in the computational basis

$$|\mathbf{t}\rangle = |t_1 \dots t_n\rangle, \quad |\mathbf{s}\rangle = |s_1 \dots s_n\rangle \quad (3.29)$$

with nontrivial matrix elements

$$\langle \mathbf{t} | U | \mathbf{t} \rangle, \quad \langle \mathbf{t} | U | \mathbf{s} \rangle, \quad \langle \mathbf{s} | U | \mathbf{t} \rangle, \quad \langle \mathbf{s} | U | \mathbf{s} \rangle \quad (3.30)$$

and the remaining trivial matrix elements $\langle \mathbf{z} | U | \mathbf{z}' \rangle = \delta_{\mathbf{z}\mathbf{z}'}$. The main idea is now to perform swap operations of computational basis states such that differ in only one digit. To find a sequence of suitable swap operations, we first find a **Gray code** connecting $|s_1 \dots s_n\rangle$ and $|t_1 \dots t_n\rangle$. This is a sequence of states that differ by exactly one bit. Since two arbitrary states can differ by at most n bits for an n bit system, one can always find such a Gray code with $m \leq n$ elements. For example, the $n = 6$ bit states $|\mathbf{s}\rangle = |010010\rangle$ and $|\mathbf{t}\rangle = |111011\rangle$ are connected via the Gray code

state	bitwise decomposition
$ \mathbf{s}\rangle = g_1\rangle$	$ 010010\rangle$
$ g_2\rangle$	$ 010011\rangle$
$ g_3\rangle$	$ 011011\rangle$
$ \mathbf{t}\rangle = g_4\rangle$	$ 111011\rangle$

Now, the agenda is to swap $|g_1\rangle \leftrightarrow |g_2\rangle$, then $|g_2\rangle \leftrightarrow |g_3\rangle$, and so on until $|g_{m-2}\rangle \leftrightarrow |g_{m-1}\rangle$, effectively transporting the computational basis state $|\mathbf{s}\rangle$ to differ by $|\mathbf{t}\rangle$ in only bit. The purpose of the Gray code construction is that this can be done without changing the order of the other states by applying controlled unitaries that are conditioned on the bits where $|g_i\rangle$ and $|g_{i+1}\rangle$ are equal and that flip the bit where they differ. Eventually, we have $U_{\text{swap}}|\mathbf{s}\rangle$ and $U_{\text{swap}}|\mathbf{t}\rangle = |\mathbf{t}\rangle$ being direct neighbours in the sense that they differ only by one bit. On this bit, we apply a controlled single-qubit unitary operation, where the control qubits are set to the qubits where $|\mathbf{t}\rangle$ and $|g_{m-1}\rangle$ are equal and the target qubit is the one where they differ. Afterwards, we order the computational basis states back to the original order by applying the same controlled operations again – just in the reverse order, see Fig. 3.8. There are at most $2n + 1$ such controlled unitaries to perform, each of them can be implemented by $\mathcal{O}(n)$ CNOT gates and single qubit rotations. With the result from the previous section, the total complexity to implement an arbitrary unitary requires

$$\mathcal{O}(n^2 4^n) \quad (3.31)$$

operations. It proves that universal quantum computation is possible using a finite number of general single-qubit rotations and CNOT gates. However, in general this can be extremely inefficient, using an exponential number of gates in the number of qubits shows that quantum computers need not be more efficient than classical ones. Good quantum algorithms must use significantly less gates (e.g. only polynomially many in the number of qubits). The decomposition of the Toffoli gate – which is an 8×8 unitary in Fig. 3.4 requires significantly less gates than $3^2 * 4^3 = 576$.

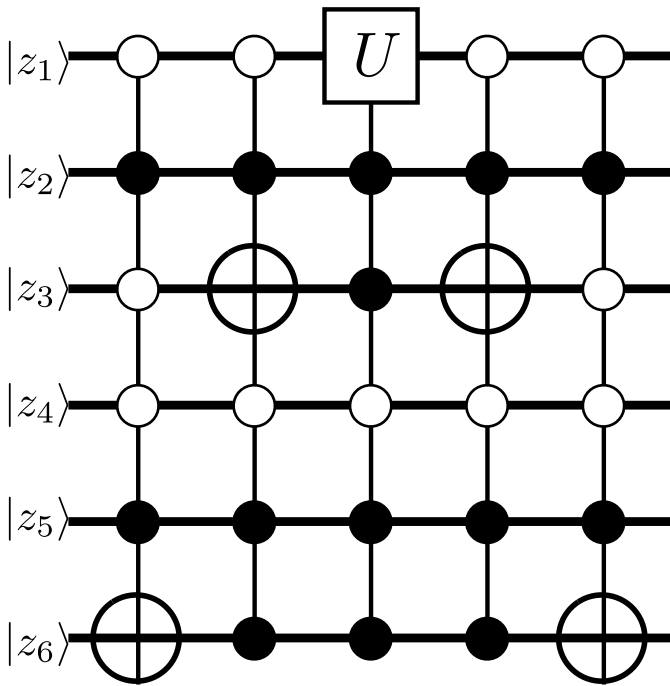


Figure 3.8: A general two-level unitary connecting the states $|010010\rangle$ and $|111011\rangle$ can be implemented by (multi-qubit) controlled NOT gates and a (multi-qubit) controlled single qubit operation, such that an overall $\mathcal{O}(n^2)$ number of CNOT and single-qubit gates is required to implement a general two-level unitary. The first gate swaps that states $|010010\rangle \leftrightarrow |010011\rangle$, whereas it leaves all other states in the computational basis invariant. The second gate then swaps states $|010011\rangle \leftrightarrow |011011\rangle$. Then, the controlled unitary only acts nontrivially on the states $|011011\rangle$ and $|111011\rangle$, after which the basis re-ordering is reversed. The individual 6-qubit controlled operations (either with U or X) can be individually implemented with the decomposition of Fig. 3.7 and Fig. 3.6.

3.4.3 Approximating single-qubit and CNOT by discrete gates

The previous two sections demonstrate that with general single-qubit rotations and CNOT gates one can implement general unitary rotations with $\mathcal{O}(n^2 4^n)$ gates. This is already quite inefficient for most unitaries. Even worse, on a realistic system such gates cannot be performed accurately. Control errors and decoherence will lead to imprecise gates, and quantum error correction codes will need to be used to account for this. Error correction codes have been developed to make the quantum algorithms work even in presence of imperfection, but they only function for a finite **universal set of gates**. Such sets are called **universal set of gates**. The **standard universal set of gates** consists of single qubit gates like the phase gate (3.16), the Hadamard gate (2.21), the $\pi/8$ -gate (3.17), and the CNOT gate (2.45) as the only entangling contribution.

We will show that with sufficiently many Hadamard gates and $\pi/8$ gates, all general single-qubit rotations can be implemented. The proof goes as follows: First, it is shown that by using Hadamard gates H and $\pi/8$ gates T , a particular unitary around a particular axis can be constructed. With using that

$$T = e^{i\pi/8} \begin{pmatrix} e^{-i\pi/8} & 0 \\ 0 & e^{+i\pi/8} \end{pmatrix} = e^{i\pi/8} e^{-i\pi/8 Z} \quad (3.32)$$

and further

$$e^{-i\pi/8} H T H = e^{-i\pi/8 X}, \quad (3.33)$$

where the global phase in front of the l.h.s. is irrelevant. Combining the two operations we get

$$\begin{aligned} T(H T H) &\propto e^{-i\pi/8 Z} e^{-i\pi/8 X} = [\cos(\pi/8)\mathbf{1} - i \sin(\pi/8)Z] [\cos(\pi/8)\mathbf{1} - i \sin(\pi/8)X] \\ &= \cos^2(\pi/8)\mathbf{1} - i \sin(\pi/8) [\cos(\pi/8)X + \sin(\pi/8)Y + \cos(\pi/8)Z]. \end{aligned} \quad (3.34)$$

The points to recognize here are that

- this is a rotation around the axis defined by

$$\mathbf{n} = \frac{1}{\sqrt{1 + \cos^2(\pi/8)}} \begin{pmatrix} \cos(\pi/8) \\ \sin(\pi/8) \\ \cos(\pi/8) \end{pmatrix} \quad (3.35)$$

- by an angle defined by

$$\cos(\theta_0/2) = \cos^2(\pi/8). \quad (3.36)$$

Importantly, *the angle θ_0 defined by the above relation is an irrational multiple of 2π !* This irrationality implies that by re-iterating the above rotation a number of times, we can reach any point on circles around the Bloch sphere that are perpendicular to the vector \mathbf{n} and go through the initial state. By contrast, if θ_0 was a rational multiple of 2π , i.e., $\bar{\theta}_0 = P/Q2\pi$ with integers P and Q , we would see that after Q iterations, no new points would be added along the circle. More formally, it allows us to approximate any rotation

$$R_{\mathbf{n}}(\theta) = \exp \left\{ -i \frac{\theta}{2} \mathbf{n} \cdot \boldsymbol{\sigma} \right\} = \cos \left(\frac{\theta}{2} \right) \mathbf{1} - i \sin \left(\frac{\theta}{2} \right) \mathbf{n} \cdot \boldsymbol{\sigma} \quad : \quad \mathbf{n} \cdot \mathbf{n} = 1 \quad (3.37)$$

now for arbitrary $\theta \neq \theta_0$ just with H and T gates.

Unfortunately, this construction so far does not allow to switch between different circles. To cover the rest of the Bloch sphere surface, we use that with

$$HXH = Z, \quad HYH = -Y, \quad HZH = X \quad (3.38)$$

we generate a rotation about another axis

$$HR_{\mathbf{n}}(\theta)H = R_{\mathbf{m}}(\theta) \quad : \quad \mathbf{m} = \frac{1}{\sqrt{1 + \cos^2(\pi/8)}} \begin{pmatrix} \cos(\pi/8) \\ -\sin(\pi/8) \\ \cos(\pi/8) \end{pmatrix}. \quad (3.39)$$

Since \mathbf{m} and \mathbf{n} are not aligned, this generates a rotation around a different axis, and by combining the rotations $R_{\mathbf{n}}$ and $R_{\mathbf{m}}$ we can eventually cover the whole Bloch sphere. More formally, this can be written in the statement that any unitary single-qubit transformation (disregarding an overall phase) can be written as

$$U = R_{\mathbf{n}}(\theta)R_{\mathbf{m}}(\phi)R_{\mathbf{n}}(\gamma) \quad : \quad \mathbf{m} \cdot \mathbf{m} = \mathbf{n} \cdot \mathbf{n} = 1, \mathbf{m} \neq a\mathbf{n}, \quad (3.40)$$

compare e.g. Eq. (2.26) for an example with $\mathbf{n} = \mathbf{e}_z$ and $\mathbf{m} = \mathbf{e}_y$.

The construction rather proves feasibility of approximating arbitrary unitaries by the discrete ones H and T rather than efficiency. In fact, the construction is quite inefficient as the number of discrete gates required to approximate a gate to a desired error ϵ increases exponentially like $\mathcal{O}(2^{1/\epsilon})$ with the inverse error. However, it is actually possible to do this much more efficient (see e.g. the Solovay Kitaev theorem in App. 3 of [1]) with a complexity that is only $\mathcal{O}(\ln^c(1/\epsilon))$ with $c \approx 2$, which is acceptable.

So why do we need in addition a phase gate? This is not really required for universality, but is required to make the computation fault-tolerant. The whole necessity of discrete quantum gates comes from the possibility of making the considered universal set of gates fault tolerant.

3.5 Quantum Fourier Transform

The classical **discrete Fourier transform** (DFT) takes N complex numbers x_j as input and generates N complex numbers y_k as output

$$\begin{aligned} y_k &= \frac{1}{\sqrt{N}} \sum_{j=0}^{N-1} x_j e^{+2\pi i j k / N}, \\ x_j &= \frac{1}{\sqrt{N}} \sum_{k=0}^{N-1} y_k e^{-2\pi i j k / N}. \end{aligned} \quad (3.41)$$

The DFT has many applications e.g. in pattern recognition or image compression (e.g. in the well-known jpg format). When we write it in matrix form $y_k = \sum_j U_{kj} x_j$, one can see that the transformation matrix is actually unitary, e.g. via

$$\sum_j U_{kj} U_{j\ell}^\dagger = \sum_j U_{kj} U_{\ell j}^* = \sum_j \frac{1}{N} e^{+2\pi i j k / N} e^{-2\pi i j \ell / N} = \delta_{k\ell}. \quad (3.42)$$

Therefore, we know that there must exist a quantum algorithm implementing the **quantum Fourier transform** (QFT), which when applied to a computational basis state $|j\rangle$ yields

$$\text{QFT } |j\rangle = \frac{1}{\sqrt{N}} \sum_{k=0}^{N-1} e^{2\pi i j k / N} |k\rangle. \quad (3.43)$$

From Sec. 3.4 we know that this must be implementable by CNOT gates and single qubit operations. The QFT is built upon the observation that the above definition can be written in product form once the binary decomposition of the computational basis state is made explicit for an n -qubit system

$$|j\rangle = |j_1 j_2 \dots j_n\rangle, \quad |k\rangle = |k_1 k_2 \dots k_n\rangle, \quad (3.44)$$

for which we have $N = 2^n$ basis states. For the numbers denoting the computational basis states, we can write

$$k = k_1 2^{n-1} + k_2 2^{n-2} + \dots + k_{n-1} 2^1 + k_n 2^0 = \sum_{\alpha=1}^n k_\alpha 2^{n-\alpha}. \quad (3.45)$$

We get just by splitting the sum over all computational basis states into the individual qubit sums

$$\begin{aligned}
\text{QFT } |j\rangle &= \frac{1}{2^{n/2}} \sum_{k=0}^{2^n-1} \exp \left\{ 2\pi i j 2^{-n} \sum_{\alpha=1}^n k_\alpha 2^{n-\alpha} \right\} |k_1 \dots k_n\rangle \\
&= \frac{1}{2^{n/2}} \sum_{k_1=0}^1 \dots \sum_{k_n=0}^1 \bigotimes_{\alpha=1}^n \exp \{ 2\pi i j k_\alpha 2^{-\alpha} \} |k_\alpha\rangle \\
&= \frac{1}{2^{n/2}} \bigotimes_{\alpha=1}^n \left[\sum_{k_\alpha=0}^1 \exp \{ 2\pi i j k_\alpha 2^{-\alpha} \} |k_\alpha\rangle \right] \\
&= \frac{1}{2^{n/2}} \bigotimes_{\alpha=1}^n \left[|0\rangle + \exp \left\{ 2\pi i \frac{j}{2^\alpha} \right\} |1\rangle \right] \\
&= \frac{|0\rangle + e^{2\pi i j/2} |1\rangle}{\sqrt{2}} \otimes \frac{|0\rangle + e^{2\pi i j/4} |1\rangle}{\sqrt{2}} \otimes \dots \otimes \frac{|0\rangle + e^{2\pi i j/2^{n-1}} |1\rangle}{\sqrt{2}} \otimes \frac{|0\rangle + e^{2\pi i j/2^n} |1\rangle}{\sqrt{2}}.
\end{aligned} \tag{3.46}$$

Now, using that the exponential function is periodic, we can fully discard the integer contribution of $j/2^\alpha$

$$\begin{aligned}
e^{2\pi i j/2^\alpha} &= \exp \left\{ 2\pi i \sum_{\beta=1}^n j_\beta 2^{n-\beta-\alpha} \right\} = \exp \left\{ 2\pi i \sum_{\beta=n-\alpha+1}^n j_\beta 2^{n-\beta-\alpha} \right\} \\
&= \exp \left\{ 2\pi i [j_{n-\alpha+1} 2^{-1} + j_{n-\alpha+2} 2^{-2} + \dots + j_n 2^{n-\alpha}] \right\} \\
&\equiv e^{2\pi i 0.j_{n-\alpha+1} j_{n-\alpha+2} \dots j_{n-1} j_n},
\end{aligned} \tag{3.47}$$

where the notation

$$0.j_a \dots j_{a+b} \equiv j_a \frac{1}{2} + \dots + j_{a+b} \frac{1}{2^{b+1}} \tag{3.48}$$

is understood. Thereby, we write the QFT as

$$\begin{aligned}
\text{QFT } |j\rangle &= \frac{|0\rangle + e^{2\pi i 0.j_n} |1\rangle}{\sqrt{2}} \otimes \frac{|0\rangle + e^{2\pi i 0.j_{n-1} j_n} |1\rangle}{\sqrt{2}} \otimes \dots \\
&\quad \otimes \frac{|0\rangle + e^{2\pi i 0.j_2 \dots j_{n-1} j_n} |1\rangle}{\sqrt{2}} \otimes \frac{|0\rangle + e^{2\pi i 0.j_1 j_2 \dots j_{n-1} j_n} |1\rangle}{\sqrt{2}}.
\end{aligned} \tag{3.49}$$

Here, we see that the QFT is just generated by a superposition of all computational basis states, where the FT is encoded in a phase factor of the amplitudes. This product decomposition leads us to introduce the phase gate

$$R_k = \begin{pmatrix} 1 & 0 \\ 0 & e^{2\pi i 2^{-k}} \end{pmatrix} \quad : \quad R_2 = S, \quad R_3 = T, \tag{3.50}$$

which we apply as a controlled unitary operation

$$R_k^{nm} = (R_k)_n \left(\frac{1}{2}(\mathbf{1} - \sigma^z) \right)_m + (\mathbf{1})_n \left(\frac{1}{2}(\mathbf{1} + \sigma^z) \right)_m, \tag{3.51}$$

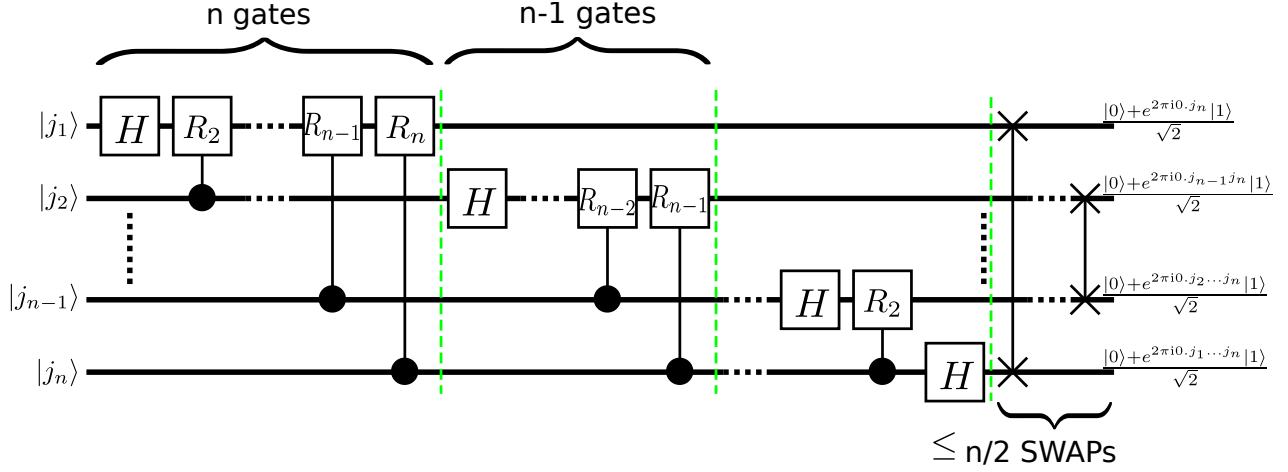


Figure 3.9: Circuit representation for the QFT algorithm, based on a controlled application of phase gates (3.50) and Hadamard gates (2.21) and final SWAP gates (2.65) reversing the order of qubits. In total, $\mathcal{O}(n^2)$ gates are required, thus rendering the QFT exponentially faster than the Fast Fourier Transform $\mathcal{O}(n2^n)$ or the naive DFT $\mathcal{O}(4^n)$.

as discussed in Sec. 3.3 together with a Hadamard gate. The quantum circuit in Fig. 3.9 implements the QFT [8]. To see that this yields the QFT, we consider the operations on the first qubit

$$\begin{aligned}
 R_n^{1n} \dots R_2^{12} H_1 |j_1 j_2 \dots j_n\rangle &= \frac{1}{\sqrt{2}} R_n^{1n} \dots R_2^{12} [|0\rangle + (-1)^{j_1} |1\rangle] \otimes |j_2 \dots j_n\rangle \\
 &= \frac{1}{\sqrt{2}} R_n^{1n} \dots R_2^{12} [|0\rangle + e^{2\pi i 0 \cdot j_1} |1\rangle] \otimes |j_2 \dots j_n\rangle \\
 &= \frac{1}{\sqrt{2}} R_n^{1n} \dots R_3^{13} [|0\rangle + e^{2\pi i 0 \cdot j_1 j_2} |1\rangle] \otimes |j_2 \dots j_n\rangle \\
 &= \frac{1}{\sqrt{2}} [|0\rangle + e^{2\pi i 0 \cdot j_1 j_2 \dots j_n} |1\rangle] \otimes |j_2 \dots j_n\rangle, \tag{3.52}
 \end{aligned}$$

compare the first vertical dashed line in Fig. 3.9. After the operations on the second qubit, the state is

$$R_{n-1}^{2n} \dots R_2^{23} H_2 R_n^{1n} \dots R_2^{12} H_1 |j_1 \dots j_n\rangle = \frac{1}{\sqrt{2}} [|0\rangle + e^{2\pi i 0 \cdot j_1 j_2 \dots j_n} |1\rangle] \otimes \frac{1}{\sqrt{2}} [|0\rangle + e^{2\pi i 0 \cdot j_2 \dots j_n} |1\rangle] \otimes |j_3 \dots j_n\rangle, \tag{3.53}$$

and so on until all Hadamard and controlled phase gates have been applied, yielding

$$H_n \dots H_1 |j_1 \dots j_n\rangle = \frac{|0\rangle + e^{2\pi i 0 \cdot j_1 j_2 \dots j_n} |1\rangle}{\sqrt{2}} \otimes \dots \otimes \frac{|0\rangle + e^{2\pi i 0 \cdot j_n} |1\rangle}{\sqrt{2}}, \tag{3.54}$$

compare the second and third vertical dashed lines in Fig. 3.9, respectively. This corresponds to (3.49), but the order of qubits is reversed. Correcting this with $[n/2]$ SWAP gates, we see that the QFT circuit exactly reproduces (3.49), validating the quantum circuit. The circuit can be reversed by reversing the order of gates and simultaneously reverting the controlled phase gates via $R_k \rightarrow R_k^\dagger$, such that likewise, the inverse QFT can be computed. Now, knowing how QFT acts on a basis state of the computational basis, we can equivalently apply the QFT to superposition

states

$$\text{QFT} \sum_j x_j |j\rangle = \sum_j x_j \text{QFT} |j\rangle = \sum_k y_k |k\rangle . \quad (3.55)$$

This is the most impressive quantum speedup known so far: An algorithm that uses exponential time in the input size classically (e.g. $\mathcal{O}(n2^n)$ for the Fast Fourier Transform or even $\mathcal{O}(4^n)$ for the naive Fourier transform) could be performed in $\mathcal{O}(n^2)$ time on a quantum computer – given that each gate can be performed with a maximum cost. Additionally, one has to think deeply how to use the QFT as upon a measurement of the final qubits, the state will be collapsed, as in any quantum algorithm.

Simulating the QFT on a classical computer will require exponential resources. However, we can use the QFT circuit to even speed up the classical computation of the DFT. To see this, we first note that multiplying an $N \times N$ unitary matrix to an N -dimensional vector – where $N = 2^n$ – requires N^2 multiplications, such that the naive DFT complexity scales as $\mathcal{O}(N^2) = \mathcal{O}(4^n)$ in the size of the bit length n

$$\begin{pmatrix} y_0 \\ \vdots \\ y_{2^n-1} \end{pmatrix} = \begin{pmatrix} u_{0,0} & \dots & u_{0,2^n-1} \\ \vdots & & \vdots \\ u_{2^n-1,0} & \dots & u_{2^n-1,2^n-1} \end{pmatrix} \begin{pmatrix} x_0 \\ \vdots \\ x_{2^n-1} \end{pmatrix} . \quad (3.56)$$

This computes the entries of the Fourier transform in an inefficient way. The product representation of the QFT has the additional advantage that by adding a qubit before the first one

$$|j\rangle = |j_1 \dots j_n\rangle \rightarrow |j_0 j_1 \dots j_n\rangle , \quad (3.57)$$

we see that in Eq. (3.49) this amounts to adding another qubit behind the last one

$$\begin{aligned} \text{QFT} |j_0 j_1 \dots j_n\rangle &= \frac{|0\rangle + e^{2\pi i 0 \cdot j_n} |1\rangle}{\sqrt{2}} \otimes \frac{|0\rangle + e^{2\pi i 0 \cdot j_{n-1} j_n} |1\rangle}{\sqrt{2}} \otimes \dots \\ &\quad \otimes \frac{|0\rangle + e^{2\pi i 0 \cdot j_2 \dots j_{n-1} j_n} |1\rangle}{\sqrt{2}} \otimes \frac{|0\rangle + e^{2\pi i 0 \cdot j_1 j_2 \dots j_{n-1} j_n} |1\rangle}{\sqrt{2}} \otimes \frac{|0\rangle + e^{2\pi i 0 \cdot j_0 j_1 j_2 \dots j_{n-1} j_n} |1\rangle}{\sqrt{2}} \\ &= [\text{QFT} |j_1 \dots j_n\rangle] \otimes \frac{|0\rangle + e^{2\pi i 0 \cdot j_0 j_1 j_2 \dots j_{n-1} j_n} |1\rangle}{\sqrt{2}} . \end{aligned} \quad (3.58)$$

Classically, the last bit however just signifies whether a number is even or odd. Having computed all the DFT components for n bits $y_k^{(n)}$, we can therefore store this result with a factor of $1/\sqrt{2}$ in the even components of $y_k^{(n+1)}$ and the same result with a factor of $e^{2\pi i 0 \cdot j_0 j_1 \dots j_n} / \sqrt{2}$ in the odd components of $y_k^{(n+1)}$. By doing so, we have to do $\mathcal{O}(n2^n)$ operations in this step, where the exponential comes from iterating through the 2^n components of $y_k^{(n)}$ and the correction n from the determination of the phase factor $e^{2\pi i 0 \cdot j_0 j_1 \dots j_n}$. Applying this recursively, the total complexity requires

$$\mathcal{O}\left(\sum_{i=1}^n i2^i\right) = \mathcal{O}(2 + (n-1)2^{n+1}) = \mathcal{O}(n2^n) \quad (3.59)$$

operations, which is a lot faster than the naive matrix-matrix multiplication and which is actually used a lot in signal processing algorithms.

The most prominent application of the QFT is Peter Shor's factoring algorithm that was introduced in 1994 [9]. It is built on the use of the QFT in phase estimation and order finding and takes a composite number $N = N_1 N_2$ as an input with unknown factors N_i and returns as an output one of the previously unknown factors. Classically, finding the factors of a number scales in the worst case exponentially in the number of input bits (or in the number of digits of that number). Quantum-mechanically, Shor's algorithm requires $\mathcal{O}((\ln N)^3)$ operations, i.e., it scales polynomially in the number of input bits. This has raised a lot of attention to quantum computers as many of our encryption protocols such as the RSA public-key cryptosystem rely on factoring. Therefore, quantum computers could actually break this kind of cryptography. Currently, we do not have a working quantum computer that could compete with classical computers on the factoring problem. Nevertheless, a proof-of-principle has been provided for the factoring algorithm by factoring $15 = 5 * 3$ on a quantum computer [10].

3.6 Quantum search

The quantum search algorithm has been suggested by Lov Grover in 1995 [11]. Grover's algorithm makes use of the *ability to recognize a solution* to a problem instead of the ability to find it. In the Grover search algorithm, this ability is hidden in a unitary called **oracle**. For many problems, such an oracle can be built without knowing the solution to a problem. For example, given a biprime (a product of two prime numbers) it will in general take you a long time to find the prime factors if the biprime is just sufficiently large. Instead, if somebody gives you two potential prime factors, it is very simple in terms of a computational complexity scaling only polynomially in the length of the prime factors to find out whether their product equals the biprime or not.

A typical search problem for which such an oracle can be relevant is the search in an unsorted database, e.g. imagine being given a telephone number without a name and try to find a name in the phone book. Whereas classically, given N entries in the phone book and the promise that at least one name matches the number in the book, we would have to consult the phone book in the worst case $N - 1$ times to find the solution. To be more concrete, for a database with N items and $M < N$ solutions to the search problems, the promise of Grover's search algorithm is that we only need to consult the oracle $\mathcal{O}\left(\sqrt{\frac{N}{M}}\right)$ times to find one solution. That is not as impressive as the QFT speedup but is more generally applicable as the cost is hidden in the basic building block – the construction of the oracle. Formally, the oracle performs the unitary operation

$$O |\mathbf{x}\rangle \otimes |q\rangle = |\mathbf{x}\rangle \otimes |q \oplus f(\mathbf{x})\rangle, \quad (3.60)$$

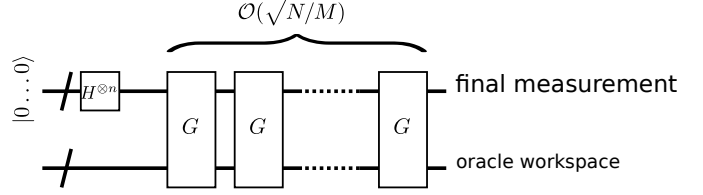
just as in the Deutsch- and Deutsch-Jozsa algorithms. The function $f(\mathbf{x})$ by definition returns

$$f(\mathbf{x}) = \begin{cases} 1 & : \mathbf{x} \text{ is a solution to the search problem} \\ 0 & : \text{else} \end{cases} \quad (3.61)$$

This means that the oracle flips its qubit $q \oplus f(\mathbf{x})$ if the fed-in state $\mathbf{x} = x_1 \dots x_n$ is a solution to the search problem and leaves it invariant otherwise. Usually, the initial oracle state is chosen as $\frac{1}{\sqrt{2}}[|0\rangle - |1\rangle]$, such that

$$O |\mathbf{x}\rangle \otimes \frac{1}{\sqrt{2}}[|0\rangle - |1\rangle] = |\mathbf{x}\rangle \frac{1}{\sqrt{2}}[|0 \oplus f(\mathbf{x})\rangle - |1 \oplus f(\mathbf{x})\rangle] = (-1)^{f(\mathbf{x})} |\mathbf{x}\rangle \otimes \frac{1}{\sqrt{2}}[|0\rangle - |1\rangle]. \quad (3.62)$$

Figure 3.10: Quantum circuit of the Grover algorithm. The initial Hadamard gates simply generate a superposition of all computational basis states. Depending on the number of solutions and search items, only a fixed number of Grover iterations is necessary.



This is just an overall phase, and the oracle qubit remains invariant, such that we do not even need to make the action of the oracle explicit

$$\bar{O} |\mathbf{x}\rangle = (-1)^{f(\mathbf{x})} |\mathbf{x}\rangle . \quad (3.63)$$

The effective action of the oracle on its workspace qubits is simply to mark a solution by a phase factor.

Thinking in terms of a control Hamiltonian that is diagonal in the computational basis

$$H_{\text{oracle}} = \sum_{\mathbf{z}} E_{\mathbf{z}} |\mathbf{z}\rangle \langle \mathbf{z}| = \sum_{z_1} \dots \sum_{z_n} E_{z_1 \dots z_n} |z_1\rangle \langle z_1| \otimes \dots \otimes |z_n\rangle \langle z_n| \quad (3.64)$$

and operates for a gate operation time T_{oracle} , one could implement an oracle Hamiltonian if e.g. the eigenvalue of the solution $\bar{\mathbf{z}}$ vanishes $E_{\bar{\mathbf{z}}} = 0$ whereas all other eigenvalues have unit value $E_{\mathbf{z} \neq \bar{\mathbf{z}}} = 1$. Then, the oracle operation could be expressed with $T_{\text{oracle}} = \pi$

$$\bar{O} = e^{-i\pi[\mathbf{1} + H_{\text{oracle}}]} , \quad (3.65)$$

and we would have $\bar{O} |\bar{\mathbf{z}}\rangle = -|\bar{\mathbf{z}}\rangle$ and $\bar{O} |\mathbf{z} \neq \bar{\mathbf{z}}\rangle = +|\mathbf{z}\rangle$. Importantly, for many problems such Hamiltonians can be constructed without knowing the solution $\bar{\mathbf{z}}$ in advance. For example, the Hamiltonian

$$H_{\text{oracle}} = \mathbf{1} - (\hat{z}_1 + \hat{z}_2 + \hat{z}_3) + 2(\hat{z}_1\hat{z}_2 + \hat{z}_1\hat{z}_3 + \hat{z}_2\hat{z}_3) - 3\hat{z}_1\hat{z}_2\hat{z}_3 \quad : \quad \hat{z}_i = \frac{1}{2}[\mathbf{1} - \sigma_i^z] \quad (3.66)$$

assigns with $\hat{z}_i |z_1 z_2 z_3\rangle = z_i |z_1 z_2 z_3\rangle$ an eigenvalue 0 only to the three solution states $|001\rangle$, $|010\rangle$, and $|100\rangle$ and eigenvalue 1 to the other 5 states in the computational basis of three qubits. It can be used for an oracle marking the solution to the question "Which states have in total only one bit set?"

The quantum search algorithm is modularized into some initial Hadamard gates that generate superpositions of computational basis states

$$H^{\otimes n} |0 \dots 0\rangle = \frac{1}{2^{n/2}} \sum_{z_1=0}^1 \dots \sum_{z_n=0}^1 |z_1\rangle \otimes \dots \otimes |z_n\rangle = \frac{1}{2^{n/2}} \sum_{\mathbf{z}=0}^{2^n-1} |\mathbf{z}\rangle \equiv |S\rangle , \quad (3.67)$$

and the repeated application of so-called **Grover iterations** as in Fig. 3.10. The purpose of the initial Hadamard gates is simply to generate a superposition of all basis states, such that this superposition can be evaluated at once. In this circuit, each call of the Grover iteration G can be further decomposed into an oracle call, Hadamard transforms, and conditional phase shifts as depicted in Fig. 3.11. The oracle call will come with an associated cost, which we assume to be constant or only mildly scaling with the problem size (e.g. polynomial in n). Additionally, the Hadamard gates correspond to $2n$ operations, and the controlled phase gate can be written as

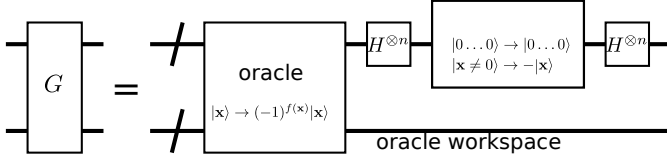


Figure 3.11: Single application of the Grover iteration. The cost of the oracle call is assumed to be independent of the database size (number of qubits) or to scale only polynomially in the number of qubits $n = \log_2 N$. Both the Hadamard gates as well as the controlled phase gate require $\mathcal{O}(n)$ gates.

a multi-qubit controlled operation. Such controlled operations require with Sec. 3.3 again $\mathcal{O}(n)$ operations, such that the cost of one Grover iteration is $\mathcal{O}(n)$ plus the cost of the oracle call.

Discarding the action of the oracle on its workspace, the effect of the Grover iteration can be written as

$$G = H^{\otimes n} [2|0\dots 0\rangle\langle 0\dots 0| - \mathbf{1}] H^{\otimes n} O = [2|S\rangle\langle S| - \mathbf{1}] O, \quad (3.68)$$

where we have used Eq. (3.67) and the fact that $H^2 = \mathbf{1}$. To analyze in detail what a Grover iteration does to the superposition of all states, we define for a search problem with N items and $1 \leq M < N$ solutions the superposition of all non-solutions $|\alpha\rangle$ and the superposition of all solutions $|\beta\rangle$, respectively

$$|\alpha\rangle = \frac{1}{\sqrt{N-M}} \sum_{\mathbf{x}'' : f(\mathbf{x}'')=0} |\mathbf{x}''\rangle, \quad |\beta\rangle = \frac{1}{\sqrt{M}} \sum_{\mathbf{x}' : f(\mathbf{x}')=1} |\mathbf{x}'\rangle. \quad (3.69)$$

By construction, they are orthonormal $\langle\alpha|\alpha\rangle = \langle\beta|\beta\rangle = 1$ and $\langle\alpha|\beta\rangle = 0$, and we can decompose the total superposition state

$$\begin{aligned} |S\rangle &= \sqrt{\frac{N-M}{N}} |\alpha\rangle + \sqrt{\frac{M}{N}} |\beta\rangle \\ &\equiv \cos \frac{\theta}{2} |\alpha\rangle + \sin \frac{\theta}{2} |\beta\rangle, \end{aligned} \quad (3.70)$$

where θ is some angle defined for the moment for convenience. By construction, we can write the action of the oracle as

$$O|\alpha\rangle = +|\alpha\rangle, \quad O|\beta\rangle = -|\beta\rangle, \quad (3.71)$$

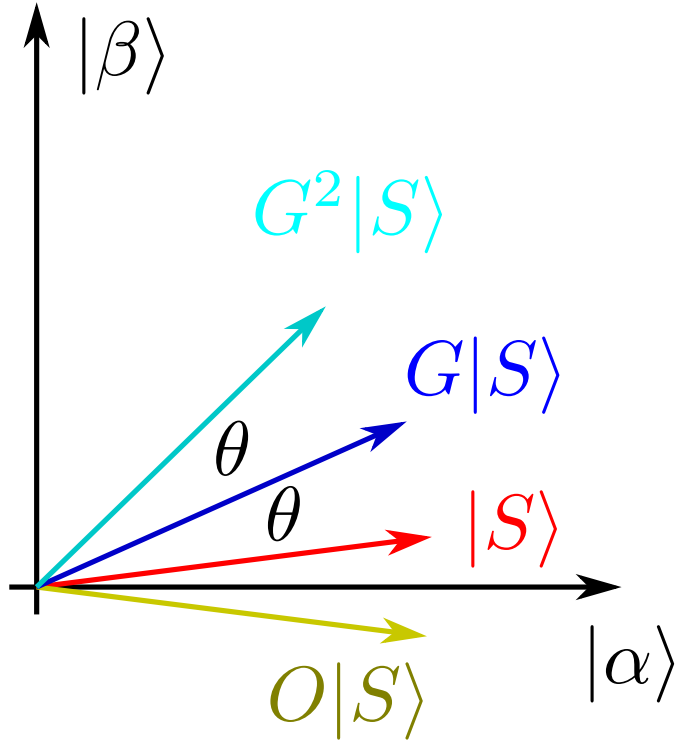
or $O|S\rangle = \cos \frac{\theta}{2} |\alpha\rangle - \sin \frac{\theta}{2} |\beta\rangle$. This means that the application of the oracle O reflects the state $|S\rangle$ about the state $|\alpha\rangle$. Likewise, the operator $[2|S\rangle\langle S| - \mathbf{1}]$ performs a reflection about the vector $|S\rangle$. Since G is a product of two reflections then, it can be interpreted as a rotation. Formally, we find

$$\begin{aligned} G|S\rangle &= [2|S\rangle\langle S| - \mathbf{1}] O|S\rangle = [2|S\rangle\langle S| - \mathbf{1}] \left[\cos \frac{\theta}{2} |\alpha\rangle - \sin \frac{\theta}{2} |\beta\rangle \right] \\ &= \cos \frac{3\theta}{2} |\alpha\rangle + \sin \frac{3\theta}{2} |\beta\rangle, \end{aligned} \quad (3.72)$$

which demonstrates that by the application of G , we do not leave the plane spanned by $|\alpha\rangle$ and $|\beta\rangle$. Computing the action of the Grover iteration on the individual components

$$G|\alpha\rangle = \dots = \cos \theta |\alpha\rangle + \sin \theta |\beta\rangle, \quad G|\beta\rangle = \dots = -\sin \theta |\alpha\rangle + \cos \theta |\beta\rangle, \quad (3.73)$$

Figure 3.12: Visualization of the Grover iteration in the plane spanned by the vectors of non-solution superpositions $|\alpha\rangle$ and solution superpositions $|\beta\rangle$. One Grover iteration (blue) can be composed from a reflection about $|\alpha\rangle$ and a reflection about $|S\rangle$ and effectively implements a rotation by an angle θ . The goal of the Grover iterations is to rotate the initial state vector $|S\rangle$ to the solution vector $|\beta\rangle$.



we see that in the $|\alpha\rangle$ and $|\beta\rangle$ plane, the Grover iteration performs a rotation by the angle θ , which is determined by the number of items and the number of solutions

$$\cos \frac{\theta}{2} \equiv \sqrt{\frac{N-M}{N}}, \quad (3.74)$$

see Fig. 3.12. We can now ask how many iterations G of the oracle call are necessary to rotate the initial state $|S\rangle$ to the solution vector $|\beta\rangle$. If we denote the number of Grover iterations by R , this is defined by

$$\left(R + \frac{1}{2}\right) \theta \approx \frac{\pi}{2}. \quad (3.75)$$

Which we can solve for integer R as

$$R = \left\lceil \frac{\pi}{4 \arccos \sqrt{\frac{N-M}{N}}} \right\rceil. \quad (3.76)$$

If the number of solutions is significantly less than the number of items (which is the typical range of application) $M \ll N$, we can expand the above formula yielding

$$R = \left\lceil \frac{\pi}{4} \sqrt{\frac{N}{M}} \right\rceil. \quad (3.77)$$

Grover iterations will suffice to rotate near the solution, which yields a quadratic speedup compared to the classical oracle query complexity of $\mathcal{O}(N/M)$. Since in general we can be off by an angle $\theta/2 \approx \sqrt{\frac{M}{N}}$, the error probability in a subsequent measurement would be $P_{\text{err}} \approx M/N$, such that the Grover rotations are quite useful. The most intriguing advantage of the Grover iteration is

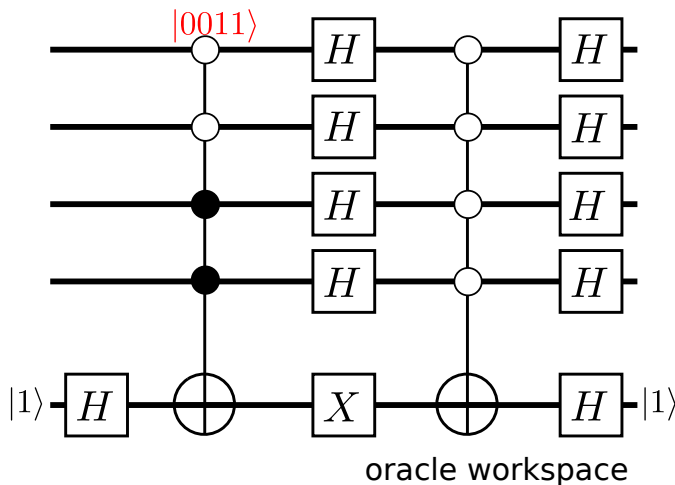


Figure 3.13: Example of a Grover iteration for a 4-qubit system with a single qubit oracle workspace. The first Hadamard on the oracle workspace simply generates an antisymmetric state with respect to a bitflip, such that the first CCCCNOT operation will generate a sign for the unique solution $|0011\rangle$. Additionally, the oracle workspace is re-used to implement the phase flip $2|0000\rangle\langle 0000| - \mathbf{1}$ by acting with X on the workspace and the second controlled CCCCNOT gate. The final Hadamard serves to recover the ancilla state.

however that it is modularized in an abstract way and can be combined with any oracle function to optimize quantum search. Counting the total complexity, we see that if the oracle costs are only polynomial in $P_{\text{oracle}}(n)$, the total complexity of Grover search is $\mathcal{O}\left(\sqrt{\frac{N}{M}}P_{\text{oracle}}(\log_2 N)\right)$.

An example of a Grover iteration G with an oracle conditioned on recognizing the unique solution $|0011\rangle$ is presented in Fig. 3.13. In this example, the oracle ‘recognizes’ the solution to the trivial question “What computational basis state has the binary decomposition 0011”. In the figure, the first Hadamard and the CCCCNOT gate implement the oracle operation O , which simply yields a sign when the solution $|0011\rangle$ is fed in and does nothing otherwise on the work qubits. Counting the number of gates, we see that this particular Grover iteration can be implemented with $\mathcal{O}(n)$ gates. As written, we would need to know the solution beforehand to implement the oracle, but one can imagine a situation where the oracle scans a global property of the state (like e.g. the number of 1s). This suggests that $R \approx 2.6 \approx 3$ iterations of the oracle should suffice to find the correct solution out of 16 states. To run a search algorithm with a different search question, we simply have to use a different oracle. In figure 3.13 we could for example discard the constraint on the second qubit in the oracle, reducing the number of solutions to two.

In general, one can prove that the Grover search algorithm is optimal, i.e., given an oracle problem one cannot do the quantum search problem faster than with $\mathcal{O}\left(\sqrt{\frac{N}{M}}\right)$ oracle calls.

3.7 Control errors

Unfortunately, we do never have perfect control over the qubits of a quantum computer. When performing a single qubit rotation, this can in principle be corrected by performing additional rotations since merely the direction of the control Hamiltonian is slightly off the intended direction. This however becomes more difficult if one has undesired couplings to additional components (e.g. other qubits).

As an example, we can investigate what happens when we intend to perform a Hadamard gate on the first qubit of a two-qubit system

$$U_{H,1} = \frac{1}{\sqrt{2}}(\sigma_1^x + \sigma_1^z) = e^{i\pi/2} e^{-i\pi/2 \frac{1}{\sqrt{2}}(\sigma_1^x + \sigma_1^z)}, \quad (3.78)$$

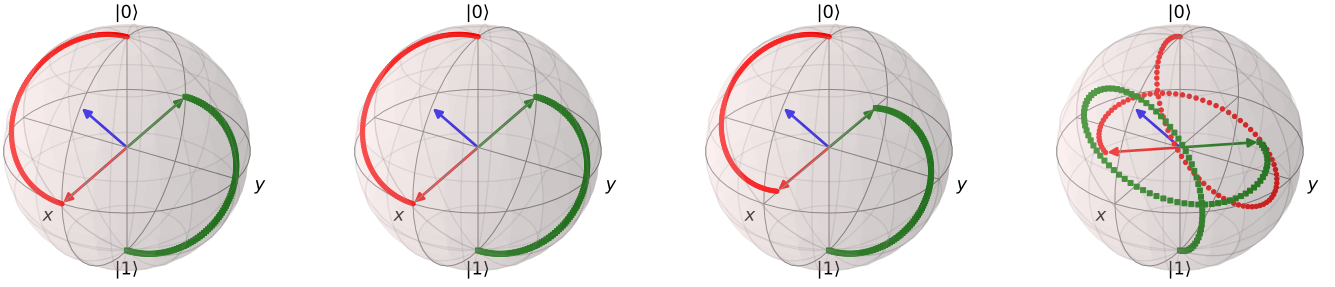


Figure 3.14: Bloch sphere representation of the evolution of two different initial states $|0\rangle$ (red) and $|1\rangle$ (green) under a Hadamard gate H in presence of a non-vanishing coupling to a second qubit that is initialized in state $|0\rangle$. From left to right, the coupling strength is increased from $\lambda/\Omega \in \{0, 0.01, 0.1, 1.0\}$, such that the leftmost panel shows the intended gate operation. The blue arrow shows the direction of the intended control Hamiltonian $H_0(t)$.

which should work with a control Hamiltonian of the form (the global phase factor can be neglected)

$$H_0(t) = \Theta(t)\Theta\left(\frac{\pi}{\Omega} - t\right) \frac{\Omega}{2} \frac{1}{\sqrt{2}} (\sigma_1^x + \sigma_1^z) . \quad (3.79)$$

If additionally however we are coupled to a second qubit with undesired coupling strength λ

$$H(t) = H_0(t) + \lambda\sigma_1^x\sigma_2^x , \quad (3.80)$$

the actual dynamics will deviate from the intended one, see Fig. 3.14. We see that moderate coupling strength leads to non-pure states, but the gate operation roughly remains the same. Although the two qubits evolve unitarily, and pure states remain pure under unitary evolution, this only holds for the joint state of both qubits. The reduced density matrix of the first qubit $\rho_1 = \text{Tr}_2 \{\rho_{12}\}$ will appear mixed $\rho_1^2 \neq \rho_1$, or alternatively the expectation values of Pauli matrices may be inside the Bloch sphere $\langle\sigma^x\rangle^2 + \langle\sigma^y\rangle^2 + \langle\sigma^z\rangle^2 < 1$. For strong couplings however, the gate function is lost completely (rightmost panel).

Chapter 4

Open quantum systems

The previously discussed quantum algorithms would work nicely if we could arbitrarily well manipulate our qubits and turn on and off certain Hamiltonians at will. This is unfortunately not the case. By driving a parameter in the Hamiltonian in a time-dependent fashion we also couple it to the outside world – the quantum system is no longer closed but should be considered open. This coupling can not always be neglected and may have strong detrimental effects on the performance of the quantum computer. To treat an open quantum system, one has to go beyond the Schrödinger equation description but consider the density matrix formalism. The starting point is then a decomposition of the total Hamiltonian into system, interaction and reservoir parts

$$H = H_S(t) + H_I + H_B, \quad (4.1)$$

where $H_S(t)$ could be the control Hamiltonian governing the qubit dynamics, H_I denotes the system-reservoir interaction and H_B the Hamiltonian of the reservoir. For weak system-reservoir coupling one may then use a perturbative treatment of the dynamics and trace out the reservoir degrees of freedom to obtain an effective evolution equation for the system only. We provide a simplified discussion here, for a more detailed treatment see e.g. [12] or the lecture notes on quantum transport.

4.1 An exactly solvable model of decoherence

Since a reservoir typically involves an infinite number of degrees of freedom, open systems are typically not exactly solvable. An exception to this is the spin-boson pure dephasing model, which describes the interaction of a spin with a bosonic environment

$$\begin{aligned} H_S &= \frac{\Omega}{2} \sigma^z, & H_B &= \sum_k \omega_k b_k^\dagger b_k, \\ H_I &= \sigma^z \otimes \sum_k \left[h_k b_k + h_k^* b_k^\dagger \right], \end{aligned} \quad (4.2)$$

where Ω denotes the splitting of the system Hamiltonian and b^\dagger creates a boson with frequency ω_k in the reservoir.

We can apply the so-called **polaron transformation** (also: Lang-Firsov) to the whole Hamiltonian

$$U = \exp \left\{ -\sigma^z \sum_k \left(\frac{h_k}{\omega_k} b_k - \frac{h_k^*}{\omega_k} b_k^\dagger \right) \right\}. \quad (4.3)$$

We note the following relations

$$\begin{aligned}
U\sigma^zU^\dagger &= \sigma^z, \\
U\sigma^\pm U^\dagger &= e^{\pm 2\sum_k \left(\frac{h_k^* b_k^\dagger}{\omega_k} - \frac{h_k b_k}{\omega_k} \right)} \sigma^\pm, \\
Ub_k U^\dagger &= b_k - \frac{h_k^*}{\omega_k} \sigma^z.
\end{aligned} \tag{4.4}$$

While the first is evident, the other can be demonstrated by application of the Baker-Campbell-Hausdorf formula. From this we conclude that the unitary decouples system and reservoir

$$\begin{aligned}
UHU^\dagger &= \frac{\Omega}{2}\sigma^z + \sigma^z \sum_k \left(h_k b_k + h_k^* b_k^\dagger - 2\frac{|h_k|^2}{\omega_k} \sigma^z \right) + \sum_k \omega_k \left(b_k^\dagger - \frac{h_k}{\omega_k} \sigma^z \right) \left(b_k - \frac{h_k^*}{\omega_k} \sigma^z \right) \\
&= \frac{\Omega}{2}\sigma^z - \sum_k \frac{|h_k|^2}{\omega_k} + \sum_k \omega_k b_k^\dagger b_k.
\end{aligned} \tag{4.5}$$

Consequently, we can e.g. compute the expectation value of σ^α via

$$\begin{aligned}
\langle \sigma^\alpha \rangle &= \text{Tr} \left\{ e^{+iHt} \sigma^\alpha e^{-iHt} \rho_0 \right\} = \text{Tr} \left\{ U^\dagger U e^{+iHt} U^\dagger U \sigma^\alpha U^\dagger U e^{-iHt} U^\dagger U \rho_0 \right\} \\
&= \text{Tr} \left\{ U^\dagger e^{+iUHU^\dagger t} U \sigma^\alpha U^\dagger e^{-iUHU^\dagger t} U \rho_0 \right\} \\
&= \text{Tr} \left\{ U^\dagger e^{+i\Omega t/2\sigma^z} e^{+i\sum_k \omega_k t b_k^\dagger b_k} U \sigma^\alpha U^\dagger e^{-i\sum_k \omega_k t b_k^\dagger b_k} e^{-i\Omega t/2\sigma^z} U \rho_0 \right\}.
\end{aligned} \tag{4.6}$$

For $\alpha = +$ we further calculate

$$\begin{aligned}
\langle \sigma^+ \rangle &= \text{Tr} \left\{ U^\dagger e^{+i\sum_k \omega_k t b_k^\dagger b_k} e^{2\sum_k \left(\frac{h_k^* b_k^\dagger}{\omega_k} - \frac{h_k b_k}{\omega_k} \right)} e^{-i\sum_k \omega_k t b_k^\dagger b_k} e^{+i\Omega/2t\sigma^z} \sigma^+ e^{-i\Omega/2t\sigma^z} U \rho_0 \right\} \\
&= e^{+i\Omega t} \text{Tr} \left\{ U^\dagger e^{2\sum_k \left(\frac{h_k^* b_k^\dagger}{\omega_k} e^{+i\omega_k t} - \frac{h_k b_k}{\omega_k} e^{-i\omega_k t} \right)} U U^\dagger \sigma^+ U \rho_0 \right\} \\
&= e^{+i\Omega t} \text{Tr} \left\{ e^{2\sum_k \left(\frac{h_k^*}{\omega_k} (b_k^\dagger + \frac{h_k}{\omega_k} \sigma^z) e^{+i\omega_k t} - \frac{h_k}{\omega_k} (b_k + \frac{h_k^*}{\omega_k} \sigma^z) e^{-i\omega_k t} \right)} e^{-2\sum_k \left(\frac{h_k^* b_k^\dagger}{\omega_k} - \frac{h_k b_k}{\omega_k} \right)} \sigma^+ \rho_0 \right\} \\
&= e^{+i\Omega t} \text{Tr} \left\{ e^{4i\sum_k \frac{|h_k|^2}{\omega_k^2} \sin(\omega_k t) \sigma^z} \sigma^+ \rho_S^0 \right\} \text{Tr} \left\{ e^{2\sum_k \left(\frac{h_k^* b_k^\dagger}{\omega_k} e^{+i\omega_k t} - \frac{h_k b_k}{\omega_k} e^{-i\omega_k t} \right)} e^{-2\sum_k \left(\frac{h_k^* b_k^\dagger}{\omega_k} - \frac{h_k b_k}{\omega_k} \right)} \bar{\rho}_B \right\} \\
&= e^{+i\Omega t} \text{Tr} \left\{ e^{4i\sum_k \frac{|h_k|^2}{\omega_k^2} \sin(\omega_k t) \sigma^z} \sigma^+ \rho_S^0 \right\} B(t),
\end{aligned} \tag{4.7}$$

where we have used initial factorization $\rho_0 = \rho_S^0 \otimes \bar{\rho}_B$. Using that $e^X e^Y = e^{X+Y+[X,Y]/2}$ when $[X, [X, Y]] = [Y, [X, Y]] = 0$, we can further evaluate the decoherence factor resulting from the reservoir

$$\begin{aligned}
B(t) &= \text{Tr} \left\{ \exp \left\{ 2 \sum_k \left[\frac{h_k^* b_k^\dagger}{\omega_k} (e^{+i\omega_k t} - 1) - \frac{h_k b_k}{\omega_k} (e^{-i\omega_k t} - 1) \right] \right\} \bar{\rho}_B \right\} e^{-4i\sum_k \frac{|h_k|^2}{\omega_k^2} \sin(\omega_k t)} \\
&= \text{Tr} \left\{ \exp \left\{ +2 \sum_k \frac{h_k^* b_k^\dagger}{\omega_k} (e^{+i\omega_k t} - 1) \right\} \exp \left\{ -2 \sum_k \frac{h_k b_k}{\omega_k} (e^{-i\omega_k t} - 1) \right\} \bar{\rho}_B \right\} \times \\
&\quad \times e^{-4\sum_k \frac{|h_k|^2}{\omega_k^2} [1 - \cos(\omega_k t) + i \sin(\omega_k t)]}.
\end{aligned} \tag{4.8}$$

Now, we can use that for a thermal reservoir $\bar{\rho}_B = e^{-\beta H_B} / \text{Tr} \{ e^{-\beta H_B} \}$ we have expressions like

$$\begin{aligned} \text{Tr} \left\{ e^{+\alpha_k b_k^\dagger} e^{-\alpha_k^* b_k} \frac{e^{-\beta \omega_k b_k^\dagger b_k}}{Z_k} \right\} &= \sum_{n,m=0}^{\infty} \frac{(+\alpha_k)^n (-\alpha_k^*)^m}{n!m!} \text{Tr} \left\{ (b_k^\dagger)^n b_k^m \frac{e^{-\beta \omega_k b_k^\dagger b_k}}{Z_k} \right\} \\ &= \sum_{q=0}^{\infty} \sum_{n=0}^q \frac{(-|\alpha_k|^2)^n}{(n!)^2} (1 - e^{-\beta \omega_k}) e^{-\beta \omega_k q} \frac{q!}{(q-n)!} \\ &= e^{-|\alpha_k|^2 n_B(\omega_k)} \end{aligned} \quad (4.9)$$

with $|\alpha_k|^2 = 8|h_k|^2/\omega_k^2[1 - \cos(\omega_k t)]$. This then implies for the decoherence factor

$$B(t) = \exp \left\{ -4 \sum_k \frac{|h_k|^2}{\omega_k^2} [1 - \cos(\omega_k t)] [1 + 2n_B(\omega_k)] \right\} \exp \left\{ -4i \sum_k \frac{|h_k|^2}{\omega_k^2} \sin(\omega_k t) \right\}. \quad (4.10)$$

Eventually, it follows that the populations remain unaffected and that the coherences decay in the long-term limit, i.e., leading to **decoherence**. In the interaction picture we can simply write

$$\begin{aligned} \rho(t) &= \begin{pmatrix} \rho_{00}(0) & \rho_{01}(0)e^{-f(t)} \\ \rho_{10}(0)e^{-f(t)} & \rho_{11}(0) \end{pmatrix} \xrightarrow{t \rightarrow \infty} \begin{pmatrix} \rho_{00}(0) & 0 \\ 0 & \rho_{11}(0) \end{pmatrix}, \\ f(t) &= 8 \sum_k |h_k|^2 \frac{\sin^2(\omega_k t/2)}{\omega_k^2} \coth \left(\frac{\beta \omega_k}{2} \right) = \frac{4}{\pi} \int_0^\infty J(\omega) \frac{\sin^2(\omega t/2)}{\omega^2} \coth \left(\frac{\beta \omega}{2} \right) d\omega \geq 0, \end{aligned} \quad (4.11)$$

where we have used the spectral density $J(\omega) = 2\pi \sum_k |h_k|^2 \delta(\omega - \omega_k)$. This result holds in a similar fashion also for multiple qubits as long as all the interactions do mutually commute [13]. For later comparison, we note that the above solution is also the solution of the **exact master equation**

$$\dot{\rho} = +\dot{f}(t) \frac{e^{-f(t)}}{2} (\sigma^z \rho \sigma^z - \rho), \quad (4.12)$$

and that $\dot{f} < 0$ may occur for specific times, depending on the specific form of $J(\omega)$. The qualitative effect of this exact master equation for the simplified case where $\dot{f}(t) \frac{e^{-f(t)}}{2} \approx \gamma$ is constant and positive over the time interval is depicted in Fig. 4.1. It exemplifies that in order to remain with a pure state representation, quantum gates have to be performed significantly faster than the decoherence rate.

4.2 Lindblad master equation: Microscopic derivation

The previous example was a very specific decoherence model because the energy of the system was kept constant all the time. To model the loss of coherence in a more general fashion, we take H_S as generic but assume it to be constant in the time of the gate duration. For simplicity (this can be generalized in a straightforward way) we also assume a generic single-operator interaction of the form

$$H_I = S \otimes \sum_k \left(h_k b_k + h_k^* b_k^\dagger \right) \equiv S \otimes B, \quad (4.13)$$

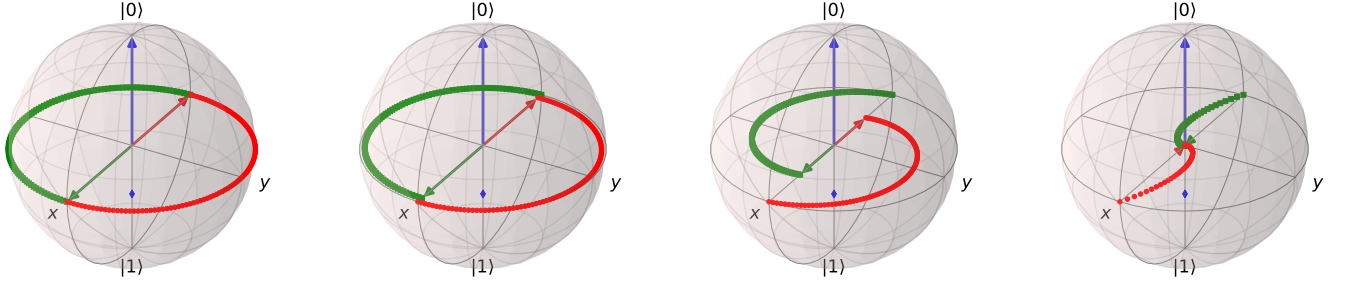


Figure 4.1: Bloch sphere representation of the evolution of two different initial states $\frac{1}{\sqrt{2}}[|0\rangle \pm |1\rangle]$ (red/green) under the Hamiltonian $H_S = \frac{\Omega}{2}\sigma^z$ (blue arrow) in presence for time $t \in [0, \pi/\Omega]$ of a pure-dephasing master equation $\dot{\rho} = -i[H_S, \rho] + \gamma[\sigma^z \rho \sigma^z - \rho]$ for constant γ . From left to right, the coupling strength is increased from $\gamma/\Omega \in \{0, 0.01, 0.1, 1.0\}$.

where S is a generic system operator and h_k denote spontaneous emission amplitudes of bosonic modes b_k and a harmonic oscillator reservoir

$$H_B = \sum_k \omega_k b_k^\dagger b_k, \quad (4.14)$$

characterized by oscillator frequencies $\omega_k > 0$. In an ion-trap quantum computer the bosonic modes could represent vibrations (phonons) of trapped ion clouds and the Pauli matrices describe two selected internal levels of an ion. The evolution of the full universe density matrix σ is then described by

$$\dot{\sigma} = -i[H_S + H_I + H_B, \sigma]. \quad (4.15)$$

In order to obtain a perturbative expression in the system-reservoir coupling strength, we transform into an interaction picture with respect to system and reservoir Hamiltonians (bold symbols)

$$\dot{\boldsymbol{\sigma}} = -i[\boldsymbol{H}_I(t), \boldsymbol{\sigma}], \quad (4.16)$$

where

$$\boldsymbol{H}_I(t) = e^{+i(H_S+H_B)t} H_I e^{-i(H_S+H_B)t} = \boldsymbol{S}(t) \otimes \boldsymbol{B}(t) \quad (4.17)$$

denotes the interaction Hamiltonian in the interaction picture. The advantage of this representation is that we can now treat the Hamiltonian perturbatively. Formally integrating both sides of the von-Neumann equation yields

$$\boldsymbol{\sigma}(t) - \boldsymbol{\sigma}(0) = -i \int_0^t [\boldsymbol{H}_I(t'), \boldsymbol{\sigma}(t')] dt', \quad (4.18)$$

which we can solve for $\boldsymbol{\sigma}(t)$ on the l.h.s. and re-insert the result into Eq. (4.16)

$$\dot{\boldsymbol{\sigma}} = -i[\boldsymbol{H}_I(t), \boldsymbol{\sigma}(0)] - \int_0^t dt' [\boldsymbol{H}_I(t), [\boldsymbol{H}_I(t'), \boldsymbol{\sigma}(t')]]. \quad (4.19)$$

This equation is still exact and still concerns the density matrix of the total universe. To obtain a density matrix for the system only, we perform the partial trace over the reservoir degrees of freedom

$$\boldsymbol{\rho}(t) \equiv \text{Tr}_B \{ \boldsymbol{\sigma}(t) \} , \quad (4.20)$$

which yields

$$\dot{\boldsymbol{\rho}} = -i \text{Tr}_B \{ [\mathbf{H}_I(t), \boldsymbol{\sigma}(0)] \} - \int_0^t dt' \text{Tr}_B \{ [\mathbf{H}_I(t), [\mathbf{H}_I(t'), \boldsymbol{\sigma}(t')]] \} . \quad (4.21)$$

This equation is still exact but impossible to solve since the r.h.s. still depends on $\boldsymbol{\sigma}$. Now, we have to apply approximations to transform this equation into a practical evolution equation for the system density matrix. Having in mind that the interaction is small $H_I = \mathcal{O}(\lambda)$ and the reservoir is large and that initially, system and reservoir are not yet coupled, it is reasonable to assume that system and reservoir remain approximately in some tensor product form, where the reservoir is hardly influenced by the system. The **Born approximation** does just this

$$\boldsymbol{\sigma}(t) = \boldsymbol{\rho}(t) \otimes \bar{\rho}_B + \mathcal{O}(\lambda) = \boldsymbol{\rho}(t) \otimes \frac{e^{-\beta H_B}}{\text{Tr}_B \{ e^{-\beta H_B} \}} + \mathcal{O}(\lambda) , \quad (4.22)$$

where we have assumed that the reservoir is in a canonical equilibrium state characterized by inverse temperature β . Inserting it in the previous equation we find that now we obtain a closed but complicated integro-differential equation

$$\begin{aligned} \dot{\boldsymbol{\rho}} &= -i \mathbf{S}(t) \boldsymbol{\rho}(0) \text{Tr}_B \{ \mathbf{B}(t) \bar{\rho}_B \} + i \boldsymbol{\rho}(0) \mathbf{S}(t) \text{Tr}_B \{ \bar{\rho}_B \mathbf{B}(t) \} \\ &\quad - \int_0^t dt' \text{Tr}_B \{ [\mathbf{S}(t) \mathbf{B}(t), [\mathbf{S}(t') \mathbf{B}(t'), \boldsymbol{\rho}(t') \bar{\rho}_B]] \} + \mathcal{O}(\lambda^3) . \end{aligned} \quad (4.23)$$

Now, we can make the interaction picture time-dependence of the coupling operators explicit

$$\begin{aligned} \mathbf{S}(t) &= e^{+iH_S t} S e^{-iH_S t} = \sum_{a,b} S_{ab} e^{+i(E_a - E_b)t} |a\rangle \langle b| , \\ \mathbf{B}(t) &= e^{+iH_B t} B e^{-iH_B t} = \sum_k \left(h_k b_k e^{-i\omega_k t} + h_k^* b_k^\dagger e^{+i\omega_k t} \right) , \end{aligned} \quad (4.24)$$

where $S_{ab} = \langle a | S | b \rangle$ are the matrix elements of the coupling operator in the energy eigenbasis of the system

$$H_S |a\rangle = E_a |a\rangle . \quad (4.25)$$

With this, one can see that the first terms involving only linear expectation values of \mathbf{B} are not problematic since with

$$\text{Tr}_B \left\{ b_k e^{-\beta \omega_k b_k^\dagger b_k} \right\} = \text{Tr}_B \left\{ b_k^\dagger e^{-\beta \omega_k b_k^\dagger b_k} \right\} = 0 \quad (4.26)$$

it follows that

$$\text{Tr}_B \{ \mathbf{B} \bar{\rho}_B \} = \text{Tr}_B \{ B \bar{\rho}_B \} = \sum_k \left[\frac{h_k}{Z_k} \text{Tr} \left\{ b_k e^{-\beta \omega_k b_k^\dagger b_k} \right\} + \frac{h_k^*}{Z_k} \text{Tr} \left\{ b_k^\dagger e^{-\beta \omega_k b_k^\dagger b_k} \right\} \right] = 0 . \quad (4.27)$$

We are left with the **non-Markovian master equation**

$$\begin{aligned}\dot{\rho} &= \int_0^t \left[-\mathbf{S}(t)\mathbf{S}(t')\rho(t')\text{Tr}_B\{\mathbf{B}(t)\mathbf{B}(t')\bar{\rho}_B\} + \mathbf{S}(t)\rho(t')\mathbf{S}(t')\text{Tr}_B\{\mathbf{B}(t)\bar{\rho}_B\mathbf{B}(t')\} \right. \\ &\quad \left. + \mathbf{S}(t')\rho(t')\mathbf{S}(t)\text{Tr}_B\{\mathbf{B}(t')\bar{\rho}_B\mathbf{B}(t)\} - \rho(t')\mathbf{S}(t')\mathbf{S}(t)\text{Tr}_B\{\bar{\rho}_B\mathbf{B}(t')\mathbf{B}(t)\} \right] + \mathcal{O}(\lambda^3) \\ &= \int_0^t C(t-t') [\mathbf{S}(t')\rho(t'), \mathbf{S}(t)] dt' + \text{h.c.} + \mathcal{O}(\lambda^3),\end{aligned}\quad (4.28)$$

where we have introduced the **reservoir correlation function**

$$C(t-t') = \text{Tr}_B\{\mathbf{B}(t)\mathbf{B}(t')\bar{\rho}_B\} = \text{Tr}_B\{\mathbf{B}(t-t')\mathbf{B}\bar{\rho}_B\} = C^*(t'-t). \quad (4.29)$$

The above master equation can only be solved for a few special cases, since it has a memory delay kernel. It does not necessarily yield a proper system density matrix: Although it preserves trace and hermiticity, one may get non-positive density matrices.

The explicit evaluation of the correlation function is tedious, but it can be related to the expectation values of quadratic bosonic observables in a thermal state

$$\begin{aligned}C(\tau) &= \sum_{kq} \text{Tr} \left\{ \left[h_k b_k e^{-i\omega_k \tau} + h_k^* b_k^\dagger e^{+i\omega_k \tau} \right] \left[h_q b_q + h_q^* b_q^\dagger \right] \bar{\rho}_B \right\} \\ &= \sum_k |h_k|^2 \left(e^{-i\omega_k \tau} \langle b_k b_k^\dagger \rangle + e^{+i\omega_k \tau} \langle b_k^\dagger b_k \rangle \right) \\ &= \sum_k |h_k|^2 \left(e^{-i\omega_k \tau} [1 + n_B(\omega_k)] + e^{+i\omega_k \tau} n_B(\omega_k) \right),\end{aligned}\quad (4.30)$$

where

$$n_B(\omega) = \frac{1}{e^{\beta\omega} - 1} \quad (4.31)$$

is the **Bose-Einstein distribution** function and we have used that

$$\text{Tr} \left\{ b_k^\dagger b_q \bar{\rho}_B \right\} = \delta_{kq} n_B(\omega_k), \quad \text{Tr} \left\{ b_k b_q \bar{\rho}_B \right\} = \text{Tr} \left\{ b_k^\dagger b_q^\dagger \bar{\rho}_B \right\} = 0 \quad (4.32)$$

together with the bosonic commutation relations $[b_k, b_q^\dagger] = \delta_{kq}$. To be able to treat the continuum reservoir limit we introduce the **spectral coupling density**

$$\bar{J}(\omega) = 2\pi \sum_k |h_k|^2 \delta(\omega - \omega_k), \quad (4.33)$$

which parametrizes the coupling strength and frequency distribution of the reservoir energy modes. Since $\omega_k \geq 0$, the original spectral density must vanish at negative frequencies. Analytically continuing the spectral density for negative frequencies as an odd function

$$J(|\omega|) = \bar{J}(|\omega|), \quad J(-\omega) = -J(\omega) \quad (4.34)$$

allows us with $n_B(-\omega) = -[1 + n_B(\omega)]$ to write the correlation function as

$$\begin{aligned}C(\tau) &= \frac{1}{2\pi} \int_0^\infty J(\omega) \left(e^{-i\omega\tau} [1 + n_B(\omega)] + e^{+i\omega\tau} n_B(\omega) \right) d\omega \\ &= \frac{1}{2\pi} \int_{-\infty}^{+\infty} d\omega J(\omega) [1 + n_B(\omega)] e^{-i\omega\tau}.\end{aligned}\quad (4.35)$$

From this, we can read off the Fourier transform of the reservoir correlation function

$$\gamma(\omega) \equiv \int C(\tau) e^{+i\omega\tau} d\tau = J(\omega)[1 + n_B(\omega)]. \quad (4.36)$$

We observe that for a thermal reservoir, the correlation functions (here, their Fourier transforms) obey additional thermal properties

$$\frac{\gamma(-\omega)}{\gamma(+\omega)} = \frac{J(-\omega)}{J(+\omega)} \frac{1 + n_B(-\omega)}{1 + n_B(+\omega)} = \frac{n_B(+\omega)}{1 + n_B(+\omega)} = e^{-\beta\omega}, \quad (4.37)$$

which are known as **Kubo-Martin-Schwinger** relations.

The specific behaviour now depends on what model is chosen for a spectral density. For example, many reservoirs are well described by an ohmic spectral density that grows linearly at small frequencies and has some cutoff at large frequencies

$$J(\omega) = J_0 \frac{\omega}{\omega_c} e^{-|\omega|/\omega_c}, \quad (4.38)$$

and we see that for small frequencies $\omega \ll \omega_c$ and large temperatures $\beta\omega \ll 1$ we have that the Fourier transform of the correlation function does not vary much

$$\lim_{\omega \rightarrow 0} J(\omega)[1 + n_B(\omega)] = \frac{J_0 \frac{\omega}{\omega_c}}{\beta\omega} = \frac{J_0}{\beta\omega_c}. \quad (4.39)$$

In turn this means that when the Fourier transform is flat, the correlation function is a rapidly decaying function of time. Revisiting Eq. (4.28) with this insight, we can replace $\rho(t') \rightarrow \rho(t)$, which is known as **first Markov approximation**. This yields the **Redfield-I equation**

$$\begin{aligned} \dot{\rho} &= \int_0^t C(t-t') [\mathbf{S}(t')\rho(t), \mathbf{S}(t)] dt' + \text{h.c.} \\ &= \int_0^t C(\tau) [\mathbf{S}(t-\tau)\rho(t), \mathbf{S}(t)] d\tau + \text{h.c.}, \end{aligned} \quad (4.40)$$

where we have replaced $\tau = t - t'$. It preserves hermiticity and trace (though not necessarily positivity) but as a practical drawback has some time-dependent coefficients. With essentially the same reasoning that the reservoir correlation function $C(\tau)$ decays very fast, we may as well extend the upper integration bound to ∞ , which is known as **second Markov approximation** and yields the **Redfield-II equation**

$$\dot{\rho} = \int_0^\infty C(\tau) [\mathbf{S}(t-\tau)\rho(t), \mathbf{S}(t)] d\tau + \text{h.c.} \quad (4.41)$$

When we introduce the **half-sided Fourier transform**

$$\Gamma(\omega) = \int_0^\infty C(\tau) e^{+i\omega\tau} d\tau, \quad (4.42)$$

it follows that we can absorb the integration over τ into a coefficient

$$\dot{\rho} = \sum_{ab} S_{ab} \Gamma(E_b - E_a) [e^{+iHst} |a\rangle \langle b| e^{-iHst} \rho(t), \mathbf{S}(t)] + \text{h.c.}, \quad (4.43)$$

from which it follows that after transforming back to the Schrödinger picture, one obtains a time-independent master equation with constant coefficients

$$\dot{\rho} = -i[H_S, \rho] + \left(\sum_{ab} S_{ab} \Gamma(E_b - E_a) [|a\rangle \langle b| \rho(t), S] + \text{h.c.} \right), \quad (4.44)$$

which preserves trace and hermiticity of the density matrix but not necessarily positivity. To obtain a generator that preserves all density matrix properties, it is necessary to apply yet another approximation. Making the time-dependencies explicit, we can write (4.41) in the form

$$\dot{\rho} = \sum_{abcd} \Gamma(E_b - E_a) S_{ab} S_{cd} e^{i(E_a - E_b + E_c - E_d)t} [|a\rangle \langle b| \rho, |c\rangle \langle d|] + \text{h.c.} \quad (4.45)$$

If the system splittings are sufficiently large, the oscillatory terms will average out, such that the **secular approximation** consists in keeping only the terms satisfying the resonance condition $E_a - E_b + E_c - E_d = 0$. After some rewriting and renaming of indices and with $L_{ab} \equiv |a\rangle \langle b|$ we can write the master equation as

$$\dot{\rho} = \sum_{abcd} \delta_{E_b - E_a, E_d - E_c} S_{ab} S_{dc} \left[\Gamma(E_b - E_a) \left(L_{ab} \rho L_{cd}^\dagger - \rho L_{cd}^\dagger L_{ab} \right) + \Gamma^*(E_b - E_a) \left(L_{ab} \rho L_{cd}^\dagger - L_{cd}^\dagger L_{ab} \rho \right) \right]. \quad (4.46)$$

This equation preserves all density matrix properties since it is of Gorini-Kossakowski-Sudarshan-Lindblad (GKSL) form [14, 15]. To see that, we split the half-sided Fourier transforms into real and imaginary part (this would generalize to hermitian and anti-hermitian parts for many coupling operators)

$$\Gamma(\omega) = \frac{1}{2} \gamma(\omega) + \frac{1}{2} \sigma(\omega) \quad (4.47)$$

with $\gamma(\omega) \in \mathbb{R}$ and $\sigma(\omega) \in i\mathbb{R}$ such that $\sigma^*(\omega) = -\sigma(\omega)$. Indeed one finds that

$$\begin{aligned} \gamma(\omega) &= \Gamma(\omega) + \Gamma^*(\omega) = \int C(\tau) e^{+i\omega\tau} d\tau, \\ \sigma(\omega) &= \Gamma(\omega) - \Gamma^*(\omega) = \int C(\tau) \text{sgn}(\tau) e^{+i\omega\tau} d\tau. \end{aligned} \quad (4.48)$$

Inserting it all, we get the **Born-Markov-secular master equation**

$$\begin{aligned} \dot{\rho} &= -i \left[\sum_{ab} \delta_{E_a, E_b} S_{cb} S_{ac} \frac{\sigma(E_b - E_c)}{2i} L_{ab}, \rho \right] \\ &+ \sum_{abcd} \delta_{E_b - E_a, E_d - E_c} S_{ab} S_{dc} \gamma(E_b - E_a) \left[L_{ab} \rho L_{cd}^\dagger - \frac{1}{2} \left\{ L_{cd}^\dagger L_{ab}, \rho \right\} \right]. \end{aligned} \quad (4.49)$$

This equation has many interesting properties

- It is of GKSL form and thereby preserves all density matrix properties. Specifically, this can be seen by showing that $H_{\text{LS}} = \sum_{ab} \delta_{E_a, E_b} S_{cb} S_{ac} \frac{\sigma(E_b - E_c)}{2i} L_{ab} = H_{\text{LS}}^\dagger$ is hermitian and that $\gamma_{ab, cd} = \delta_{E_b - E_a, E_d - E_c} S_{ab} S_{dc} \gamma(E_b - E_a)$ is a positive semidefinite matrix (i.e., $\sum_{ab, cd} x_{ab}^* \gamma_{ab, cd} x_{cd} \geq 0$).

- The correction to the control Hamiltonian commutes with the control Hamiltonian.
- For a non-degenerate system, it decouples populations and coherences in the system energy eigenbasis. Specifically, the populations obey a rate equation, the so-called **Pauli master equation**

$$\dot{\rho}_{aa} = \sum_b \gamma_{ab,ab} \rho_{bb} - \sum_b \gamma_{ba,ba} \rho_{aa} \quad : \quad \gamma_{ab,ab} = |S_{ab}|^2 \gamma(E_b - E_a) \quad (4.50)$$

- For a thermal reservoir $\bar{\rho}_B \propto e^{-\beta H_B}$, the system will thermalize with the reservoir temperature, i.e., $\bar{\rho}_S \propto e^{-\beta H_S}$ is a stationary state of the master equation.

The thermalization can be seen by considering the ratio of rates between two energy eigenstates

$$\frac{\gamma_{ab,ab}}{\gamma_{ba,ba}} = \frac{\gamma(E_b - E_a)}{\gamma(E_a - E_b)} \frac{n_B(E_a - E_b)}{1 + n_B(E_a - E_b)} = e^{-\beta(E_a - E_b)}. \quad (4.51)$$

Specifically for a qubit with two non-degenerate levels $|-\rangle$ and $|+\rangle$ defined by the eigenstates of the control Hamiltonian, equation (4.49) becomes in the Schrödinger picture

$$\begin{aligned} \dot{\rho} = & -i[H_S + \sigma_{--} |-\rangle \langle -| + \sigma_{++} |+\rangle \langle +|, \rho] \\ & + |S_{-+}|^2 \gamma(E_+ - E_-) \left[L_{-+} \rho L_{-+}^\dagger - \frac{1}{2} \{L_{-+} L_{-+}^\dagger, \rho\} \right] \\ & + |S_{+-}|^2 \gamma(E_- - E_+) \left[L_{+-} \rho L_{+-}^\dagger - \frac{1}{2} \{L_{+-} L_{+-}^\dagger, \rho\} \right]. \end{aligned} \quad (4.52)$$

The effect of the Hamiltonian correction (Lamb-shift) term is merely a shift of the system energy levels which induces a different splitting and effectively introduces an irrelevant global phase and changes the gate operation time. The dissipative term however severely affects the dynamics, as it drags the system to a mixed stationary state and thereby destroys coherences. Exemplifying this for a Hadamard gate

$$H_S = \frac{\Omega}{\sqrt{2}} (\sigma^x + \sigma^z) \quad T_{\text{gt}} = \frac{\pi}{\Omega}, \quad (4.53)$$

one can see that strong dissipation inhibits the intended gate operation, see Fig. 4.2. To analyze the fixed point of the master equation dynamics with the thermal state, it is helpful to note that for $\mathbf{n} \cdot \mathbf{n} = 1$

$$e^{-\beta\Omega/2 \mathbf{n} \cdot \boldsymbol{\sigma}} = \cosh\left(\frac{\beta\Omega}{2}\right) \mathbf{1} - \sinh\left(\frac{\beta\Omega}{2}\right) \mathbf{n} \cdot \boldsymbol{\sigma}, \quad (4.54)$$

from which it follows that

$$\langle \sigma^\alpha \rangle_{\text{th}} = -\tanh\left(\frac{\beta\Omega}{2}\right) n_\alpha. \quad (4.55)$$

For high temperatures $\beta \rightarrow 0$, this just tends towards the center of the Bloch sphere. Since all trajectories converge to the thermal state of the system Hamiltonian, the information about the initial state is lost.

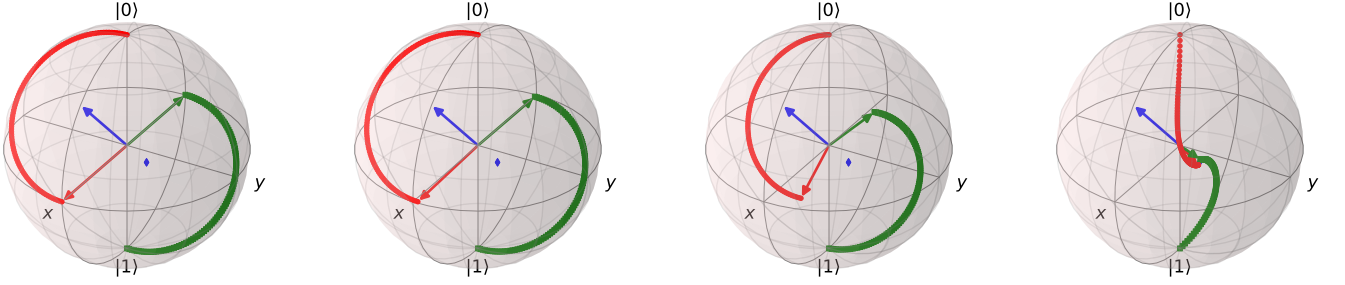


Figure 4.2: Bloch sphere representation of the evolution of two different initial states $|0\rangle$ (red) and $|1\rangle$ (green) under a Hadamard gate H in presence of decoherence due to a generic coupling operators S and neglecting a dephasing channel $J(0) = 0$. From left to right, the dissipation strength is increased from $\gamma/\Omega \in \{0, 0.01, 0.1, 1.0\}$, where $\gamma = J(\Omega)|\langle -|S|+\rangle|^2$, such that the leftmost panel shows the intended gate operation. The blue arrow shows the direction of the control Hamiltonian, and the blue dot shows the expectation value of the thermal state of the control Hamiltonian, to which for strong dissipation or slow gates all states decay. The Lamb-shift has been neglected. Other parameters: $\beta\omega = 1.0$.

4.3 Lindblad master equation: General properties

We have written the Lindblad equation so far in the form

$$\dot{\rho} = -i[H, \rho] + \sum_{\alpha\beta} \gamma_{\alpha\beta} \left[L_{\alpha}\rho L_{\beta}^{\dagger} - \frac{1}{2} \{L_{\beta}^{\dagger}L_{\alpha}, \rho\} \right], \quad (4.56)$$

where $H = H^{\dagger}$ is a self-adjoint operator (which usually is given by the system Hamiltonian of the isolated quantum system plus some Lamb-shift corrections due to the system-reservoir interactions) and $\gamma_{\alpha\beta} = \gamma_{\beta\alpha}^*$ is a hermitian and **positive semidefinite** matrix

$$\sum_{\alpha\beta} x_{\alpha}^* \gamma_{\alpha\beta} x_{\beta} \geq 0 \quad (4.57)$$

with positive semidefinite eigenvalues. In the previous section, we have expressed these summations by double summations over energy eigenstates, i.e., $\sum_{\alpha} f_{\alpha} \hat{=} \sum_{ab} f_{ab}$.

From this form, it is immediately evident that trace and hermiticity of the density matrix ρ are preserved. To see that the above equation also preserves the positive definiteness of ρ , one may use that a hermitian density matrix has a spectral decomposition

$$\rho = \sum_{\tilde{a}} \rho_{\tilde{a}}(t) |\tilde{a}(t)\rangle \langle \tilde{a}(t)|, \quad (4.58)$$

where $\rho_{\tilde{a}}$ are the eigenvalues and the tilde is used to emphasize that the eigenstates of the density matrix need not coincide with the eigenstates of the system Hamiltonian. By evaluating the evolution of the eigenvalues, we get from $\langle \dot{\tilde{a}}|\tilde{a}\rangle + \langle \tilde{a}|\dot{\tilde{a}}\rangle = \frac{d}{dt} \langle \tilde{a}|\tilde{a}\rangle = 0$ (eigenstates are normalized) that the eigenvalues of the density matrix obey a rate equation

$$\begin{aligned} \dot{\rho}_{\tilde{b}} &= \sum_{\tilde{a}} \left(\sum_{\alpha\beta} \gamma_{\alpha\beta} \langle \tilde{b}|L_{\alpha}|\tilde{a}\rangle \langle \tilde{a}|L_{\beta}^{\dagger}|\tilde{b}\rangle \right) \rho_{\tilde{a}} - \left(\sum_{\tilde{a}} \sum_{\alpha\beta} \gamma_{\alpha\beta} \langle \tilde{b}|L_{\beta}^{\dagger}|\tilde{a}\rangle \langle \tilde{a}|L_{\alpha}|\tilde{b}\rangle \right) \rho_{\tilde{b}} \\ &= \sum_{\tilde{a}} R_{\tilde{a} \rightarrow \tilde{b}} \rho_{\tilde{a}} - \sum_{\tilde{a}} R_{\tilde{b} \rightarrow \tilde{a}} \rho_{\tilde{b}}, \end{aligned} \quad (4.59)$$

and in particular the requirement of positive definiteness leads to the insight that the transition rates are positive

$$R_{\tilde{a} \rightarrow \tilde{b}} = \sum_{\alpha\beta} \langle \tilde{a} | L_\alpha^\dagger | \tilde{b} \rangle^* \gamma_{\alpha\beta} \langle \tilde{a} | L_\beta^\dagger | \tilde{b} \rangle \geq 0. \quad (4.60)$$

Trace-preserving rate equations with positive transition rates however always preserve positivity of the eigenvalues $\rho_{\tilde{a}}$: If one of the eigenvalues approaches zero (while the others are still positive), its change will always be positive, such that its value can no longer decrease.

One can write the Lindblad equation in an even simpler form: By writing $L_\alpha = \sum_{\tilde{a}} u_{\alpha\tilde{a}} \tilde{K}_{\tilde{a}}$ with unitary $u_{\alpha\tilde{a}}$ we can choose to diagonalize the dampening matrix, yielding

$$\dot{\rho} = -i[H, \rho] + \sum_{\alpha} \gamma_{\alpha} \left[\tilde{K}_{\alpha} \rho \tilde{K}_{\alpha}^\dagger - \frac{1}{2} \{ \tilde{K}_{\alpha}^\dagger \tilde{K}_{\alpha}, \rho \} \right] \quad (4.61)$$

with $\gamma_{\alpha} \geq 0$ representing the eigenvalues of the positive definite density matrix. Even more, we can absorb the dampening coefficient in the jump operators $K_{\alpha} = \sqrt{\gamma_{\alpha}} \tilde{K}_{\alpha}$, yielding the simplest form of a **Lindblad equation**

$$\dot{\rho} = -i[H, \rho] + \sum_{\alpha} \left[K_{\alpha} \rho K_{\alpha}^\dagger - \frac{1}{2} \{ K_{\alpha}^\dagger K_{\alpha}, \rho \} \right] \equiv \mathcal{L} \rho, \quad (4.62)$$

where the calligraphic notation is conventionally used to mark a **superoperator**.

Specifically, Lindblad master equations that have a thermal stationary state [16]

$$\bar{\rho} = \frac{e^{-\beta H_S}}{\text{Tr} \{ e^{-\beta H_S} \}} \quad (4.63)$$

are sometimes also called **Lindblad-Davies** maps. Beyond the preservation of positivity, Lindblad equations obey a Spohn inequality

$$\sigma = -\text{Tr} \{ (\mathcal{L} \rho) [\ln \rho - \ln \bar{\rho}] \} \geq 0, \quad (4.64)$$

where $\mathcal{L} \bar{\rho} = 0$ defines a stationary solution. Specifically, when $\bar{\rho} = e^{-\beta H_S} / Z_S$ is thermal, the above inequality allows an interpretation as the second law via

$$\sigma = \frac{d}{dt} S_{\text{sys}} + \frac{d}{dt} S_{\text{res}} \geq 0, \quad (4.65)$$

such that σ can also be interpreted as **entropy production rate**.

Chapter 5

Adiabatic quantum computation

The previous approaches to quantum computation worked well when the system was isolated from its environment. One can try to make the gates significantly faster than the effects of decoherence and to use quantum error correction to compensate the coherence losses. This will presumably require enormous resources. Alternatively, one may try to engineer the interaction with the reservoir in a way that the environment even assists to bring the system into a desired state. For example, the stationary state of the Lindblad master equation could be a pure state with some desired properties. Unfortunately, the specifics of the interaction can hardly be controlled. Nevertheless, we have seen that at least under specific conditions (weak coupling, large system energy splitting, Markovian reservoir such that the Born-, Markov-, and secular approximations are applicable) the reservoir generically induces thermalization of the system. This allows for the solution of computational problems by encoding them into the ground state of a quantum system. When the reservoir temperature is low in comparison to the energy gap above the ground state $\beta\Omega \gg 1$, the system will be mainly in the ground state. For an N -dimensional Hilbert space we can estimate the thermal ground state occupation probability as

$$P_0 = 1 - P_1 - \dots - P_{N-1} \geq 1 - (N-1)P_1 = 1 - (N-1)e^{-\beta\Omega}P_0, \quad (5.1)$$

from which we get a lower bound

$$P_0 \geq \frac{1}{1 + (N-1)e^{-\beta\Omega}}. \quad (5.2)$$

Thereby, to achieve a sufficiently large occupation of the ground state, e.g. $P_0 \geq 1/2$, the inverse temperature in the worst case needs to scale only logarithmically in the Hilbert space dimension $\beta\Omega \geq \ln(N-1)$ (or linearly in the number of qubits).

It is therefore believed that a quantum computer encoding the solution to some computational problem in its well-gapped ground state could be less vulnerable to decoherence. With a Hamiltonian encoding the solution to some problem in its ground state, one could simply connect to a low temperature reservoir and wait until the system has cooled down. This however is not expected to be efficient in the weak-coupling limit where the master equations apply. Instead, it has been proposed to use the adiabatic theorem for computation, which works also in absence of dissipation:

- prepare the system in the ground state of a simple Hamiltonian (which can be easily reached by e.g. dissipative relaxation)
- slowly deform the simple Hamiltonian into the problem Hamiltonian

- measure the state properties and thereby get the solution.

To see how this works, we revisit the adiabatic theorem.

5.1 The adiabatic theorem for closed systems

We consider the time-dependent Schrödinger equation

$$|\dot{\Psi}\rangle = -iH(t)|\Psi(t)\rangle . \quad (5.3)$$

Here, $|\Psi(t)\rangle$ denotes the normalized wave function, where the normalization is preserved as long as the system Hamiltonian $H(t) = H^\dagger(t)$ is self-adjoint. In this sense, the results in this section apply to all time-dependent first order ODEs with a self-adjoint generator, which can be written in the form of Eq. (5.3).

Thanks to the hermiticity of $H(t)$, we can at each instant in time define an orthonormal energy eigenbasis of the instantaneous Hamiltonian

$$H(t)|n(t)\rangle = E_n(t)|n(t)\rangle . \quad (5.4)$$

Since the basis is complete $\sum_n |n(t)\rangle \langle n(t)| = \mathbf{1}$, we can always expand the state vector in this energy eigenbasis

$$|\Psi(t)\rangle = \sum_n a_n(t) \exp\left\{-i \int_0^t E_n(t') dt'\right\} |n(t)\rangle , \quad (5.5)$$

where $a_n(t) \in \mathbb{C}$ obey $\sum_n |a_n(t)|^2 = 1$ and where the exponential integral factor has just been introduced for convenience. The coefficients $a_n(t)$ tell us the distribution of the state vector over the different energy eigenstates. For example, the energy of the state is given by $\langle E \rangle = \sum_n E_n(t) |a_n(t)|^2$.

Inserting this in the Schrödinger equation one directly obtains a coupled system of ordinary differential equations for the coefficients

$$\dot{a}_m = - \sum_n a_n(t) \exp\left\{-i \int_0^t [E_n(t') - E_m(t')] dt'\right\} \langle m(t)|\dot{n}(t)\rangle . \quad (5.6)$$

Since we aim at an expression quantifying the transitions between different energy eigenstates, we pull the term with $n = m$ to the l.h.s., yielding

$$\begin{aligned} \dot{a}_m + a_m \langle m(t)|\dot{m}(t)\rangle &= - \sum_{n:n \neq m} a_n(t) \exp\left\{-i \int_0^t [E_n(t') - E_m(t')] dt'\right\} \langle m(t)|\dot{n}(t)\rangle \\ &= - \sum_{n:n \neq m} a_n(t) \exp\left\{-i \int_0^t [E_n(t') - E_m(t')] dt'\right\} \frac{\langle m(t)|\dot{H}|n(t)\rangle}{E_n(t) - E_m(t)} . \end{aligned} \quad (5.7)$$

In the last step, we have assumed that the system is non-degenerate, i.e., $E_n(t) \neq E_m(t)$, which enables one to obtain the used relation from the time derivative of equation (5.4). Multiplying both sides with $e^{-i\gamma_m(t)}$ with the **Berry phase**

$$\gamma_m(t) = i \int_0^t \langle m(t')|\dot{m}(t')\rangle dt' , \quad (5.8)$$

we can also write this as

$$\frac{d}{dt} (a_m e^{-i\gamma_m}) = - \sum_{n:n \neq m} a_n(t) e^{-i\gamma_m(t)} \exp \left\{ -i \int_0^t [E_n(t') - E_m(t')] dt' \right\} \frac{\langle m(t) | \dot{H} | n(t) \rangle}{E_n(t) - E_m(t)}. \quad (5.9)$$

Assuming that the r.h.s. is small (slow evolution), we aim at solving the equation perturbatively for slow evolutions. First, we formally integrate the equation, yielding

$$\begin{aligned} a_m(t) e^{-i\gamma_m(t)} - a_m^0 &= - \sum_{n:n \neq m} \int_0^t dt' a_n(t') e^{-i\gamma_m(t')} \exp \left\{ -i \int_0^{t'} [E_n(t'') - E_m(t'')] dt'' \right\} \times \\ &\quad \times \frac{\langle m(t') | \dot{H}(t') | n(t') \rangle}{E_n(t') - E_m(t')} \\ &= -i \sum_{n:n \neq m} \int_0^t dt' \frac{\langle m(t') | \dot{H}(t') | n(t') \rangle}{[E_n(t') - E_m(t')]^2} a_n(t') e^{-i\gamma_m(t')} \times \\ &\quad \times \frac{d}{dt'} \exp \left\{ -i \int_0^{t'} [E_n(t'') - E_m(t'')] dt'' \right\}, \end{aligned} \quad (5.10)$$

which we can solve for $a_m(t)$ on the l.h.s. and iteratively insert this on the r.h.s. However, provided that the **adiabaticity condition**

$$\left| \frac{\langle m(t') | \dot{H}(t') | n(t') \rangle}{[E_n(t') - E_m(t')]^2} \right| \ll 1 \quad (5.11)$$

holds for all times $0 < t' < t$, the evolution is adiabatic at all times, and we can completely neglect the r.h.s. above. In this case, the adiabatic evolution yields

$$a_m(t) \approx a_m^0 e^{+i\gamma_m(t)}. \quad (5.12)$$

Therefore, we see that for such slowly driven systems (in comparison to the energy gap), the coefficient $a_m(t)$ just acquires a phase factor, and effectively, the system remains in its instantaneous energy eigenstate. This is the essence of the adiabatic theorem: Slowly driven quantum systems that are initially in a particular energy eigenstate remain in the corresponding instantaneous energy eigenstate. In terms of a time-evolution operator, we could therefore approximate

$$U(t) \approx U_{\text{ad}}(t) = \sum_n e^{-i \int_0^t E_n(t') dt'} e^{+i\gamma_n(t)} |n(t)\rangle \langle n(0)|, \quad (5.13)$$

with the **Berry phase** $\gamma_n(t)$ and **dynamical phase** $\int_0^t E_n(t') dt'$. This decomposition however also shows that superpositions of initial energy eigenstates need not remain the same because the relative phase can change.

5.2 Adiabatic qubit control

For a qubit, parametrized by the time-dependent Hamiltonian

$$H(t) = \frac{\omega(t)}{2} \mathbf{n}(t) \cdot \boldsymbol{\sigma} \quad : \quad \mathbf{n} = \begin{pmatrix} \sin \theta(t) \cos \phi(t) \\ \sin \theta(t) \sin \phi(t) \\ \cos \theta(t) \end{pmatrix}, \quad (5.14)$$

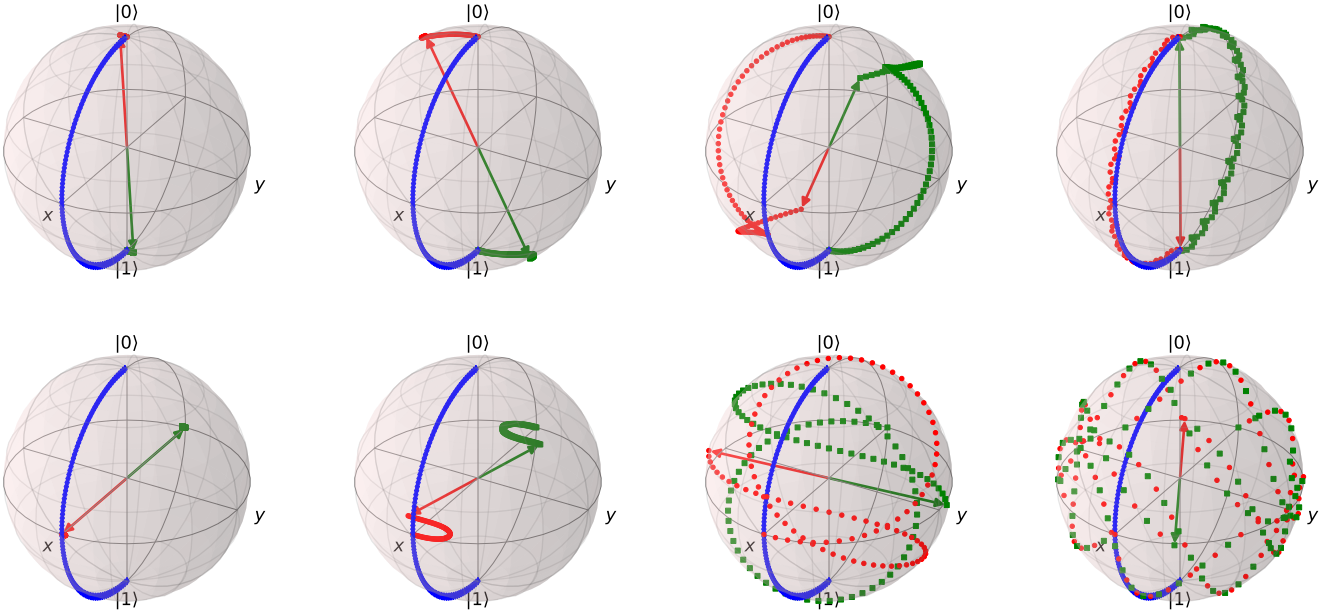


Figure 5.1: Bloch sphere evolution of specific initial states under the evolution parametrized by a time-dependent Hamiltonian (blue). From left to right, the evolution time is increased as $\omega T \in \{0.1, 1.0, 10.0, 100.0\}$, such that the rightmost panel in the top row indicates the adiabatic limit with the desired flip operation $|0\rangle \leftrightarrow |1\rangle$, and the leftmost panels indicate highly non-adiabatic evolution where the system cannot follow the Hamiltonian at all. The bottom row shows however that superpositions of eigenstates may pick up a relative phase even in the adiabatic limit, such that this adiabatic gate does not perform an X -gate operation.

we can directly compute the time-dependent energy eigenstates $n \in \{-, +\}$

$$\begin{aligned}
 E_-(t) &= -\frac{\omega(t)}{2}, & |-(t)\rangle &= \frac{\cos \theta(t) - 1}{\sqrt{2 - 2 \cos \theta(t)}} |0\rangle + \frac{e^{+i\phi(t)} \sin \theta(t)}{\sqrt{2 - 2 \cos \theta(t)}} |1\rangle, \\
 E_+(t) &= +\frac{\omega(t)}{2}, & |+(t)\rangle &= \frac{e^{-i\phi(t)} \sin \theta(t)}{\sqrt{2 - 2 \cos \theta(t)}} |0\rangle + \frac{1 - \cos \theta(t)}{\sqrt{2 - 2 \cos \theta(t)}} |1\rangle.
 \end{aligned} \tag{5.15}$$

The Berry phases become

$$\gamma_-(t) = - \int_0^t \cos^2 \left(\frac{\theta(t')}{2} \right) \dot{\phi}(t') dt' = -\gamma_+(t). \tag{5.16}$$

Considering the specific realization

$$\omega(t) = \omega, \quad \theta(t) = \pi \frac{t}{T}, \quad \phi(t) = 0, \tag{5.17}$$

such that $H(0) = \frac{\omega}{2} \sigma^z$ and $H(T) = -\frac{\omega}{2} \sigma^z$. With $|+(0)\rangle = |0\rangle$ and $|-(0)\rangle = |1\rangle$ and $|+(T)\rangle \propto |1\rangle$ and $|-(T)\rangle \propto |0\rangle$, we see that a sufficiently slow evolution transforms $|0\rangle \rightarrow |1\rangle$ and vice versa as shown in Fig. 5.1. However, care should be taken when one considers superpositions of energy eigenstates. These may pick up relative geometric and dynamical phase factors. In this case, the resulting dynamical phase yields in the adiabatic limit the solutions $\Psi(T) \approx \frac{1}{\sqrt{2}} [|0\rangle \pm e^{-i\omega T} |1\rangle]$.

5.3 Adiabatic control in presence of thermal dissipation

For a time-dependent Hamiltonian, an exact master equation is not so simple to get, since already the transformation into the interaction picture is non-trivial. However, explicit forms can be derived when the evolution is adiabatic. The transformation into the interaction picture can in the adiabatic limit be written as

$$\mathbf{H}_I(t) = U_{\text{ad}}^\dagger(t) e^{+iH_B t} H_I e^{-iH_B t} U_{\text{ad}}(t) = U_{\text{ad}}^\dagger(t) S U_{\text{ad}}(t) \otimes e^{+iH_B t} B e^{-iH_B t}, \quad (5.18)$$

with the adiabatic time evolution operator (5.13). Provided that the slow driving does not increase the effective system-reservoir coupling nor speed up the system dynamics, Born- and Markov approximations can be performed in analogy, since the evolution of bath coupling operators $\mathbf{B}(t)$ is fully analogous to the undriven case. We therefore directly start from the Redfield-II equation (4.41) in the interaction picture

$$\begin{aligned} \dot{\rho} = & \int_0^\infty C(+\tau) [\mathbf{S}(t-\tau) \rho(t) \mathbf{S}(t) - \mathbf{S}(t) \mathbf{S}(t-\tau) \rho(t)] d\tau \\ & + \int_0^\infty C(-\tau) [\mathbf{S}(t) \rho(t) \mathbf{S}(t-\tau) - \rho(t) \mathbf{S}(t-\tau) \mathbf{S}(t)] d\tau. \end{aligned} \quad (5.19)$$

Now inserting the adiabatic time evolution operator

$$\begin{aligned} \mathbf{S}(t) &= U_{\text{ad}}^\dagger(t) S U_{\text{ad}}(t) = \sum_{ab} e^{+i \int_0^t [E_a(t') - E_b(t')] dt'} e^{-i[\gamma_a(t) - \gamma_b(t)]} \langle a(t) | S | b(t) \rangle \cdot |a(0)\rangle \langle b(0)|, \\ \mathbf{S}(t-\tau) &= \sum_{cd} e^{+i \int_0^{t-\tau} [E_c(t') - E_d(t')] dt'} e^{-i[\gamma_c(t-\tau) - \gamma_d(t-\tau)]} \langle c(t-\tau) | S | d(t-\tau) \rangle \cdot |c(0)\rangle \langle d(0)| \\ &= \sum_{cd} e^{+i \int_0^t [E_c(t') - E_d(t')] dt'} e^{-i \int_{t-\tau}^t [E_c(t') - E_d(t')] dt'} e^{-i[\gamma_c(t) - \gamma_d(t)]} e^{+i^2 \int_{t-\tau}^t [\langle c(t') | \dot{c}(t') \rangle - \langle d(t') | \dot{d}(t') \rangle] dt'} \times \\ &\quad \times \langle c(t-\tau) | S | d(t-\tau) \rangle \cdot |c(0)\rangle \langle d(0)| \\ &\approx \sum_{cd} e^{+i \int_0^t [E_c(t') - E_d(t')] dt'} e^{-i\tau [E_c(t) - E_d(t)]} e^{-i[\gamma_c(t) - \gamma_d(t)]} \langle c(t) | S | d(t) \rangle \cdot |c(0)\rangle \langle d(0)|, \end{aligned} \quad (5.20)$$

where in the last line we have performed approximations similar to a third Markov approximation, meaning that the dominant contribution to the integral arises always when τ is small: Then, we can write $\int_{t-\tau}^t E_c(t') dt' \approx \tau E_c(t)$, $\int_{t-\tau}^t \langle c(t') | \dot{c}(t') \rangle dt' \approx 0$, and $|c(t-\tau)\rangle \approx |c(t)\rangle$. The secular approximation can now be performed in a similar fashion, yielding the neglect of all terms where a t -dependence remains [17]. Upon transferring back to the Schrödinger picture, we get the same master equation (4.49), just in the time-dependent system energy eigenbasis

$$\begin{aligned} \dot{\rho} = & -i \left[H_S(t) + \sum_{ab} \delta_{\tilde{E}_a(t), \tilde{E}_b(t)} S_{cb}(t) S_{ac}(t) \frac{\sigma(E_b(t) - E_c(t))}{2i} L_{ab}(t), \rho \right] \\ & + \sum_{abcd} \delta_{\tilde{E}_b(t) - \tilde{E}_a(t), \tilde{E}_d(t) - \tilde{E}_c(t)} S_{ab}(t) S_{dc}(t) \gamma(E_b(t) - E_a(t)) \left[L_{ab}(t) \rho L_{cd}^\dagger(t) - \frac{1}{2} \left\{ L_{cd}^\dagger(t) L_{ab}(t), \rho \right\} \right]. \end{aligned} \quad (5.21)$$

Here, the \sim symbols just mark that the averaging procedure is over the more complicated exponential factors. The net effect is that we get the conventional BMS equation, just with the time-dependent parameters of the Hamiltonian inserted a posteriori. Nevertheless, the above derivation

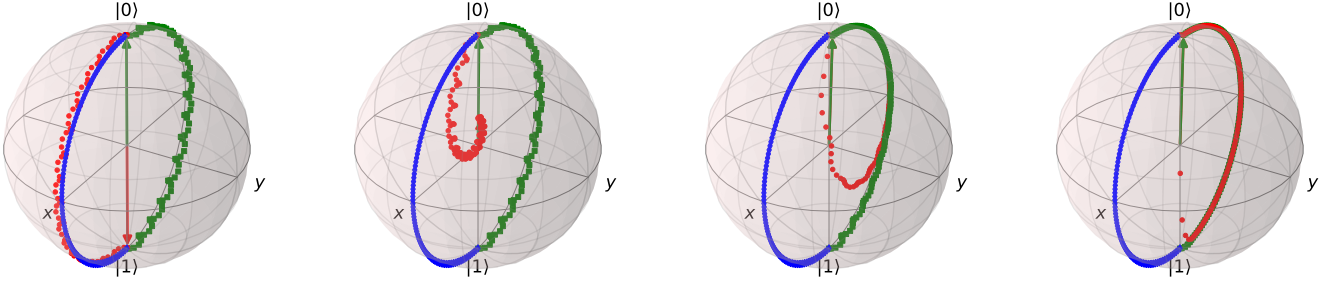


Figure 5.2: Evolution under the same time-dependent Hamiltonian like in Fig. 5.1, but now for fixed runtime $\omega T = 100$ (adiabatic limit) and low temperature $\beta\omega = 10$ and from left-to right increasing dissipation strength $\gamma = |S_{-+}(t)|^2\gamma(E_+(t) - E_-(t)) \in \{0, 0.01, 0.1, 1.0\}\omega$. Whereas the low-temperature dissipation improves the ground state (green) fidelity, it quickly destroys the fidelity of the excited state (red).

is not really rigorous, one could have performed the approximations in a slightly different fashion and would end up with a different master equation. For just two levels the above master equation would become

$$\begin{aligned} \dot{\rho} = & -i[H_S(t) + \sigma_{--}(t)|-(t)\rangle\langle-(t)| + \sigma_{++}(t)|+(t)\rangle\langle+(t)|, \rho] \\ & + |S_{-+}(t)|^2\gamma(E_+(t) - E_-(t)) \left[L_{-+}(t)\rho L_{-+}^\dagger(t) - \frac{1}{2} \{L_{-+}(t)L_{-+}^\dagger(t), \rho\} \right] \\ & + |S_{+-}(t)|^2\gamma(E_-(t) - E_+(t)) \left[L_{+-}(t)\rho L_{+-}^\dagger(t) - \frac{1}{2} \{L_{+-}(t)L_{+-}^\dagger(t), \rho\} \right]. \end{aligned} \quad (5.22)$$

The qualitative effect of this is that at low temperatures, the evolution of the ground state is protected against thermal dissipation, whereas the excited state evolution is not, see Fig. 5.2. It follows that under a thermalizing dissipator, only a (well-gapped) ground state can be protected against the influence of decoherence. So instead of trying to apply unitary gates to a fragile quantum state, can we encode the solution to difficult problems into the ground state of an interacting Hamiltonian? The answer is affirmative, but what is the scaling behaviour of such an adiabatic quantum computer? We shall try to understand this below.

5.4 The adiabatic Grover search

There is an adiabatic analogue of the Grover search algorithm, and it also makes use of an oracle Hamiltonian

$$H_F = \Omega[\mathbf{1} - |W\rangle\langle W|], \quad (5.23)$$

where $|W\rangle$ marks a superposition of all solutions to a search problem and Ω is some global energy scale. Like before, we stress that by merely writing this Hamiltonian in a projector form, we do not require the state $|W\rangle$ to be known beforehand. Rather, we know certain properties of the solution, and the above projector gives an eigenvalue 0 to the solution and assigns an energy penalty $+\Omega$ to all non-solutions. The adiabatic Grover search [18] consists of a linear interpolation

$$H(t) = [1 - s(t)]H_I + s(t)H_F \quad (5.24)$$

between the final (problem) Hamiltonian and some initial Hamiltonian

$$H_I = \Omega[\mathbf{1} - |S\rangle\langle S|], \quad (5.25)$$

where $|S\rangle$ is the superposition of all computational basis states, with variable speed, expressed by the function

$$s(t) \quad : \quad s(0) = 0 = 1 - s(T). \quad (5.26)$$

The implementation of such projection operators may require many-qubit interactions, as is visible via

$$\begin{aligned} |S\rangle\langle S| &= \frac{1}{2}[\mathbf{1} + \sigma^x] \otimes \dots \otimes \frac{1}{2}[\mathbf{1} + \sigma^x], \\ |W\rangle\langle W| &= \frac{1}{2}[\mathbf{1} + (-1)^{W_1}\sigma^z] \otimes \dots \otimes \frac{1}{2}[\mathbf{1} + (-1)^{W_n}\sigma^z]. \end{aligned} \quad (5.27)$$

By analyzing the spectrum of the complete model, we will see that we will need to adapt the time-dependent evolution speed. The spectrum in turn can be computed analytically, where we first note that

$$\langle W|S\rangle = \sqrt{\frac{M}{N}} \equiv \sqrt{\alpha}, \quad (5.28)$$

where N is the dimension of the (Hilbert) search space and M is the number of solutions. We can introduce the orthonormal basis $\{|W\rangle, |W_\perp\rangle, \dots\}$, where the first non-trivial vector is given by

$$|W_\perp\rangle = \frac{|S\rangle - \langle W|S\rangle|W\rangle}{\sqrt{1 - |\langle W|S\rangle|^2}}, \quad (5.29)$$

and the remaining basis vectors are chosen orthonormal in some arbitrary order (this is known as Gram-Schmidt orthonormalization procedure). Like in Eq. (3.70), we can also express the full superposition state by solution states $|W\rangle$ and non-solution states $|W_\perp\rangle$

$$|S\rangle = \sqrt{1 - \frac{M}{N}}|W_\perp\rangle + \sqrt{\frac{M}{N}}|W\rangle. \quad (5.30)$$

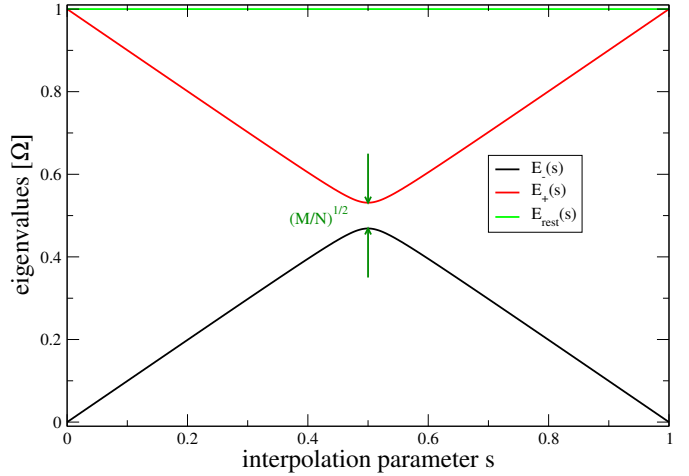
With this, we can write the total Hamiltonian with $\alpha \equiv \frac{M}{N}$ as

$$\begin{aligned} H(s)/\Omega &= \mathbf{1} - (1-s)|S\rangle\langle S| - s|W\rangle\langle W| \\ &= \mathbf{1} - ((1-s)\alpha + s)|W\rangle\langle W| - (1-s)(1-\alpha)|W_\perp\rangle\langle W_\perp| \\ &\quad - (1-s)\sqrt{\alpha(1-\alpha)}[|W_\perp\rangle\langle W| + |W\rangle\langle W_\perp|]. \end{aligned} \quad (5.31)$$

In the new basis, the Hamiltonian has the matrix representation

$$H(s)/\Omega = \left(\begin{array}{cc|ccc} 1 - [(1-s)\alpha + s] & -(1-s)\sqrt{\alpha(1-\alpha)} & & & \\ -(1-s)\sqrt{\alpha(1-\alpha)} & 1 - (1-s)(1-\alpha) & & & \\ \hline & & 1 & & \\ & & & \ddots & \\ & & & & 1 \end{array} \right), \quad (5.32)$$

Figure 5.3: Spectrum of the adiabatic Grover Hamiltonian (5.31) as a function of the interpolation parameter s for $n = 8$ qubits leading to a search space dimension of $N = 2^n = 256$ and a single solution $M = 1$.



and we see that only the top 2×2 block creates non-trivial eigenvalues (black spaces indicate zeroes)

$$E_{\pm}(s) = \frac{\Omega}{2} \left[1 \pm \sqrt{1 - (1 - \alpha)4s(1 - s)} \right], \quad (5.33)$$

whereas the remaining eigenvalues remain at $E_{\text{rest}} = \Omega$. From this, we find that there is an avoided crossing at $s = 1/2$ with a minimum energy gap

$$g_{\min} = E_{+}(1/2) - E_{-}(1/2) = \Omega\sqrt{\alpha} = \Omega\sqrt{\frac{M}{N}}, \quad (5.34)$$

see also Fig. 5.3. This shows, that to remain adiabatic, the evolution speed needs to be adapted near the position of the minimum energy gap. In a more detailed fashion, for a general interpolation speed $s(t)$ we get

$$\begin{aligned} \frac{d}{dt}H(s(t)) &= \Omega\dot{s}(t) [|S\rangle\langle S| - |W\rangle\langle W|] \\ &= \Omega\dot{s} \left[(1 - \alpha) |W_{\perp}\rangle\langle W_{\perp}| + (\alpha - 1) |W\rangle\langle W| + \sqrt{\alpha(1 - \alpha)} (|W_{\perp}\rangle\langle W| + |W\rangle\langle W_{\perp}|) \right]. \end{aligned} \quad (5.35)$$

A more detailed analysis of the eigenvectors now shows that at the critical point

$$\langle E_{-}(s) | \dot{H} | E_{+}(s) \rangle |_{s=1/2} = \Omega\dot{s}(1/2)\sqrt{1 - \alpha}. \quad (5.36)$$

This means that with a constant speed interpolation with adiabatic runtime T

$$s(t) = \frac{t}{T} \quad (5.37)$$

we need – to satisfy the adiabaticity condition (5.11) also in the vicinity of the minimum gap – to scale the adiabatic runtime as

$$T \propto \frac{N}{M}. \quad (5.38)$$

Therefore, for constant interpolation speed there is no speedup in comparison to classical search algorithms.

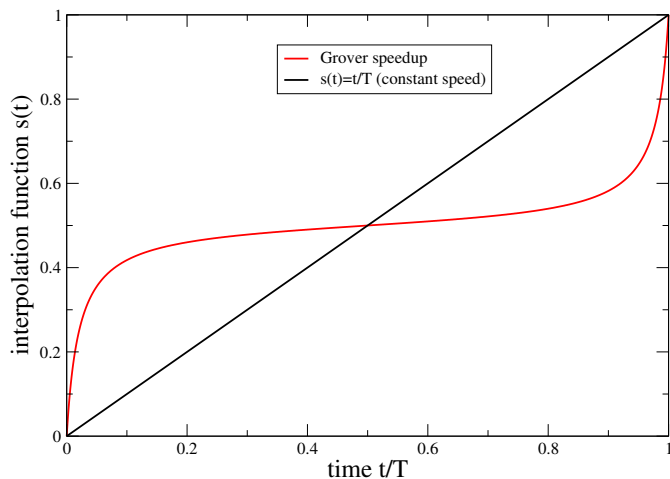


Figure 5.4: Plot of interpolation functions $s(t)$ vs. dimensionless time t/T . The black line corresponds to a ramp with constant speed, whereas the red curve is defined by (5.39) for $\alpha = 1/2^8$ and $\sigma\Omega = 1.0$.

Another approach considers a variable interpolation speed, given by the solution to the differential equation

$$\dot{s} = \sigma g^2(s) = \sigma\Omega^2 [1 - (1 - \alpha)4s(1 - s)] \quad : \quad s(0) = 0, \quad (5.39)$$

with a small constant σ and the adiabatic runtime implicitly defined via $s(T) = 1$. This has the advantage that in the adiabaticity condition (5.11), the dependence on the energy gap cancels. However, to reach $s(T) = 1$, we have to satisfy the condition (separate the variables in the above equation)

$$\int_0^1 \frac{ds}{1 - (1 - \alpha)4s(1 - s)} = \sigma\Omega^2 T = \frac{\arctan(\sqrt{1/\alpha - 1})}{\sqrt{\alpha(1 - \alpha)}} \approx \frac{\pi}{2} \frac{1}{\sqrt{\alpha}}. \quad (5.40)$$

Therefore, the adiabatic runtime will need to scale as

$$T \propto \sqrt{\frac{N}{M}}, \quad (5.41)$$

which reproduces the original Grover search scaling with an adiabatic algorithm. Effectively, this just requires slow speeds near the minimum energy gap to maintain the adiabaticity and fast speeds in regions where the gap is large to obtain a short overall runtime, compare Fig. 5.4.

5.5 Adiabatic approaches to an NP-complete problem

The previous example of Grover search may seem a bit hard to implement, considering that to implement the projection operators, one requires n -qubit interactions, whereas physically realistic models have at most two-body interactions. Nevertheless, they can be understood as effective Hamiltonians. An example where it is quite straightforward to construct a final problem Hamiltonian with only few-body interactions that nevertheless encode a solution to some non-trivial problem in their ground state is the problem class 3-SAT. The **3-SAT problem** (from 3-satisfiability) is a search problem for an n -bit bitstring $b_1 \dots b_n$ with $b_i \in \{0, 1\}$ that fulfills a set of constraints (clauses) that involve three bits each. These constraints can be of very different nature, and given a set of constraints, it is classically extremely hard to find a solution satisfying all the constraints (which do of course overlap). However, given a candidate solution bitstring, it is a matter of $\mathcal{O}(m)$

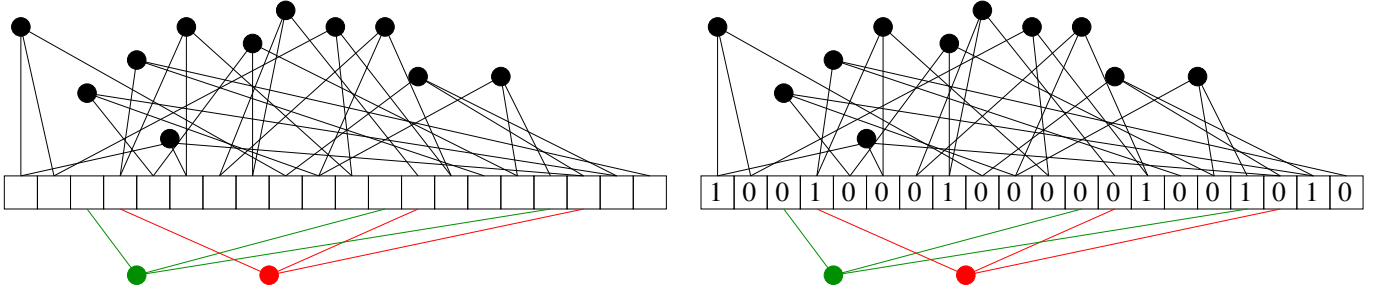


Figure 5.5: Example EC3 problem for 20 bits (boxes) and 13 clauses involving three different bits each (spheres with legs). There exists only a unique satisfying solution for all clauses (right), where the sum of bits belonging to every clause equals one. This solution however is very hard to find and essentially requires brute force methods with exponential runtime in the number of bits. In general, there is no known classical algorithm that finds solutions to such problems in a time that scales polynomially in the number of bits.

operations to check whether the bitstring fulfils the search problem. The problem is part of the problem class NP (for non-deterministic polynomial). Even more, it is even NP-complete, meaning that any problem in NP (e.g. factoring) can be mapped to 3-SAT with a polynomial overhead. This implies that if an efficient (scaling polynomially in the size of the problem) algorithm for an NP-complete problem was known, all other problems in the NP problem class could be solved with polynomial effort.

To make things simpler, we consider only a special case of a 3-SAT problem called **EC-3** (from exact-cover 3), which is also NP-complete. It is defined by

- m intersecting conditions on an unknown n -bit bitstring $b_1 \dots b_n : b_i \in \{0, 1\}$
- each condition C_i ($1 \leq i \leq m$) involves three (different) bits $C_i = (p_i^1, p_i^2, p_i^3) : 1 \leq i \leq m$ with $1 \leq p_i^\alpha \leq n$
- problem: find the bitstring that fulfils for all constraints

$$b_{p_i^1} + b_{p_i^2} + b_{p_i^3} = 1 \quad (5.42)$$

The problem seems trivial if one has only three bits $b_1 b_2 b_3$. In this case, there are 8 possible states, there is only one clause $C_1 = (1, 2, 3)$ and there are three solutions 100, 010, 001. However, things become difficult for larger problems when the clauses overlap. For a 20 bits with 13 clauses, this is exemplified in Fig. 5.5. One may now wonder how to encode the solution to such a problem in the ground state of a Hamiltonian. Since it is part of the problem class NP, this does not require to know the solution, we just need to know its local properties, i.e., for an EC3 problem we need to know the clauses that the solution has to satisfy. With this knowledge, we can build an energy penalty Hamiltonian with just two-body spin-spin interactions [19]

$$\begin{aligned} H_F &= \sum_{c=1}^m \Omega \left[\mathbf{1} - \hat{z}_{p_c^1} - \hat{z}_{p_c^2} - \hat{z}_{p_c^3} \right]^2 = \sum_{c=1}^m \Omega \left[\mathbf{1} - \frac{1}{2} \left(\mathbf{1} - \sigma_{p_c^1}^z \right) - \frac{1}{2} \left(\mathbf{1} - \sigma_{p_c^2}^z \right) - \frac{1}{2} \left(\mathbf{1} - \sigma_{p_c^3}^z \right) \right]^2 \\ &= \Omega \left[m\mathbf{1} - \sum_{i=1}^n \frac{n_i}{2} \sigma_i^z + \sum_{i,j=1}^n \frac{n_{ij}}{4} \sigma_i^z \sigma_j^z \right], \end{aligned} \quad (5.43)$$

where m is the total number of clauses, n_i is the number of clauses that involve the i th bit, and n_{ij} is the number of clauses that involve the bits i and j . These parameters can be determined in polynomial time. The ground state of the Hamiltonian violates the fewest constraints since the individual terms are positive semidefinite. Actually, if solution(s) exist, the ground state manifold will violate no constraint at all. If no solutions exist, the ground state manifold will be composed of states that violate the smallest number of constraints. For a violation of a clause, one gets an energy penalty of either Ω (for the configurations 000, 011, 101, 110) or even 4Ω (for the configuration 111), so one knows that the ground state is well-gapped by at least Ω from the excited states. If there exists a solution to the search problem, it will violate no clause and will end up at energy zero. Known classical minimization algorithms are not efficient and will get stuck in local minima.

The adiabatic quantum computing approach in contrast only requires an initial Hamiltonian whose ground state can be easily prepared

$$H_I = \Omega \sum_{i=1}^n \frac{1}{2} [1 - \sigma_i^x]. \quad (5.44)$$

The ground state of this Hamiltonian is just the superposition state of all states in the computational basis

$$|S\rangle = \frac{1}{\sqrt{2}}[|0\rangle + |1\rangle] \otimes \dots \otimes \frac{1}{\sqrt{2}}[|0\rangle + |1\rangle], \quad (5.45)$$

By interpolating with a constant speed interpolation between such Hamiltonians

$$H(t) = [1 - s(t)] H_I + s(t) H_F \quad : \quad s(t) = \frac{t}{T}, \quad (5.46)$$

a seminal numerical study [20] did reveal quite favorable scaling behaviours. The way such an adiabatic algorithm works is depicted in Fig. 5.6. One can see that during the evolution, there exists a minimum energy gap, and to remain adiabatic all the time, we have to satisfy the adiabaticity condition also at the minimum gap. From the maximum eigenvalues of the Hamiltonians we get the bound

$$\left| \langle E_n(t) | \dot{H} | E_m(t) \rangle \right| \leq \dot{s} |\langle E_n(t) | H_I | E_m(t) \rangle| + \dot{s} |\langle E_n(t) | H_F | E_m(t) \rangle| \leq \dot{s} \Omega (n + 4m) = \frac{(n + 4m)\Omega}{T}, \quad (5.47)$$

which shows that the scaling of the matrix element in the adiabatic condition (5.11) is not very dramatic. Solving for the runtime, we get

$$T \gg \frac{(n + 4m)\Omega}{g_{\min}^2}, \quad (5.48)$$

where g_{\min} denotes the minimum energy gap encountered during the evolution (which also scales as Ω). The main obstacle is therefore how the minimum energy gap scales with the problem size n . In particular, for the naive approach it has been argued that at least for some problems one may always encounter an exponentially small energy gap in the system size [22].

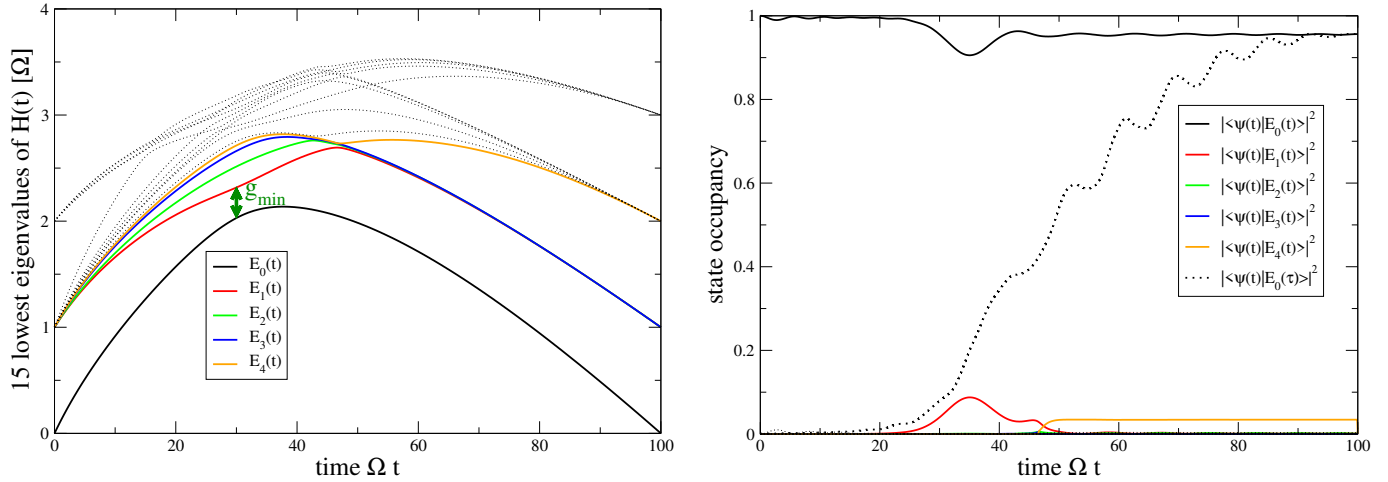


Figure 5.6: Left: Typical spectrum for an EC3 problem with 10 qubits, adapted from Ref. [21]. For initial and final Hamiltonian, there is a well-gapped ground state, but in between the evolution, there exists a smaller energy gap that determines the complexity of the adiabatic algorithm. Right: Plot of the corresponding overlap between state $|\Psi(t)\rangle$ and the corresponding instantaneous eigenstate of the time-dependent Hamiltonian $|E_n(t)\rangle$. The dotted curve shows the overlap with the final ground state $|E_0(T)\rangle$.

5.6 An adiabatic adder

To engineer an adiabatic algorithm that encodes the sum of two given binary numbers $x_1 \dots x_n$ and $y_1 \dots y_n$ with n digits in the ground state of a multi-qubit Hamiltonian, we can consider the binary summation scheme as shown in the table below:

x_1	\dots	x_{n-1}	x_n	
y_1	\dots	y_{n-1}	y_n	
c_1	c_2	\dots	c_n	.
z_1	z_2	\dots	z_n	z_{n+1}

Here, $z_1 \dots z_{n+1}$ encode the bits of the result of the summation, and $c_1 \dots c_n$ the possible carries. These carries can for example be represented by auxiliary bits. Accordingly, we have to fulfil the equations

$$\begin{aligned}
 z_{n+1} &= x_n + y_n - 2x_n y_n = x_n + y_n - 2c_n, \\
 c_n &= x_n y_n, \\
 &\vdots \\
 z_\ell &= \frac{1}{2} [1 - (1 - 2x_{\ell-1})(1 - 2y_{\ell-1})(1 - 2c_\ell)] & : & \quad 2 \leq \ell \leq n, \\
 c_{\ell-1} &= x_{\ell-1} y_{\ell-1} + [x_{\ell-1} + y_{\ell-1} - 2x_{\ell-1} y_{\ell-1}] c_\ell & : & \quad 2 \leq \ell \leq n, \\
 &\vdots \\
 z_1 &= c_1.
 \end{aligned} \tag{5.49}$$

We see immediately that it would be straightforward to eliminate some of the carries, but for illustrational purposes we will keep them. To promote this into an adiabatic ground state search

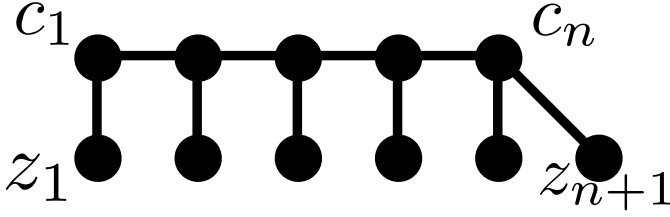


Figure 5.7: Sketch of the required two-body interactions (lines) between qubits (dots) for $n = 5$ to implement the problem Hamiltonian for an adiabatic adder.

problem, we advance the carry bits and the solution bits to operators

$$\begin{aligned} z_\ell &\rightarrow \hat{z}_\ell = \frac{1}{2} [\mathbf{1} - \sigma_\ell^z], \\ c_\ell &\rightarrow \hat{c}_\ell = \frac{1}{2} [\mathbf{1} - \sigma_{n+1+\ell}^z] \end{aligned} \quad (5.50)$$

while x_ℓ and y_ℓ remain numbers that are defined by the integers we would like to add. The (unique) solution is found by fulfilling all the above $2n + 1$ equations. If a particular combination $\{z_\ell, c_\ell\}$ violates any of these equations, it is no solution. Therefore, to construct an energy penalty Hamiltonian for violating an equation, we write the above summation equations into the form $0 = f_i(\{x_j, y_j, \hat{z}_j, \hat{c}_j\})$ and – since f_i is a hermitian observable with real eigenvalues – we get a positive semidefinite Hamiltonian by adding the appropriate penalties as

$$\begin{aligned} H_F(x, y) &= \Omega [\hat{z}_{n+1} - x_n - y_n + 2\hat{c}_n]^2 + \Omega [\hat{c}_n - x_n y_n]^2 \\ &\quad + \dots + \Omega \left[\hat{z}_\ell - \frac{1}{2} [1 - (1 - 2x_{\ell-1})(1 - 2y_{\ell-1})(1 - 2\hat{c}_\ell)] \right]^2 \\ &\quad + \Omega [\hat{c}_{\ell-1} - x_{\ell-1} y_{\ell-1} - [x_{\ell-1} + y_{\ell-1} - 2x_{\ell-1} y_{\ell-1}] \hat{c}_\ell]^2 \\ &\quad + \dots + \Omega [\hat{z}_1 - \hat{c}_1]^2 \\ &= \Omega [\hat{z}_{n+1} + 2\hat{c}_n - x_n - y_n]^2 + \Omega [\hat{c}_n - x_n y_n]^2 + \Omega [\hat{z}_1 - \hat{c}_1]^2 \\ &\quad + \Omega \sum_{\ell=2}^n \left[\hat{z}_\ell - (1 - 2x_{\ell-1})(1 - 2y_{\ell-1})\hat{c}_\ell - \frac{1}{2} [1 - (1 - 2x_{\ell-1})(1 - 2y_{\ell-1})] \right]^2 \\ &\quad + \Omega \sum_{\ell=2}^n [\hat{c}_{\ell-1} - [x_{\ell-1} + y_{\ell-1} - 2x_{\ell-1} y_{\ell-1}] \hat{c}_\ell - x_{\ell-1} y_{\ell-1}]^2, \end{aligned} \quad (5.51)$$

where Ω is some energy scale. This construction yields a final Hamiltonian that consists of two-body interactions at most (i.e., of terms linear and quadratic in the Pauli matrices) and comes with the promise that any non-solution gets an energy penalty of at least Ω . The interaction topology of the above penalty Hamiltonian is sketched in Fig. 5.7. It follows that for an adiabatic adder, as the number of qubits is increased, only neighbouring qubits need to be coupled to each other. When we combine this with the same initial Hamiltonian as used before

$$H_I = \sum_{i=1}^{2n-1} \frac{1}{2} [\mathbf{1} - \sigma_i^x], \quad (5.52)$$

a straight-line interpolation between the two Hamiltonians

$$H(t) = [1 - s(t)]H_I + s(t)H_F \quad : \quad s(t) = \frac{t}{T} \quad (5.53)$$

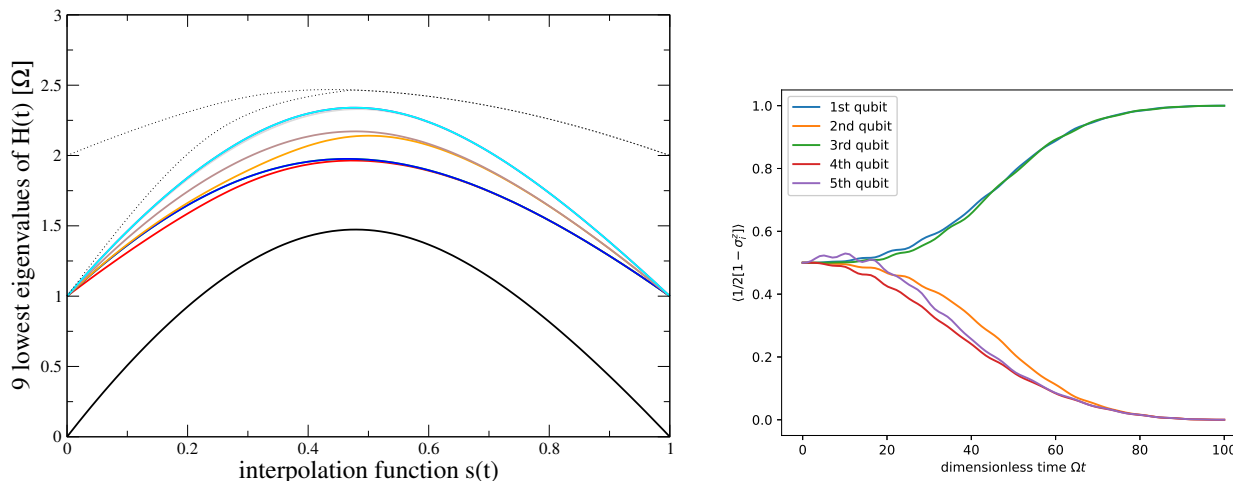


Figure 5.8: Adiabatic performance of an adder algorithm computing the sum of $1001 + 1011 = 10100$. The left panel shows only a very mild gap reduction during the course of the computation. The right panel shows the evolution of $\langle z_j \rangle = \langle \frac{1}{2}[\mathbf{1} - \sigma_j^z] \rangle$ for the first five qubits $1 \leq j \leq 5$ (which encode the solution) in the adiabatic limit $\Omega T = 100$. Altogether, we need 9 qubits (5 encoding the solution and 4 for the carry bits). The initial ground state is $|S\rangle$, and the final ground state for this example is $|10100|1011\rangle$.

reveals a smoothly varying spectrum, see Fig. 5.8 left panel. Accordingly, when we prepare the system in the initial ground state $|S\rangle$ and evolve adiabatically the time, at the end of the computation the system will be in the final ground state

$$|\Psi_0(t = T)\rangle = |z|c\rangle, \quad (5.54)$$

and a measurement of σ_j^z would reveal the solution and the carry bits.

5.7 An adiabatic multiplier

In a similar way one can proceed if one would like to multiply two binary numbers $x_1 \dots x_n$ and $y_1 \dots y_m$, where without loss of generality we can assume that $m \leq n$. Then, one can use that bitwise multiplication can be reduced to single-bit multiplication and subsequent addition, as exemplified by the bitwise multiplication table for multiplying two four-bit numbers:

$$\begin{array}{r} 1\ 0\ 0\ 1 \cdot 1\ 0\ 1\ 1 \\ \hline 1\ 0\ 0\ 1 \\ 0\ 0\ 0\ 0 \\ 1\ 0\ 0\ 1 \\ 1\ 0\ 0\ 1 \\ \hline 1\ 1\ 0\ 0\ 0\ 1\ 1 \end{array}$$

Here, we first multiply the n bits of the first number with the bit y_i of the second number, yielding in total m numbers with n bits each

$$\begin{aligned} \mathbf{z}_1 &= (x_1 y_1, x_2 y_1, \dots, x_n y_1), \\ &\vdots \end{aligned} \quad (5.55)$$

$$\mathbf{z}_m = (x_1 y_m, x_2 y_m, \dots, x_n y_m). \quad (5.56)$$

Afterwards, the result is obtained by just adding these m numbers, appropriately shifted by one digit

$$z = 2^{m-1}z_1 + 2^{m-2}z_2 + \dots + 2z_{m-1} + z_m. \quad (5.57)$$

Since the multiplication with 2^α is just a shift, this can be broken up into $m - 1$ additions, e.g. for the previous example these would be written as

$$\begin{array}{r} 1 \ 0 \ 0 \ 1 \ \cdot \ 1 \ 0 \ 1 \ 1 \\ \hline 1 \ 0 \ 0 \ 1 \\ \quad 0 \ 0 \ 0 \ 0 \\ \hline 1 \ 0 \ 0 \ 1 \ 0 \\ \quad \quad 1 \ 0 \ 0 \ 1 \\ \hline 1 \ 0 \ 1 \ 1 \ 0 \ 1 \\ \quad \quad \quad 1 \ 0 \ 0 \ 1 \\ \hline 1 \ 1 \ 0 \ 0 \ 0 \ 1 \ 1 \end{array}$$

The first addition concerns an n -bit and an $n + 1$ -bit number, so we write it as the sum of two $n + 1$ bit numbers, which requires with the previous section $(n + 2) + (n + 1) = 2n + 3$ bits (intermediate result of the sum and the carries). The next addition concerns two $n + 2$ -bit numbers, requiring $2n + 5$ bits, and so on. Altogether, one can see that the number of auxiliary bits required to implement multiplication scales quadratically. To convert this into an adiabatic quantum algorithm, we leave $x_1 \dots x_n$ and $y_1 \dots y_m$ as numbers and promote the unknown ancillas (intermediate results and carry bits) to operators. It is then straightforward to write down explicit quadratic expressions that fine a violation of an equation with an energy penalty of at least Ω . The final Hamiltonian then encodes the solution of all ancillas and the final product in its multi-qubit ground state, and in total, it can be implemented with two-body interactions only (i.e., involving only products of at most two Pauli matrices at once).

Finally, we also note that the problem can be reversed to approach the factoring problem [21]. If we are given a biprime $z_1 \dots z_n$, we have the promise that it can be written as the product of just two integers. Thereby we can first choose the partition $z = \mathbf{x} \cdot \mathbf{y}$ with an $n - k$ -digit number \mathbf{x} and a k -digit number \mathbf{y} and set up the factorization equations as before. The only difference is now that z_i remain numbers and x_i and y_i become operators.

5.8 The 1d quantum Ising model in a transverse field

The quantum Ising model in a transverse field for n spins

$$H = -g \sum_{i=1}^n \sigma_i^x - J \sum_{i=1}^n \sigma_i^z \sigma_{i+1}^z, \quad n \text{ even} \quad (5.58)$$

where $g \propto B$ describes the coupling to an external magnetic field in \mathbf{x} -direction, J the inter-chain coupling to nearest neighbors, and periodic boundary conditions are assumed $\sigma_{n+1}^z \equiv \sigma_1^z$ is a paradigmatic model to describe quantum-critical behaviour [23]. Although rather a technical constraint, we note explicitly that we consider here only the case where n is even. The model is analytically diagonalizable for finite n and displays a second order quantum phase transition at $g = J$. One can distinguish easily the behaviour in the simple cases where one coefficient vanishes

- When $J = 0$, the model behaves either paramagnetic or diamagnetic, depending on how the magnetic field enters the constant g .

- When $g = 0$, the model may describe ferromagnetic behaviour when $J > 0$ (in the ground state, all spins are aligned) or anti-ferromagnetic behaviour when $J < 0$ (all spins tend to anti-align)

We will just consider the paramagnetic-ferromagnetic transition here by assuming $g \geq 0$ and $J \geq 0$.

We can introduce a dimensionless phase parameter by fixing $\Omega s = J$ and $\Omega(1 - s) = g$ with energy scale Ω

$$H(s) = -\Omega(1 - s) \sum_{i=1}^n \sigma_i^x - \Omega s \sum_{i=1}^n \sigma_i^z \sigma_{i+1}^z = (1 - s)H_I + sH_F. \quad (5.59)$$

Another interpretation of this Hamiltonian is that of an adiabatic algorithm, where the initial ground state is unique

$$|\Psi_0(s = 0)\rangle = |\rightarrow\rangle \otimes \dots \otimes |\rightarrow\rangle = |S\rangle, \quad (5.60)$$

whereas the final ground state is two-fold degenerate

$$|\Psi_0(s = 1)^a\rangle = |0 \dots 0\rangle, \quad |\Psi_0(s = 1)^b\rangle = |1 \dots 1\rangle. \quad (5.61)$$

However, one can also check that both $H_{I/F}$ commute with the **bitflip parity** operator flipping all bits

$$\Sigma^x = \bigotimes_{\ell=1}^n \sigma_\ell^x, \quad (5.62)$$

which can be explicitly seen from

$$\begin{aligned} [\sigma_i^z \sigma_{i+1}^z, \sigma_i^x \sigma_{i+1}^x] &= \sigma_i^x [\sigma_i^z \sigma_{i+1}^z, \sigma_{i+1}^x] + [\sigma_i^z \sigma_{i+1}^z, \sigma_i^x] \sigma_{i+1}^x \\ &= \sigma_i^x \sigma_i^z (2i\sigma_{i+1}^y) + (2i\sigma_i^y) \sigma_{i+1}^z \sigma_{i+1}^x \\ &= (-i\sigma_i^y)(2i\sigma_{i+1}^y) + (2i\sigma_i^y)(+i\sigma_{i+1}^y) = 0. \end{aligned} \quad (5.63)$$

It follows that the full Ising model Hamiltonian commutes with the operator, such that the bitflip parity is actually a conserved quantity. Since the eigenvalues of Σ^x are just ± 1 , we conclude that it must be possible to classify the eigenvalues of the Hamiltonian into two groups of even (+) and odd (−) bitflip parity. Furthermore, since the initial ground state is even under bitflip $\Sigma^x |\Psi_0(s = 0)\rangle = + |\Psi_0(s = 0)\rangle$, an adiabatic evolution between H_I and H_F would actually prepare the even superposition

$$|\Psi_{\text{ad}}^0(s = 1)\rangle = \frac{1}{\sqrt{2}} [|0 \dots 0\rangle + |1 \dots 1\rangle], \quad (5.64)$$

which is actually a Schrödinger cat state.

5.8.1 Exact Diagonalization

Apart from these qualitative considerations, the Ising Hamiltonian can be diagonalized exactly also for finite spin numbers n . The successive application of Jordan-Wigner, Fourier-, and Bogoliubov

transforms maps the system Hamiltonian into two mutually commuting parts $H = H^- + H^+$ of non-interacting fermions

$$H^\pm = \sum_k \epsilon_k^\pm \gamma_{k\pm}^\dagger \gamma_{k\pm} + \sigma^\pm \mathbf{1} \quad (5.65)$$

with fermionic annihilation operators γ_k that describe quasi-particles and shifts σ^\pm . Here, the quasi-momentum k may assume discrete values only, and the single-particle excitation energies – that correspond to excitation energies of the full model – can be explicitly computed. The standard path to diagonalize the Ising model can be broken down into three steps.

Jordan-Wigner transform

The **Jordan-Wigner transform** (JWT)

$$\sigma_\ell^x = \mathbf{1} - 2c_\ell^\dagger c_\ell, \quad \sigma_\ell^z = -(c_\ell + c_\ell^\dagger) \prod_{m=1}^{\ell-1} (\mathbf{1} - 2c_m^\dagger c_m) \quad (5.66)$$

maps the spin-1/2 Pauli matrices non-locally to spinless fermionic operators c_m obeying **fermionic anticommutation relations** $\{c_m, c_\ell^\dagger\} = \delta_{m\ell}$ and $\{c_m, c_\ell\} = 0$. For reference, we also note that this implies

$$\sigma_\ell^y = i(c_\ell^\dagger - c_\ell) \prod_{m=1}^{\ell-1} (\mathbf{1} - 2c_m^\dagger c_m). \quad (5.67)$$

Additionally, it may also be useful to note the inverted JWT

$$c_\ell = -\frac{1}{2} [\sigma_\ell^z - i\sigma_\ell^y] \prod_{m=1}^{\ell-1} \sigma_m^x, \quad (5.68)$$

which (possibly after some convenient single-qubit rotations) can be used to co construct fermionic annihilation and creation operators from the Pauli matrices.

Inserting the JWT into the Ising Hamiltonian, one has to treat the boundary term with special care

$$\begin{aligned} H &= -g \sum_{\ell=1}^n (\mathbf{1} - 2c_\ell^\dagger c_\ell) - J \sum_{\ell=1}^{n-1} (c_\ell + c_\ell^\dagger)(c_{\ell+1} + c_{\ell+1}^\dagger)(\mathbf{1} - 2c_\ell^\dagger c_\ell) \\ &\quad - J(c_n + c_n^\dagger) \left[\prod_{\ell=1}^{n-1} (\mathbf{1} - 2c_\ell^\dagger c_\ell) \right] (c_1 + c_1^\dagger) \\ &= -g \sum_{\ell=1}^n (\mathbf{1} - 2c_\ell^\dagger c_\ell) - J \sum_{\ell=1}^{n-1} (c_\ell^\dagger - c_\ell)(c_{\ell+1}^\dagger + c_{\ell+1}) \\ &\quad + J(c_n^\dagger - c_n)(c_1^\dagger + c_1) \left[\prod_{\ell=1}^n (\mathbf{1} - 2c_\ell^\dagger c_\ell) \right], \end{aligned} \quad (5.69)$$

where we have extensively used the fermionic anticommutation relations. Introducing the projection operators on the subspaces with even (+) and odd (-) total number of fermion quasiparticles

$$\mathcal{P}^\pm \equiv \frac{1}{2} [\mathbf{1} \pm \Sigma^x] = \frac{1}{2} \left[\mathbf{1} \pm \prod_{m=1}^n (\mathbf{1} - 2c_m^\dagger c_m) \right], \quad (5.70)$$

we may also write the Hamiltonian (5.69) as $H = (\mathcal{P}^+ + \mathcal{P}^-)H(\mathcal{P}^+ + \mathcal{P}^-)$. It is straightforward to see that terms with different projectors and with $\ell < n$ vanish

$$\begin{aligned} 0 &= \mathcal{P}^+ (\mathbf{1} - 2c_\ell^\dagger c_\ell) \mathcal{P}^- = \mathcal{P}^- (\mathbf{1} - 2c_\ell^\dagger c_\ell) \mathcal{P}^+, \\ 0 &= \mathcal{P}^+ (c_\ell^\dagger - c_\ell)(c_{\ell+1}^\dagger + c_{\ell+1}) \mathcal{P}^- = \mathcal{P}^- (c_\ell^\dagger - c_\ell)(c_{\ell+1}^\dagger + c_{\ell+1}) \mathcal{P}^+. \end{aligned} \quad (5.71)$$

For the boundary terms one finds similarly

$$\begin{aligned} &(\mathcal{P}^+ + \mathcal{P}^-)(c_n^\dagger - c_n)(c_1^\dagger + c_1) \left[\prod_{\ell=1}^n (\mathbf{1} - 2c_\ell^\dagger c_\ell) \right] (\mathcal{P}^+ + \mathcal{P}^-) \\ &= (\mathcal{P}^+ + \mathcal{P}^-)(c_n^\dagger - c_n)(c_1^\dagger + c_1)(2\mathcal{P}^+ - \mathbf{1})(\mathcal{P}^+ + \mathcal{P}^-) \\ &= \mathcal{P}^+(c_n^\dagger - c_n)(c_1^\dagger + c_1)\mathcal{P}^+ - \mathcal{P}^-(c_n^\dagger - c_n)(c_1^\dagger + c_1)\mathcal{P}^-. \end{aligned} \quad (5.72)$$

The prefactor of the last term with the \mathcal{P}^- is negative as it should be, but the first is positive. We can correct for this by demanding anti-periodic boundary conditions in the even subspace. Eventually, we can write the Hamiltonian (5.69) as the sum of two non-interacting parts with either an even or an odd total number of fermionic quasiparticles

$$\begin{aligned} H &= \mathcal{P}^+ H^+ \mathcal{P}^+ + \mathcal{P}^- H^- \mathcal{P}^- \\ &= \mathcal{P}^+ \left[-g \sum_{\ell=1}^n (\mathbf{1} - 2c_\ell^\dagger c_\ell) - J \sum_{\ell=1}^n (c_\ell^\dagger - c_\ell)(c_{\ell+1}^\dagger + c_{\ell+1}) \right] \mathcal{P}^+ \\ &\quad + \mathcal{P}^- \left[-g \sum_{\ell=1}^n (\mathbf{1} - 2c_\ell^\dagger c_\ell) - J \sum_{\ell=1}^n (c_\ell^\dagger - c_\ell)(c_{\ell+1}^\dagger + c_{\ell+1}) \right] \mathcal{P}^-. \end{aligned} \quad (5.73)$$

Although the Hamiltonians in the brackets look formally identical, we stress that to arrive at this expression, we need to demand antiperiodic boundary conditions in the even (+) subspace and periodic boundary conditions in the odd (-) subspace

$$c_{n+1,(+)} \equiv -c_{1,(+)}, \quad c_{n+1,(-)} \equiv +c_{1,(-)}. \quad (5.74)$$

Even subspace diagonalization

We first seek to diagonalize the even part of the Hamiltonian

$$H^+ = -g \sum_{\ell=1}^n (\mathbf{1} - 2c_\ell^\dagger c_\ell) - J \sum_{\ell=1}^n (c_\ell^\dagger - c_\ell)(c_{\ell+1}^\dagger + c_{\ell+1}) \quad (5.75)$$

with antiperiodic boundary conditions $c_{n+1} = -c_1$. This is often the only part considered, since it contains the ground state (with zero quasi-particles). Translational invariance suggests to use the

discrete Fourier transform (DFT, preserving the anticommutation relations due to its unitarity by construction)

$$c_\ell = \frac{e^{-i\pi/4}}{\sqrt{n}} \sum_k \tilde{c}_k e^{+ik\ell \frac{2\pi}{n}}, \quad (5.76)$$

which is a specific case of a **Bogoliubov transformation**. By construction, the DFT is unitary and since it does not mix between annihilation and creation operators, it leaves the fermionic anticommutation relations invariant (as one can check). The factor $e^{-i\pi/4}$ in front has just been inserted for convenience (to obtain real-valued Bogoliubov coefficients later-on). The DFT is compatible with the antiperiodic boundary conditions $c_{n+1} = -c_1$ when k takes half-integer values

$$k \in \left\{ \pm \frac{1}{2}, \pm \frac{3}{2}, \pm \frac{5}{2}, \dots \right\}, \quad \text{where} \quad |k| \leq \frac{n-1}{2}. \quad (5.77)$$

Therefore, for even n , we get n different k values. The DFT maps the Hamiltonian into

$$H^+ = -gn\mathbf{1} + \sum_k \left\{ 2[g - J \cos(k2\pi/n)] \tilde{c}_k^\dagger \tilde{c}_k + J \sin(k2\pi/n) \left[\tilde{c}_k^\dagger \tilde{c}_{-k}^\dagger + \tilde{c}_{-k} \tilde{c}_k \right] \right\}. \quad (5.78)$$

Now, the observation that only positive and negative frequencies couple (conservation of one-dimensional quasi-momentum), suggests to use the reduced **Bogoliubov transform**

$$\tilde{c}_k = u_{+k} \gamma_{+k} + v_{-k}^* \gamma_{-k}^\dagger, \quad (5.79)$$

which mixes positive and negative momenta and where the a priori unknown coefficients have already been labeled suggestively (a more general ansatz would eventually of course yield the same solution). Since the new operators γ_k should be fermionic, we obtain from the orthonormality conditions

$$1 = |u_{+k}|^2 + |v_{-k}|^2, \quad 0 = u_{+k} v_{+k}^* + u_{-k} v_{-k}^* = (v_{+k}^*, v_{-k}^*) \begin{pmatrix} u_{+k} \\ u_{-k} \end{pmatrix}. \quad (5.80)$$

Demanding that the Bogoliubov transform eliminates all non-diagonal terms (of the form $\gamma_{-k} \gamma_{+k}$ etc.) yields (by combining positive and negative k) the equation

$$\begin{aligned} 0 &= 2 \left[g - J \cos \left(k \frac{2\pi}{n} \right) \right] (u_{+k} v_{-k} - u_{-k} v_{+k}) + 2J \sin \left(k \frac{2\pi}{n} \right) (u_{-k} u_{+k} + v_{-k} v_{+k}) \\ &= (v_{-k}, u_{-k}) \begin{pmatrix} +2 \left[g - J \cos \left(k \frac{2\pi}{n} \right) \right] & +2J \sin \left(k \frac{2\pi}{n} \right) \\ +2J \sin \left(k \frac{2\pi}{n} \right) & -2 \left[g - J \cos \left(k \frac{2\pi}{n} \right) \right] \end{pmatrix} \begin{pmatrix} u_{+k} \\ v_{+k} \end{pmatrix} \\ &\equiv (v_{-k}, u_{-k}) \mathcal{M} \begin{pmatrix} u_{+k} \\ v_{+k} \end{pmatrix}. \end{aligned} \quad (5.81)$$

All equations can be fulfilled when we choose $(u_{+k}, v_{+k})^T$ as the normalized positive energy eigenstate of the matrix \mathcal{M} with eigenvalue

$$\varepsilon_k^+ = +2\sqrt{g^2 + J^2 - 2gJ \cos(k2\pi/n)} \equiv \epsilon_k \quad (5.82)$$

and $(v_{-k}^*, u_{-k}^*)^T = (-v_{+k}^*, +u_{+k}^*)^T$ as its negative energy eigenstate with eigenvalue $\varepsilon_k^- = -2\sqrt{g^2 + J^2 - 2gJ \cos(k2\pi/n)}$. To be more explicit, we have

$$\begin{aligned} u_k &= \frac{g - J \cos(k2\pi/n) + \sqrt{g^2 + J^2 - 2gJ \cos(k2\pi/n)}}{\sqrt{\left[g - J \cos(k2\pi/n) + \sqrt{g^2 + J^2 - 2gJ \cos(k2\pi/n)}\right]^2 + [J \sin(k2\pi/n)]^2}}, \\ v_k &= \frac{J \sin(k2\pi/n)}{\sqrt{\left[g - J \cos(k2\pi/n) + \sqrt{g^2 + J^2 - 2gJ \cos(k2\pi/n)}\right]^2 + [J \sin(k2\pi/n)]^2}}. \end{aligned} \quad (5.83)$$

As a sanity check, we see that when the interaction vanishes $J \rightarrow 0$, we get that the modes no longer mix $u_k \rightarrow 1$ and $v_k \rightarrow 0$.

Using these solutions, we obtain when n is even

$$H^+ = \sum_k 2\sqrt{g^2 + J^2 - 2gJ \cos\left(k\frac{2\pi}{n}\right)} \left(\gamma_k^\dagger \gamma_k - \frac{1}{2}\right). \quad (5.84)$$

From this, we conclude the single-particle energies

$$\varepsilon_k^+ = 2\sqrt{g^2 + J^2 - 2gJ \cos\left(k\frac{2\pi}{n}\right)} = 2\Omega\sqrt{(1-s)^2 + s^2 - 2s(1-s) \cos\left(k\frac{2\pi}{n}\right)}. \quad (5.85)$$

The ground state has zero quasi-particles, and we can compute the ground state energy for large chain lengths n explicitly by converting the sum into an integral

$$E_0 = -\frac{1}{2} \sum_k \varepsilon_k^+ \xrightarrow{n \rightarrow \infty} -\Omega \frac{n}{2} \int_{-1}^{+1} d\kappa \sqrt{(1-s)^2 + s^2 - 2s(1-s) \cos(\pi\kappa)}, \quad (5.86)$$

where $\kappa = 2k/n$. Accordingly, the ground state energy density per spin becomes

$$\varepsilon(s) = \frac{E_0}{n} = -\Omega \int_0^1 d\kappa \sqrt{(1-s)^2 + s^2 - 2s(1-s) \cos(\pi\kappa)} = -\frac{2\Omega}{\pi} \epsilon(4s(1-s)), \quad (5.87)$$

where $\epsilon(x)$ is an elliptic integral of the second kind. This function has the peculiar property that although its value at $s = 1/2$ is continuous, its second derivative diverges there logarithmically, see Fig. 5.9. The next excited state in the subspace of an even quasiparticle number would be to put two quasiparticles. To get the lowest excitation, we take the quasiparticles with $k = \pm 1/2$, which yields for the excitation gap

$$G(s) = E_1(s) - E_0(s) = 2\varepsilon_{1/2}^+ = 4\Omega\sqrt{s^2 + (1-s)^2 - 2s(1-s) \cos\left(\frac{\pi}{n}\right)}. \quad (5.88)$$

By expanding the cos for large n and considering only the value of the gap at the critical point $s \rightarrow 1/2$, the critical gap becomes

$$G_{\text{crit}} \approx \Omega \frac{\pi}{n}. \quad (5.89)$$

It is a general feature of quantum-critical models that the gap above the ground state vanishes as $n \rightarrow \infty$. The scaling for the Ising model is rather mild, connected to the fact that it has a second order quantum phase transition.

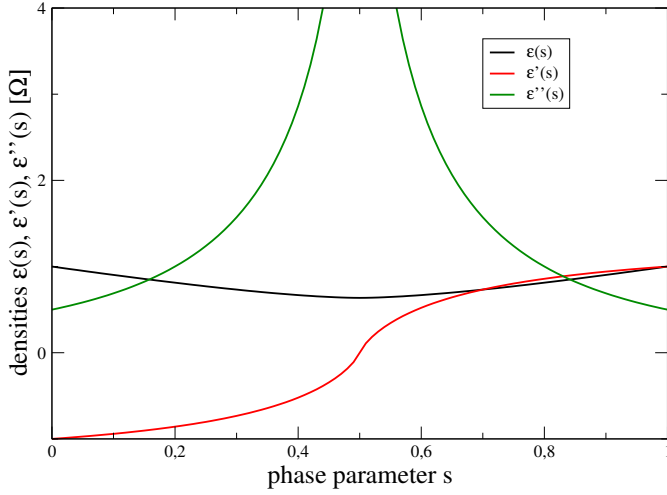


Figure 5.9: Plot of the (negative) ground state energy density $\varepsilon(s)$ (black) and its first two derivatives versus s . At the critical point $s^* = 1/2$, the second derivative diverges.

Odd subspace diagonalization

The procedure for the odd subspace is essentially analogous, except that the Fourier transform should now be compatible with periodic boundary conditions $c_{n+1} = +c_1$. The **Discrete Fourier transform**

$$c_\ell = \frac{1}{\sqrt{n}} \sum_k \tilde{c}_k e^{+ik\ell \frac{2\pi}{n}} \quad (5.90)$$

is compatible with the periodic boundary conditions when k takes only integer values

$$k \in \left\{ 0, \pm 1, \pm 2, \pm 3, \dots, \pm \left(\frac{n}{2} - 1 \right), +\frac{n}{2} \right\}, \quad (5.91)$$

which holds for even values of n (we treat only this case) and then yields n different k -values. From this choice, it also follows that $\tilde{c}_{-n/2} = \tilde{c}_{+n/2}$. We get in analogy to the even subspace calculations the relations

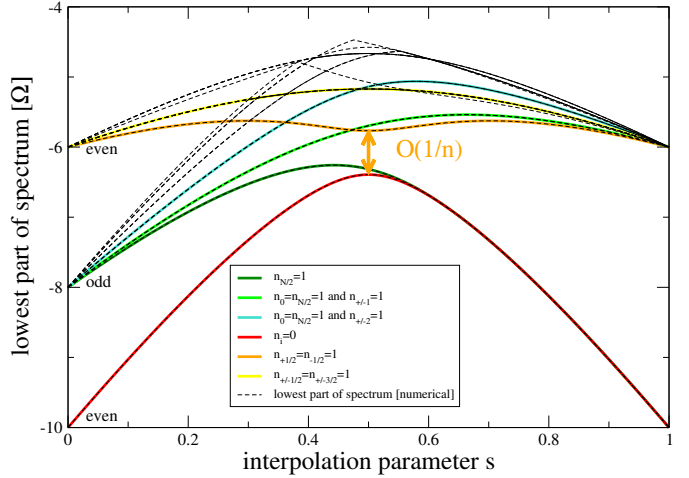
$$\begin{aligned} \sum_{i=1}^{n-1} c_i c_{i+1} + c_n c_1 &= \sum_k \tilde{c}_{+k} \tilde{c}_{-k} e^{-ik \frac{2\pi}{n}}, & \sum_{i=1}^{n-1} c_{i+1}^\dagger c_i^\dagger + c_1^\dagger c_n^\dagger &= \sum_k \tilde{c}_{-k}^\dagger \tilde{c}_{+k}^\dagger e^{+ik \frac{2\pi}{n}}, \\ \sum_{i=1}^{n-1} c_i^\dagger c_{i+1} + c_n^\dagger c_1 &= \sum_k \tilde{c}_{+k}^\dagger \tilde{c}_{+k} e^{-ik \frac{2\pi}{n}}, & \sum_{i=1}^{n-1} c_{i+1}^\dagger c_i + c_1^\dagger c_n &= \sum_k \tilde{c}_{+k}^\dagger \tilde{c}_{+k} e^{+ik \frac{2\pi}{n}}, \end{aligned} \quad (5.92)$$

and inserting them into the Hamiltonian H^- we get

$$\begin{aligned} H^- &= gn\mathbf{1} - 2g \sum_k \tilde{c}_{+k}^\dagger \tilde{c}_{+k} - J \sum_k \left[\tilde{c}_{+k} \tilde{c}_{-k} e^{-ik \frac{2\pi}{n}} + \tilde{c}_{-k}^\dagger \tilde{c}_{+k}^\dagger e^{+ik \frac{2\pi}{n}} \right] \\ &\quad + J \sum_k \tilde{c}_{+k}^\dagger \tilde{c}_{+k} \left(e^{+ik \frac{2\pi}{n}} + e^{-ik \frac{2\pi}{n}} \right) \\ &= gn\mathbf{1} - 2(g - J)c_0^\dagger c_0 - 2(g + J)c_{n/2}^\dagger c_{n/2} + \sum_{k=1}^{n/2-1} H_k^-. \end{aligned} \quad (5.93)$$

Here, the two additional terms arise from $k = 0$ and $k = n/2$, which is due to the different boundary conditions in the odd subspace. The excitation energies of these modes can become negative. The

Figure 5.10: Comparison of analytical (bold, colored) predictions with numerical (thin dashed, black) results for the lower part of the spectrum for $n = 10$. Other parameters have been chosen as $g = \Omega(1 - s)$ and $J = \Omega s$. At the critical point $s^* = 1/2$, the indicated gap between ground state and first excited state of the even subspace closes in the continuum limit $n \rightarrow \infty$.



diagonalization of the quasimomentum pair Hamiltonian H_k^- proceeds in full analogy to H_k^+ , we only have to take the different values of k into account

$$\begin{aligned}
 H_k^- &= \left[2J \cos\left(\frac{2\pi k}{n}\right) - 2g \right] c_{+k}^\dagger c_{+k} + \left[2J \cos\left(\frac{2\pi k}{n}\right) - 2g \right] c_{-k}^\dagger c_{-k} \\
 &\quad - 2iJ \sin\left(\frac{2\pi k}{n}\right) c_{-k} c_{+k} + 2iJ \sin\left(\frac{2\pi k}{n}\right) c_{+k}^\dagger c_{-k}^\dagger \\
 &= \epsilon_k^- \left[\gamma_{-k}^\dagger \gamma_{-k} + \gamma_{+k}^\dagger \gamma_{+k} \right] + \omega_k^- \mathbf{1}, \\
 \omega_k^- &= -2 \left(\sqrt{g^2 + J^2 - 2gJ \cos\left(\frac{2\pi k}{n}\right)} + g - J \cos\left(\frac{2\pi k}{n}\right) \right), \\
 \epsilon_k^- &= 2 \sqrt{g^2 + J^2 - 2gJ \cos\left(\frac{2\pi k}{n}\right)}. \tag{5.94}
 \end{aligned}$$

After some rewriting, we can write the total Hamiltonian in the odd subspace as

$$\begin{aligned}
 H^- &= -2(g - J) \left(\gamma_0^\dagger \gamma_0 - \frac{1}{2} \right) - 2(g + J) \left(\gamma_{n/2}^\dagger \gamma_{n/2} - \frac{1}{2} \right) \\
 &\quad + \sum_{k=1}^{n/2-1} \epsilon_k^- \left[\left(\gamma_{+k}^\dagger \gamma_{+k} - \frac{1}{2} \right) + \left(\gamma_{-k}^\dagger \gamma_{-k} - \frac{1}{2} \right) \right]. \tag{5.95}
 \end{aligned}$$

From these excitation energies we can successively compute the full spectrum in the odd subspace. First, we compute the lowest energy eigenstate by putting a single (odd subspace) quasiparticle with minimum energy (this is for our parameters the one with $k = +n/2$) into the system. Further energies can be computed by putting quasiparticles with larger energies, always obeying the constraint that in this subspace, the total number of quasi-particles must be odd. Other odd branches are obtained by inserting three quasi-particles and so on.

Fig. 5.10 illustrates the analytic calculation of the eigenvalues for both even and odd subspaces by comparing with a full-scale numerical solution for $n = 10$ spins, which yields in total $2^n = 1024$ eigenvalues. One can see that by knowing the single-quasiparticle energies and the ground state energy in the separate subspaces, we can successively build up the complete spectrum of the model – which numerically (dashed curves) requires the diagonalization of a $2^n \times 2^n$ matrix.

5.8.2 Adiabatic criterion

To see how fast the final ground state can be prepared from the initial one by a convex quench, we consider the adiabatic criterion (5.11), which for a straight-line interpolation just involves the matrix element $H_F - H_I$ in the time-dependent system energy eigenbasis. If $s(t) = t/T$, we can use the very same argument as before to find that $T \propto g_{\min}^{-2} \propto n^2$ will suffice to ensure for adiabatic evolution, such that the Schrödinger cat state can be prepared in a time that is quadratic in the number of qubits [24]. However, similar to the adiabatic Grover model, when the interpolation speed is adapted to the energy gap, one can do better.

Since $[H_F - H_I, \Sigma^x] = 0$, we will only consider the even parity sector, as there are no allowed transitions between these sectors. To compute it, it is helpful to represent the individual contributions of the Ising model Hamiltonian in terms of the even subspace fermions (compare Eq. (5.78) for either $g = 0$ or $J = 0$)

$$\begin{aligned}
\sum_{\ell} \sigma_{\ell}^x &= n\mathbf{1} - 2 \sum_{\ell} c_{\ell}^{\dagger} c_{\ell} = n \cdot \mathbf{1} - 2 \sum_k \tilde{c}_k^{\dagger} \tilde{c}_k = n \cdot \mathbf{1} - 2 \sum_k \left(u_k^* \gamma_k^{\dagger} + v_{-k} \gamma_{-k} \right) \left(u_k \gamma_k + v_{-k}^* \gamma_{-k}^{\dagger} \right) \\
&= n\mathbf{1} - 2 \sum_k \left[|u_k|^2 \gamma_k^{\dagger} \gamma_k + |v_{-k}|^2 \gamma_{-k} \gamma_{-k}^{\dagger} + u_k^* v_{-k}^* \gamma_k^{\dagger} \gamma_{-k}^{\dagger} + u_k v_{-k} \gamma_{-k} \gamma_k \right], \\
\sum_{\ell} \sigma_{\ell}^z \sigma_{\ell+1}^z &= \sum_{\ell} (c_{\ell}^{\dagger} - c_{\ell})(c_{\ell+1}^{\dagger} + c_{\ell+1}) = \sum_k \left[2 \cos(2\pi k/n) \tilde{c}_k^{\dagger} \tilde{c}_k - \sin(2\pi k/n) \left(\tilde{c}_k^{\dagger} \tilde{c}_{-k}^{\dagger} + \tilde{c}_{-k} \tilde{c}_k \right) \right] \\
&= \sum_k \left[2 \cos \left(\frac{2\pi k}{n} \right) \left(u_k^* \gamma_k^{\dagger} + v_{-k} \gamma_{-k} \right) \left(u_k \gamma_k + v_{-k}^* \gamma_{-k}^{\dagger} \right) \right. \\
&\quad \left. - \sin \left(\frac{2\pi k}{n} \right) \left[\left(u_k^* \gamma_k^{\dagger} + v_{-k} \gamma_{-k} \right) \left(u_{-k}^* \gamma_{-k}^{\dagger} + v_k \gamma_k \right) + \left(u_{-k} \gamma_{-k} + v_k^* \gamma_k^{\dagger} \right) \left(u_k \gamma_k + v_{-k}^* \gamma_{-k}^{\dagger} \right) \right] \right], \\
\end{aligned} \tag{5.96}$$

where the coefficients are defined by (5.83). This helps with $|E_0(s)\rangle = |0\rangle$ and $|E_1(s)\rangle = \gamma_{-1/2}^{\dagger} \gamma_{+1/2}^{\dagger} |0\rangle$ to evaluate the matrix elements between ground state and first excited state in the even particle number subspace, since only terms with two matching annihilation operators will survive. Explicitly, one obtains

$$\begin{aligned}
\langle E_0(s) | \sum_i \sigma_i^x | E_1(s) \rangle &= \langle 0 | \left(\sum_i \sigma_i^x \right) \gamma_{-1/2}^{\dagger} \gamma_{+1/2}^{\dagger} | 0 \rangle \\
&= -2u_{1/2} v_{-1/2} \langle 0 | \gamma_{-1/2} \gamma_{+1/2} \gamma_{-1/2}^{\dagger} \gamma_{+1/2}^{\dagger} | 0 \rangle \\
&\quad - 2u_{-1/2} v_{+1/2} \langle 0 | \gamma_{+1/2} \gamma_{-1/2} \gamma_{-1/2}^{\dagger} \gamma_{+1/2}^{\dagger} | 0 \rangle \\
&= 2u_{1/2} v_{-1/2} - 2u_{-1/2} v_{+1/2} = -4u_{1/2} v_{1/2}, \\
\langle E_0(s) | \sum_i \sigma_i^z \sigma_{i+1}^z | E_1(s) \rangle &= \langle 0 | \left(\sum_i \sigma_i^z \sigma_{i+1}^z \right) \gamma_{-1/2}^{\dagger} \gamma_{+1/2}^{\dagger} | 0 \rangle \\
&= 2 \cos \left(\frac{\pi}{n} \right) [-v_{-1/2} u_{+1/2} + v_{+1/2} u_{-1/2}] - \sin \left(\frac{\pi}{n} \right) [-v_{-1/2} v_{1/2} - u_{-1/2} u_{+1/2}] \\
&\quad + \sin \left(\frac{\pi}{n} \right) [v_{1/2} v_{-1/2} + u_{1/2} u_{-1/2}] \\
&= 4 \cos \left(\frac{\pi}{n} \right) u_{1/2} v_{1/2} + 2 \sin \left(\frac{\pi}{n} \right) [u_{1/2}^2 - v_{1/2}^2]. \\
\end{aligned} \tag{5.97}$$

Altogether, this implies

$$\begin{aligned} \langle E_0(s) | \dot{H} | E_1(s) \rangle &= \Omega \dot{s} \left\{ -4 \left[1 + \cos \left(\frac{\pi}{n} \right) \right] u_{1/2} v_{1/2} - 2 \sin \left(\frac{\pi}{n} \right) [u_{1/2}^2 - v_{1/2}^2] \right\} \\ &= \frac{-2\Omega \dot{s} \sin \left(\frac{\pi}{n} \right)}{\sqrt{1 - 2s(1-s)} \left[1 + \cos \left(\frac{\pi}{n} \right) \right]} = \frac{-8\Omega^2 \sin \left(\frac{\pi}{n} \right)}{G(s)} \dot{s} \xrightarrow{n \rightarrow \infty} -4\Omega \dot{s}, \end{aligned} \quad (5.98)$$

with the energy gap (5.88). Altogether, the locally adiabatic criterion (5.11) reads

$$\frac{8\Omega^2 \sin \left(\frac{\pi}{n} \right)}{G^3(s)} \dot{s} \ll 1. \quad (5.99)$$

For large n , since $\sin(\pi/n)/G(s)$ remains bounded, it suffices to choose $\dot{s} = \sigma G^2(s)$ with a small constant σ to satisfy the adiabatic condition. From solving

$$\int_0^1 \frac{ds}{G^2(s)} = \frac{2 \arctan \left[\sqrt{\frac{1+\cos(\pi/n)}{1-\cos(\pi/n)}} \right]}{\sqrt{1-\cos^2(\pi/n)}} = \int_0^T \sigma dt = \sigma T = n - 1 + \mathcal{O}(1/n) \quad (5.100)$$

one then finds that in the large- n limit, an adiabatic runtime of $T \propto n$ actually suffices to prepare the final Schrödinger cat ground state. So as with the Grover model in Sec. 5.4 one may get a quadratic speedup by taking the varying gap into account. The difference however is that the main obstacle, the energy gap, in the Grover model becomes exponentially small in the system size $g_{\min}^{\text{Grover}} = \Omega N^{-1/2} = \Omega 2^{-n/2}$, whereas in the Ising model it is only polynomially small $g_{\min}^{\text{Ising}} = 4\Omega \sin \left(\frac{\pi}{2n} \right) \rightarrow 2\Omega \frac{\pi}{n}$.

5.8.3 Non-straight interpolation

In presence of a thermal reservoir a reducing energy gap would still be problematic: Even if non-adiabatic excitations can be controlled, a finite reservoir temperature will imply that thermal excitations still pose a problem for large n . Fortunately, for the Ising model a different path may be chosen along which a lower bound on the energy gap can be guaranteed. Instead of performing a global quench which homogeneously changes the field $g(t) = \Omega[1 - s(t)]$ and the interaction $J(t) = \Omega s(t)$ for all spins, one may sequentially turn on interactions and turn off local fields, i.e.,

one may interpolate along the series of Hamiltonians

$$\begin{aligned}
H_0 &= -\Omega \sum_{i=1}^n \sigma_i^x = H_1, \\
H_1 &= -\Omega \sigma_1^z \sigma_2^z - \Omega \sum_{i=3}^n \sigma_i^x, \\
&\vdots \\
H_k &= -\Omega \sum_{i=1}^k \sigma_i^z \sigma_{i+1}^z - \Omega \sum_{i=k+2}^n \sigma_i^x, \\
&\vdots \\
H_{n-1} &= -\Omega \sum_{i=1}^{n-1} \sigma_i^z \sigma_{i+1}^z, \\
H_n &= -\Omega \sum_{i=1}^n \sigma_i^z \sigma_{i+1}^z = H_F,
\end{aligned} \tag{5.101}$$

which connects the same initial and final Hamiltonians, but now via a different path. Formally, the time-dependent Hamiltonian is given by

$$H(t) = \sum_{k=0}^{n-1} \Theta[s_k(t)] \Theta[1 - s_k(t)] \{ [1 - s_k(t)] H_k + s_k(t) H_{k+1} \}, \tag{5.102}$$

where $\Theta(x)$ denotes the Heavyside step function and $s_k(t) = \frac{t-k\Delta t}{\Delta t}$ encodes a constant speed interpolation with $n\Delta t = T$ such that $s_k[(k+1)\Delta t] = 1 = 1 - s_{k+1}[(k+1)\Delta t]$ and $H(\tau) = H_F$.

Given a spin chain with (constant) $\sigma_i^z \sigma_{i+1}^z$ -interactions, one has to apply a correspondingly stronger external field to achieve an effective decoupling of the spins. The above nonlinear scheme could be approximated by a strong transverse magnetic field that within the distance between two spins rises linearly from zero to maximum and then travels at constant speed along the spin chain. Conversely, one might imagine to slowly pull the spin chain out of a region with a strong stationary transverse field if it is open, or to move and rotate it across an interface if it is closed, to realize the above scheme.

Note that the interpolation path (5.101) does not destroy the bitflip symmetry, since $\left[H_k, \bigotimes_{\ell=1}^n \sigma_\ell^x \right] = 0$. The initial ground state is just the total superposition state

$$|\Psi_0^{0,\text{even}}\rangle = |S\rangle = \mathcal{H}_1 \dots \mathcal{H}_n |0 \dots 0\rangle, \tag{5.103}$$

where $\mathcal{H}_k = \frac{1}{\sqrt{2}} (\sigma_k^x + \sigma_k^z)$ denotes the Hadamard gate on qubit k . It is easy to see that the ground state of a single Hamiltonian H_k in (5.101) (within the subspace of even bit-flip parity) is for $1 \leq k \leq n-1$ given by

$$|\Psi_k^{0,\text{even}}\rangle = \frac{1}{\sqrt{2}} [\mathbf{1} + \sigma_1^x \dots \sigma_{k+1}^x] \mathcal{H}_{k+2} \dots \mathcal{H}_n |0 \dots 0\rangle, \tag{5.104}$$

such that the overlap between two successive ground states yields $\langle \Psi_k^{0,\text{even}} | \Psi_{k+1}^{0,\text{even}} \rangle = 1/\sqrt{2}$ for $0 \leq k \leq n-2$. In the last interpolation step, the ground state is even invariant $\langle \Psi_{n-1}^{0,\text{even}} | \Psi_n^{0,\text{even}} \rangle = 1$.

Hence, in every single step only slight transformations of the ground state are performed and intuitively, one may expect that adiabatic preparation along this modified path should be more efficient than in the conventional scheme.

For the first interpolation step in (5.101)

$$\begin{aligned} H_0(s) &\equiv (1-s)H_0 + sH_1 \\ &= -(1-s)\Omega(\sigma_1^x + \sigma_2^x) - \Omega s\sigma_1^z\sigma_2^z - \Omega \sum_{i=3}^n \sigma_i^x, \end{aligned} \quad (5.105)$$

the first two qubits evolve independently from the rest of the system and it is straightforward to obtain the nontrivial eigenvalue contribution generated by their four-dimensional subspace

$$\begin{aligned} \lambda_0/\Omega &= -\sqrt{5s^2 - 8s + 4}, \\ \lambda_1/\Omega &= -s, \\ \lambda_2/\Omega &= +s, \\ \lambda_3/\Omega &= +\sqrt{5s^2 - 8s + 4}, \end{aligned} \quad (5.106)$$

to which the (well-gapped) excitations resulting from decoupled qubits $3 \dots n$ – that are still subject to a local external field – have to be added. Here, the relevant even subspace leads to an energy gap $g_0(s) = \lambda_3(s) - \lambda_0(s)$ in the first step that is evidently independent of the total chain length n .

For the intermediate steps we have

$$\begin{aligned} H_k(s) &\equiv (1-s)H_k + sH_{k+1} \\ &= -\Omega \sum_{i=1}^k \sigma_i^z\sigma_{i+1}^z - \Omega(1-s)\sigma_{k+2}^x - \Omega s\sigma_{k+1}^z\sigma_{k+2}^z - \Omega \sum_{i=k+3}^n \sigma_i^x \end{aligned} \quad (5.107)$$

in (5.101) for $1 \leq k \leq n-2$, such that some non-trivial dynamics only takes place in the coefficients of qubits $k+1$ and $k+2$. These are decoupled from qubits $j \geq k+3$ but still coupled to qubits $j \leq k$. However, with a suitable CNOT gate transformation (2.45), we can decouple them. One can show that

$$\begin{aligned} \text{CNOT}_{ij} [\sigma_i^z \otimes \mathbf{1}_j] \text{CNOT}_{ij} &= \sigma_i^z \otimes \mathbf{1}_j, \\ \text{CNOT}_{ij} [\sigma_i^z \otimes \sigma_j^z] \text{CNOT}_{ij} &= \mathbf{1}_i \otimes \sigma_j^z, \\ \text{CNOT}_{ij} [\mathbf{1}_i \otimes \sigma_j^x] \text{CNOT}_{ij} &= \mathbf{1}_i \otimes \sigma_j^x. \end{aligned} \quad (5.108)$$

This means that a CNOT gate can be used to effectively decouple certain interactions, where we only have local σ^z terms on the control qubit, local σ^x terms on the target qubit, and a $\sigma^z \otimes \sigma^z$ interaction between the two. Using the CNOT transformation at the transition region, the Hamiltonian (5.107) is mapped to

$$\text{CNOT}_{k+1,k+2} H_k(s) \text{CNOT}_{k+1,k+2} = -\Omega \sum_{i=1}^k \sigma_i^z\sigma_{i+1}^z - \Omega \sum_{i=k+3}^n \sigma_i^x - \Omega(1-s)\sigma_{k+2}^x - \Omega s\sigma_{k+2}^z, \quad (5.109)$$

where it is visible that the qubit sets $\{1, \dots, (k+1)\}$, $\{(k+2)\}$, and $\{(k+3), \dots, n\}$ are mutually decoupled. Then, one obtains for qubits $1 \dots (k+1)$ just the eigenvalues of the Ising model in the

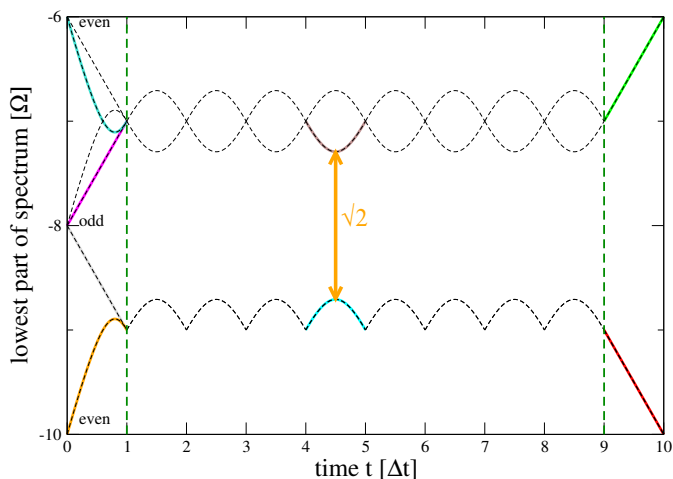


Figure 5.11: Spectrum of an interpolation scheme for the Ising model for $n = 10$, along which – in contrast to Fig. 5.10 – a lower bound on the energy gap can be guaranteed, adapted from Ref. [25]. The solid curves represent the analytical results from Eqns (5.106) (left), (5.110) (middle), and (5.111) (right) that are shifted by the corresponding negative energy contributions of the decoupled qubits, whereas thin dashed lines represent numerical solutions.

ferromagnetic phase with open boundary conditions (i.e., with minimum energy $-k\Omega$ for a two-fold degenerate ground state and fundamental energy gap 2Ω) and for qubits $(k+3), \dots, n$ a minimum energy of $-(n-k-2)\Omega$ for the unique ground state and a fundamental energy gap of 2Ω . The nontrivial part of the spectrum arises from the subspace of qubit $(k+2)$, where one obtains for the eigenvalues

$$\lambda_{\pm}/\Omega = \pm\sqrt{1-2s(1-s)}. \quad (5.110)$$

The final step is then trivial. Here, the two Hamiltonians do mutually commute, and the spectrum accordingly just consists of straight lines

$$\lambda_0/\Omega = (1-s)[-(n-1)] + s[-n], \quad \lambda_1/\Omega = (1-s)[-(n-3)] + s[-(n-4)]. \quad (5.111)$$

Therefore, the minimum fundamental energy gap along the whole sequence of (5.101) within the even subspace equates to $g_{\min}^{\text{even}} = \Omega\sqrt{2}$, which is independent on the system size, see figure 5.11. Accordingly, with a non-straight interpolation path, it is possible to prepare the final Schrödinger cat state adiabatically also in $\mathcal{O}(n)$ time (we have a constant energy gap but need n steps), with a lower bound on the energy gap. Here, the model is built such that one may never have any coupling between subspaces of even and odd quasiparticle number, which follows from $[H(s), \Sigma^x] = 0$. Some imperfections within the model or coupling to reservoirs not preserving the parity would lead to transitions between even and odd subspaces. For this (and for purposes of numerical separation), we note that by adding a penalty Hamiltonian

$$H_{\text{pen}} = \frac{\Omega}{2} \left[1 - \bigotimes_{\ell} \sigma_{\ell}^x \right] \quad (5.112)$$

the odd subspace is lifted by an energy penalty Ω , whereas the even subspace is not affected. A review on adiabatic quantum computation is provided in Ref. [26].

Chapter 6

Information measures

We have seen that some unintuitive properties like entanglement and coherence are vital for quantum computation to work. Unfortunately however, quantum computers are far from perfect and in particular for an open system, the Schrödinger equation alone is not sufficient to describe their dynamics. To see how well a quantum device works, we need some objective measures for distances between states [1] and we would like to have a method for measuring or quantifying entanglement. With such a measure, we could say for quantum state preparation, how well a quantum algorithm (e.g. Grover search) approximates the target state.

6.1 Quantum operations

For closed systems, we always used unitary evolution to describe the system dynamics. When we perform a measurement on the system, we have to act on the density matrix with projection operators to obtain the post-measurement state. For an open system, we integrate a master equation, thereby mapping an initial density matrix to a final one. These are possible maps between two density matrices.

The master equation formalism however rested on several approximations which in general will not be applicable. In standard treatment of open systems, it is always assumed that the global (full universe) density matrix evolves unitarily. If then initially, system and reservoir can be written in a product form $\rho_{SB} = U_{SB}(t)\rho_S^0 \otimes \rho_B^0 U_{SB}^\dagger(t)$, it follows by simply inserting a tensor product decomposition of the time evolution operator $U_{SB}(t) = \sum_\alpha A_\alpha \otimes B_\alpha$, that the exact reduced density matrix of the system can be written as

$$\rho_S(t) = \sum_{\alpha\beta} A_\alpha \rho_S^0 A_\beta^\dagger C_{\alpha\beta}, \quad (6.1)$$

where the positive semidefinite matrix $C_{\alpha\beta} = \text{Tr}_B \{ B_\beta^\dagger B_\alpha \rho_B^0 \}$ ensures that $\sum_{\alpha\beta} C_{\alpha\beta} A_\beta^\dagger A_\alpha = \mathbf{1}$. Even further representing the operators by unitary transformations $A_\alpha = \sum_{\bar{\alpha}} u_{\alpha\bar{\alpha}} \bar{K}_{\bar{\alpha}}$ of new operators $\bar{K}_{\bar{\alpha}}$ with the aim to diagonalize the $C_{\alpha\beta}$ matrix, we can with the eigenvalues $C_\alpha \geq 0$ write the above equation as

$$\rho_S(t) = \sum_{\alpha} C_\alpha \bar{K}_\alpha \rho_S^0 \bar{K}_\alpha^\dagger. \quad (6.2)$$

Finally, we introduce the operators $K_\alpha = \sqrt{C_\alpha} \bar{K}_\alpha$ which then obey $\sum_\alpha K_\alpha^\dagger K_\alpha = \mathbf{1}$ to conclude that the most general quantum operation on a density matrix ρ_S^0 is given by a **Kraus map** [27]

$$\rho_S(t) = \sum_\alpha K_\alpha \rho_S^0 K_\alpha^\dagger \equiv \mathcal{E}(\rho_S^0) \quad : \quad \sum_\alpha K_\alpha^\dagger K_\alpha = \mathbf{1}. \quad (6.3)$$

This is more general than Lindblad evolution, and the form of the above equation also includes the unitary case as well as the evolution under measurements. Conversely, if a map can be written as above, it is straightforward to show that it preserves all density matrix properties, e.g. for positivity

$$\langle \Psi | \rho_S(t) | \Psi \rangle = \sum_\alpha \sum_n \rho_n^0 \langle \Psi | K_\alpha | n \rangle \langle n | K_\alpha^\dagger | \Psi \rangle = \sum_\alpha \sum_n \rho_n^0 |\langle \Psi | K_\alpha | n \rangle|^2 \geq 0, \quad (6.4)$$

where we have used the spectral decomposition of $\rho_S^0 = \sum_n \rho_n^0 |n\rangle \langle n|$.

6.2 Comparing density matrices

6.2.1 Trace Distance

A classical distance measure between two probability distributions $\{p_n\}$ and $\{q_n\}$ (i.e., we have $p_n \geq 0$ and $\sum_n p_n = 1$) is the **Kolmogorov distance**

$$D_{\text{KD}}(\{p_n\}, \{q_n\}) = \frac{1}{2} \sum_n |p_n - q_n|. \quad (6.5)$$

It is actually even a **metric**, since it is positive, vanishes if and only if $q = p$, it is symmetric, and it obeys the triangle inequality

$$\begin{aligned} D_{\text{KD}}(\{p_n\}, \{q_n\}) &\geq 0, \\ D_{\text{KD}}(\{p_n\}, \{q_n\}) &= 0 \leftrightarrow p_n = q_n \forall n, \\ D_{\text{KD}}(\{p_n\}, \{q_n\}) &= D_{\text{KD}}(\{q_n\}, \{p_n\}), \\ D_{\text{KD}}(\{p_n\}, \{q_n\}) &\leq D_{\text{KD}}(\{p_n\}, \{\ell_n\}) + D_{\text{KD}}(\{\ell_n\}, \{q_n\}). \end{aligned} \quad (6.6)$$

All these requirements are sensible ones to define a proper distance. In addition, one can give the Kolmogorov distance an operational meaning: It is also given by the maximum probability difference for an event S to occur

$$D_{\text{KD}}(\{p_n\}, \{q_n\}) = \max_S |p(S) - q(S)| = \max_S \left| \sum_{n \in S} (p_n - q_n) \right|. \quad (6.7)$$

To see this, define $r_n = p_n - q_n$ and define the sets $N_+ = \{n : r_n > 0\}$ and $N_- = \{n : r_n < 0\}$, such that $\sum_n r_n = \sum_{n \in N_+} r_n + \sum_{n \in N_-} r_n = 0$. With this, we can write

$$D_{\text{KD}}(\{p_n\}, \{q_n\}) = \frac{1}{2} \sum_n |r_n| = \frac{1}{2} \left[\sum_{n \in N_+} r_n - \sum_{n \in N_-} r_n \right] = \sum_{n \in N_+} r_n = \max_S \left| \sum_{n \in S} r_n \right|, \quad (6.8)$$

which shows the above representation.

Quantum systems are not just characterized by a discrete probability distribution, in addition we need to specify the states corresponding to the probabilities. This is done with the density matrix formalism $\rho = \sum_n p_n |\Phi_n\rangle \langle \Phi_n|$ (recall that in general $\langle \Phi_n | \Phi_m \rangle \neq \delta_{nm}$), and correspondingly we need a measure to quantify the distance between two density matrices. The trace distance generalizes its classical analogue, the Kolmogorov distance, to the quantum world. The **trace distance** between two density matrices ρ and σ is defined as

$$D_{\text{TD}}(\rho, \sigma) = \frac{1}{2} \text{Tr} \{ |\rho - \sigma| \} \equiv \frac{1}{2} \text{Tr} \left\{ \sqrt{(\rho - \sigma)^\dagger (\rho - \sigma)} \right\} = \frac{1}{2} \text{Tr} \left\{ \sqrt{(\rho - \sigma)^2} \right\}. \quad (6.9)$$

- Practically, it can be computed by computing the real eigenvalues λ_n of $\rho - \sigma$, and summing up their absolute values $D_{\text{TD}}(\rho, \sigma) = \frac{1}{2} \sum_n |\lambda_n|$.
- Similar to the Kolmogorov distance, we can write the trace distance as a maximization over all possible projectors $P^2 = P$

$$D_{\text{TD}}(\rho, \sigma) = \max_P \text{Tr} \{ P(\rho - \sigma) \}, \quad (6.10)$$

which means that for any two states, there is an optimal measurement outcome P that distinguishes best between the two states, and the trace distance is then given by the difference of outcome probabilities for this optimal outcome. To see that such a projector P_{max} exists, we note that

$$\rho - \sigma = \sum_n \lambda_n |n\rangle \langle n| = \underbrace{\sum_{n:\lambda_n>0} \lambda_n |n\rangle \langle n|}_{R_+} - \underbrace{\sum_{n:\lambda_n<0} (-\lambda_n) |n\rangle \langle n|}_{R_-} \quad (6.11)$$

with positive operators R_\pm obeying $R_+ R_- = R_- R_+ = 0$ and $\text{Tr} \{ R_+ \} - \text{Tr} \{ R_- \} = \text{Tr} \{ \rho - \sigma \} = 0$. This decomposition formally allows to evaluate

$$D_{\text{TD}}(\rho, \sigma) = \frac{1}{2} \text{Tr} \{ |\rho - \sigma| \} = \frac{1}{2} \text{Tr} \{ R_+ + R_- \} = \text{Tr} \{ R_+ \}. \quad (6.12)$$

Therefore, we can choose P_{max} as the projector onto the support of R_+ , i.e.,

$$P_{\text{max}} = \sum_{n:\lambda_n>0} |n\rangle \langle n|, \quad (6.13)$$

such that $P_{\text{max}} R_+ = R_+$ and $P_{\text{max}} R_- = 0$. With this, we get

$$D_{\text{TD}}(\rho, \sigma) = \text{Tr} \{ R_+ \} = \text{Tr} \{ P_{\text{max}}(R_+ - R_-) \} = \text{Tr} \{ P_{\text{max}}(\rho - \sigma) \}. \quad (6.14)$$

In contrast, for an arbitrary projector $P = P^2 \neq P_{\text{max}}$, we have

$$\text{Tr} \{ P(\rho - \sigma) \} = \text{Tr} \{ P(R_+ - R_-) \} \leq \text{Tr} \{ P R_+ \} \leq \text{Tr} \{ R_+ \} = D_{\text{TD}}(\rho, \sigma), \quad (6.15)$$

which shows (6.10).

- The trace distance is a **metric**: It is evidently positive, it vanishes if and only if $\rho = \sigma$, and it is symmetric. Additionally, one can show the triangle inequality

$$\begin{aligned} D_{\text{TD}}(\rho, \tau) &= \text{Tr} \{ P_{\text{max}}^{\rho\tau} (\rho - \tau) \} = \text{Tr} \{ P_{\text{max}}^{\rho\tau} (\rho - \sigma + \sigma - \tau) \} \\ &\leq D_{\text{TD}}(\rho, \sigma) + D_{\text{TD}}(\sigma, \tau). \end{aligned} \quad (6.16)$$

This is useful to compare distances to each other: The direct distance should always be smaller than the distance along a detour.

- When the two density matrices commute $[\rho, \sigma] = 0$, we can denote their eigenvalues by ρ_ℓ and σ_ℓ , and the trace distance falls back to the previously introduced Kolmogorov distance between two distributions

$$D_{\text{TD}}(\rho, \sigma) \rightarrow \frac{1}{2} \sum_n |\rho_n - \sigma_n|. \quad (6.17)$$

- For a qubit, the trace distance between two states can be mapped to the ordinary euclidian distance within the Bloch sphere, where with $|\mathbf{n}|, |\mathbf{m}| \leq 1$ we have

$$\begin{aligned} D_{\text{TD}}(\rho, \sigma) &= D_{\text{TD}}\left(\frac{1}{2}[\mathbf{1} - \mathbf{n}\boldsymbol{\sigma}], \frac{1}{2}[\mathbf{1} - \mathbf{m}\boldsymbol{\sigma}]\right) = \frac{1}{2} \text{Tr} \left\{ \sqrt{\left[\frac{1}{2}(\mathbf{n} - \mathbf{m}) \cdot \boldsymbol{\sigma}\right]^2} \right\} \\ &= \frac{1}{4} 2|\mathbf{n} - \mathbf{m}| = \frac{|\mathbf{n} - \mathbf{m}|}{2}, \end{aligned} \quad (6.18)$$

where we have used that the eigenvalues of $\boldsymbol{\alpha} \cdot \boldsymbol{\sigma}$ are given by $\pm|\boldsymbol{\alpha}|$.

- Any rotation on the Bloch sphere leaves the distance between two states invariant, but this holds more generally for unitary transformations beyond the single-qubit case

$$D_{\text{TD}}(U\rho U^\dagger, U\sigma U^\dagger) = D_{\text{TD}}(\rho, \sigma). \quad (6.19)$$

This also implies that the trace distance does not depend on the basis within which we represent the density matrices ρ and σ .

A remarkable property of trace-preserving quantum operations (6.3) that becomes apparent by using the trace-distance is that these operations are **contractive**. Writing again $\rho - \sigma = R_+ - R_-$ with positive definite operators R_\pm , we find

$$\begin{aligned} D_{\text{TD}}(\mathcal{E}(\rho), \mathcal{E}(\sigma)) &= \text{Tr} \{P_{\text{max}}[\mathcal{E}(\rho) - \mathcal{E}(\sigma)]\} = \text{Tr} \{P_{\text{max}}[\mathcal{E}(R_+) - \mathcal{E}(R_-)]\} \\ &\leq \text{Tr} \{P_{\text{max}}[\mathcal{E}(R_+)]\} \\ &\leq \text{Tr} \{\mathcal{E}(R_+)\} \\ &= \text{Tr} \{R_+\} = \frac{1}{2} \text{Tr} \{R_+ + R_-\} = \frac{1}{2} \text{Tr} \{|R_+ - R_-|\} = \frac{1}{2} \text{Tr} \{|\rho - \sigma|\} = D_{\text{TD}}(\rho, \sigma), \end{aligned} \quad (6.20)$$

such that we get

$$D_{\text{TD}}(\mathcal{E}(\rho), \mathcal{E}(\sigma)) \leq D_{\text{TD}}(\rho, \sigma). \quad (6.21)$$

- Unitary operations are thus an example of quantum-operations, where the equality is reached

$$D_{\text{TD}}(U\rho_0 U^\dagger, U\sigma_0 U^\dagger) = D_{\text{TD}}(\rho_0, \sigma_0). \quad (6.22)$$

- Under Lindblad evolution $\dot{\rho} = \mathcal{L}\rho$ and $\dot{\sigma} = \mathcal{L}\sigma$, any two states can only get closer

$$D_{\text{TD}}(e^{\mathcal{L}t}\rho_0, e^{\mathcal{L}t}\sigma_0) \leq D_{\text{TD}}(\rho_0, \sigma_0). \quad (6.23)$$

In fact, we can even write this for infinitesimal time intervals using the divisibility of Markovian evolution $\rho(t + \Delta t) = e^{\mathcal{L}\Delta t}\rho(t)$

$$D_{\text{TD}}(e^{\mathcal{L}\Delta t}\rho(t), e^{\mathcal{L}\Delta t}\sigma(t)) \leq D_{\text{TD}}(\rho(t), \sigma(t)), \quad (6.24)$$

which means that under GKSL-dynamics, the distance between any two states must monotonously decrease. We have already observed this in Fig. 4.2.

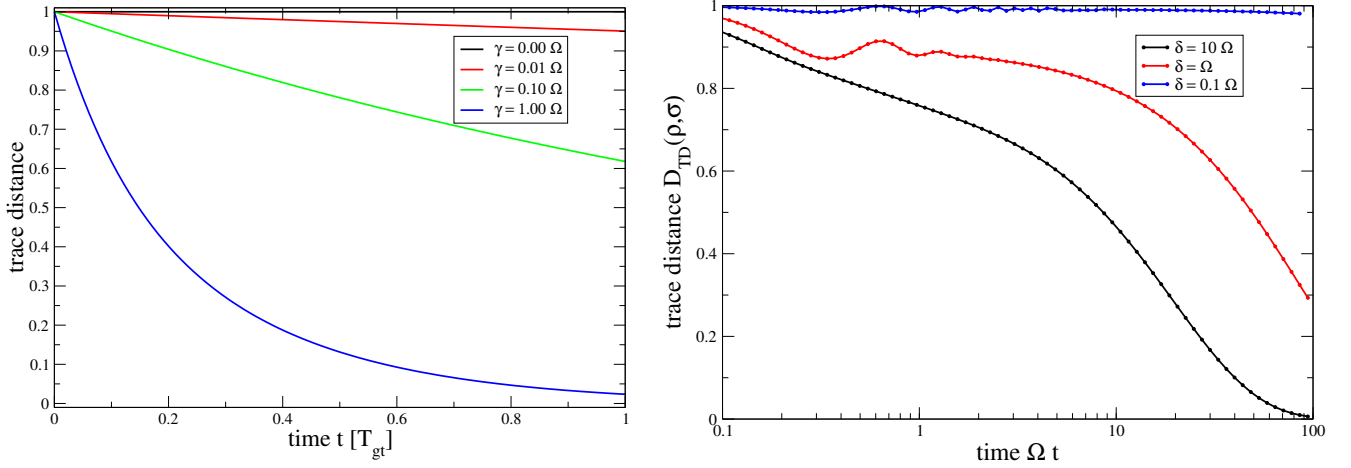


Figure 6.1: Left: Evolution of trace distance between the two states depicted in Fig. 4.2 over the full gate operation time $\Omega T_{\text{gt}} = \pi$ (same parameters as there). The trace distance decreases monotonously, which is a general feature of Lindblad evolution. Right: Evolution of the trace distance between the exact solutions of the pure-dephasing spin-boson model for the initial states $\rho_0 = |+\rangle\langle+|$ and $\sigma_0 = |-\rangle\langle-|$. Parameters $J_0\Omega = 1.0$, $\bar{\omega} = 5\Omega$, $\beta\Omega = 10$.

- For the exact solution of the pure-dephasing model (4.11) however, we only have

$$D_{\text{TD}}(\rho(t), \sigma(t)) \leq D_{\text{TD}}(\rho_0, \sigma_0), \quad (6.25)$$

which can be used as a measure to distinguish Markovian (continuously contractive) from non-Markovian evolution [28].

For a single qubit, this can be directly visualized with the euclidean distance between two states, which is visualized in Fig. 6.1. If we compare this to the exact solution of the spin-boson pure-dephasing model (4.11), we would for $|\pm\rangle = \frac{1}{\sqrt{2}}[|0\rangle \pm |1\rangle]$ gave

$$D_{\text{TD}}(\mathcal{E}(|-\rangle\langle-|), \mathcal{E}(|+\rangle\langle+|)) = e^{-f(t)}, \quad (6.26)$$

with $f(t)$ also defined in Eq. (4.11). From its definition, one can see that $f(t) \geq 0$, but its derivative

$$\begin{aligned} \frac{d}{dt}f(t) &= \frac{4}{\pi} \int_0^\infty J(\omega) \frac{d \sin^2(\omega t/2)}{dt} \frac{1}{\omega^2} \coth(\beta\omega/2) d\omega \\ &= \frac{2}{\pi} \int_0^\infty J(\omega) \frac{\sin(\omega t)}{\omega} \coth(\beta\omega/2) d\omega \end{aligned} \quad (6.27)$$

can become negative, in particular when $J(\omega) \coth(\beta\omega/2)$ is a strongly peaked function. For example, parametrizing the spectral density as

$$J(\omega) = J_0 \frac{\omega 4\bar{\omega} \delta^2}{[(\omega - \bar{\omega})^2 + \delta^2][(\omega + \bar{\omega})^2 + \delta^2]}, \quad (6.28)$$

which for $\bar{\omega} \gg \delta$ has a maximum of height J_0 and width δ at $\omega = \bar{\omega}$, one can achieve a non-monotonously decreasing trace distance, see Fig. 6.1 right panel.

We see that while with $f(t) \geq 0 = f(0)$, the trace distance always decreases with respect to its initial value

$$D_{\text{TD}}(\rho(t), \sigma(t)) \leq D_{\text{TD}}(\rho_0, \sigma_0), \quad (6.29)$$

it does not need not decrease monotonously under the exact evolution of the pure-dephasing spin-boson model, which highlights non-Markovian evolution [28].

6.2.2 Fidelity

The trace distance does not simplify significantly in case of pure states, as one can visualize in the Bloch sphere representation. Therefore, also other measures have been introduced.

The **classical fidelity** between two classical distributions is given by

$$F(\{p_n\}, \{q_n\}) = \sum_n \sqrt{p_n q_n}. \quad (6.30)$$

If the distributions are equal, we get $F(\{p_n\}, \{p_n\}) = \sum_n p_n = 1$, which demonstrates that the fidelity is not a metric. One can however construct a metric from the fidelity.

The quantum generalization yields the **fidelity between states** ρ and σ

$$F(\rho, \sigma) = \text{Tr} \left\{ \sqrt{\sqrt{\rho} \sigma \sqrt{\rho}} \right\}, \quad (6.31)$$

where often also the square is used $F(\rho, \sigma) \rightarrow F^2(\rho, \sigma)$.

- Since ρ and σ are density matrices, the above expression is well-defined. For example, by using the spectral decomposition $\rho = \sum_n \rho_n |n\rangle \langle n|$ we know that $\sqrt{\rho}$ is well-defined and positive. Then also using $\sigma = \sum_\alpha \sigma_\alpha |\alpha\rangle \langle \alpha|$ we see that the operator below the large root is positive

$$\langle \Psi | \sqrt{\rho} \sum_\alpha \sigma_\alpha |\alpha\rangle \langle \alpha| \sqrt{\rho} | \Psi \rangle = \sum_\alpha \sigma_\alpha |\langle \alpha | \sqrt{\rho} | \Psi \rangle|^2 \geq 0. \quad (6.32)$$

- When both states are pure $\rho = |\Psi\rangle \langle \Psi| = \sqrt{\rho}$ and $\sigma = |\Phi\rangle \langle \Phi|$, the fidelity reduces to the overlap between the states

$$F(\rho, \sigma) \rightarrow \text{Tr} \left\{ \sqrt{|\Psi\rangle \langle \Psi| |\Phi\rangle \langle \Phi| |\Psi\rangle \langle \Psi|} \right\} = |\langle \Psi | \Phi \rangle|. \quad (6.33)$$

- In the limit where both states commute $[\rho, \sigma] = 0$, we can use the spectral decomposition $\rho = \sum_n \rho_n |n\rangle \langle n|$ and $\sigma = \sum_n \sigma_n |n\rangle \langle n|$ to conclude that the fidelity reduces to the classical one (just as for the trace distance)

$$F(\rho, \sigma) \rightarrow \text{Tr} \left\{ \sqrt{\sum_n \rho_n^{1/2} \sigma_n \rho_n^{1/2} |n\rangle \langle n|} \right\} = \text{Tr} \left\{ \sum_n \sqrt{\rho_n \sigma_n} |n\rangle \langle n| \right\} = \sum_n \sqrt{\rho_n \sigma_n}. \quad (6.34)$$

This also implies that $F(\rho, \rho) = 1$.

- Unitary transformations do not change the fidelity

$$\begin{aligned} F(\rho, \sigma) &= \text{Tr} \left\{ U^\dagger U \sqrt{U^\dagger U \sqrt{\rho} U^\dagger U \sigma U^\dagger U \sqrt{\rho} U^\dagger U} \right\} \\ &= \text{Tr} \left\{ \sqrt{\sqrt{U \rho U^\dagger} U \sigma U^\dagger \sqrt{U \rho U^\dagger}} \right\} = F(U \rho U^\dagger, U \sigma U^\dagger). \end{aligned} \quad (6.35)$$

- The symmetry can be seen by writing the fidelity as a trace norm

$$F(\rho, \sigma) = \text{Tr} \left\{ \sqrt{(\sqrt{\sigma}\sqrt{\rho})^\dagger \sqrt{\sigma}\sqrt{\rho}} \right\} = \text{Tr} \left\{ \sqrt{\sqrt{\sigma}\sqrt{\rho} (\sqrt{\sigma}\sqrt{\rho})^\dagger} \right\} = F(\sigma, \rho). \quad (6.36)$$

- A metric can be constructed by (compare e.g. [1])

$$D_{\text{FD}}(\rho, \sigma) = \arccos F(\rho, \sigma). \quad (6.37)$$

For two states on the surface of the Bloch sphere, this metric then corresponds to the angle between the states.

- Quantum operations can only increase the fidelity between two states (which decreases the derived metric above)

$$F(\mathcal{E}(\rho), \mathcal{E}(\sigma)) \geq F(\rho, \sigma). \quad (6.38)$$

- There exist relations between fidelity and trace distance like

$$1 - F(\rho, \sigma) \leq D_{\text{TD}}(\rho, \sigma) \leq \sqrt{1 - F^2(\rho, \sigma)}. \quad (6.39)$$

In Fig. 5.6 right panel, we have actually already used the (squared) fidelity to quantify the distance between the time-dependent solution of the Schrödinger equation and individual energy eigenstates.

6.2.3 Quantum relative entropy

The **von-Neumann entropy** of a density matrix ρ is given by

$$S(\rho) = -\text{Tr} \{ \rho \ln \rho \}. \quad (6.40)$$

- It is well-defined since ρ is a positive definite matrix and can therefore be computed by the eigenvalues $S(\rho) = -\sum_n \rho_n \ln \rho_n$, from which we can conclude $0 \leq S(\rho)$, and where it is understood that $\lim_{\rho_n \rightarrow 0} \rho_n \ln \rho_n = 0$. If ρ_n are interpreted as probabilities, the expression is the entropy for a classical probability distribution and typically termed **Shannon entropy**.
- Often, one uses \log_2 in the definition, which merely then differs by a factor.
- From the expressions above one can see that the von-Neumann entropy of a pure state vanishes $S(|\Psi\rangle\langle\Psi|) = 0$.
- One can maximize the entropy subject to the constraint that $\sum_n \rho_n = 1 = \text{Tr} \{ \rho \}$ (e.g. with the method of Lagrange multipliers), and one then finds that the maximally mixed state is the one with maximum entropy

$$S\left(\frac{1}{N}\mathbf{1}\right) = \ln N, \quad (6.41)$$

such that we have $0 \leq S(\rho) \leq \ln N$ for a Hilbert space dimension N .

- In a similar fashion, one can show that the maximum entropy state at given mean energy $E = \text{Tr} \{H\rho\}$ is the canonical equilibrium state

$$\rho_c = \frac{e^{-\beta H}}{\text{Tr} \{e^{-\beta H}\}}, \quad (6.42)$$

where the Lagrange multiplier β assumes the role of the inverse temperature.

- For given mean energy $E = \text{Tr} \{H\rho\}$ and particle number $N = \text{Tr} \{\hat{N}\rho\}$, the grand-canonical equilibrium state also maximizes the entropy

$$\rho_{\text{gc}} = \frac{e^{-\beta(H-\mu N)}}{\text{Tr} \{e^{-\beta(H-\mu N)}\}}. \quad (6.43)$$

- The entropy of a tensor product is additive

$$\begin{aligned} S(\rho_A \otimes \rho_B) &= -\text{Tr} \{\rho_A \otimes \rho_B \ln(\rho_A \otimes \rho_B)\} = -\text{Tr} \{\rho_A \otimes \rho_B [(\ln \rho_A) \otimes \mathbf{1} + \mathbf{1} \otimes (\ln \rho_B)]\} \\ &= -\text{Tr}_A \{\rho_A \ln \rho_A\} - \text{Tr}_B \{\rho_B \ln \rho_B\} = S(\rho_A) + S(\rho_B), \end{aligned} \quad (6.44)$$

where we have used that the matrix logarithm of a product of two commuting (!) matrices behaves like the conventional logarithm.

Another way to quantify the distance between two quantum states is then the **quantum relative entropy**

$$D_{\text{QRE}}(\rho, \sigma) = \text{Tr} \{\rho[\ln \rho - \ln \sigma]\} = -S(\rho) - \text{Tr} \{\rho \ln \sigma\}. \quad (6.45)$$

- It is positive, which can be seen by introducing the spectral decomposition of both density matrices

$$\begin{aligned} \rho &= \sum_{\ell} \rho_{\ell} |\ell\rangle \langle \ell|, & 0 \leq \rho_{\ell} \leq 1, & \quad \sum_{\ell} \rho_{\ell} = 1, \\ \sigma &= \sum_{\alpha} \sigma_{\alpha} |\alpha\rangle \langle \alpha|, & 0 \leq \sigma_{\alpha} \leq 1, & \quad \sum_{\alpha} \sigma_{\alpha} = 1. \end{aligned} \quad (6.46)$$

Inserting them for the quantum relative entropy yields

$$\begin{aligned} -D_{\text{QRE}}(\rho, \sigma) &= \sum_{\ell} \rho_{\ell} [\langle \ell | \ln \sigma | \ell \rangle - \ln \rho_{\ell}] = \sum_{\ell} \rho_{\ell} \left[\sum_{\alpha} \ln(\sigma_{\alpha}) |\langle \ell | \alpha \rangle|^2 - \ln \rho_{\ell} \right] \\ &= \sum_{\ell} \rho_{\ell} \left[\sum_{\alpha} \ln(\sigma_{\alpha}) |\langle \ell | \alpha \rangle|^2 - \ln(\rho_{\ell}) \sum_{\alpha} |\langle \ell | \alpha \rangle|^2 \right] = \sum_{\ell} \sum_{\alpha} \rho_{\ell} |\langle \ell | \alpha \rangle|^2 \ln \frac{\sigma_{\alpha}}{\rho_{\ell}} \\ &\leq \sum_{\ell} \sum_{\alpha} \rho_{\ell} |\langle \ell | \alpha \rangle|^2 \left[\frac{\sigma_{\alpha}}{\rho_{\ell}} - 1 \right] = \sum_{\alpha} \sigma_{\alpha} - \sum_{\ell} \rho_{\ell} = 0, \end{aligned} \quad (6.47)$$

where we have used $\ln(x) \leq x - 1$, such that accordingly $D_{\text{QRE}}(\rho, \sigma) \geq 0$.

- When ρ and σ commute, we obtain the classical limit, the **Kullback-Leibler-divergence**

$$D_{\text{QRE}}(\rho, \sigma) \rightarrow \sum_{\ell} \rho_{\ell} \ln \frac{\rho_{\ell}}{\sigma_{\ell}}, \quad (6.48)$$

where ρ_{ℓ} and σ_{ℓ} are the eigenvalues of ρ and σ (in the same basis, with the same ordering).

- It is not a metric (it is evidently not even symmetric).
- Completely positive trace-preserving maps (trace-preserving quantum operations) reduce the relative entropy [29]

$$D_{\text{QRE}}(\mathcal{E}(\rho), \mathcal{E}(\sigma)) \leq D_{\text{QRE}}(\rho, \sigma). \quad (6.49)$$

- An important inequality for Lindblad dynamics $\mathcal{E}(\rho) = e^{\mathcal{L}t}\rho$ can be derived from this by taking $\sigma = \bar{\rho}$. One can write for Lindblad dynamics and $\Delta t > 0$ for the evolution of distances then

$$\begin{aligned} 0 &\geq \frac{1}{\Delta t} [D_{\text{QRE}}(e^{\mathcal{L}\Delta t}\rho(t), e^{\mathcal{L}\Delta t}\bar{\rho}) - D_{\text{QRE}}(\rho(t), \bar{\rho})] \\ &= \frac{1}{\Delta t} [D_{\text{QRE}}(\rho(t + \Delta t), \bar{\rho}) - D_{\text{QRE}}(\rho(t), \bar{\rho})] \\ &= \frac{1}{\Delta t} \text{Tr} \{ \rho(t + \Delta t) \ln(\rho(t + \Delta t)) - \rho(t + \Delta t) \ln \bar{\rho} - \rho(t) \ln \rho(t) + \rho(t) \ln \bar{\rho} \} \\ &= \frac{1}{\Delta t} [\Delta t \text{Tr} \{ [\mathcal{L}\rho(t)] \ln \rho(t) \} + \Delta t \text{Tr} \{ \rho(t) \rho^{-1}(t) [\mathcal{L}\rho(t)] \} - \Delta t [\mathcal{L}\rho(t)] \ln \bar{\rho} + \mathcal{O}(\Delta t^2)] \\ &\stackrel{\Delta t \rightarrow 0}{\rightarrow} \text{Tr} \{ [\mathcal{L}\rho(t)] [\ln \rho(t) - \ln \bar{\rho}] \}. \end{aligned} \quad (6.50)$$

Eventually, we can write this as **Spohn's inequality** [30]

$$-\text{Tr} \{ (\mathcal{L}\rho) [\ln \rho - \ln \bar{\rho}] \} \geq 0, \quad (6.51)$$

which has to hold for any Lindblad master equation where $\mathcal{L}\bar{\rho} = 0$ is a steady state.

- The quantum relative entropy can be straightforwardly related to the (quantum) **mutual information**, which measures (quantum and classical) correlation between two systems A and B via

$$I(A, B) \equiv S(\rho_A) + S(\rho_B) - S(\rho_{AB}) = D_{\text{QRE}}(\rho_{AB}, \rho_A \otimes \rho_B). \quad (6.52)$$

The mutual information evidently vanishes for product states but is finite also for classical correlations, as can be exemplified with the mixture $\rho_{AB} = \frac{1}{2} |00\rangle \langle 00| + \frac{1}{2} |11\rangle \langle 11|$, for which one gets $S(\rho_A) = S(\rho_B) = S(\rho_{AB}) = \ln 2$.

6.3 Entanglement

Being an obscure property of multipartite quantum systems that is however necessary for the quantum speedup, we would like to quantify entanglement between the constituents of bipartite (or multipartite) quantum systems.

6.3.1 Entanglement entropy

When $\rho_{AB} = |\Psi_{AB}\rangle \langle \Psi_{AB}|$ is a pure state, where in general

$$|\Psi_{AB}\rangle = \sum_{n_A} \sum_{m_B} c_{n_A, m_B} |n_A\rangle \otimes |m_B\rangle \quad (6.53)$$

denotes the tensor-product representation with coefficients c_{n_A, m_B} and basis states $|n_A\rangle$ and $|m_B\rangle$, respectively, one would like to have a measure for the non-classical correlations shared by A and B . The mutual information measures also the classical correlations, such that it is not sufficient. For this, it is helpful to note that any bipartite quantum state can also be written as

$$|\Psi_{AB}\rangle = \sum_{\alpha} \lambda_{\alpha} |a_{\alpha}\rangle \otimes |b_{\alpha}\rangle \quad : \quad \sum_{\alpha} \lambda_{\alpha}^2 = 1, \quad \lambda_{\alpha} \geq 0, \quad (6.54)$$

where $|a_{\alpha}\rangle$ and $|b_{\alpha}\rangle$ denote respective orthonormal bases in subsystem A and B (that in general are different from the original bases). The above decomposition is known as **Schmidt decomposition** with **Schmidt coefficients** λ_{α} . It is helpful because the single summation makes it simple to compute reduced states: Since $|a_{\alpha}\rangle$ and $|b_{\alpha}\rangle$ are orthonormal bases, we can evaluate the partial trace in them

$$\begin{aligned} \rho_A &= \text{Tr}_B \{ |\Psi_{AB}\rangle \langle \Psi_{AB}| \} = \sum_{\alpha} \lambda_{\alpha}^2 |a_{\alpha}\rangle \langle a_{\alpha}|, \\ \rho_B &= \text{Tr}_A \{ |\Psi_{AB}\rangle \langle \Psi_{AB}| \} = \sum_{\alpha} \lambda_{\alpha}^2 |b_{\alpha}\rangle \langle b_{\alpha}|. \end{aligned} \quad (6.55)$$

In turn, this provides us with a recipe to obtain the bases $\{|a_{\alpha}\rangle\}$ and $\{|b_{\alpha}\rangle\}$ and the Schmidt coefficients λ_{α} by the spectral decompositions of the reduced density matrices.

For pure bipartite states, a measure for the entanglement between subsystems A and B is the **entanglement entropy**, which is given by the von-Neumann entropy of the reduced state

$$E(|\Psi_{AB}\rangle) = S(\text{Tr}_B \{ |\Psi_{AB}\rangle \langle \Psi_{AB}| \}). \quad (6.56)$$

- The entanglement entropy is evidently positive as it inherits this property from the von-Neumann entropy. Particularly, it vanishes for separable states

$$E(|\Psi_A\rangle \otimes |\Psi_B\rangle) = S(|\Psi_A\rangle \langle \Psi_A|) = 0, \quad (6.57)$$

whereas for all other states (that have more than one term in their Schmidt decomposition), the reduced density matrix in A is mixed, such that the von-Neumann entropy is positive

$$E(|\Psi_{AB}\rangle) = - \sum_{\alpha} \lambda_{\alpha}^2 \ln \lambda_{\alpha}^2 > 0. \quad (6.58)$$

- The entanglement entropy of the state between two d -level systems

$$|\Psi_{\max}\rangle = \frac{1}{\sqrt{d}} [|1\rangle \otimes |1\rangle + \dots + |d\rangle \otimes |d\rangle] \quad (6.59)$$

is then given by

$$E(|\Psi_{\max}\rangle) = S\left(\frac{1}{d} [|1\rangle \langle 1| + \dots + |d\rangle \langle d|]\right) = \ln d, \quad (6.60)$$

which assumes its maximum value, and hence, the above state is considered as **maximally entangled state**. Such states (and equivalent ones connected to the above by local unitary transformations) can serve as a resource and are therefore like a currency standard to which one can compare.

- It does not matter which system is traced out: One always has with $\rho_A = \text{Tr}_B \{ |\Psi_{AB}\rangle \langle \Psi_{AB}| \}$ and $\rho_B = \text{Tr}_A \{ |\Psi_{AB}\rangle \langle \Psi_{AB}| \}$

$$S(\rho_A) = S(\rho_B). \quad (6.61)$$

Note that this even holds when A and B have different dimension, because it is a direct consequence of the Schmidt decomposition introduced before. Indeed, when looking at Eq. (6.55) one can see that ρ_A and ρ_B have the same non-vanishing eigenvalues.

6.3.2 Examples

Bell states

The Bell states are maximally entangled ones, because they are assigned the maximum entanglement entropy, e.g.

$$E\left(\frac{|01\rangle + |10\rangle}{\sqrt{2}}\right) = S\left(\frac{1}{2}|0\rangle\langle 0| + \frac{1}{2}|1\rangle\langle 1|\right) = \ln 2. \quad (6.62)$$

Asymmetric partitions

To work through a simple asymmetric example, consider the three-qubit state

$$|\Psi\rangle = \frac{1}{\sqrt{3}} [|001\rangle + |010\rangle + |100\rangle]. \quad (6.63)$$

The reduced state of the first qubit $A = \{1\}$ is

$$\rho_1 = \text{Tr}_{23} \{ |\Psi\rangle \langle \Psi| \} = \frac{2}{3} |0\rangle\langle 0| + \frac{1}{3} |1\rangle\langle 1|, \quad (6.64)$$

which has entropy $S(\rho_1) = \ln(3/2^{2/3}) \approx 0.637$. The reduced state of the other two qubits $B = \{2, 3\}$ is

$$\begin{aligned} \rho_{23} &= \text{Tr}_1 \{ |\Psi\rangle \langle \Psi| \} = \frac{1}{3} [|01\rangle\langle 01| + |01\rangle\langle 10| + |10\rangle\langle 01| + |10\rangle\langle 10| + |00\rangle\langle 00|] \\ &= \frac{2}{3} \frac{|01\rangle + |10\rangle}{\sqrt{2}} \frac{\langle 01| + \langle 10|}{\sqrt{2}} + \frac{1}{3} |00\rangle\langle 00|, \end{aligned} \quad (6.65)$$

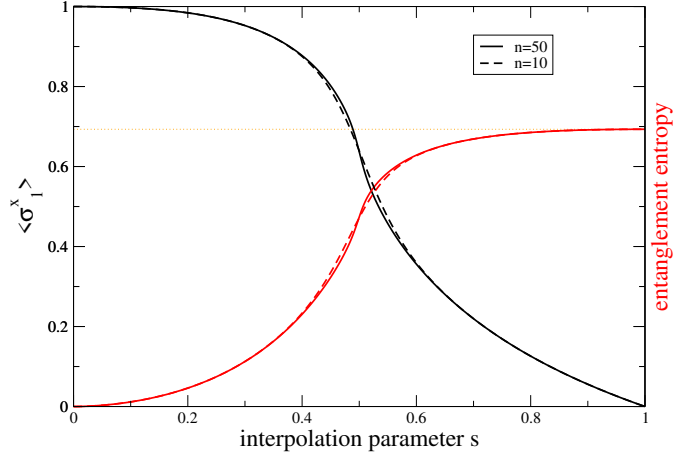
which has the same non-vanishing eigenvalues as ρ_1 , such that $S(\rho_1) = S(\rho_{23})$, despite the fact that B has a four-dimensional Hilbert space, whereas A has a two-dimensional one. From this, we can also find the Schmidt decomposition

$$|\Psi\rangle = \sqrt{\frac{2}{3}} |0\rangle \otimes \frac{|01\rangle + |10\rangle}{\sqrt{2}} + \sqrt{\frac{1}{3}} |1\rangle \otimes |00\rangle. \quad (6.66)$$

Ising model entanglement

If we revisit the Ising model (5.59), we can ask about the entanglement between any spin and the rest of the chain, when the global system is prepared in the ground state $|\Psi_0(s)\rangle$. Since the whole

Figure 6.2: Expectation value of $\langle \sigma_\ell^x \rangle$ (black) and the derived entanglement entropy (red) for the entanglement between a single spin of the Ising model and the rest of the chain versus interpolation parameter s . The thin dotted line at $\ln 2$ provides the upper bound for the entanglement entropy of a single spin. The limits $s = 0$ (no entanglement) and $s = 1$ (Schrödinger ket state $\frac{1}{\sqrt{2}}[|0\dots 0\rangle + |1\dots 1\rangle]$) can be understood analytically.



model is invariant under cyclic permutations of the spins, without loss of generality we consider the first

$$\rho_1 = \text{Tr}_{2\dots n} \{ |\Psi_0(s)\rangle \langle \Psi_0(s)| \} = \frac{1}{2} [\mathbf{1} + \mathbf{n} \cdot \boldsymbol{\sigma}]. \quad (6.67)$$

We can evaluate along the Jordan-Wigner (5.66), DFT (5.76), and Bogoliubov (5.79) transforms employed in the diagonalization of the Ising model to find

$$\begin{aligned} n_x &= \langle \Psi_0(s) | \sigma_1^x | \Psi_0(s) \rangle = \langle \Psi_0(s) | (\mathbf{1} - 2c_1^\dagger c_1) | \Psi_0(s) \rangle = 1 - \frac{2}{n} \sum_{kq} e^{-i(k-q)2\pi/n} \langle \Psi_0(s) | \tilde{c}_k^\dagger \tilde{c}_q | \Psi_0(s) \rangle \\ &= 1 - \frac{2}{n} \sum_{kq} e^{-i(k-q)2\pi/n} \langle \Psi_0(s) | \left(u_k^* \gamma_{+k}^\dagger + v_{-k} \gamma_{-k} \right) \left(u_q \gamma_q + v_{-q}^* \gamma_{-q}^\dagger \right) | \Psi_0(s) \rangle \\ &= 1 - \frac{2}{n} \sum_k |v_{-k}|^2, \\ n_y &= \langle \Psi_0(s) | i(c_1^\dagger - c_1) | \Psi_0(s) \rangle = \dots = 0, \\ n_z &= -\langle \Psi_0(s) | (c_1^\dagger + c_1) | \Psi_0(s) \rangle = \dots = 0, \end{aligned} \quad (6.68)$$

where the first expectation value can be made explicit by Eq. (5.83) and in the other equations we have used that the DFT and Bogoliubov transforms are linear transformations of annihilation and creation operators, such that their expectation value in the Ising ground state vanishes. The result is then depicted in Fig. 6.2. The entanglement entropy does depend on the chosen partition. For the Ising model for example, we may equally well split the ring into two equally-sized parts. One then observes that the entanglement entropy of the ground state develops a peak near the critical point, with a height that scales mildly with the system size [31, 32], see Fig. 6.3. The scaling laws of the ground state entanglement entropy are an interesting research subject of its own [33].

Since adiabatic algorithms with a small energy gap are in some sense analogous to quantum-critical phenomena, a scaling entanglement entropy has also been used to measure the performance of such algorithms [21].

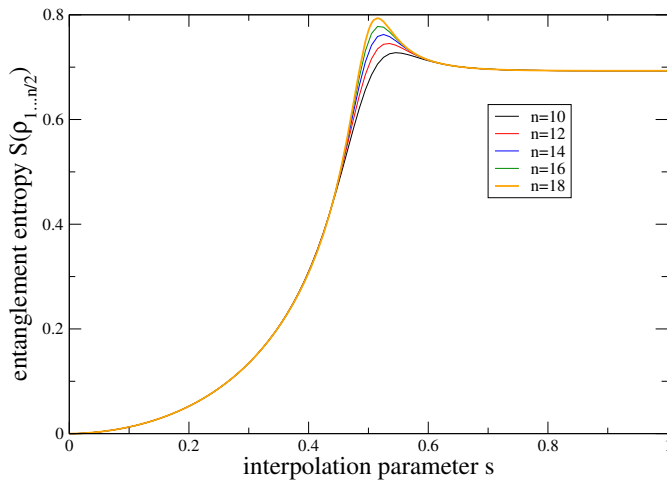


Figure 6.3: Entanglement entropy of one half Ising ring in the global Ising ground state for different lengths n . The peak in the middle scales with the system size n and denotes a finite-size precursor of a quantum phase transition. For $n \rightarrow \infty$, it scales logarithmically with the chain length $S_{\max} \propto \ln n$ (which is significantly smaller than the maximum possible scaling which would be $S \leq \ln d = \frac{n}{2} \ln 2$) and its position moves to $s = 1/2$.

Collective spin models

In collective spin models, characterized by a Hamiltonian $H(J^x, J^y, J^z)$ with large spins

$$J^\alpha = \frac{1}{2} \sum_{i=1}^n \sigma_i^\alpha, \quad (6.69)$$

one can via the commutation relations

$$[J^x, J^y] = \frac{1}{4} \sum_{ij} [\sigma_i^x, \sigma_j^y] = \frac{i}{2} \sum_i \sigma_i^z = iJ^z \quad (6.70)$$

and cyclic permutations thereof conclude that the large spin operators commute with the total angular momentum operator, e.g.

$$\begin{aligned} [J^x, (J^x)^2 + (J^y)^2 + (J^z)^2] &= J^y [J^x, J^y] + [J^x, J^y] J^y + J^z [J^x, J^z] + [J^x, J^z] J^z \\ &= iJ^y J^z + iJ^z J^y - iJ^z J^y - iJ^y J^z = 0 \end{aligned} \quad (6.71)$$

and likewise for the other components. From this, we can conclude that for such Hamiltonians, the total angular momentum is conserved

$$[H, J^2] = [H, (J^x)^2 + (J^y)^2 + (J^z)^2] = 0, \quad (6.72)$$

and one can classify the eigenstates of such Hamiltonians according to their total angular momentum. Within each subspace of given total angular momentum

$$J^2 |j, m\rangle = j(j+1) |j, m\rangle \quad (6.73)$$

one can use the eigenstates of J^z

$$J^z |j, m\rangle = m |j, m\rangle \quad (6.74)$$

as a basis, and by introducing the **ladder operators**

$$J^\pm = \frac{1}{2} \sum_{i=1}^n (\sigma_i^x \pm i\sigma_i^y) = \sum_i \sigma_i^\pm = J^x \pm iJ^y, \quad (6.75)$$

one can see that they allow to construct the other basis members from just one of a given angular momentum sector

$$J^\pm |j, m\rangle = \sqrt{j(j+1) - m(m \pm 1)} |j, m \pm 1\rangle \quad : \quad -j \leq m \leq +j. \quad (6.76)$$

For n qubits one has $j_{\max} = n/2$.

One example of such a collective is the Dicke model of superradiant decay that describes the collective coupling of n two-level atoms (qubits) to a bosonic reservoir (the surrounding electromagnetic field)

$$H = \Omega J^z + 2J^x \otimes \sum_k \left(h_k b_k + h_k b_k^\dagger \right) + \sum_k \omega_k b_k^\dagger b_k. \quad (6.77)$$

The master equation for the system then assumes the form

$$\begin{aligned} \dot{\rho}_S = & -i \left[\Omega J^z + \Delta E_+ J^+ J^- + \Delta E_- J^- J^+, \rho_S \right] \\ & + J(\Omega) [1 + n_B(\Omega)] \left[J^- \rho_S J^+ - \frac{1}{2} \{ J^+ J^-, \rho_S \} \right] + J(\Omega) n_B(\Omega) \left[J^+ \rho_S J^- - \frac{1}{2} \{ J^- J^+, \rho_S \} \right], \end{aligned} \quad (6.78)$$

where Ω is the splitting of an individual atom, $J(\Omega)$ is the spectral density, and ΔE_\pm denote Lamb-shift terms. For low temperatures $n_B(\omega) \rightarrow 0$ the master equation predicts a striking collective speedup of relaxation from the state $|m = +n/2\rangle = |0 \dots 0\rangle$ down to the state $|m = -n/2\rangle = |1 \dots 1\rangle$ as compared to the independent decay of two-level systems [34]. This speedup becomes possible due to the increased transition rates around $m \approx 0$, and we can ask for the role of entanglement in this process.

For example, for $n = 3$ we would have for the relevant maximum angular momentum states

$$\begin{aligned} \left| \frac{3}{2}, +\frac{3}{2} \right\rangle &= |000\rangle, \\ \left| \frac{3}{2}, +\frac{1}{2} \right\rangle &= \frac{1}{\sqrt{3}} [|001\rangle + |010\rangle + |100\rangle], \\ \left| \frac{3}{2}, -\frac{1}{2} \right\rangle &= \frac{1}{\sqrt{3}} [|110\rangle + |101\rangle + |011\rangle], \\ \left| \frac{3}{2}, -\frac{3}{2} \right\rangle &= |111\rangle, \end{aligned} \quad (6.79)$$

and we note that these states (also known as **Dicke states**) are always completely symmetric superpositions of computational basis states with a given total number of 1s

$$\left| \frac{n}{2}, m \right\rangle \equiv |m\rangle = \frac{1}{\sqrt{\binom{n}{\frac{n}{2}-m}}} \sum_{\mathbf{z}: \langle \mathbf{z} | J^z | \mathbf{z} \rangle = m} |\mathbf{z}\rangle. \quad (6.80)$$

To compute the entanglement in such a Dicke state, we compute the reduced density matrix of just one qubit, where from symmetry considerations it does not matter which we choose

$$\rho_i = \text{Tr}_{1 \dots (i-1), (i+1) \dots n} \{ |m\rangle \langle m| \} = \frac{1}{2} [\mathbf{1} + \mathbf{n} \cdot \boldsymbol{\sigma}]. \quad (6.81)$$

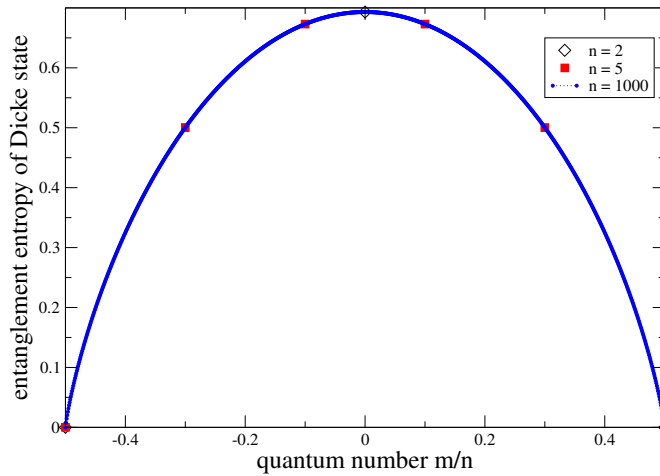


Figure 6.4: Entanglement entropy between a single qubit and the others in the Dicke states $|m\rangle$ vs. m/n and for different n . For $m = 0$, it reaches the maximum value $\ln 2$ for all n .

The coefficients in the Bloch sphere representation can be computed from expectation values

$$n_\alpha = \langle m | \sigma_i^\alpha | m \rangle = \frac{2}{n} \langle m | J^\alpha | m \rangle, \quad (6.82)$$

where we have again used the symmetry of the Dicke states. This implies

$$n_x = n_y = 0, \quad -1 \leq n_z = \frac{2m}{n} \leq +1, \quad \rho_i = \frac{1}{2} \begin{pmatrix} 1 + \frac{2m}{n} & 0 \\ 0 & 1 - \frac{2m}{n} \end{pmatrix}, \quad (6.83)$$

for which we can readily compute the von-Neumann entropy, see Fig. 6.4. It follows that the Dicke states are highly entangled, in particular those with $|m| \ll n/2$. This however is just a statement about the entanglement in the basis states that are convenient to treat this particular problem.

6.3.3 Entanglement of mixed states

Unfortunately however, the naive application of the entanglement entropy to mixed global states leads to problems. Consider, for example, the two-qubit density matrix

$$\rho_{AB} = \frac{1}{2} \frac{|00\rangle + |11\rangle}{\sqrt{2}} \frac{\langle 00| + \langle 11|}{\sqrt{2}} + \frac{1}{2} \frac{|00\rangle - |11\rangle}{\sqrt{2}} \frac{\langle 00| - \langle 11|}{\sqrt{2}}, \quad (6.84)$$

which one could interpret as a statistical mixture of two (maximally entangled) Bell states. However, simple expansion also shows that

$$\rho_{AB} = \frac{1}{2} |00\rangle \langle 00| + \frac{1}{2} |11\rangle \langle 11|, \quad (6.85)$$

which is a mixture of two separable states that are not entangled at all. The naive application of the entropy of entanglement recipe would yield the maximal entanglement of the Bell state $S(\text{Tr}_B \{\rho_{AB}\}) = S(\frac{1}{2} |0\rangle \langle 0| + \frac{1}{2} |1\rangle \langle 1|) = \ln 2$. To the contrary, to define an entanglement measure for a mixed state, the following properties should be met [35]

- Separable states contain no entanglement. Such **separable states** can be written in the form

$$\rho_{AB} = \sum_i p_i \rho_A^i \otimes \rho_B^i \quad (6.86)$$

with probabilities $0 \leq p_i \leq 1$ and $\sum_i p_i = 1$ and where ρ_A^i and ρ_B^i are valid density matrices (trace-normalized, hermitian, and positive) in subsystem A and B , respectively. The above example would thereby not contain any entanglement.

- To the contrary, all non-separable states are entangled.
- The entanglement between two parties does not increase under local operations and classical communication operations (**LOCC operations**). As a special case we note that entanglement does not change at all under local unitary operations.
- There exist maximally entangled states, e.g. for two parties with d -dimensional subsystems the state

$$|\Psi_{\max}\rangle = \frac{|1, 1\rangle + \dots + |d, d\rangle}{\sqrt{d}} \quad (6.87)$$

is maximally entangled. One example for this are the Bell states. Since one can prepare essentially all other states by LOCC operations from the maximally entangled ones, the maximally entangled states provide some reference to which one can compare.

A way to respect this would be to use the **entanglement of formation**

$$E_F(\rho) = \inf_{\{p_i, |\Psi_i\rangle\} : \rho = \sum_i p_i |\Psi_i\rangle\langle\Psi_i|} p_i S(\text{Tr}_B \{|\Psi_i\rangle\langle\Psi_i|\}), \quad (6.88)$$

which for the example above would yield $E_F(\rho) = 0$. In general however, finding the infimum decomposition of a density matrix is a hard problem.

6.3.4 Concurrence

For general mixed states of only two qubits, this problem has been solved [36]. The **entanglement of formation** $E_F(\rho)$ for a mixed two-qubit density matrix ρ is given by

$$E_F(\rho) = s\left(\frac{1 + \sqrt{1 - C^2(\rho)}}{2}\right) \quad : \quad s(x) = -x \ln x - (1 - x) \ln(1 - x),$$

$$C(\rho) = \max\{0, \lambda_1 - \lambda_2 - \lambda_3 - \lambda_4\}, \quad (6.89)$$

where the quantity $C(\rho)$ is known as **concurrence** (and often used independently), the function $s(x)$ computes the von-Neumann entropy of a single-qubit density matrix with eigenvalues x and $1 - x$, and $\lambda_1 \geq \lambda_2 \geq \lambda_3 \geq \lambda_4$ are the sorted eigenvalues of the matrix

$$R = \sqrt{\sqrt{\rho} [\sigma_y \otimes \sigma_y \rho^* \sigma_y \otimes \sigma_y] \sqrt{\rho}}, \quad (6.90)$$

where ρ^* denotes the complex conjugate density matrix.

One can see that these definitions remain sensible.

- You may see other definitions. For example, to compare with the entropy of formation where the entropy is taken with \log_2 , one has to replace $\ln \rightarrow \log_2$. Likewise, instead of calculating the eigenvalues of R , an equivalent representation asks to calculate the squareroots of the (nevertheless positive) eigenvalues of the non-hermitian matrix $R'^2 = \rho[\sigma_y \otimes \sigma_y \rho^* \sigma_y \otimes \sigma_y]$.

- As with our discussion of fidelity, since ρ^* is a valid density matrix and $[\sigma_y \otimes \sigma_y \rho^* \sigma_y \otimes \sigma_y]$ is also valid (it is just a spin-flipped state of ρ^*), it leads to a valid density matrix, such that what is under the root is positive definite.
- For a two-qubit pure state

$$|\Psi\rangle = c_{00}|00\rangle + c_{01}|01\rangle + c_{10}|10\rangle + c_{11}|11\rangle \quad : \quad \rho = |\Psi\rangle\langle\Psi| = \sqrt{\rho}, \quad (6.91)$$

this falls back to the entanglement entropy $S(\text{Tr}_2\{|\Psi\rangle\langle\Psi|\})$. Particularly, we get

$$\begin{aligned} R &= \sqrt{|\Psi\rangle\langle\Psi| \sigma_y \otimes \sigma_y |\Psi^*\rangle\langle\Psi^*| \sigma_y \otimes \sigma_y |\Psi\rangle\langle\Psi|} \\ &= |\langle\Psi| \sigma_y \otimes \sigma_y |\Psi^*\rangle| |\Psi\rangle\langle\Psi|, \end{aligned} \quad (6.92)$$

from which one can see that $\lambda_1 = |\langle\Psi| \sigma_y \otimes \sigma_y |\Psi^*\rangle| = 2|c_{01}^*c_{10}^* - c_{00}^*c_{11}^*|$ whereas $\lambda_2 = \lambda_3 = \lambda_4 = 0$. The concurrence of a pure state is thereby given by

$$C(|\Psi\rangle\langle\Psi|) = 2|c_{01}^*c_{10}^* - c_{00}^*c_{11}^*|. \quad (6.93)$$

This can take values $0 \leq C(|\Psi\rangle\langle\Psi|) \leq 1$, and if we compute the reduced state of a two-qubit state

$$\rho_1 = \frac{1}{2}[\mathbf{1} + \mathbf{n} \cdot \boldsymbol{\sigma}] = \text{Tr}_2\{|\Psi\rangle\langle\Psi|\}, \quad (6.94)$$

we can readily compute its eigenvalues $\lambda_{\pm} = \frac{1}{2}[1 \pm |\mathbf{n}|]$, and by explicitly computing $n_{\alpha} = \text{Tr}\{\sigma_1^{\alpha} |\Psi\rangle\langle\Psi|\} = \langle\Psi| \sigma_1^{\alpha} |\Psi\rangle$ one finds

$$\begin{aligned} \langle\Psi| \sigma_1^x |\Psi\rangle &= c_{00}c_{10}^* + c_{01}c_{11}^* + c_{10}c_{00}^* + c_{11}c_{01}^*, \\ \langle\Psi| \sigma_1^y |\Psi\rangle &= ic_{00}c_{10}^* + ic_{01}c_{11}^* - ic_{10}c_{00}^* - ic_{11}c_{01}^*, \\ \langle\Psi| \sigma_1^z |\Psi\rangle &= c_{00}c_{00}^* + c_{01}c_{01}^* - c_{10}c_{10}^* - c_{11}c_{11}^*, \end{aligned} \quad (6.95)$$

with which after some calculations one finds that

$$\mathbf{n} \cdot \mathbf{n} = 1 - C^2(|\Psi\rangle\langle\Psi|). \quad (6.96)$$

This shows that the reduced state is mixed (witnessing entanglement in $|\Psi\rangle$) when the concurrence is positive. The agreement however demonstrates that the above entanglement of formation falls back to the entanglement entropy for pure two-qubit states, since in the above entanglement of formation formula we can identify $x = 1/2[1 + |\mathbf{n}|]$ and $1 - x = 1/2[1 - |\mathbf{n}|]$.

- For a product state $\rho_{AB} = \rho_A \otimes \rho_B$ we get by inspection that the matrix R has four identical eigenvalues $\lambda_i = \lambda$ and hence $C(\rho_A \otimes \rho_B) = 0$.
- The maximum concurrence $C(\rho) = 1$ is achieved for pure Bell states, and the entanglement of formation is then $\ln 2$. For example, we get for the pure Bell state $C\left(\frac{|01\rangle+|10\rangle}{\sqrt{2}}\frac{\langle 01|+\langle 10|}{\sqrt{2}}\right) = 1$, such that the entropy becomes $\ln 2$ (or 1 if \log_2 is chosen).

6.3.5 Examples

Bell states

Let us consider a mixture of Bell states

$$\rho_{AB} = p \frac{|00\rangle + |11\rangle}{\sqrt{2}} \frac{\langle 00| + \langle 11|}{\sqrt{2}} + (1-p) \frac{|00\rangle - |11\rangle}{\sqrt{2}} \frac{\langle 00| - \langle 11|}{\sqrt{2}} \quad (6.97)$$

with $0 \leq p \leq 1$ parametrizing the mixture. Then, the eigenvalues of the matrix R are given by

$$\lambda_i \in \{1-p, p, 0, 0\}, \quad (6.98)$$

such that the concurrence becomes

$$C(\rho_{AB}) = |1-2p|, \quad (6.99)$$

and the derived entanglement of formation

$$E_F(\rho_{AB}) = -\frac{1+2\sqrt{p(1-p)}}{2} \ln \frac{1+2\sqrt{p(1-p)}}{2} - \frac{1-2\sqrt{p(1-p)}}{2} \ln \frac{1-2\sqrt{p(1-p)}}{2} \quad (6.100)$$

becomes maximal when $p=0$ or $p=1$ (pure Bell state) and vanishes if and only if $p=1/2$ (which reproduces our previous example).

Ising model ground state

We can revisit the Ising model (5.59) ground state $|\Psi_0(s)\rangle$ and from this derive the mixed state of any two different qubits $i \neq j$

$$\rho_{ij} = \text{Tr}_{k \neq i,j} \{ |\Psi_0(s)\rangle \langle \Psi_0(s)| \}. \quad (6.101)$$

For this – in general mixed – density matrix, we can find the mutual information

$$I(\rho_{ij}) = S(\rho_i) + S(\rho_j) - S(\rho_{ij}) \quad (6.102)$$

and via the concurrence $C(\rho_{ij})$ also the entanglement of formation

$$E_F(\rho_{ij}) = S \left(\frac{1}{2} [\mathbf{1} + \sqrt{1 - C^2(\rho_{ij}) \sigma^z}] \right) \quad (6.103)$$

between any two qubits on the Ising chain. One finds that whereas classical correlations quickly build up for $s > 0$, the entanglement of formation between two qubits is only finite between next neighbours and next-next-neighbours, see Fig. 6.5. For the Ising model, this can actually be made explicit analytically [37, 38]. In the figure, we also see that the mutual information is always larger than the entanglement of formation. However, this need not generally be the case [39].

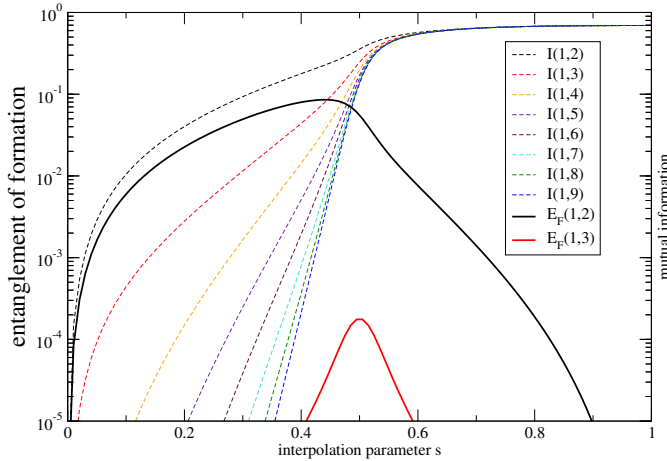


Figure 6.5: Correlations between pairs of qubits in the ground state of an Ising model (5.59) with $n = 18$ spins. Whereas general (quantum and classical) correlations as measured by the mutual information (dashed) quickly build up with the ferromagnetic interaction ($s > 0$), quantum entanglement of formation (solid) only exists between neighbouring and next-neighbouring qubits.

Completely symmetric spin states

For fully symmetric spin systems – such as e.g. the Dicke model describing the collective coupling – the two-spin density matrix of arbitrary two qubits must be fully symmetric under exchange of the qubits, which imposes some constraints on its matrix elements. In the computational basis for two qubits $\{|00\rangle, |01\rangle, |10\rangle, |11\rangle\}$, we can therefore give its matrix representation as

$$\rho_{12} = \begin{pmatrix} v_+ & x_+^* & x_+^* & u^* \\ x_+ & w & y & x_-^* \\ x_+ & y & w & x_-^* \\ u & x_- & x_- & v_- \end{pmatrix}, \quad (6.104)$$

which has 7 parameters, and taking into account the trace condition we only have 6 instead of 15 possible parameters in the two-qubit density matrix. From this, we can compute the reduced matrices ρ_1 and ρ_2 , the mutual information $I_{12} = S(\rho_1) + S(\rho_2) - S(\rho_{12}) = 2S(\rho_1) - S(\rho_{12})$ and the concurrence. The parameters can be expressed by expectation values of Pauli matrices

$$\begin{aligned} v_{\pm} &= \text{Tr} \left\{ \frac{1}{4} (\mathbf{1} \pm 2\sigma_1^z + \sigma_1^z \sigma_2^z) \rho_{12} \right\}, \\ x_{\pm} &= \text{Tr} \left\{ \frac{1}{2} (\sigma_1^+ \pm \sigma_1^+ \sigma_2^z) \rho_{12} \right\}, \\ w &= \text{Tr} \left\{ \frac{1}{4} (\mathbf{1} - \sigma_1^z \sigma_2^z) \rho_{12} \right\}, \\ y &= \text{Tr} \left\{ \frac{1}{4} (\sigma_1^x \sigma_2^x + \sigma_1^y \sigma_2^y) \rho_{12} \right\}, \\ u &= \text{Tr} \left\{ \frac{1}{4} (\sigma_1^x \sigma_2^x - \sigma_1^y \sigma_2^y + 2i\sigma_1^x \sigma_2^y) \rho_{12} \right\}. \end{aligned} \quad (6.105)$$

The important point is now that for a fully symmetric system, these expectation values of arbitrary two qubits (1 and 2 can correspond to any different labels) can be linked to the expectation values

of large-spin operators [40]. For the relevant ones one gets

$$\begin{aligned}
\langle \sigma_1^\alpha \rangle &= \frac{2}{n} \langle J^\alpha \rangle, & \langle \sigma_1^+ \rangle &= \frac{1}{n} \langle J^+ \rangle, \\
\langle \sigma_1^\alpha \sigma_2^\alpha \rangle &= \frac{4 \langle (J^\alpha)^2 \rangle - n}{n(n-1)}, \\
\langle \sigma_1^x \sigma_2^y \rangle &= \frac{2 \langle \{J^x, J^y\} \rangle}{n(n-1)}, \\
\langle \sigma_1^+ \sigma_2^z \rangle &= \frac{\langle \{J^+, J^z\} \rangle}{n(n-1)}.
\end{aligned} \tag{6.106}$$

Here, the first line becomes evident by inserting the definition of J^α or J^+ in terms of Pauli matrices and using that due to symmetry, all individual resulting terms must be identical. The other terms also become evident by inserting the definitions of the large-spin operators, using that $\langle \sum_i (\sigma_i^\alpha)^2 \rangle = \langle \mathbf{1}n \rangle = n$ and that in the product of large spin operators one gets $n(n-1)$ terms where the Pauli matrices act on different spins, e.g.

$$\begin{aligned}
\text{Tr} \{ (J^\alpha J^\beta + J^\beta J^\alpha) \rho_{\text{symm}} \} &= \frac{1}{4} \sum_{ij} \text{Tr} \{ (\sigma_i^\alpha \sigma_j^\beta + \sigma_i^\beta \sigma_j^\alpha) \rho_{\text{symm}} \} \\
&= \frac{n}{2} + \frac{1}{4} \sum_{i \neq j} \text{Tr} \{ (\sigma_i^\alpha \sigma_j^\beta + \sigma_j^\beta \sigma_i^\alpha) \rho_{\text{symm}} \} \\
&= \frac{n}{2} + \frac{1}{4} n(n-1) \text{Tr} \{ (\sigma_1^\alpha \sigma_2^\beta + \sigma_2^\beta \sigma_1^\alpha) \rho_{\text{symm}} \},
\end{aligned} \tag{6.107}$$

where in the last line we have used that by symmetry they will all get the same expectation values. From this, one finds that the density matrix of arbitrary two qubits of a fully symmetric system – and thereby the concurrence between any two qubits chosen from that fully symmetric system – can be linked to expectation values of large-spin operators. The concurrence between any two qubits in the maximum angular momentum Dicke state has been calculated [40]

$$C(\text{Tr}_{3\dots n} \{ |m\rangle \langle m| \}) = \frac{1}{2n(n-1)} \left[n^2 - 4m^2 - \sqrt{(n^2 - 4m^2)[(n-2)^2 - 4m^2]} \right], \tag{6.108}$$

from which we can see that the concurrence (and hence the entanglement) vanishes for $m = \pm n/2$. Interestingly, the states with $m = -n/2 + 1$ and $m = +n/2 - 1$ are the ones with the highest concurrence $C_{\text{max}} = 2/n$ (and hence largest pairwise entanglement), and not the ones with $m \approx 0$ (which have the largest qubit-remainder entanglement). The derived maximum pairwise entanglement for these states $E_{\text{max}} = (1 + 2 \ln n)/n^2 + \mathcal{O}((\ln n)/n^4)$ is significantly smaller than the qubit-remainder entanglement depicted in Fig. 6.4. Furthermore, for $n = 2$ and $m = 0$ the concurrence reaches the maximum possible value $C \rightarrow 1$, such that the derived entanglement of formation becomes maximal. However, the corresponding Dicke state

$$|1, 0\rangle = \frac{1}{\sqrt{2}} [|01\rangle + |10\rangle] \tag{6.109}$$

is just one of the Bell states, such that this outcome is to be expected. For large n , the pairwise entanglement in the Dicke states, see Fig. 6.6 is significantly smaller than the entanglement between a single qubit and the rest.

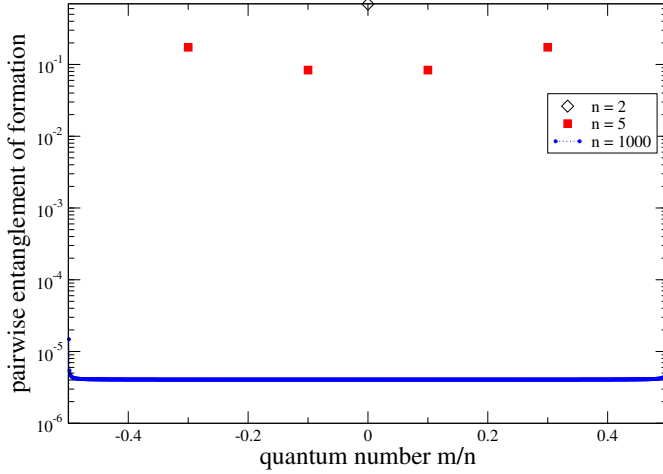


Figure 6.6: Entanglement of formation between two different qubits when the atomic cloud is purely prepared in one of the Dicke states $|m\rangle$ vs. m/n and for different n . For $m = -n/2 + 1$ and $m = +n/2 - 1$, it reaches its maximum value for all n . The pairwise entanglement is thus for $n > 2$ significantly smaller than the entanglement between a single qubit and the rest depicted in Fig. 6.4.

Superradiant decay

For systems that are fully symmetric under particle exchange, the two-qubit density matrix of any two qubits (6.104) can be fully expressed by expectation values of large spin operators. From this mixed reduced density matrix we can get the concurrence and from the concurrence the entanglement of formation. The expectation value of large-spin operators can be obtained by solving the master equation

$$\begin{aligned} \dot{\rho}_S = & -i \left[\Omega J^z + \frac{\sigma(\Omega)}{2i} J^+ J^- + \frac{\sigma(\Omega)}{2i} J^- J^+, \rho_S \right] \\ & + J(\Omega)[1 + n_B(\Omega)] \left[J^- \rho_S J^+ - \frac{1}{2} \{ J^+ J^-, \rho_S \} \right] + J(\Omega)n_B(\Omega) \left[J^+ \rho_S J^- - \frac{1}{2} \{ J^- J^+, \rho_S \} \right], \end{aligned} \quad (6.110)$$

where Ω is the splitting of an individual atom, $n_B(\Omega) = [e^{\beta\Omega} - 1]^{-1}$ and $\sigma(\pm\Omega)$ denote Lamb-shift terms. We parametrize the spectral density as

$$J(\omega) = \Gamma \frac{4\omega\bar{\omega}\delta^2}{[(\omega - \bar{\omega})^2 + \delta^2][(\omega + \bar{\omega})^2 + \delta^2]}, \quad (6.111)$$

which is an odd function of ω and for $\delta \ll \bar{\omega}$ has a peak of height Γ at position $\bar{\omega}$ with a width δ . For such a spectral density an explicit analytic calculation of the Lamb-shift terms in the zero-temperature limit is possible

$$\sigma(\omega) = \frac{i}{\pi} \mathcal{P} \int \frac{J(\omega')[1 + n_B(\omega')]}{\omega - \omega'} d\omega' \rightarrow \frac{i}{\pi} \mathcal{P} \int_0^\infty \frac{J(\omega')}{\omega - \omega'} d\omega', \quad (6.112)$$

such that we can numerically solve the full master equation. However, if initially no coherences in the Dicke basis are present, the density matrix can at all times be written as a statistical mixture of Dicke states

$$\rho_S(t) = \sum_m P_m(t) |m\rangle \langle m|, \quad (6.113)$$

Figure 6.7: Superradiant decay of a cloud of n two-level systems according to Eq. (6.110) vs. dimensionless time for zero temperature. The collective effect leads to a quadratic speedup of relaxation, which in the radiated energy current (inset) shows up as a peak of the radiation intensity with a height scaling as n^2 . Parameters: $J(\Omega) = \Gamma$.

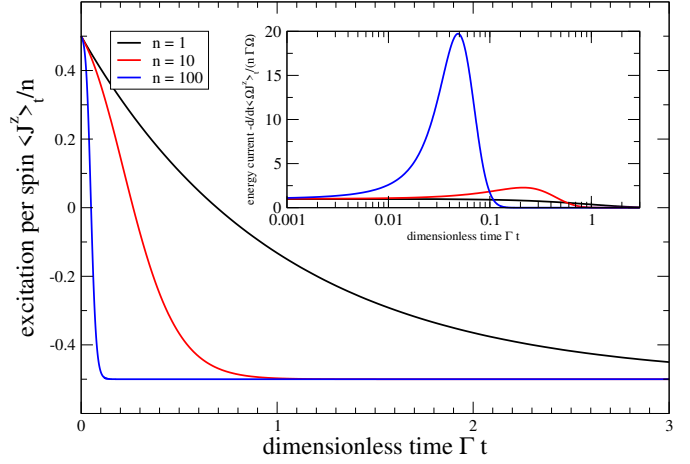
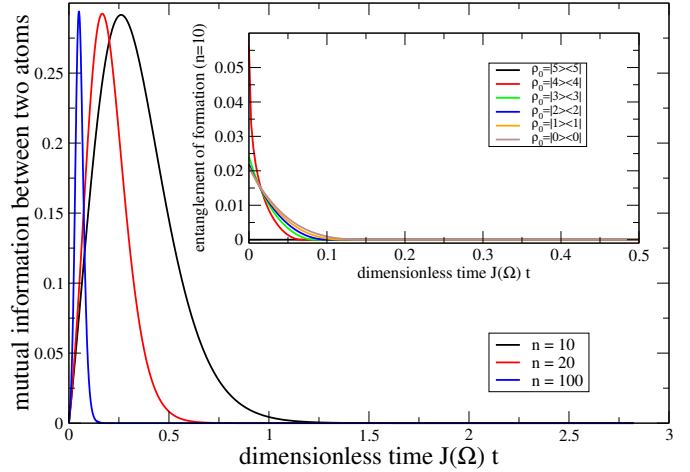


Figure 6.8: Main: Mutual information between two atoms during superradiant decay when initialized in $|n/2\rangle\langle n/2|$. For larger n , the strong correlations between all atomic pairs only persist for a short time. Inset: The entanglement of formation (and concurrence) between two atoms is only finite if one starts with a finite entanglement, i.e., with $|m| \neq n/2$ and even in this case decays quickly.



where the evolution of the probabilities $P_m(t)$ is governed by a rate equation

$$\begin{aligned} \dot{P}_m &= \langle m | \dot{\rho}_S | m \rangle \\ &= J(\Omega)[1 + n_B(\Omega)] \left[\frac{n}{2} \left(\frac{n}{2} + 1 \right) - m(m+1) \right] P_{m+1} + J(\Omega)n_B(\Omega) \left[\frac{n}{2} \left(\frac{n}{2} + 1 \right) - m(m-1) \right] P_{m-1} \\ &\quad - J(\Omega)[1 + n_B(\Omega)] \left[\frac{n}{2} \left(\frac{n}{2} + 1 \right) - m(m-1) \right] P_m - J(\Omega)n_B(\Omega) \left[\frac{n}{2} \left(\frac{n}{2} + 1 \right) - m(m+1) \right] P_m, \end{aligned} \quad (6.114)$$

which is inert to the Lamb-shift terms.

At small temperatures or large Ω such that $n_B(\Omega) \rightarrow 0$, the evolution of $\langle J^z \rangle$ for example shows drastic collective effects for large n [41, 34], compare e.g. Fig. 6.7. In contrast to the decay of a single atom (or N single atoms decaying independently), the collective decay is significantly faster, formally explained by the scaling of the coefficients in the rate equation (6.114).

From the full master equation (6.110) however we may also obtain other large spin expectation values. From the solution, we can with the results of the previous section deduce the concurrence and entanglement of formation and also the mutual information between two qubits during the superradiant decay, which is depicted in fig. 6.8. As one would expect, the collective interaction with the reservoir strongly correlates any pair of atoms during the superradiant decay. This correlation could not be there if the atoms would couple to the reservoir independently, since then the total density matrix would always be a tensor product of the individual ones.

From the finite concurrence we have deduced before for the Dicke states, one might have

expected that also a finite two-atom entanglement of formation may be generated in the course of the evolution. However, this is not the case, as is exemplified in the inset. When initialized in the state $|n/2, n/2\rangle$, the concurrence (and the derived entanglement of formation will remain zero) throughout the evolution. Also when initialized in other Dicke states, the two-atom entanglement of formation quickly decays. Going back to the original microscopic model (6.77), this does make some sense: The coupling between the single atoms and the modes of the electromagnetic field cannot generate entanglement between the atoms if the electromagnetic field is kept unperturbed (as we assume in the derivation of the master equation by keeping the reservoir in a fixed state).

Chapter 7

Quantum Thermodynamics

7.1 Nonequilibrium thermodynamics

Interestingly, we can use some of the information measures introduced to connect the globally unitary evolution of quantum systems that generates correlations between system and reservoirs to the second law of thermodynamics – without resorting to weak-coupling assumptions [42]. We start from a microscopic setting where both system and interaction Hamiltonians are allowed to be time-dependent

$$H(t) = H_S(t) + \sum_{\nu} H_I^{(\nu)}(t) + \sum_{\nu} H_B^{(\nu)}, \quad (7.1)$$

whereas the reservoir Hamiltonians $H_B^{(\nu)}$ are constant. The index ν labels different reservoirs, thus allowing for a non-equilibrium context.

The only assumption is that initially, we assume that the system and reservoirs are uncorrelated, and that the reservoirs are initially at (grand-canonical) thermal equilibrium states

$$\rho(0) = \rho_S(0) \bigotimes_{\nu} \bar{\rho}_{\nu}, \quad \bar{\rho}_{\nu} = \frac{e^{-\beta_{\nu}(H_B^{(\nu)} - \mu_{\nu} N_B^{(\nu)})}}{Z_{\nu}}, \quad (7.2)$$

where Z_{ν} and $N_B^{(\nu)}$ denote partition function and reservoir particle number of reservoir ν , respectively, and β_{ν} and μ_{ν} are the inverse temperature and chemical potential. We will only assume this at the initial time, but not for $t > 0$. In fact, the treatment is so general that the reservoirs can be arbitrarily small, they can even consist of single qubits and they can move arbitrarily far away from any product state during the evolution. The only formal requirement is that they are initially represented as a thermal equilibrium state, which can be decomposed as a mixture of reservoir energy eigenstates.

Since the evolution of the total universe is unitary, its total von-Neumann entropy is a constant of motion

$$\frac{d}{dt} \Sigma(t) = -\frac{d}{dt} \text{Tr} \{ \rho(t) \ln \rho(t) \} = -\text{Tr} \left\{ \dot{\rho} \ln \rho + \rho \frac{d}{dt} \ln \rho \right\} = 0. \quad (7.3)$$

While it is obvious from the von-Neumann equation that the first term on the r.h.s. above vanishes

$$\text{Tr} \{ \dot{\rho} \ln \rho \} = -i \text{Tr} \{ [H\rho - \rho H] \ln \rho \} = -i \text{Tr} \{ H[\rho \ln(\rho) - \ln(\rho)\rho] \} = 0, \quad (7.4)$$

the second term should be treated a bit more carefully as the density matrix need not commute with its derivative. Nevertheless, since ρ is always a valid density matrix, there exists a unitary transformation $V(t)$ that diagonalizes it $\rho(t) = V(t)\rho_D(t)V^\dagger(t)$, where $\rho_D(t)$ is a diagonal matrix. From this, we find that also the second term vanishes

$$\begin{aligned}
\text{Tr} \left\{ \rho \frac{d}{dt} \ln \rho \right\} &= \text{Tr} \left\{ V(t)\rho_D(t)V^\dagger(t) \frac{d}{dt} \ln[V(t)\rho_D(t)V^\dagger(t)] \right\} \\
&= \text{Tr} \left\{ V(t)\rho_D(t)V^\dagger(t) \frac{d}{dt} V(t) [\ln \rho_D(t)] V^\dagger(t) \right\} \\
&= \text{Tr} \left\{ \rho_D(t)V^\dagger(t)\dot{V} [\ln \rho_D(t)] + \rho_D(t)\rho_D^{-1}(t)\dot{\rho}_D + V(t)\rho_D(t) [\ln \rho_D(t)]\dot{V}^\dagger \right\} \\
&= \text{Tr} \left\{ [\ln \rho_D(t)]\rho_D(t)V^\dagger\dot{V} + \rho_D(t) [\ln \rho_D(t)]\dot{V}^\dagger V \right\} \\
&= \text{Tr} \left\{ \rho_D(t) [\ln \rho_D(t)] [\dot{V}^\dagger V + V^\dagger \dot{V}] \right\} = 0.
\end{aligned} \tag{7.5}$$

This means that the entropy of the universe remains constant and is given by the sum of the initial entropies

$$\Sigma(t) = -\text{Tr} \{ \rho(t) \ln \rho(t) \} = -\text{Tr} \{ \rho(0) \ln \rho(0) \} = -\text{Tr}_S \{ \rho_S(0) \ln \rho_S(0) \} - \sum_{\nu} \text{Tr}_{\nu} \{ \bar{\rho}_{\nu} \ln \bar{\rho}_{\nu} \}, \tag{7.6}$$

where we have used that for an initial product state the von-Neumann entropy is additive in system and reservoir contributions. Now, we introduce the exact (i.e., without any master equation approximation) local reduced density matrices of system and reservoirs via

$$\rho_S(t) = \text{Tr}_{\{\nu\}} \{ \rho(t) \}, \quad \rho_{\nu}(t) = \text{Tr}_{S, \nu' \neq \nu} \{ \rho(t) \}. \tag{7.7}$$

When we look at the entropy of the system

$$S(t) \equiv -\text{Tr}_S \{ \rho_S(t) \ln \rho_S(t) \}, \tag{7.8}$$

we see that its initial value is related to the full entropy of the universe via $\Sigma(0) = \Sigma(t)$ as

$$S(0) = \Sigma(t) + \sum_{\nu} \text{Tr}_{\nu} \{ \bar{\rho}_{\nu} \ln \bar{\rho}_{\nu} \}. \tag{7.9}$$

Its change with respect to the initial value can therefore be written as

$$\begin{aligned}
\Delta S(t) &\equiv S(t) - S(0) \\
&= -\text{Tr}_S \{ \rho_S(t) \ln \rho_S(t) \} + \text{Tr} \{ \rho(t) \ln \rho(t) \} - \sum_{\nu} \text{Tr}_{\nu} \{ \bar{\rho}_{\nu} \ln \bar{\rho}_{\nu} \} \\
&= -\text{Tr} \{ \rho(t) \ln \rho_S(t) \} + \text{Tr} \{ \rho(t) \ln \rho(t) \} - \sum_{\nu} \text{Tr}_{\nu} \{ \bar{\rho}_{\nu} \ln \bar{\rho}_{\nu} \} \\
&= -\text{Tr} \left\{ \rho(t) \ln \left[\rho_S(t) \otimes_{\nu} \bar{\rho}_{\nu} \right] \right\} + \text{Tr} \{ \rho(t) \ln \rho(t) \} + \sum_{\nu} \text{Tr}_{\nu} \{ [\rho_{\nu}(t) - \bar{\rho}_{\nu}] \ln \bar{\rho}_{\nu} \} \\
&= D_{\text{QRE}} \left(\rho(t), \rho_S(t) \otimes_{\nu} \bar{\rho}_{\nu} \right) - \sum_{\nu} \beta_{\nu} \text{Tr}_{\nu} \left\{ [\rho_{\nu}(t) - \bar{\rho}_{\nu}] \left[H_B^{(\nu)} - \mu_{\nu} N_B^{(\nu)} \right] \right\},
\end{aligned} \tag{7.10}$$

where the first term is nothing but the distance – expressed in terms of the quantum relative entropy, compare Eq. (6.45) – between the actual exact density matrix of the full universe $\rho(t)$ and the product state of the exact reduced system density matrix and the initial reservoir states. The first term is thus positive and vanishes if system and bath are not correlated at all and when the baths remain at their initial states (e.g. decoupled evolution of system and reservoirs). Since it has the standard form, it will be denoted as the **entropy production**

$$\Delta_i S(t) = D_{\text{QRE}} \left(\rho(t), \rho_S(t) \bigotimes_{\nu} \bar{\rho}_{\nu} \right) \geq 0. \quad (7.11)$$

We see that the entropy production is large when system and reservoir become strongly correlated or also when the reservoirs are driven far away from their initial states. For finite-size reservoirs, recurrences can occur, and the entropy production can behave periodically. We therefore note that its production rate need not be positive. In particular, for periodically evolving universes we must observe times where $\frac{d}{dt} \Delta_i S(t) < 0$. Note that also for just a single reservoir, the entropy production is not the mutual information between system and reservoir, because $\bar{\rho}_{\nu}$ is not the exact reduced density matrix of the reservoir.

By contrast, the second term in (7.10) can be related to the heat leaving the reservoirs during $[0, t]$

$$\begin{aligned} \Delta_e S(t) &= - \sum_{\nu} \beta_{\nu} \text{Tr}_{\nu} \left\{ [\rho_{\nu}(t) - \bar{\rho}_{\nu}] \left[H_B^{(\nu)} - \mu_{\nu} N_B^{(\nu)} \right] \right\} \\ &= \sum_{\nu} \beta_{\nu} \Delta Q_{\nu}(t), \end{aligned} \quad (7.12)$$

where the the heat flowing out of the reservoir ν is defined as

$$\Delta Q_{\nu}(t) = \left\langle H_B^{(\nu)} - \mu_{\nu} N_B^{(\nu)} \right\rangle_0 - \left\langle H_B^{(\nu)} - \mu_{\nu} N_B^{(\nu)} \right\rangle_t. \quad (7.13)$$

Summarizing, the second law can be written as $\Delta S(t) = \Delta_i S(t) + \sum_{\nu} \beta_{\nu} \Delta Q_{\nu}(t)$ or solving for the entropy production, the **second law of thermodynamics** reads

$$\Delta_i S(t) = \Delta S(t) - \sum_{\nu} \beta_{\nu} \Delta Q_{\nu}(t) \geq 0. \quad (7.14)$$

- The first term on the r.h.s. is the entropy change of the system only, whereas the other terms correspond to the entropy changes of an initial equilibrium reservoir $\Delta S_{\nu} = \beta_{\nu} \Delta Q_{\nu}$.
- By performing the operation $\lim_{t \rightarrow \infty} \frac{1}{t} [\dots]$ on Eq. (7.14), we find for a finite-sized system and a constant global Hamiltonian

$$- \sum_{\nu} \beta_{\nu} \lim_{t \rightarrow \infty} \frac{\langle H_{\nu} - \mu_{\nu} N_{\nu} \rangle_0 - \langle H_{\nu} - \mu_{\nu} N_{\nu} \rangle_t}{t} = \lim_{t \rightarrow \infty} \frac{\Delta_i S(t)}{t} \geq 0. \quad (7.15)$$

Now, if the currents leaving the reservoirs assume steady state values in the long-time limit (it is an assumption that these limits exist)

$$\lim_{t \rightarrow \infty} \frac{d}{dt} \langle H_{\nu} \rangle_t \equiv -\bar{I}_E^{\nu}, \quad \lim_{t \rightarrow \infty} \frac{d}{dt} \langle N_{\nu} \rangle_t \equiv -\bar{I}_M^{\nu}, \quad (7.16)$$

we can invoke the rule of l'Hospital to evaluate the limit, yielding

$$-\sum_{\nu} \beta_{\nu} (\bar{I}_E^{\nu} - \mu_{\nu} \bar{I}_M^{\nu}) \geq 0. \quad (7.17)$$

This shows that under the assumption of stationary currents, the conventional form of the second law at steady state also holds beyond weak coupling and also if interactions are present inside the system, thus confirming and generalizing considerations based on the Landauer formula [43] (compare lecture on quantum transport).

- In general (for $t > 0$) the total entropy is not just the sum of system entropy (7.8) and reservoir entropies

$$S_{\nu}(t) = -\text{Tr} \{ \rho_{\nu}(t) \ln \rho_{\nu}(t) \}. \quad (7.18)$$

Instead, it is modified by the correlations between system and reservoir (e.g. entanglement). The **correlation entropy** is therefore defined as

$$S_c(t) = \Sigma(t) - S(t) - \sum_{\nu} S_{\nu}(t). \quad (7.19)$$

For a single reservoir only, the correlation entropy corresponds to the negative mutual information (6.52) between system and reservoir, such that it generalizes this concept to multipartite systems. Due to the assumption of an initial product state we have $S_c(0) = 0$, and therefore with $\Sigma(t) = \Sigma(0)$ the relation

$$S_c(t) = S_c(t) - S_c(0) = -\Delta S(t) - \sum_{\nu} \Delta S_{\nu}(t) \quad (7.20)$$

In analogy to the mutual information, we can also express the correlation entropy by a distance

$$\begin{aligned} D_{\text{QRE}} \left(\rho(t), \rho_S(t) \otimes_{\nu} \rho_{\nu}(t) \right) &= \text{Tr} \{ \rho(t) \ln \rho(t) \} - \text{Tr} \left\{ \rho(t) \left[\ln \rho_S(t) + \sum_{\nu} \ln \rho_{\nu}(t) \right] \right\} \\ &= -\Sigma(t) - \text{Tr}_S \{ \rho_S(t) \ln \rho_S(t) \} - \sum_{\nu} \text{Tr}_{\nu} \{ \rho_{\nu}(t) \ln \rho_{\nu}(t) \} \\ &= -\Sigma(t) + S(t) + \sum_{\nu} S_{\nu}(t) = -S_c(t) \geq 0. \end{aligned} \quad (7.21)$$

The correlation entropy is thereby always negative. Now, one can write the sum of entropy production and correlation entropy as

$$\begin{aligned} \Delta_i S(t) + S_c(t) &= D_{\text{QRE}} \left(\rho(t), \rho_S(t) \otimes_{\nu} \bar{\rho}_{\nu} \right) - D_{\text{QRE}} \left(\rho(t), \rho_S(t) \otimes_{\nu} \rho_{\nu}(t) \right) \\ &= -\text{Tr} \left\{ \rho(t) \ln [\rho_S(t) \otimes_{\nu} \bar{\rho}_{\nu}] \right\} + \text{Tr} \left\{ \rho(t) \ln [\rho_S(t) \otimes_{\nu} \rho_{\nu}(t)] \right\} \\ &= \sum_{\nu} [-\text{Tr}_{\nu} \{ \rho_{\nu}(t) \ln \bar{\rho}_{\nu} \} + \text{Tr}_{\nu} \{ \rho_{\nu}(t) \ln \rho_{\nu}(t) \}] = \sum_{\nu} D_{\text{QRE}}(\rho_{\nu}(t), \bar{\rho}_{\nu}) \geq 0 \end{aligned} \quad (7.22)$$

as a distance quantifying how much the reservoirs are driven away from their initial states. Since this is always positive, we conclude that the entropy production is always larger or equal than the negative correlation entropy

$$\Delta_i S(t) \geq -S_c(t) \geq 0. \quad (7.23)$$

- We can solve Eq. (7.10) for the entropy production $\Delta_i S(t) = S(t) - S(0) - \sum_\nu \beta_\nu \Delta Q_\nu(t) \geq 0$ and perform a time derivative on both sides

$$\frac{d}{dt} \Delta_i S(t) = \dot{S}(t) - \sum_\nu \beta_\nu \Delta \dot{Q}_\nu(t), \quad (7.24)$$

where $\dot{Q}_\nu(t)$ now denotes the heat current entering the system from reservoir ν . In general, this quantity $\frac{d}{dt} \Delta_i S(t)$ need not be positive. However, for a master equation approach where all reservoirs enter additively

$$\mathcal{L} = \mathcal{L}_0 + \sum_\nu \mathcal{L}_\nu \quad (7.25)$$

and individually thermalize the system to its reservoir-specific local equilibrium state

$$\mathcal{L}_\nu \bar{\rho}_S^\nu = \mathcal{L}_\nu e^{-\beta_\nu (H_S - \mu_\nu N_S)} / Z_\nu = 0, \quad (7.26)$$

we can write Spohn's inequality as

$$\begin{aligned} - \sum_\nu \text{Tr} \{ (\mathcal{L}_\nu \rho(t)) [\ln \rho(t) - \ln \bar{\rho}_S^\nu] \} &= \dot{S}(t) - \sum_\nu \beta_\nu \text{Tr} \{ (\mathcal{L}_\nu \rho(t)) [H_S - \mu_\nu N_S] \} \\ &= \dot{S}(t) - \sum_\nu \beta_\nu [I_E^{(\nu)} - \mu_\nu I_M^{(\nu)}] \geq 0, \end{aligned} \quad (7.27)$$

and we see that the r.h.s. then just yields the same with energy currents $I_E^{(\nu)}$ and matter currents $I_M^{(\nu)}$ that enter the system from reservoir ν then just tells us that for such descriptions also the entropy production rate must be positive.

7.1.1 Example: Two coupled qubits

To begin with something simple, we can test the above relations with just two qubits

$$H = \frac{\omega_1}{2} \sigma_1^z + \frac{\omega_2}{2} \sigma_2^z + \lambda \sigma_1^x \sigma_2^x, \quad (7.28)$$

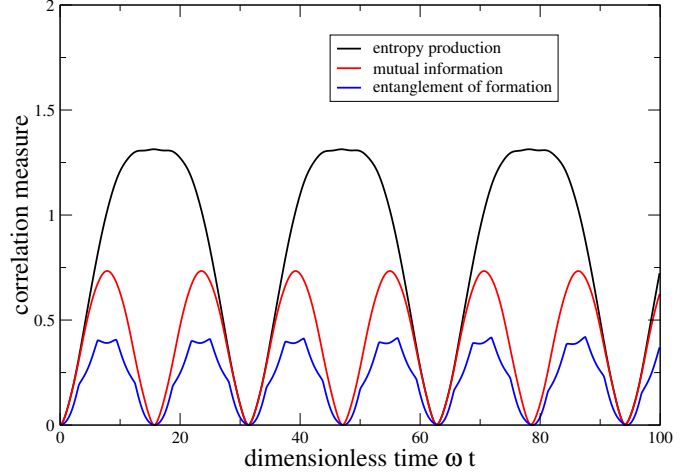
where λ parametrizes the coupling strength between them. The first qubit can be considered as the system, whereas the second mimics the "reservoir". We consider the initial state

$$\rho(0) = \rho_1^0 \otimes \bar{\rho}_2 = \rho_1^0 \otimes \frac{e^{-\beta_2 \omega_2 / 2 \sigma_2^z}}{Z_2}, \quad (7.29)$$

where the initial state of the system ρ_1^0 is arbitrary. Then, we compute the exact solution via

$$\rho(t) = e^{-iHt} \rho(0) e^{+iHt}. \quad (7.30)$$

Figure 7.1: Plot of the correlation measures entropy production (black) from (7.32) and negative correlation entropy/mutual information (red) from (7.33), and entanglement of formation (blue) from (6.89) for a universe composed of two interacting qubits. The entropy production (black) is always greater than the mutual information (red), and both quantities are positive. In times where the mutual information vanishes with finite entropy production, the global density matrix is of product form, but the bath is driven away from its initial equilibrium state. For $\lambda \rightarrow 0$, all quantities vanish. Parameters: $\omega_1 = \omega_2 = \omega$, $\lambda = 0.1\omega$, $\rho_1^0 = (1 - 10^{-3})|0\rangle\langle 0| + 10^{-3}|1\rangle\langle 1|$, $\beta_2\omega_2 = 1.0$.



From this, we can compute the reduced density matrices

$$\rho_1(t) = \text{Tr}_2 \{ \rho(t) \} , \quad \rho_2(t) = \text{Tr}_1 \{ \rho(t) \} . \quad (7.31)$$

and the entropy production

$$\Delta_i S(t) = D_{\text{QRE}}(\rho(t), \rho_1(t) \otimes \bar{\rho}_2) \quad (7.32)$$

and the mutual information (negative correlation entropy)

$$I_{12}(t) = -S_c(t) = D_{\text{QRE}}(\rho(t), \rho_1(t) \otimes \rho_2(t)) . \quad (7.33)$$

The result is shown in Fig. 7.1 and confirms relation (7.23).

7.1.2 Numeric example: Ising model

If we consider the Ising model (5.59), we can simply isolate one spin and call it system, and the remaining open chain is then called reservoir. Thus, we consider the Hamiltonian of the universe to be composed as $H = H_S + H_B + H_I$ with

$$H_S = \Omega(1 - s)\sigma_1^x , \quad H_B = \Omega(1 - s) \sum_{i=2}^n \sigma_i^x + \Omega s \sum_{i=2}^{n-1} \sigma_i^z \sigma_{i+1}^z , \quad H_I = \Omega s [\sigma_1^z \sigma_2^z + \sigma_n^z \sigma_1^z] . \quad (7.34)$$

In this representation, the coupling between system and reservoir is parametrized by s and is not independent of the reservoir-internal coupling. We consider the product initial state which we can numerically propagate

$$\rho_0 = \rho_S^0 \otimes \rho_B^0 \quad : \quad \rho_B^0 = \frac{e^{-\beta H_B}}{Z_B} \quad \implies \quad \rho(t) = e^{-i[H_S + H_B + H_I]t} \rho_0 e^{+i[H_S + H_B + H_I]t} . \quad (7.35)$$

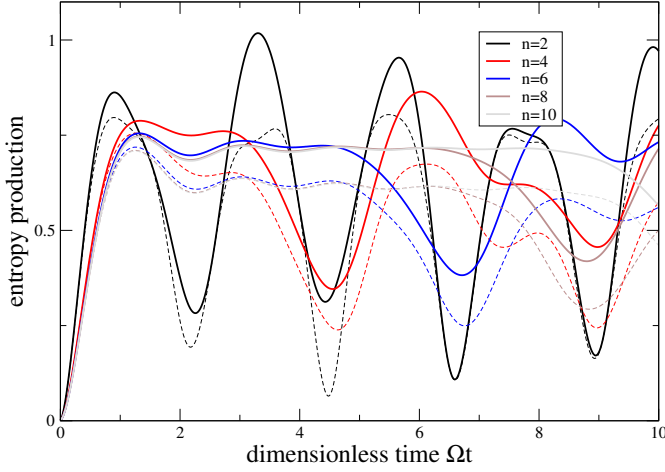


Figure 7.2: Plot of the entropy production vs. dimensionless time for Ising chains of different lengths n , regarding a single qubit as system and the rest of the ring as reservoir. With increasing chain length, the intermediate plateau is assumed for longer times. Dashed lines denote the mutual information. Other parameters $\beta\Omega = 1.0$, $\rho_S^0 = \frac{1}{2}[\mathbf{1} + \sigma^x]$, $s = 0.5$.

We may numerically trace the evolution of the entropy production

$$\begin{aligned}
 D_{\text{QRE}}(\rho(t), \rho_S(t) \otimes \rho_B^0) &= \text{Tr} \{ \rho(t) \ln \rho(t) \} - \text{Tr} \{ \rho(t) \ln \rho_S(t) \otimes \rho_B^0 \} \\
 &= \text{Tr} \{ \rho(t) \ln \rho(t) \} - \text{Tr} \{ \rho(t) [\ln \rho_S(t)] \otimes \mathbf{1} \} - \text{Tr} \{ \rho(t) \mathbf{1} \otimes [\ln \rho_B^0] \} \\
 &= S(\rho_S(t)) - S(\rho(t)) + \beta \langle H_B \rangle_t + \ln Z_B,
 \end{aligned} \tag{7.36}$$

which can thereby be related to a time-dependent expectation value of the reservoir energy and the entropies of system and universe, which can be determined by computing the eigenvalues of the respective density matrices. Altogether, one finds some highly oscillatory behaviour, which however develops into a plateau when the chain becomes longer (the reservoir becomes larger), see Fig. 7.2.

7.1.3 Example: Transient entropy production for pure-dephasing

We had solved the pure dephasing version of the spin-boson model

$$H = \Omega/2\sigma^z + \sigma^z \otimes \sum_k \left(h_k b_k + h_k^* b_k^\dagger \right) + \sum_k \omega_k b_k^\dagger b_k. \tag{7.37}$$

before. For the system, we would in the eigenbasis of σ^z simply obtain stationary populations and decaying coherences

$$|\rho_{01}|(t) = e^{-f(t)} |\rho_{01}^0|, \quad f(t) = \frac{4}{\pi} \int_0^\infty J(\omega) \frac{\sin^2(\omega t/2)}{\omega^2} \coth\left(\frac{\beta\omega}{2}\right) d\omega, \tag{7.38}$$

compare Eq. (4.11). For the pure-dephasing model it is actually much simpler to compute the change of the reservoir energy by going to the Heisenberg picture (marked with a $\tilde{O}(t) = e^{+iHt} O e^{-iHt}$). Performing a time-derivative, operators that are constant in the Schrödinger picture obey

$$\frac{d}{dt} \tilde{O}(t) = i e^{+iHt} [H, O] e^{-iHt}, \tag{7.39}$$

and by explicitly computing all the commutators one can see that the Heisenberg operators will obey a system of coupled differential equations (which may be infinite-dimensional). Fortunately,

for the pure-dephasing model, these operator equations do already close

$$\begin{aligned}\frac{d}{dt}\tilde{\sigma}^z &= 0, \\ \frac{d}{dt}\tilde{b}_k &= -i\omega_k\tilde{b}_k - ih_k^*\tilde{\sigma}^z, \\ \frac{d}{dt}\tilde{b}_k^\dagger &= +i\omega_k\tilde{b}_k^\dagger + ih_k\tilde{\sigma}^z.\end{aligned}\tag{7.40}$$

They are therefore solved by

$$\begin{aligned}\tilde{\sigma}^z(t) &= \sigma^z, \\ \tilde{b}_k(t) &= b_k e^{-i\omega_k t} + \frac{h_k^*}{\omega_k} \sigma^z (e^{-i\omega_k t} - 1), \\ \tilde{b}_k^\dagger(t) &= b_k^\dagger e^{+i\omega_k t} + \frac{h_k}{\omega_k} \sigma^z (e^{+i\omega_k t} - 1),\end{aligned}\tag{7.41}$$

which also respects the initial condition $\tilde{b}_k(0) = b_k$. This already tells us that the total expectation value of the reservoir energy becomes

$$\begin{aligned}\langle E \rangle_t &= \sum_k \omega_k \text{Tr} \left\{ \left(e^{+i\omega_k t} b_k^\dagger + \frac{h_k}{\omega_k} (e^{+i\omega_k t} - 1) \sigma^z \right) \times \right. \\ &\quad \left. \times \left(e^{-i\omega_k t} b_k + \frac{h_k^*}{\omega_k} (e^{-i\omega_k t} - 1) \sigma^z \right) \rho_S^0 \otimes \rho_B \right\} \\ &= \langle E \rangle_0 + \sum_k \frac{|h_k|^2}{\omega_k} [2 - 2 \cos(\omega_k t)] = \langle E \rangle_0 + \int_0^\infty \frac{J(\omega)}{2\pi\omega} [2 - 2 \cos(\omega t)] \\ &= \langle E \rangle_0 + \frac{2}{\pi} \int_0^\infty \frac{J(\omega)}{\omega} \sin^2 \left(\frac{\omega t}{2} \right) d\omega,\end{aligned}\tag{7.42}$$

where

$$\langle E \rangle_0 = \sum_k \omega_k \langle b_k^\dagger b_k \rangle_{\text{th}} = \sum_k \omega_k \sum_{n_k=0}^\infty n_k e^{-\beta(\omega_k - \mu)n_k} / Z_k,\tag{7.43}$$

where convergence requires that $\omega_k - \mu > 0$. Therefore, the difference to the initial reservoir energy is then given by

$$\Delta E(t) = \frac{2}{\pi} \int_0^\infty \frac{J(\omega)}{\omega} \sin^2 \left(\frac{\omega t}{2} \right) d\omega,\tag{7.44}$$

which is always positive. In complete analogy one can compute the change of the reservoir particle number

$$\Delta N(t) = \frac{2}{\pi} \int_0^\infty \frac{J(\omega)}{\omega^2} \sin^2 \left(\frac{\omega t}{2} \right) d\omega.\tag{7.45}$$

For a single reservoir, Eq. (7.10) becomes

$$\Delta_i S(t) = S(t) - S(0) + \beta [\Delta E(t) - \mu \Delta N(t)].\tag{7.46}$$

Using that $\Delta E(t) > 0$, $\Delta N(t) > 0$, and for bosons $\mu \leq 0$ (actually, we would normally drop it for photons), we can already conclude that the second term that describes the reservoir entropy production is separately positive. Also, if we would let $t \rightarrow \infty$, the final density matrix of the system would be diagonal, such that we can conclude that $S(\infty) - S(0) > 0$, but does this hold for all times? Parametrizing the density matrix by the occupation ρ_{11} and the time-dependent coherence $\rho_{01}(t)$, its von-Neumann entropy becomes

$$S(t) = -\frac{1}{2} \left[1 - \sqrt{(1 - 2\rho_{11})^2 + 4|\rho_{01}(t)|^2} \right] \ln \frac{1}{2} \left[1 - \sqrt{(1 - 2\rho_{11})^2 + 4|\rho_{01}(t)|^2} \right] - \frac{1}{2} \left[1 + \sqrt{(1 - 2\rho_{11})^2 + 4|\rho_{01}(t)|^2} \right] \ln \frac{1}{2} \left[1 + \sqrt{(1 - 2\rho_{11})^2 + 4|\rho_{01}(t)|^2} \right]. \quad (7.47)$$

Using that as time increases, the coherences become smaller $|\rho_{01}(t)|^2 = e^{-2f(t)}|\rho_{01}^0|^2$, we find (in the regime $0 \leq (1 - 2\rho_{11})^2 + 4|\rho_{01}(t)|^2 \leq 1$ that is allowed for a valid density matrix), that $S(t) = -(1-x)/2 \ln(1-x)/2 - (1+x)/2 \ln(1+x)/2$ is a decaying function with $\sqrt{(1 - 2\rho_{11})^2 + 4|\rho_{01}(t)|^2} = x \in [0, 1]$. Therefore, we conclude $S(t) > S(0)$, and consequently

$$\Delta_i S(t) = S(t) - S(0) + \beta [\Delta E(t) - \mu \Delta N(t)] \geq 0, \quad (7.48)$$

confirming the validity of the second law for the pure-dephasing model. Here, the first term gives the entropy increase in the system. The time derivative of these terms may become negative (similar to the discussion of the trace distance).

7.1.4 Use of Spohn's inequality

In the master equation limit, the entropy production is a monotonously growing function in time, which is expressed by Spohn's inequality even in a non-equilibrium environment (7.27)

$$\dot{S}(t) - \sum_{\nu} \beta_{\nu} [I_E^{(\nu)}(t) - \mu_{\nu} I_M^{(\nu)}(t)] \geq 0 \quad (7.49)$$

labeled by the different reservoirs ν , from which energy and matter currents may enter the system

$$I_E^{(\nu)}(t) \equiv \text{Tr} \{ H_S [\mathcal{L}_{\nu} \rho_S(t)] \}, \quad I_M^{(\nu)}(t) \equiv \text{Tr} \{ N_S [\mathcal{L}_{\nu} \rho_S(t)] \}. \quad (7.50)$$

In the long-term limit, for a finite-size system, the system will reach a stationary state

$$\lim_{t \rightarrow \infty} \rho_S(t) = \bar{\rho}_S, \quad (7.51)$$

and the von-Neumann entropy of the system will saturate

$$\lim_{t \rightarrow \infty} \dot{S}(t) = 0. \quad (7.52)$$

In this limit, also the currents will then assume stationary limits

$$\lim_{t \rightarrow \infty} I_E^{(\nu)}(t) = \bar{I}_E^{(\nu)}, \quad \lim_{t \rightarrow \infty} I_M^{(\nu)}(t) = \bar{I}_M^{(\nu)}, \quad (7.53)$$

and Spohn's inequality then reads

$$- \sum_{\nu} \beta_{\nu} [\bar{I}_E^{(\nu)} - \mu_{\nu} \bar{I}_M^{(\nu)}] \geq 0. \quad (7.54)$$

Formally, the same inequality has to be satisfied whenever stationary currents exist and the system entropy saturates, compare Eq. (7.17). The difference however is then that in the master equation treatment currents are defined phenomenologically from the system perspective (e.g. $I_E(t) = \text{Tr} \{H_S(\mathcal{L}_\nu \rho_S(t))\}$), whereas in the full treatment the currents can be defined microscopically (e.g. $I_E(t) = -\text{Tr} \{H_B \rho(t)\}$).

This has been the basis for the analysis of many heat engines operating at steady state [44, 45].

- For a single reservoir described by inverse temperature β and chemical potential μ we first note that all stationary currents must vanish since we discuss master equations where then $\mathcal{L}e^{-\beta[H_S - \mu N_S]}/Z_S = 0$. The same holds for many different reservoirs that are at the same equilibrium state $\beta_\nu = \beta$ and $\mu_\nu = \mu$.
- For just two reservoirs $\nu \in \{L, R\}$, the energy currents and matter currents at steady state must cancel

$$\bar{I}_E \equiv \bar{I}_E^{(L)} = -\bar{I}_E^{(R)}, \quad \bar{I}_M \equiv \bar{I}_M^{(L)} = -\bar{I}_M^{(R)}. \quad (7.55)$$

With this, the second law inequality (7.17) becomes

$$-\beta_L(\bar{I}_E - \mu_L \bar{I}_M) + \beta_R(\bar{I}_E - \mu_R \bar{I}_M) = (\beta_R - \beta_L)\bar{I}_E + (\beta_L \mu_L - \beta_R \mu_R)\bar{I}_M \geq 0. \quad (7.56)$$

- For equal temperatures $\beta_L = \beta_R = \beta$, this just leads to the inequality $(\mu_L - \mu_R)\bar{I}_M \geq 0$, which states that the matter current going through the system must be directed from high chemical potential to low chemical potential.
- For equal chemical potentials $\mu_L = \mu_R = \mu$, this yields $(\beta_R - \beta_L)(\bar{I}_E - \mu \bar{I}_M) \geq 0$, which states that the heat current going through the system from left to right reservoirs always goes from hot (small β_ν) to cold (large β_ν) – the Clausius formulation of the second law.
- Without loss of generality we assume $\mu_L < \mu_R$ and $\beta_L < \beta_R$ (i.e., the left reservoir is hotter than the right one). Then, it is possible to generate chemical work (in case of electrons electric power) by utilizing heat from the hot reservoir. The **efficiency** of this generator is then given by the ratio of the generated electric power (or chemical work rate) $P = -\bar{I}_M(\mu_L - \mu_R)$ divided by the heat current entering the system from the hot reservoir

$$\begin{aligned} \eta &= \frac{-\bar{I}_M(\mu_L - \mu_R)}{\bar{I}_E - \mu_L \bar{I}_M} = \frac{-(\beta_R - \beta_L)(\mu_L - \mu_R)\bar{I}_M}{(\beta_R - \beta_L)\bar{I}_E - (\beta_R - \beta_L)\mu_L \bar{I}_M} \\ &= \frac{-(\beta_R - \beta_L)(\mu_L - \mu_R)\bar{I}_M}{(\beta_R - \beta_L)\bar{I}_E + (\mu_L \beta_L - \mu_R \beta_R)\bar{I}_M - (\mu_L \beta_L - \mu_R \beta_R)\bar{I}_M - (\beta_R - \beta_L)\mu_L \bar{I}_M} \\ &\leq \frac{-(\beta_R - \beta_L)(\mu_L - \mu_R)\bar{I}_M}{-(\mu_L \beta_L - \mu_R \beta_R)\bar{I}_M - (\beta_R - \beta_L)\mu_L \bar{I}_M} = \frac{(\beta_R - \beta_L)(\mu_L - \mu_R)}{(\mu_L \beta_L - \mu_R \beta_R) + (\beta_R - \beta_L)\mu_L} \\ &= 1 - \frac{\beta_L}{\beta_R} = 1 - \frac{T_R}{T_L} = 1 - \frac{T_{\text{cold}}}{T_{\text{hot}}} = \eta_{\text{Carnot}}. \end{aligned} \quad (7.57)$$

The efficiency of such a generator is bounded by **Carnot efficiency**, irrespective of the microscopic details.

- For a system that is coupled via three terminals to different reservoirs characterized only by a temperature

$$\beta_w < \beta_h < \beta_c, \quad (7.58)$$

we only have to satisfy energy conservation

$$\bar{I}_E^{(w)} + \bar{I}_E^{(h)} + \bar{I}_E^{(c)} = 0. \quad (7.59)$$

The second law

$$\beta_w[\bar{I}_E^{(h)} + \bar{I}_E^{(c)}] - \beta_h \bar{I}_E^{(h)} - \beta_c \bar{I}_E^{(c)} \geq 0 \quad (7.60)$$

then allows to use heat from the (hottest) work reservoir to cool the coldest reservoir, i.e., to achieve

$$\bar{I}_E^{(c)} > 0. \quad (7.61)$$

The **coefficient of performance** for this process is then also upper-bounded by a corresponding Carnot value. One can see this by considering the infinite temperature limit for the work reservoir $\beta_w \rightarrow 0$, from which we get $-\beta_h \bar{I}_E^{(h)} - \beta_c \bar{I}_E^{(c)} \geq 0$ or alternatively $-\frac{\bar{I}_E^{(h)}}{\bar{I}_E^{(c)}} \geq \frac{\beta_c}{\beta_h}$. This then implies

$$\begin{aligned} \text{COP}_{\text{cooling}} &= \frac{\bar{I}_E^{(c)}}{\bar{I}_E^{(w)}} = \frac{\bar{I}_E^{(c)}}{-\bar{I}_E^{(h)} - \bar{I}_E^{(c)}} = \frac{1}{-\frac{\bar{I}_E^{(h)}}{\bar{I}_E^{(c)}} - 1} \\ &\leq \frac{1}{\frac{\beta_c}{\beta_h} - 1} = \frac{T_c}{T_h - T_c}, \end{aligned} \quad (7.62)$$

which is the well-known classical limit.

7.2 Quantum Otto cycle

Thermodynamic cycles were useful to separate heat and work contributions clearly from each other. Some classical cycles can be straightforwardly transferred into the quantum domain. During some strokes of such a thermodynamic cycle, the working fluid of a heat engine could be subjected to a constant Hamiltonian and coupled to a single reservoir. In these strokes, any energetic change can be interpreted as heat, and the quantum system is evolving towards thermal equilibrium with its coupled reservoir. In other strokes, the system is decoupled from any reservoir and only subject to a time-dependent Hamiltonian. In such strokes, any energetic change of the system can be seen as work. If the reservoirs that we couple to are kept at different temperature, one may construct cycles like in the classical limit.

The ideal **Otto cycle** consists of four strokes

- A→B A parameter in the classical system is varied such that no heat is exchanged with the reservoir (this is also called adiabatic). Quantum-mechanically, this would transfer to the solution of a time-dependent von-Neumann equation, which however is not necessarily quantum adiabatic if the driving of the Hamiltonian is fast.
- B→C The system is coupled to a hot reservoir while keeping its internal parameters constant until it has equilibrated with the reservoir. Quantum-mechanically, this could be modeled by the evolution under a thermalizing Lindblad equation.

- C→D The parameters are varied back while the system is decoupled from any reservoir, such that formally this step is similar to the first one.
- D→A The system is coupled to a cold reservoir, such that the formal description is similar to the second step.

Since we have model equations for every step of the cycle, it is straightforward to transfer the Otto cycle into the quantum domain and to take the final density matrix after every stroke as the initial one to the next stroke.

The simplest example for this is a harmonic oscillator with a time-dependent frequency

$$H(t) = \frac{p^2}{2m} + \frac{1}{2}m\omega^2(t)x^2, \quad (7.63)$$

where x and p are the usual position and momentum operators obeying $[x, p] = i$ (recall $\hbar = 1$). Now, the usual transformation to creation and annihilation operators becomes time-dependent

$$x = \sqrt{\frac{1}{2m\omega(t)}}(a^\dagger(t) + a(t)), \quad p = i\sqrt{\frac{m\omega(t)}{2}}(a^\dagger(t) - a(t)), \quad (7.64)$$

but still allows to represent the Hamiltonian by ladder operators

$$H(t) = \omega(t) [a^\dagger(t)a(t) + 1/2]. \quad (7.65)$$

Here it is important to realize that the Hamilton-Operator will not commute with itself at different times

$$[H(t), H(t')] \neq 0, \quad (7.66)$$

since the annihilation and creation operators

$$a(t) = \sqrt{\frac{m\omega(t)}{2}}x + i\frac{1}{\sqrt{2m\omega(t)}}p, \quad a^\dagger(t) = \sqrt{\frac{m\omega(t)}{2}}x - i\frac{1}{\sqrt{2m\omega(t)}}p \quad (7.67)$$

will at different times not obey the usual commutation relations

$$[a(t), a^\dagger(t')] = \frac{1}{2} \left[\sqrt{\frac{\omega(t)}{\omega(t')}} + \sqrt{\frac{\omega(t')}{\omega(t)}} \right]. \quad (7.68)$$

When $\omega(t) = \omega(t')$, this falls back to the known commutation relations.

7.2.1 Modeling of closed (unitary) strokes

While the system is decoupled from the reservoirs, we change the parameter of oscillator frequency, leading to the time-dependent von-Neumann equation

$$\dot{\rho} = -i[H(t), \rho]. \quad (7.69)$$

Formally, this is solved by

$$\rho(t) = U(t)\rho(0)U^\dagger(t), \quad (7.70)$$

with time evolution operator $U(t)$ defined by

$$\dot{U} = -iH(t)U(t). \quad (7.71)$$

In general, it will have to be obtained numerically. If the evolution of the frequency however is very slow, we can use the quantum adiabatic approximation from Sec. 5.1. It states that density operator which is initially diagonal in the initial energy eigebasis (because it was thermalized with a reservoir) remains diagonal. Specific for the oscillator, the initial energy eigenbasis would be given by the initial Fock states $a^\dagger(0)a(0)|n(0)\rangle = n|n(0)\rangle$, and an initially diagonal state would be given by

$$\rho(0) = \sum_n p_n^0 |n(0)\rangle \langle n(0)| \quad : \quad p_n^0 = e^{-\beta\omega(n+1)}(e^{\beta\omega} - 1). \quad (7.72)$$

When we apply the adiabatically approximated time evolution operator $U_{\text{ad}(t)}$ from Eq. (5.13) we obtain a state that is diagonal in the final Fock states

$$\rho(t) = \sum_n p_n^0 |n(t)\rangle \langle n(t)|, \quad (7.73)$$

which are defined by $a^\dagger(t)a(t)|n(t)\rangle = n|n(t)\rangle$. The net effect is that although $|n(t)\rangle \neq |n(0)\rangle$, the probabilities for these states do not change.

7.2.2 Modeling of open (dissipative) strokes

While coupled to the reservoir, we leave the parameter ω constant and model the dynamics of the system with a Lindblad equation

$$\begin{aligned} \dot{\rho} = & -i[H, \rho(t)] + \Gamma[1 + n_B(\omega)] \left[a\rho a^\dagger - \frac{1}{2}a^\dagger a\rho - \frac{1}{2}\rho a^\dagger a \right] \\ & + \Gamma n_B(\omega) \left[a^\dagger \rho a - \frac{1}{2}a a^\dagger \rho - \frac{1}{2}\rho a a^\dagger \right]. \end{aligned} \quad (7.74)$$

Here, Γ is a coupling strength to the reservoir and

$$n_B(\omega) = \frac{1}{e^{\beta\omega} - 1} \quad (7.75)$$

is the Bose distribution at inverse reservoir temperature β . For $H = \omega(a^\dagger a + 1/2)$ one can now show that the stationary state of this equation is the thermalized one

$$\bar{\rho} = \frac{e^{-\beta H}}{\text{Tr}\{e^{-\beta H}\}}. \quad (7.76)$$

If one considers the dynamics of populations $\langle n|\rho|n\rangle \equiv \rho_{nn}$ one finds that they decouple from the coherences and correspond to a rate equation system

$$\dot{\rho}_{nn} = \Gamma[1 + n_B(\omega)] [(n+1)\rho_{n+1,n+1} - n\rho_{nn}] + \Gamma n_B(\omega) [n\rho_{n-1,n-1} - (n+1)\rho_{nn}]. \quad (7.77)$$

From this, one finds that the ratio of relaxation and excitation processes

$$\frac{R_{n \rightarrow n+1}}{R_{n+1 \rightarrow n}} = \frac{\Gamma n_B(\omega)}{\Gamma[1 + n_B(\omega)]} = e^{-\beta\omega} \quad (7.78)$$

obeys detailed balance. Furthermore, in the long-term limit, the coherences $\langle n|\rho|m\rangle$ with $n \neq m$ will just decay, such that thermalization becomes immediately evident.

7.2.3 Strokes in the quantum Otto cycle

For the quantum Otto cycle with a harmonic oscillator we can construct the cycle from two unitary (no heat exchange – classically adiabatic) and two dissipative (with a cold reservoir coupling Γ_c and a hot reservoir coupling Γ_h) strokes:

$A \rightarrow B$: In this first stroke the frequency of the oscillator is changed from $\omega(t_A) = \omega_c$ to $\omega(t_B) = \omega_h$ by a rather arbitrary protocol, while the reservoirs are decoupled $\Gamma_c(t) = \Gamma_h(t) = 0$ for all $t \in [t_A, t_B]$. Since only the parameter ω is changed, all energetic changes of the working fluid are interpreted as work. The time evolution is modeled by the von-Neumann equation and is not necessarily quantum adiabatic (but termed classically adiabatic as there is no heat exchange). Accordingly, the von-Neumann entropy of the system remains constant.

$B \rightarrow C$: In the second stroke the frequency is kept constant $\omega(t) = \omega_B = \omega_h$ for all $t \in [t_B, t_C]$. The system is coupled to the hot reservoir, i.e., $\Gamma_h(t) = \Gamma_h$ and $\Gamma_c(t) = 0$ for $t \in [t_B, t_C]$. The von-Neumann entropy of the system may change, but its rate of change is bounded via Spohn's inequality by the heat flux

$$\dot{S} - \beta I_E^h \geq 0. \quad (7.79)$$

$C \rightarrow D$: In the third stroke the coupling to the reservoirs is lifted and the frequency is brought back to its initial value $\omega_h \rightarrow \omega_c$, where the protocol actually need not be the reverse one of the first stroke. This corresponds to $\omega(t_C) = \omega_h$ und $\omega(t_D) = \omega_c$, and the reservoirs are decoupled $\Gamma_c(t) = \Gamma_h(t) = 0$ for all $t \in [t_C, t_D]$. In this stroke, the entropy remains constant.

$D \rightarrow A$: The cycle is closed by the last stroke via coupling to the cold reservoir, one has $\omega(t) = \omega_c$, $\Gamma_c(t) = \Gamma_c$ and $\Gamma_h(t) = 0$ for all $t \in [t_D, t_A + T]$, there T is the total duration of one cycle.

Accordingly, we can model the complete dynamics throughout the cycle as

$$\begin{aligned} \dot{\rho} = & -i [\omega(t)a^\dagger(t)a(t), \rho] \\ & + \Gamma_h(t)[1 + n_B(\omega_h)] \left[a_h \rho a_h^\dagger - \frac{1}{2} a_h^\dagger a_h \rho - \frac{1}{2} \rho a_h^\dagger a_h \right] + \Gamma_h(t) n_B(\omega_h) \left[a_h^\dagger \rho a_h - \frac{1}{2} a_h a_h^\dagger \rho - \frac{1}{2} \rho a_h a_h^\dagger \right] \\ & + \Gamma_c(t)[1 + n_B(\omega_c)] \left[a_c \rho a_c^\dagger - \frac{1}{2} a_c^\dagger a_c \rho - \frac{1}{2} \rho a_c^\dagger a_c \right] + \Gamma_c(t) n_B(\omega_c) \left[a_c^\dagger \rho a_c - \frac{1}{2} a_c a_c^\dagger \rho - \frac{1}{2} \rho a_c a_c^\dagger \right], \end{aligned} \quad (7.80)$$

where frequencies and couplings vary as described above and $a_h = a(t_B) = a(t_C)$ sowie $a_c = a(t_D) = a(t_A)$. In general, this model system will have to be solved numerically – using an appropriate cutoff $n_{\text{cut}} \beta_h \omega_h \gg 1$ and $n_{\text{cut}} \beta_c \omega_c \gg 1$, such that the time-dependent density matrix will be very far from an equilibrium state. However, in the particular case when the cycle is performed very slow (meaning slow driving and a very long coupling time to the reservoirs), a simple analytic treatment is possible:

$$t_B - t_A \rightarrow \infty, \quad t_D - t_C \rightarrow \infty, \quad t_C - t_B \rightarrow \infty, \quad t_A + T - t_D \rightarrow \infty \quad (7.81)$$

If the contact to the cold reservoir was sufficiently long, at time t_A the working fluid will be in thermal equilibrium with the cold reservoir

$$\rho(t_A) \approx \frac{e^{-\beta_c \omega_c a_c^\dagger a_c}}{\text{Tr} \left\{ e^{-\beta_c \omega_c a_c^\dagger a_c} \right\}}. \quad (7.82)$$

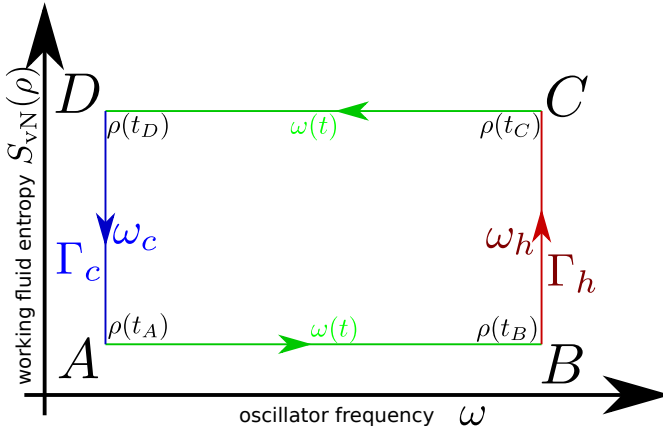


Figure 7.3: Quantum Otto cycle in the $S - \omega$ plane. The ideal limit is slow (quantum-adiabatic) driving and perfect equilibration, but for finite durations of the strokes only the horizontal lines will be closer together. Energetic changes during the unitary strokes (analogous to classically adiabatic ones) are interpreted as work (green), during the coupling to the hot (red) or cold (blue) reservoir only heat is exchanged.

Then, if the frequency change ω_c to ω_h is performed sufficiently slow (i.e., quantum-adiabatically), the working fluid will for $t \in [t_A, t_B]$ remain in the instantaneous energy eigenstates, i.e., one has

$$\rho(t_B) \approx \frac{e^{-\beta_c \omega_c a_h^\dagger a_h}}{\text{Tr} \left\{ e^{-\beta_c \omega_c a_h^\dagger a_h} \right\}}. \quad (7.83)$$

However, for $\beta_c > \beta_h$, this is not the equilibrium state with the hot reservoir. If we couple in the next stroke to the hot reservoir, the state will evolve into a new equilibrium state (through a sequence of non-equilibrium ones), such that after long time, the system will equilibrate with the hot reservoir

$$\rho(t_C) \approx \frac{e^{-\beta_h \omega_h a_h^\dagger a_h}}{\text{Tr} \left\{ e^{-\beta_h \omega_h a_h^\dagger a_h} \right\}}. \quad (7.84)$$

When now the frequency is changed back from ω_h to ω_c , the system remains in its instantaneous energy eigenstates, which is however not the equilibrium state of the cold reservoir

$$\rho(t_D) \approx \frac{e^{-\beta_h \omega_h a_c^\dagger a_c}}{\text{Tr} \left\{ e^{-\beta_h \omega_h a_c^\dagger a_c} \right\}}. \quad (7.85)$$

Coupling the system for a long time then to the cold reservoir leads to $\rho(t_A + T) = \rho(t_A)$, which closes the cycle. During the unitary strokes, the von-Neumann entropy of the system will remain constant. While coupled to the hot reservoir, energy will flow into the system, its entropy will increase. While coupled to the cold reservoir, energy will flow out of the system, its entropy will decrease, such that the cycle in the $S - \omega$ diagram assumes a simple shape, see Fig. 7.3.

The work applied to the system is then computed as the net work resulting from the two strokes $A \rightarrow B$ and $C \rightarrow D$

$$\begin{aligned} \Delta W_{AB} &= \text{Tr} \left\{ \omega_h (a_h^\dagger a_h + 1/2) \rho(t_B) \right\} - \text{Tr} \left\{ \omega_c (a_c^\dagger a_c + 1/2) \rho(t_A) \right\} = \frac{\omega_h - \omega_c}{e^{\beta_c \omega_c} - 1} + \frac{(\omega_h - \omega_c)}{2}, \\ \Delta W_{CD} &= \text{Tr} \left\{ \omega_c (a_c^\dagger a_c + 1/2) \rho(t_D) \right\} - \text{Tr} \left\{ \omega_h (a_h^\dagger a_h + 1/2) \rho(t_C) \right\} = \frac{\omega_c - \omega_h}{e^{\beta_h \omega_h} - 1} + \frac{(\omega_c - \omega_h)}{2}. \end{aligned} \quad (7.86)$$

The energetic changes during the other strokes are heat. The (usually positive) heat entering from the hot reservoir and (usually negative) heat entering from the cold reservoir are then calculated via

$$\begin{aligned}\Delta Q_{BC} &= \text{Tr} \left\{ \omega_h a_h^\dagger a_h [\rho(t_C) - \rho(t_B)] \right\} = \frac{\omega_h}{e^{\beta_h \omega_h} - 1} - \frac{\omega_h}{e^{\beta_c \omega_c} - 1}, \\ \Delta Q_{DA} &= \text{Tr} \left\{ \omega_c a_c^\dagger a_c [\rho(t_A) - \rho(t_D)] \right\} = \frac{\omega_c}{e^{\beta_c \omega_c} - 1} - \frac{\omega_c}{e^{\beta_h \omega_h} - 1}.\end{aligned}\quad (7.87)$$

With these formulas, we have neglected that any time-dependent coupling to the reservoir must also require a change of Hamiltonian parameters (wasted work required to let the engine run). This means that the coupling to the reservoir must remain weak enough to allow for a Lindblad description and to be able to neglect the work contribution required for coupling and decoupling.

To take up heat from the hot reservoir $\Delta Q_{BC} > 0$ we therefore require that $\beta_h \omega_h < \beta_c \omega_c$. The total work extracted from the system is then $\Delta W = -\Delta W_{AB} - \Delta W_{CD}$, which we can write as

$$\Delta W = (\omega_h - \omega_c) \left[\frac{1}{e^{\beta_h \omega_h} - 1} - \frac{1}{e^{\beta_c \omega_c} - 1} \right]. \quad (7.88)$$

The efficiency in this limit is then

$$\eta = \frac{\Delta W}{\Delta Q_{BC}} \Theta(\Delta W) = \left(1 - \frac{\omega_c}{\omega_h} \right) \Theta(\Delta W). \quad (7.89)$$

One might think that this efficiency could reach one for $\omega_h \gg \omega_c$, but additionally we have to respect the condition $\Delta W \geq 0$ (work extraction), which also requires $\beta_h \omega_h < \beta_c \omega_c$. Therefore, we can at best choose $\omega_h^{\max} = \omega_c \frac{\beta_c}{\beta_h}$ to maximize efficiency while still having a non-negative work output

$$\eta_{\max} = 1 - \frac{\beta_h}{\beta_c} = 1 - \frac{T_c}{T_h} = \eta_{Ca}. \quad (7.90)$$

Unfortunately, at this working point even the extracted work per cycle vanishes. Even when we numerically optimize ω_c and ω_h to maximize the extracted work, the extracted power would still vanish due to the assumed infinite cycle time. Individually optimizing altogether ω_c , ω_h and the protocol, one often finds numerically that the Curzon-Ahlborn or Chambadal-Novikov efficiency

$$\eta_{CA} = 1 - \sqrt{\frac{T_c}{T_h}} \quad (7.91)$$

is a much more realistic bound for the efficiency.

7.2.4 Harmonic oscillator working fluid with finite times

To numerically simulate a quantum Otto cycle, it is for most solvers useful to employ a fixed operator basis. We choose here the "cold" ladder operators that diagonalize the Hamiltonian while coupled to the cold bath

$$a_c = \sqrt{\frac{m\omega_c}{2}} x + \frac{i}{\sqrt{2m\omega_c}} p, \quad a_c^\dagger = \sqrt{\frac{m\omega_c}{2}} x - \frac{i}{\sqrt{2m\omega_c}} p. \quad (7.92)$$

Then, we need to express the ladder operators that hold for a different frequency in terms of the cold ladder operators. Since Eq. (7.67) holds at all frequencies, we can simply insert

$$x = \frac{1}{\sqrt{2m\omega_c}} (a_c^\dagger + a_c) , \quad p = i\sqrt{\frac{m\omega_c}{2}} (a_c^\dagger - a_c) , \quad (7.93)$$

to obtain a representation of the time-dependent ladder operators in terms of the cold ladder operators

$$\begin{aligned} a(t) &= \frac{1}{2} \left(\sqrt{\frac{\omega(t)}{\omega_c}} + \sqrt{\frac{\omega_c}{\omega(t)}} \right) a_c + \frac{1}{2} \left(\sqrt{\frac{\omega(t)}{\omega_c}} - \sqrt{\frac{\omega_c}{\omega(t)}} \right) a_c^\dagger , \\ a^\dagger(t) &= \frac{1}{2} \left(\sqrt{\frac{\omega(t)}{\omega_c}} + \sqrt{\frac{\omega_c}{\omega(t)}} \right) a_c^\dagger + \frac{1}{2} \left(\sqrt{\frac{\omega(t)}{\omega_c}} - \sqrt{\frac{\omega_c}{\omega(t)}} \right) a_c . \end{aligned} \quad (7.94)$$

In particular, this also defines the "hot" ladder operators that diagonalize the Hamiltonian while coupled to the hot bath

$$\begin{aligned} a_h &= \frac{1}{2} \left(\sqrt{\frac{\omega_h}{\omega_c}} + \sqrt{\frac{\omega_c}{\omega_h}} \right) a_c + \frac{1}{2} \left(\sqrt{\frac{\omega_h}{\omega_c}} - \sqrt{\frac{\omega_c}{\omega_h}} \right) a_c^\dagger , \\ a_h^\dagger &= \frac{1}{2} \left(\sqrt{\frac{\omega_h}{\omega_c}} + \sqrt{\frac{\omega_c}{\omega_h}} \right) a_c^\dagger + \frac{1}{2} \left(\sqrt{\frac{\omega_h}{\omega_c}} - \sqrt{\frac{\omega_c}{\omega_h}} \right) a_c . \end{aligned} \quad (7.95)$$

This is in fact a particular case of a **Bogoliubov transform** that mixes annihilation and creation operators a_c and a_c^\dagger to form new bosonic annihilation and creation operators $a(t)$ and $a^\dagger(t)$ that automatically obey the bosonic commutation relations.

To estimate whether the adiabatic criterion (5.11) is met, we consider to represent \dot{H} in terms of the time-dependent ladder operators

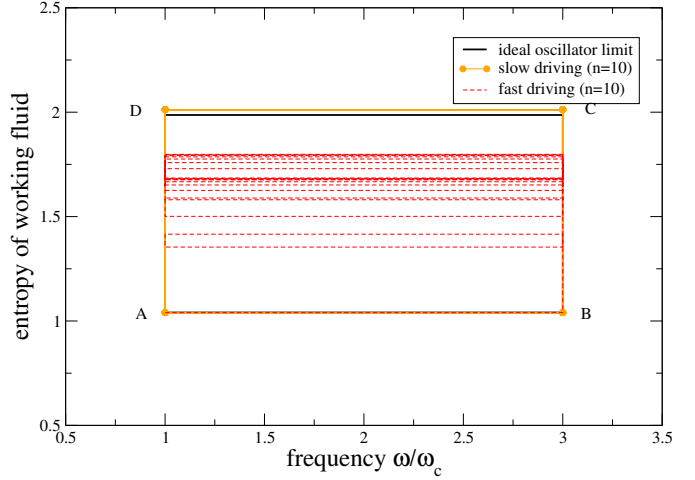
$$\dot{H} = m\omega(t)\dot{\omega}x^2 = \frac{\dot{\omega}}{2} ((a^\dagger(t))^2 + a^2(t) + a^\dagger(t)a(t) + a(t)a^\dagger(t)) , \quad (7.96)$$

from which we see that the driving of the frequency preserves the number parity of the oscillator quasiparticle (i.e., an even or odd number of quanta would remain either even or odd under this driving). Inserting this into (5.11), we conclude that adiabaticity can be maintained when $N_{\text{cut}}\dot{\omega}/\omega^2 \ll 1$, where N_{cut} denotes the bosonic cutoff of the Hilbert space.

Nevertheless, care should be taken when choosing the bosonic cutoff of the Hilbert space: Since the "hot" annihilation operators also contain a contribution from "cold" creation operators, they do not as reliably drag the system towards the vacuum state of the cold reservoir, such that the bosonic cutoff N_{cut} needs to be chosen significantly larger. If that is not taken into account, we will rather model an artificial system than a harmonic oscillator model. Nevertheless, it may show similar characteristics as a full harmonic oscillator working medium. Fig. 7.4 shows that for slow driving, the previously discussed harmonic oscillator limit is roughly approximated. For faster driving, the evolution is no longer adiabatic and the equilibration between system and reservoir is not perfect during the dissipative strokes. Therefore, the cycle in the ω -entropy plane reaches a different limit cycle which is significantly smaller.

Such models can actually be implemented in a lab [46].

Figure 7.4: Plot of 10 finite-time Otto cycle in the $\omega - S$ plane. For long cycle durations ($\omega_c T = 1000$, orange), the analytic results are approached, but for short cycle durations a limit cycle develops ($\omega_c T = 10$). Other parameters $N_{\text{cut}} = 10$, $\omega_h = 3\omega_c$, $\beta_c \omega_c = 1$, $\beta_h \omega_h = 3/8$, $\Gamma_h/\omega_c = \Gamma_c/\omega_c = 0.1$, linear ramp protocol between ω_c and ω_h , all strokes take one quarter of total cycle duration.



7.2.5 Collective spin working fluid with finite times

The quantum Otto cycle can be applied to arbitrary quantum systems. To remain quantum-adiabatic, we have to run it slowly – thereby reducing the extracted power. Further, the finite equilibration times will also reduce the overall power output.

By contrast, one can always remain quantum adiabatic by driving the Hamiltonian in the unitary strokes in a way that does not change the energy eigenstates but only the energies

$$H(t) = \sum_n E_n(t) |n\rangle \langle n|, \quad (7.97)$$

which is the case when the Hamiltonian commutes with itself at different times

$$[H(t), H(t')] = 0. \quad (7.98)$$

Any homogeneous transformation of the Hamiltonian $H(t) = g(t)H_0$ by some function $g(t)$ will implement this. This then allows to explicitly write the unitary time evolution operator as

$$U(t) = \exp \left\{ -i \int_0^t H(t') dt' \right\}, \quad (7.99)$$

which shows that under such evolution, one will always remain in the instantaneous energy eigenstate, or more generally, for an initial state expanded in the constant energy eigenstates

$$\rho = \sum_{nm} \rho_{nm} |n\rangle \langle m|, \quad (7.100)$$

one gets the time-evolved state

$$U(t)\rho U^\dagger(t) = \sum_{nm} \rho_{nm} e^{-i \int_0^t [E_n(t') - E_m(t')] dt'} |n\rangle \langle m|, \quad (7.101)$$

no matter how fast the driving is actually performed.

Additionally, one can speed up the equilibration with the reservoirs (or the energy uptake from the hot reservoir and energy radiation into the cold reservoir) by using superradiant effects. This way, the total energy exchange (e.g. total work extraction or heat uptake) will not be increased, but it will be achieved in shorter time, thereby increasing the delivered power $P = \Delta W/T$. Thereby,

instead of Eq. (7.80), we may consider an atomic cloud with a variable level splitting $\omega(t)$ – implemented e.g. by Stark or Zeeman splittings with a time-dependent external field – collectively coupled to both reservoirs

$$\begin{aligned} \dot{\rho} = & -i[\omega(t)J^z, \rho] \\ & + \Gamma_h(t)[1 + n_B(\omega_h)] \left[J^- \rho J^+ - \frac{1}{2} J^+ J^- \rho - \frac{1}{2} \rho J^+ J^- \right] + \Gamma_h(t)n_B(\omega_h) \left[J^+ \rho J^- - \frac{1}{2} J^- J^+ \rho - \frac{1}{2} \rho J^- J^+ \right] \\ & + \Gamma_c(t)[1 + n_B(\omega_c)] \left[J^- \rho J^+ - \frac{1}{2} J^+ J^- \rho - \frac{1}{2} \rho J^+ J^- \right] + \Gamma_c(t)n_B(\omega_c) \left[J^+ \rho J^- - \frac{1}{2} J^- J^+ \rho - \frac{1}{2} \rho J^- J^+ \right]. \end{aligned} \quad (7.102)$$

Technically, the advantage is that a natural time-independent basis – the eigenbasis of J^z can be employed. Furthermore, to simplify the analysis, we assume that only the subspace of maximum angular momentum $j = n/2$ contributes, such that we can constrain ourselves to the **Dicke states** $|m\rangle = |n/2, m\rangle$. In the ideal limit (perfect equilibration), the working fluid is initially in equilibrium with the cold reservoir

$$\rho_A \approx \frac{e^{-\beta_c \omega_c J^z}}{\text{Tr} \{e^{-\beta_c \omega_c J^z}\}}. \quad (7.103)$$

This state is diagonal in the Dicke basis, and therefore, no matter how fast we drive, during the unitary stroke we do not change such a state

$$\rho_B \approx \frac{e^{-\beta_c \omega_c J^z}}{\text{Tr} \{e^{-\beta_c \omega_c J^z}\}} = \frac{e^{-\beta' \omega_h J^z}}{\text{Tr} \{e^{-\beta' \omega_h J^z}\}}, \quad \beta' = \beta_c \frac{\omega_c}{\omega_h}, \quad (7.104)$$

which has an appealing interpretation of a thermal state at a different temperature. To take up heat from the hot reservoir, we require that $\beta' > \beta_h$. After an ideal equilibration with the hot reservoir, the state would be

$$\rho_C \approx \frac{e^{-\beta_h \omega_h J^z}}{\text{Tr} \{e^{-\beta_h \omega_h J^z}\}}, \quad (7.105)$$

which would be inert to the reversed unitary stroke

$$\rho_D \approx \frac{e^{-\beta_h \omega_h J^z}}{\text{Tr} \{e^{-\beta_h \omega_h J^z}\}} = \frac{e^{-\beta'' \omega_c J^z}}{\text{Tr} \{e^{-\beta'' \omega_c J^z}\}}, \quad \beta'' = \beta_h \frac{\omega_h}{\omega_c}, \quad (7.106)$$

where – to dump heat into the cold reservoir we require that $\beta'' < \beta_c$, which reproduces the previous condition.

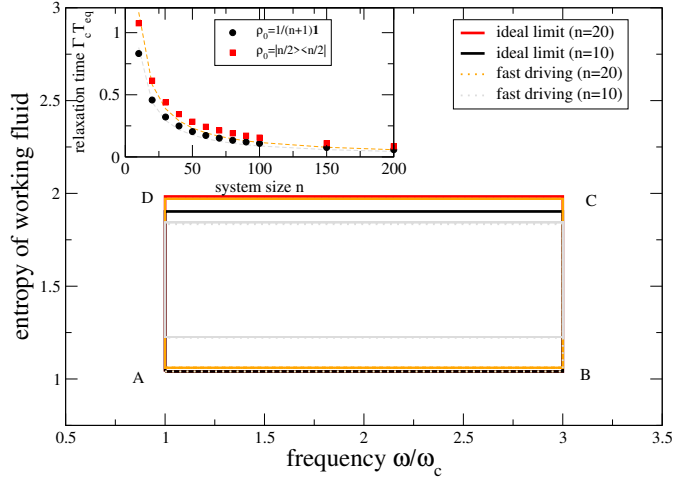
The total work extracted during one cycle is then

$$\begin{aligned} \Delta W = E_A - E_B + E_C - E_D &= \text{Tr} \{\omega_c J^z \rho_A\} - \text{Tr} \{\omega_h J^z \rho_B\} + \text{Tr} \{\omega_h J^z \rho_C\} - \text{Tr} \{\omega_c J^z \rho_D\} \\ &= (\omega_h - \omega_c) \text{Tr} \{J^z (\rho_C - \rho_A)\}, \end{aligned} \quad (7.107)$$

where we have only used that for our driving $\rho_D = \rho_C$ and $\rho_B = \rho_A$, irrespective of perfect or imperfect thermalization. Likewise, the heat uptake from the hot reservoir is

$$\Delta Q_h = E_C - E_B = \omega_h \text{Tr} \{J^z (\rho_C - \rho_B)\} = \omega_h \text{Tr} \{J^z (\rho_C - \rho_A)\}. \quad (7.108)$$

Figure 7.5: Plot of 10 quantum Otto cycles for a large spin model for slow driving (solid) and very fast driving (dotted). Whereas for $n = 10$, a fast driving time $\omega_c T = 10$ does not suffice to achieve thermalization (grey), the same driving time suffices for $n = 20$ (orange). Other parameters are chosen as in Fig. 7.4. Inset: Scaling of relaxation times during steps $D \rightarrow A$ for a zero-temperature cold reservoir, defined by a small trace distance $D_{\text{TD}}(\rho(T_{\text{eq}}), | -n/2 \rangle \langle -n/2 |) = 0.01$ for an initial infinite temperature state (black) and the original Dicke setup (red) (lines represent $1/n$ fits).



Without calculation, we therefore find that the efficiency η depends only on the ratio of the frequencies

$$\eta = \left(1 - \frac{\omega_c}{\omega_h}\right) \Theta(\Delta W) = \left(1 - \frac{\omega_c}{\omega_h}\right) \Theta(\beta_c \omega_c - \beta_h \omega_h) \leq 1 - \frac{\beta_h}{\beta_c}, \quad (7.109)$$

which eventually is again bounded by the Carnot value.

To compute the absolute value of work extracted per cycle, we note that in the subspace of maximum angular momentum $j = n/2$, everything can be derived analytically, e.g. via

$$\begin{aligned} \text{Tr} \{ e^{-\alpha J^z} \} &= \sum_{m=-n/2}^{+n/2} e^{-\alpha m} = \frac{\sinh\left(\frac{\alpha(n+1)}{2}\right)}{\sinh\left(\frac{\alpha}{2}\right)}, \\ \text{Tr} \{ J^z e^{-\alpha J^z} \} &= -\frac{d}{d\alpha} \text{Tr} \{ e^{-\alpha J^z} \}. \end{aligned} \quad (7.110)$$

The simplest result however is achieved when the hot reservoir is at infinite temperature $\beta_h \omega_h \ll 1$, such that $\rho_C \approx \frac{1}{n+1} \mathbf{1}$ and the cold reservoir is at zero temperature $\beta_c \omega_c \gg 1$ such that $\rho_A \approx | -n/2 \rangle \langle -n/2 |$. In this limit, we get the maximum extracted work for perfect thermalization as

$$\Delta W_{\text{max}} = \frac{n}{2} (\omega_h - \omega_c). \quad (7.111)$$

The power is then obtained by dividing by the cycle duration $P = \Delta W/T$. Since the unitary strokes can be performed infinitely fast, the cycle duration is composed from the contact times with both reservoirs $T = \tau_c + \tau_h$. If the times required to reach complete equilibration scale as $1/n$ (as is found in the original superradiance setup), the total power would scale quadratically with the number of qubits, thus transferring a genuine quantum effect to the classical world. Indeed, we observe that a cycle duration that for $n = 10$ does not suffice to achieve perfect equilibration manages to achieve perfect equilibration for $n = 20$, see Fig. 7.5.

For the excitation process due to the hot reservoir, the master equation (7.102) can with $\Gamma_c(t) \rightarrow 0$ and $\omega(t) \rightarrow \omega_h$ be written as

$$\begin{aligned} \dot{\rho} &= -i [\omega_h J^z, \rho] \\ &+ \Gamma_h [1 + n_B(\omega_h)] \left[J^- \rho J^+ - \frac{1}{2} J^+ J^- \rho - \frac{1}{2} \rho J^+ J^- \right] + \Gamma_h n_B(\omega_h) \left[J^+ \rho J^- - \frac{1}{2} J^- J^+ \rho - \frac{1}{2} \rho J^- J^+ \right], \end{aligned} \quad (7.112)$$

which for an infinitely hot reservoir $n_B(\omega_h) \rightarrow \infty$ will lead to an instantaneous equilibration, such that we can also perform this stroke infinitely fast in the infinite temperature limit and $T \approx \tau_c$. While coupled to the cold reservoir (effectively at zero temperature), we have to obey

$$\dot{\rho} = -i[\omega_c J^z, \rho] + \Gamma_c \left[J^- \rho J^+ - \frac{1}{2} J^+ J^- \rho - \frac{1}{2} \rho J^+ J^- \right]. \quad (7.113)$$

From this, we can derive the **dual master equation**, i.e., an equation of motion for the expectation value $\langle J^z \rangle$, using invariance of the trace and the commutation relations of the large spin operators

$$\begin{aligned} \frac{d}{dt} \langle J^z \rangle &= \Gamma_c \text{Tr} \left\{ \left(J^+ J^z J^- - \frac{1}{2} J^z J^+ J^- - \frac{1}{2} J^+ J^- J^z \right) \rho \right\} \\ &= \frac{\Gamma_c}{2} \text{Tr} \{ [J^+, J^z] J^- \rho + J^+ [J^z, J^-] \rho \} = -\Gamma_c \text{Tr} \{ J^+ J^- \rho \} \\ &= -\Gamma_c [\langle J^2 \rangle - \langle (J^z)^2 \rangle + \langle J^z \rangle]. \end{aligned} \quad (7.114)$$

A common approach to this is to apply the **mean-field approximation** $\langle (J^z)^2 \rangle \approx \langle J^z \rangle^2$, which closes the equation of motion and predicts a $1/n$ scaling of the equilibration time. Unfortunately, for the initial infinite-temperature state we have

$$\langle J^z \rangle_0 = \sum_{m=-n/2}^{+n/2} \frac{m}{n+1} = 0, \quad \langle (J^z)^2 \rangle_0 = \sum_{m=-n/2}^{+n/2} \frac{m^2}{n+1} = \frac{n(n+2)}{12}, \quad (7.115)$$

which does not comply well with the mean-field approximation. Nevertheless, the $1/n$ scaling is well observed even for starting with the most excited state, which should show the longest equilibration time. We can define an equilibration time by using the trace distance to the ground state as an equilibration measure

$$D_{\text{TD}}(\rho(T_{\text{eq}}), |-n/2\rangle \langle -n/2|) = 0.01. \quad (7.116)$$

Indeed, the inset of Fig. 7.5 shows that the equilibration times with a zero-temperature reservoir scale as $1/n$ for large n . This means that an optimal cycle time would allow to extract a power scaling quadratically in the number of qubits [47]

$$\frac{\Delta W}{T} \propto n^2. \quad (7.117)$$

7.2.6 Analogous equilibrium cycle

To optimize the cycle, we have so far exploited limits where ideally the system density matrix was close to an equilibrium state

$$\rho(t) \approx \frac{e^{-\beta(t)H(t)}}{\text{Tr} \{ e^{-\beta(t)H(t)} \}}. \quad (7.118)$$

For general protocols, this will evidently not be the case: Fast (non-adiabatic) drivings will normally yield non-thermal states $\rho_{A/B/C/D}$ (for example, they may build up coherences in the instantaneous energy eigenstates), and imperfect relaxation processes will also generate non-equilibrium states. Then, an analytic treatment is significantly harder. Nevertheless, general statements are

still possible even in this case. To each nonequilibrium state ρ and a Hamiltonian H we can define a **thermal reference state** ω and a **reference temperature** β^* by constructing the Gibbs state as the one which has the same entropy

$$\omega \equiv \frac{e^{-\beta^* H}}{\text{Tr}\{e^{-\beta^* H}\}} \quad : \quad S_{\text{vN}}(\omega) \stackrel{!}{=} S_{\text{vN}}(\rho) = -\text{Tr}\{\rho \ln \rho\} . \quad (7.119)$$

We note that for a non-degenerate ground state, this construction allows for a unique solution for β^* , since the entropy of an equilibrium state is a monotonously growing function of temperature and spans the complete range from 0 for zero temperature to $\ln d$ for infinite temperature. It will however normally have to be obtained numerically.

The advantage in this definition comes from a relation between the quantum relative entropy between the thermal reference state and the nonequilibrium state and the energetic difference

$$\begin{aligned} D_{\text{QRE}}(\rho, \omega) &= \text{Tr}\{\rho \ln \rho\} - \text{Tr}\{\rho \ln \omega\} = \text{Tr}\{\omega \ln \omega\} - \text{Tr}\{\rho \ln \omega\} \\ &= \text{Tr}\{(\omega - \rho) [-\beta^* H - \ln \text{Tr}\{e^{-\beta^* H}\} \mathbf{1}]\} = \beta^* \text{Tr}\{H(\rho - \omega)\} . \end{aligned} \quad (7.120)$$

Therefore, we can e.g. relate the heat uptake during steps $B \rightarrow C$ from the hot reservoir for a nonequilibrium state to the heat uptake of the corresponding thermal reference states

$$\begin{aligned} Q_h &= \text{Tr}\{H_B(\rho_C - \rho_B)\} = \text{Tr}\{H_B(\omega_C - \omega_B)\} - \text{Tr}\{H_B(\omega_C - \rho_C)\} + \text{Tr}\{H_B(\omega_B - \rho_B)\} \\ &= Q_h^* + (\beta_C^*)^{-1} D_{\text{QRE}}(\rho_C, \omega_C) - (\beta_B^*)^{-1} D_{\text{QRE}}(\rho_B, \omega_B) . \end{aligned} \quad (7.121)$$

Doing the same for the (negative) heat taken from the cold reservoir

$$Q_c = \text{Tr}\{H_A(\rho_A - \rho_D)\} = Q_c^* + (\beta_A^*)^{-1} D_{\text{QRE}}(\rho_A, \omega_A) - (\beta_D^*)^{-1} D_{\text{QRE}}(\rho_D, \omega_D) , \quad (7.122)$$

we can relate the efficiency at the limit cycle – where $\Delta W = Q_c + Q_h$ due to energy conservation – with the heat uptakes Q_c^* and Q_h^* of an analogous replacement circuit along thermal reference states

$$\eta = \frac{Q_c + Q_h}{Q_h} = 1 - \frac{-Q_c}{Q_h} . \quad (7.123)$$

Exploiting that the quantum relative entropy is always positive, one can find protocols for a quantum Otto cycle that optimize the efficiency [48]. For example, assuming that the reservoirs perfectly equilibrate the working fluid

$$D_{\text{QRE}}(\rho_A, \omega_A) = D_{\text{QRE}}(\omega_A, \omega_A) = 0 , \quad D_{\text{QRE}}(\rho_C, \omega_C) = D_{\text{QRE}}(\omega_C, \omega_C) = 0 , \quad (7.124)$$

the only way to increase efficiency is to bring the state at points D and B as close as possible to their thermal reference state by improving the unitary stroke protocol, see Fig. 7.6.

7.3 Quantum-mechanical evolution towards equilibrium

In the theory of closed quantum systems, the basic assumption is that all states evolve unitarily. This means that the information of the initial state $|\Psi_0\rangle$ is still fully contained in the time-dependent solution $|\Psi(t)\rangle$, and in this strict sense, any evolution towards a time-independent equilibrium state is excluded.

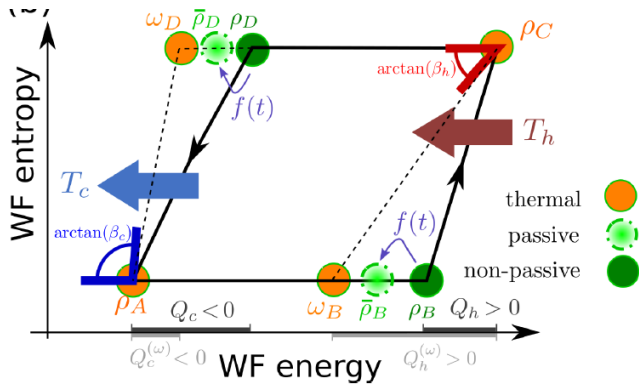


Figure 7.6: Optimization of a thermodynamic cycle by using improved unitary strokes to deliver more work, taken from Ref. [48]. By reducing the distance to the thermal reference states at points B and D , more heat is taken from the hot reservoir and less is dumped into the cold reservoir, altogether leading to an increased efficiency. Since the thermal reference states cannot always be reached, the final efficiency may not reach the Carnot value.

One may nevertheless reach a notion where a time-dependent reduced state of a globally unitarily evolving system approaches an equilibrium state [49].

Here, the main assumption is that initially, the whole universe is in a pure state

$$\rho_0 = |\Psi_0\rangle \langle \Psi_0|, \quad (7.125)$$

and under a globally unitary dynamics, this does of course remain pure

$$\rho(t) = U(t) |\Psi_0\rangle \langle \Psi_0| U^\dagger(t) = e^{-iHt} |\Psi_0\rangle \langle \Psi_0| e^{iHt} = |\Psi(t)\rangle \langle \Psi(t)| \neq \bar{\rho}. \quad (7.126)$$

The above expression could be time-independent if the initial pure state was an eigenstate of the global Hamiltonian or a superposition of energetically degenerate eigenstates. The global Hamiltonian $H = H_S + H_B + H_I$ can formally be written in its spectral representation

$$H = \sum_k E_k |E_k\rangle \langle E_k| \quad (7.127)$$

with energies E_k and eigenstates $|E_k\rangle$. The only restriction that one imposes is that the global Hamiltonian has non-degenerate energy gaps, i.e., for any four energies $\{E_n, E_m, E_k, E_\ell\}$ the condition

$$E_k - E_\ell = E_m - E_n \quad (7.128)$$

can only be trivially fulfilled, i.e., with $(E_k = E_\ell$ and $E_m = E_n)$ or with $(E_k = E_m$ and $E_\ell = E_n)$.

- This restriction excludes Hamiltonians that are not fully interactive. For such Hamiltonians, there would exist a partition into system and reservoir without an interaction remaining ($H = H'_S + H'_B$), and one would have e.g. the energies $E_1 = E_1^S + E_1^B$, $E_2 = E_1^S + E_2^B$, $E_3 = E_2^S + E_1^B$, and $E_4 = E_2^S + E_2^B$ that could fulfil the above condition $E_4 - E_3 = E_2 - E_1$ without any of the energies being equal.
- This restriction is rather mild in the sense that most slight perturbations added to a non-interacting Hamiltonian will render it interacting.

Then, notationally one defines the reduced density matrices of system and reservoir

$$\rho_S(t) = \text{Tr}_B \{\rho(t)\}, \quad \rho_B(t) = \text{Tr}_S \{\rho(t)\} \quad (7.129)$$

as usual and the **time-averaged states** of the universe, the system, and the reservoir

$$\omega = \lim_{\tau \rightarrow \infty} \frac{1}{\tau} \int_0^\tau \rho(t) dt, \quad \omega_S = \lim_{\tau \rightarrow \infty} \frac{1}{\tau} \int_0^\tau \rho_S(t) dt, \quad \omega_B = \lim_{\tau \rightarrow \infty} \frac{1}{\tau} \int_0^\tau \rho_B(t) dt. \quad (7.130)$$

Furthermore, one can also introduce an effective dimension of a mixed state by

$$d_{\text{eff}}(\rho) = \frac{1}{\text{Tr} \{\rho^2\}}. \quad (7.131)$$

For example, if we decompose the initial state into energy eigenstates of the global Hamiltonian

$$|\Psi_0\rangle = \sum_k c_k |E_k\rangle \quad : \quad \sum_k |c_k|^2 = 1, \quad (7.132)$$

we get for the time-evolved state

$$\rho(t) = \sum_{k\ell} c_k c_\ell^* e^{-i(E_k - E_\ell)t} |E_k\rangle \langle E_\ell|, \quad (7.133)$$

and for its time-averaged value (due to the non-degenerate energy gaps)

$$\omega = \sum_k |c_k|^2 |E_k\rangle \langle E_k|. \quad (7.134)$$

Simply squaring this, we have $\omega^2 = \sum_k |c_k|^4 |E_k\rangle \langle E_k|$, and the effective dimension becomes

$$d_{\text{eff}}(\omega) = \frac{1}{\sum_k |c_k|^4}. \quad (7.135)$$

Let furthermore d_S denote the Hilbert space dimension of the system. Then, one can prove the following [49]

$$\lim_{\tau \rightarrow \infty} \frac{1}{\tau} \int_0^\tau D_{\text{TD}}(\rho_S(t), \omega_S) dt \leq \frac{1}{2} \sqrt{\frac{d_S}{d_{\text{eff}}(\omega_B)}} \leq \sqrt{\frac{d_S^2}{d_{\text{eff}}(\omega)}}. \quad (7.136)$$

- If the r.h.s. is small (naturally, d_S is significantly smaller than the dimension of the full universe), then the inequality means that the time-averaged distance between actual state $\rho_S(t)$ and its time-averaged state ω_S is small.
- A small trace distance implies that any derived expectation values are small. Writing for two valid density matrices $\rho_1 - \rho_2 = \sum_n \lambda_n |n\rangle \langle n|$, we can e.g. bound

$$\begin{aligned} |\langle A_1 \rangle - \langle A_2 \rangle| &= |\text{Tr} \{A(\rho_1 - \rho_2)\}| = \left| \sum_n \langle n| A |n\rangle \lambda_n \right| \\ &\leq \sum_n |\langle n| A |n\rangle| |\lambda_n| \leq |a_{\text{max}}| 2 \frac{1}{2} \sum_n |\lambda_n| = 2|a_{\text{max}}| D_{\text{TD}}(\rho_1, \rho_2), \end{aligned} \quad (7.137)$$

where a_{max} is the eigenvalue of the observable A with the largest magnitude.

Chapter 8

Selected phenomena and applications

8.1 Reservoir models

Reservoir models are used in abundance to describe relaxation processes to thermal equilibrium. In most microscopic approaches, a reservoir is typically modeled by a bunch of non-interacting degrees of freedom

$$H_B = \sum_k \omega_k H_B^k \quad (8.1)$$

that do not directly interact $[H_B^k, H_B^q] = 0$ and which could for example be bosonic or fermionic modes $H_B^k = b_k^\dagger b_k$. Here, the energies ω_k represent excitation energies of the reservoir. The coupling between system and reservoir

$$H_I = S^\dagger \sum_k h_k B_k + \sum_k h_k^* B_k^\dagger S \quad (8.2)$$

then couples the system via the (not necessarily hermitian) system coupling operator S to every mode of the reservoir with reservoir coupling operator B_k fulfilling $[B_k, H_B^q] \stackrel{k \neq q}{=} 0$ with individual coupling strength h_k . In the limit of an infinitely large reservoir, the **spectral density** or **spectral coupling density**

$$\Gamma(\omega) = 2\pi \sum_k |h_k|^2 \delta(\omega - \omega_k) \quad (8.3)$$

describes the combined effect of system-reservoir coupling strength and reservoir level distribution. In contrast, the **density of states**

$$D(\omega) = 2\pi \sum_k \delta(\omega - \omega_k) \quad (8.4)$$

is a pure reservoir property and describes only the level distribution.

Whenever we use a continuous function to describe these quantities, we assume that the reservoir is infinitely large. In the following, we will review some particularly simple examples of reservoir models that after diagonalization give rise to a continuum of energies ω_k .

8.1.1 Tight-binding chain

Consider a chain of N identical sites that are connected by identical next-neighbour hopping amplitudes $T > 0$ (any complex phase can be absorbed in the annihilation and creation operators)

$$H_B = \epsilon \sum_{n=1}^N c_n^\dagger c_n + T \sum_{n=1}^{N-1} [c_n^\dagger c_{n+1} + c_{n+1}^\dagger c_n] = (c_1^\dagger, \dots, c_N^\dagger) \mathcal{H} \begin{pmatrix} c_1 \\ \vdots \\ c_N \end{pmatrix}. \quad (8.5)$$

Here, it does not matter whether the chain is of bosonic or fermionic nature. All that matters is that the tri-diagonal $N \times N$ matrix

$$\mathcal{H} = \begin{pmatrix} \epsilon & T & & & \\ T & \ddots & \ddots & & \\ & \ddots & \ddots & T & \\ & & & T & \epsilon \end{pmatrix} \quad (8.6)$$

can be diagonalized by a suitable unitary transformation $\mathcal{H}_D = \mathcal{U}\mathcal{H}\mathcal{U}^\dagger$. We therefore define new operators by using the unitary transformation

$$\begin{pmatrix} d_1 \\ \vdots \\ d_N \end{pmatrix} = \mathcal{U} \begin{pmatrix} c_1 \\ \vdots \\ c_N \end{pmatrix}. \quad (8.7)$$

Notably, if the c_i operators are bosons or fermions, the transformed d_k operators are of the same nature (the commutation or anticommutation relations are not changed by arbitrary unitary transformations of creation and annihilation operators). This allows us to write the Hamiltonian as

$$H_B = (c_1^\dagger, \dots, c_N^\dagger) \mathcal{U}^\dagger \mathcal{U} \mathcal{H} \mathcal{U}^\dagger \mathcal{U} \begin{pmatrix} c_1 \\ \vdots \\ c_N \end{pmatrix} = (d_1^\dagger, \dots, d_N^\dagger) \mathcal{H}_D \begin{pmatrix} d_1 \\ \vdots \\ d_N \end{pmatrix} = \sum_{k=1}^N \omega_k d_k^\dagger d_k, \quad (8.8)$$

where ω_k are the eigenvalues of \mathcal{H} . Simply by looking at the matrix \mathcal{H} , we find that its eigenvalues must be in the interval $\omega_k \in [\epsilon - 2T, \epsilon + 2T]$.

This becomes apparent e.g. by the **Gershgorin circle theorem**: To any square matrix $A \in \mathbb{C}^{N \times N}$ one can in the complex plane define the Gershgorin disks centered at the diagonal entries a_{ii} with radii determined by the sum of off-diagonals in every row

$$S_i = \left\{ z : |z - a_{ii}| \leq \sum_{j=1, j \neq i}^N |a_{ij}| \right\}. \quad (8.9)$$

Then one has that any connected set of Gershgorin disks contains as many eigenvalues as diagonal elements. The radii of the Gershgorin disks can evidently also be determined by summing the off-diagonal entries of columns instead of rows, and a tighter bound for the eigenvalues is then found by taking the smaller radius. Applied to the matrix above, we find that all N Gershgorin discs coincide with center ϵ and radius $2T$. Additionally however, the matrix is hermitian, such that all eigenvalues must be real.

For the matrix above, we can explicitly find the unitary transformation that diagonalizes it

$$U_{ij} = (U)_{ij} = \sqrt{\frac{2}{N+1}} \sin\left(\frac{\pi ij}{N+1}\right), \quad (8.10)$$

and which leads to the eigenvalues

$$\omega_k = \epsilon - 2T \cos\left(\frac{\pi k}{N+1}\right), \quad (8.11)$$

and we can write the bath Hamiltonian as

$$H_B = \sum_{k=1}^N \left[\epsilon - 2T \cos\left(\frac{\pi k}{N+1}\right) \right] d_k^\dagger d_k. \quad (8.12)$$

To see what effect such a local diagonalization of the reservoir Hamiltonian has on the coupling, consider the interaction Hamiltonian describing a coupling to the first site of the chain

$$H_I = \lambda S^\dagger c_1 + \lambda^* c_1^\dagger S, \quad (8.13)$$

where S is some arbitrary system operator that can also be hermitian (note also that for bosons, the operator order may be exchanged without additional sign). Inverting the transformation, we can express the c_1 operators in terms of the d_k operators

$$\begin{pmatrix} c_1 \\ \vdots \\ c_N \end{pmatrix} = U^\dagger \begin{pmatrix} d_1 \\ \vdots \\ d_N \end{pmatrix}, \quad (8.14)$$

or component-wise

$$c_1 = \sum_k (U^\dagger)_{1k} d_k = U_{k1}^* d_k = \sqrt{\frac{2}{N+1}} \sum_k \sin\left(\frac{\pi k}{N+1}\right) d_k. \quad (8.15)$$

Thus, from the interaction Hamiltonian

$$\begin{aligned} H_I &= \lambda S^\dagger \sum_k \sqrt{\frac{2}{N+1}} \sin\left(\frac{\pi k}{N+1}\right) d_k + \lambda^* \sum_k \sqrt{\frac{2}{N+1}} \sum_k \sin\left(\frac{\pi k}{N+1}\right) d_k^\dagger S \\ &= S^\dagger \sum_k t_k d_k + \sum_k t_k^* d_k^\dagger S \end{aligned} \quad (8.16)$$

we can identify

$$t_k = \lambda \sqrt{\frac{2}{N+1}} \sin\left(\frac{\pi k}{N+1}\right). \quad (8.17)$$

In the continuum limit $N \rightarrow \infty$, we can replace the summation in the spectral density by an integral with $\kappa = k/(N+1)$

$$\Gamma(\omega) = 2\pi \sum_k |t_k|^2 \delta(\omega - \omega_k) = 4\pi \lambda^2 \int_0^1 \sin^2(\pi \kappa) \delta(\omega - \epsilon + 2T \cos(\pi \kappa)) d\kappa. \quad (8.18)$$

Now, using a δ -function property

$$\delta(g(x)) = \sum_i \frac{\delta(x - x_i)}{|g'(x_i)|} \quad : \quad g(x_i) = 0 \quad (8.19)$$

we find that

$$\begin{aligned} \Gamma(\omega) &= 4\pi\lambda^2 \int_0^1 [1 - \cos^2(\pi\kappa)] \frac{\delta\left(\kappa - \frac{1}{\pi} \arccos\left(\frac{\epsilon - \omega}{2T}\right)\right)}{2T\pi \sin(\pi\kappa)} d\kappa \\ &= \frac{2\lambda^2}{T} \sqrt{1 - \frac{(\omega - \epsilon)^2}{4T^2}} \Theta(4T^2 - (\omega - \epsilon)^2). \end{aligned} \quad (8.20)$$

In a similar fashion, the density of states becomes

$$\begin{aligned} D(\omega) &= 2\pi N \int_0^1 \frac{\delta\left(\kappa - \frac{1}{\pi} \arccos\left(\frac{\epsilon - \omega}{2T}\right)\right)}{2T\pi \sin(\pi\kappa)} d\kappa \\ &= \frac{N}{T \sqrt{1 - \frac{(\omega - \epsilon)^2}{4T^2}}} \Theta(4T^2 - (\omega - \epsilon)^2). \end{aligned} \quad (8.21)$$

8.1.2 Example: Evolution under a 1d reservoir

We consider a fermionic Hamiltonian

$$H_S = \varepsilon d^\dagger d, \quad H_I = \lambda d^\dagger c_1 + \lambda^* c_1^\dagger d, \quad (8.22)$$

and where H_B is the finite tight-binding chain discussed in the previous section. By locally diagonalizing the reservoir, we can write this in the form

$$H = \varepsilon d^\dagger d + \sum_k \left[t_k d^\dagger d_k + t_k^* d_k^\dagger d \right] + \sum_k \omega_k d_k^\dagger d_k, \quad (8.23)$$

where

$$t_k = \lambda \sqrt{\frac{2}{N+1}} \sin\left(\frac{\pi k}{N+1}\right), \quad \omega_k = \epsilon - 2T \cos\left(\frac{\pi k}{N+1}\right). \quad (8.24)$$

Initially, the universe is in the state

$$\rho_0 = \rho_S^0 \otimes \frac{e^{-\beta(H_B - \mu N_B)}}{Z_B}, \quad (8.25)$$

where initially the reservoir is put in local thermal equilibrium with inverse temperature β and chemical potential μ . This system can be solved exactly by various methods. Note that however a direct numerical solution is usually prohibitive since the dimension of the Hilbert space scales exponentially and numerical error control is mandatory.

In the Heisenberg picture (bold symbols), the equations of motions close by considering e.g. only annihilation operators

$$\dot{\mathbf{d}} = -i\varepsilon \mathbf{d} - i \sum_k t_k \mathbf{d}_k, \quad \dot{\mathbf{d}}_k = -i\omega_k \mathbf{d}_k - it_k^* \mathbf{d}. \quad (8.26)$$

It is at this point where we have used that the operators are fermionic (some sign differences would show up for bosons). Performing a Laplace transform

$$d(z) = \int_0^\infty \mathbf{d} e^{-zt} dt, \quad d_k(z) = \int_0^\infty \mathbf{d}_k e^{-zt} dt \quad (8.27)$$

we can convert the differential equations into algebraic ones

$$zd(z) - d = -i\varepsilon d(z) - i \sum_k t_k d_k(z), \quad zd_k(z) - d_k = -i\omega_k d_k(z) - it_k^* d(z), \quad (8.28)$$

where d and d_k are the original operators in the Schrödinger picture. Of these, we can solve the second for $d_k(z)$ and insert this in the first equation, yielding an expression for the dot annihilation operator

$$d(z) = g(z)d + \sum_k g_k(z)d_k \quad (8.29)$$

with the functions

$$g(z) = \frac{1}{z + i\varepsilon + \sum_k \frac{|t_k|^2}{z + i\omega_k}}, \quad g_k(z) = \frac{-it_k}{(z + i\omega_k) \left(z + i\varepsilon + \sum_q \frac{|t_q|^2}{z + i\omega_q} \right)}. \quad (8.30)$$

Accordingly, to compute the time-dependent annihilation operator in the interaction picture

$$\mathbf{d} = g(t)d + \sum_k g_k(t)d_k \quad (8.31)$$

we need to compute the inverse Laplace transforms

$$g(t) = \frac{1}{2\pi i} \int_{\gamma-i\infty}^{\gamma+i\infty} g(z)e^{+zt} dz, \quad g_k(t) = \frac{1}{2\pi i} \int_{\gamma-i\infty}^{\gamma+i\infty} g_k(z)e^{+zt} dz \quad (8.32)$$

via the Bromwick integral. Eventually, the time-dependent dot occupation is given by

$$\langle \mathbf{d}^\dagger \mathbf{d} \rangle_t = \text{Tr} \{ \mathbf{d}^\dagger \mathbf{d} \rho_0 \} = |g(t)|^2 n_0 + \sum_{k=1}^N |g_k(t)|^2 f(\omega_k), \quad (8.33)$$

where n_0 is the initial dot occupation and $f(\omega_k) = [e^{\beta(\omega_k - \mu)} + 1]^{-1}$ is the Fermi function of the lead. For finite number of reservoir modes, this solution will exhibit recurrences. An exact solution in the continuum limit $N_c \rightarrow \infty$ can also be derived by converting the sums into integrals. For example, in case a stationary solution exists, the stationary dot occupation then becomes

$$\bar{n} = \int \frac{d\omega}{2\pi} \Gamma(\omega) f(\omega) \frac{T^2}{T^2(\varepsilon - \omega)^2 + (\varepsilon - \omega)(\omega - \epsilon)\lambda^2 + \lambda^4}, \quad (8.34)$$

which however still needs to be evaluated numerically.

We can compare this exact solution with the master equation solution (4.50) which yields a simple rate equation in the system energy eigenbasis

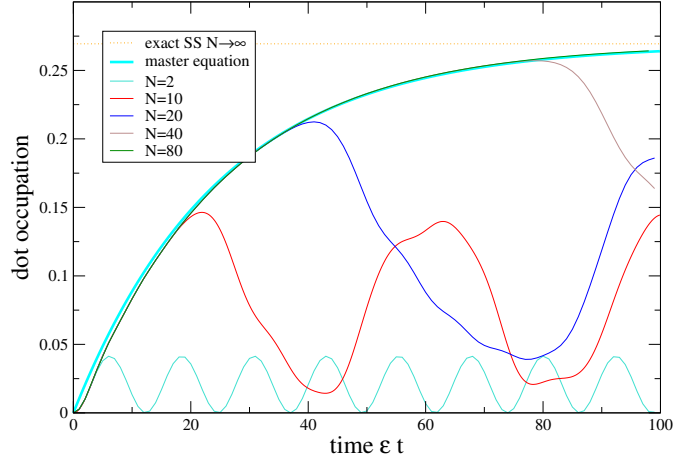
$$\begin{aligned} P_0 &= -\Gamma(\varepsilon)f(\varepsilon)P_0 + \Gamma(\varepsilon)[1 - f(\varepsilon)]P_1, \\ P_1 &= +\Gamma(\varepsilon)f(\varepsilon)P_0 - \Gamma(\varepsilon)[1 - f(\varepsilon)]P_1, \end{aligned} \quad (8.35)$$

and which has the simple solution

$$\langle \mathbf{d}^\dagger \mathbf{d} \rangle_t = e^{-\Gamma(\varepsilon)t} n_0 + f(\varepsilon) [1 - e^{-\Gamma(\varepsilon)t}]. \quad (8.36)$$

The result is depicted in Fig. 8.1. One can see that at weak couplings λ , the master equation captures the general dynamics very well, although it fits worse for small times.

Figure 8.1: Time-dependent occupation of a single quantum dot coupled to tight-binding chains of varying lengths. Thin solid curves represent exact solutions, the bold solid curve corresponds to Eq. (8.36), and the dotted line represents the stationary dot occupation according to (8.34). Parameters: $\varepsilon = \epsilon$, $T = \epsilon/2$, $\lambda = 0.1\epsilon$, $\beta\epsilon = 1$, $\mu = 0$.



8.1.3 Higher-dimensional tight-binding lattices

The diagonalization of the chain Hamiltonian in the previous section becomes evident from the identities (for integers $1 \leq k, q \leq N$)

$$\begin{aligned} \delta_{kq} &= \sum_{j=1}^N \frac{2}{N+1} \sin\left(\frac{\pi kj}{N+1}\right) \sin\left(\frac{\pi qj}{N+1}\right), \\ \delta_{kq} 2 \cos\left(\frac{\pi k}{N+1}\right) &= \sum_{j=1}^N \frac{2}{N+1} \left[\sin\left(\frac{\pi kj}{N+1}\right) \sin\left(\frac{\pi q(j+1)}{N+1}\right) \right. \\ &\quad \left. + \sin\left(\frac{\pi k(j+1)}{N+1}\right) \sin\left(\frac{\pi qj}{N+1}\right) \right], \end{aligned} \quad (8.37)$$

where the first equation simply implements the unitarity condition of the transformation (8.10). Such relations can also be employed for higher-dimensional lattices, for example, the Hamiltonian

$$H_B = \epsilon \sum_{i=1}^{N_x} \sum_{j=1}^{N_y} c_{ij}^\dagger c_{ij} + T_x \sum_{i=1}^{N_x-1} \sum_{j=1}^{N_y} \left[c_{ij}^\dagger c_{i+1,j} + c_{i+1,j}^\dagger c_{ij} \right] + T_y \sum_{i=1}^{N_x} \sum_{j=1}^{N_y-1} \left[c_{ij}^\dagger c_{i,j+1} + c_{i,j+1}^\dagger c_{ij} \right]. \quad (8.38)$$

Now, the unitary transform

$$c_{ij} = \sqrt{\frac{2}{N_x+1}} \sqrt{\frac{2}{N_y+1}} \sum_{k=1}^{N_x} \sum_{q=1}^{N_y} \sin\left(\frac{\pi ki}{N_x+1}\right) \sin\left(\frac{\pi qj}{N_y+1}\right) d_{kq} \quad (8.39)$$

will allow to map the Hamiltonian into

$$H_B = \sum_{k=1}^{N_x} \sum_{q=1}^{N_y} \left[\epsilon - 2T_x \cos\left(\frac{\pi k}{N_x+1}\right) - 2T_y \cos\left(\frac{\pi q}{N_y+1}\right) \right] d_{kq}^\dagger d_{kq}. \quad (8.40)$$

An interaction Hamiltonian of the form

$$H_I = \lambda(S^\dagger c_{11} + c_{11}^\dagger S), \quad (8.41)$$

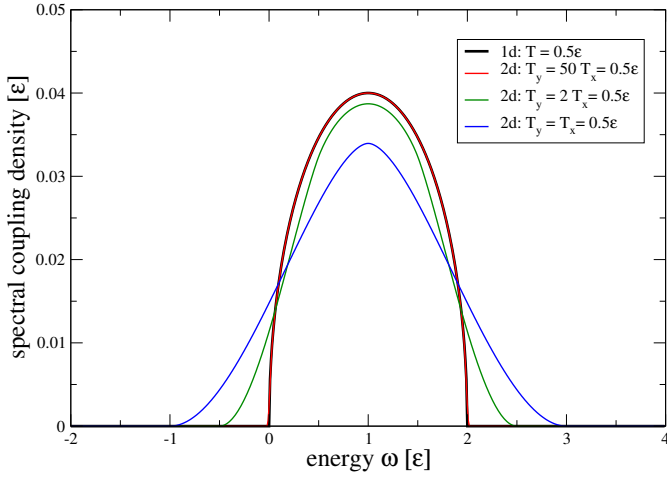


Figure 8.2: Spectral densities for infinite 1d and 2d reservoirs, characterized by tunneling amplitudes T in the 1d case and T_x and T_y in the 2d case, where the system is coupled to the end of the chain or the corner of the lattice, respectively. For $T_x \ll T_y$, the lattice becomes effectively one-dimensional.

where some system is coupled to the corner of a square lattice reservoir, is then transformed into

$$H_I = S^\dagger \sum_{kq} \lambda \sqrt{\frac{2}{N_x + 1}} \sqrt{\frac{2}{N_y + 1}} \sin\left(\frac{\pi k}{N_x + 1}\right) \sin\left(\frac{\pi q}{N_y + 1}\right) d_{kq} + \text{h.c.} \quad (8.42)$$

This allows to compute the spectral coupling density for such a corner coupling as

$$\begin{aligned} \Gamma(\omega) &= 2\pi \sum_{kq} |t_{kq}|^2 \delta\left(\omega - \epsilon + 2T_x \cos\left(\frac{\pi k}{N_x + 1}\right) + 2T_y \cos\left(\frac{\pi q}{N_y + 1}\right)\right) \\ &\rightarrow 2\pi \int_0^1 d\kappa \int_0^1 d\sigma 4\lambda^2 \sin^2(\pi\kappa) \sin^2(\pi\sigma) \delta\left(\omega - \epsilon + 2T_x \cos(\pi\kappa) + 2T_y \cos(\pi\sigma)\right) \\ &= 8\pi\lambda^2 \int_{-2T_x}^{+2T_x} dx \int_{-2T_y}^{+2T_y} dy \left[1 - \frac{x^2}{4T_x^2}\right] \left[1 - \frac{y^2}{4T_y^2}\right] \delta(\omega - \epsilon + x + y) \frac{1}{2\pi T_x \sqrt{1 - \frac{x^2}{4T_x^2}}} \frac{1}{2\pi T_y \sqrt{1 - \frac{y^2}{4T_y^2}}} \\ &= \frac{2\lambda^2}{\pi T_x T_y} \int_{-2T_x}^{+2T_x} dx \int_{-2T_y}^{+2T_y} dy \sqrt{1 - \frac{x^2}{4T_x^2}} \sqrt{1 - \frac{y^2}{4T_y^2}} \delta(\omega - \epsilon + x + y), \end{aligned} \quad (8.43)$$

which can be further reduced by using the Dirac- δ function. Essentially, for a different dimension we obtain a different shape of the spectral density – for strongly elongated reservoirs $T_x \ll T_y$ however we reproduce the previous 1d result, see Fig. 8.2. The generalization to even higher dimensions is straightforward.

8.1.4 Reservoirs with periodic boundary conditions

For a closed chain of the form

$$H_B = \epsilon \sum_{n=1}^N c_n^\dagger c_n + T \sum_{n=1}^N \left[c_n^\dagger c_{n+1} + c_{n+1}^\dagger c_n \right] = \left(c_1^\dagger, \dots, c_N^\dagger \right) \mathcal{H} \begin{pmatrix} c_1 \\ \vdots \\ c_N \end{pmatrix} \quad (8.44)$$

the matrix is no longer tridiagonal

$$\mathcal{H} = \begin{pmatrix} \epsilon & T & & T \\ T & \ddots & \ddots & \\ & \ddots & \ddots & T \\ T & & T & \epsilon \end{pmatrix}, \quad (8.45)$$

but Gershgorins circle theorem yields the same estimate on the eigenvalues. This case is even simpler: One can use the discrete Fourier transform from Eq. (5.76)

$$c_n = \frac{1}{\sqrt{N}} \sum_{k=1}^N e^{2\pi i n k / N} d_k \quad (8.46)$$

to diagonalize the Hamiltonian via exploiting

$$\sum_{n=1}^N \frac{1}{N} e^{+2\pi i n k / N} e^{-2\pi i n q / N} = \delta_{kq}. \quad (8.47)$$

Eventually, one finds

$$H_B = \sum_{k=1}^N \left[\epsilon + 2T \cos\left(\frac{2\pi k}{N}\right) \right] d_k^\dagger d_k = \sum_k \omega_k d_k^\dagger d_k. \quad (8.48)$$

Now, for a generic local coupling to the j -th site of the ring

$$H_I = \lambda S^\dagger c_j + \lambda^* c_j^\dagger S = \lambda S^\dagger \sum_k \frac{1}{\sqrt{N}} e^{2\pi i j k / N} d_k + \text{h.c.}, \quad (8.49)$$

the spectral coupling density becomes independent of the coupling site (using $\kappa = k/N$)

$$\begin{aligned} \Gamma(\omega) &= 2\pi \sum_k \frac{\lambda^2}{N} \delta\left(\omega - \epsilon - 2T \cos\left(\frac{2\pi k}{N}\right)\right) = 2\pi \lambda^2 \int_0^1 \delta(\omega - \epsilon - 2T \cos(2\pi\kappa)) d\kappa \\ &= \frac{\lambda^2}{T \sqrt{1 - \frac{(\omega - \epsilon)^2}{4T^2}}} \Theta(4T^2 - (\omega - \epsilon)^2), \end{aligned} \quad (8.50)$$

which is very different from the spectral density of a chain (8.20).

8.1.5 Spin reservoir: Ising model

Our previous considerations were limited to non-interacting bosons or fermions, such that we could consider the single-particle subspace. One can go beyond this by adding a single qubit to the Ising model (5.59)

$$\begin{aligned} H_S &= \frac{\omega_0}{2} \sigma_0^z - T \sigma_0^x, & H_I &= \frac{\lambda}{\sqrt{n}} \sigma_0^x \sum_{i=1}^n \sigma_i^x, \\ H_B &= -\Omega(1-s) \sum_{i=1}^n \sigma_i^x - \Omega s \sum_{i=1}^n \sigma_i^z \sigma_{i+1}^z \end{aligned} \quad (8.51)$$

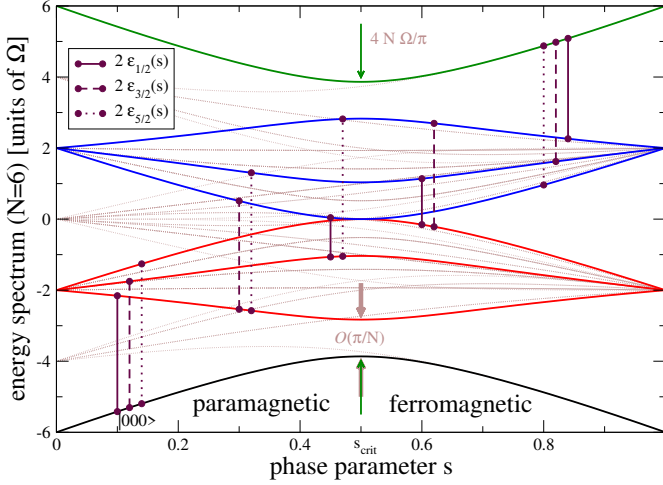


Figure 8.3: Full spectrum of the Ising model spectrum for $n = 6$ spins, adapted from Ref. [50]. A collective J^x interaction may only connect the ground state to a fraction of states in the even subspace (bold curves and vertical lines). The number of connected states is $2^{n/2}$. Vertical lines denote single-particle excitation energies. The largest single-particle excitation energy at $s = 1/2$ is 2Ω , such that the largest pair creation energy is 4Ω .

with $\sigma_{n+1}^z = \sigma_1^z$. Here, the scaling with the coupling strength has been adapted to reach a suitable continuum limit. With appropriate coding of the full Hamiltonian, we can numerically access what we did before, i.e., solve it numerically for finite (small) values of n .

However, additionally we can now derive the master equation for the system. Taking $B = \frac{\lambda}{\sqrt{n}} 2J^x$ as coupling operator, we first note that in the free fermion representation, it reads via (5.96)

$$2J^x = \sum_{\ell=1}^n \sigma_{\ell}^x = n\mathbf{1} - 2 \sum_k \left[|u_k|^2 \gamma_k^{\dagger} \gamma_k + |v_{-k}|^2 \gamma_{-k} \gamma_{-k}^{\dagger} + u_k^* v_{-k}^* \gamma_k^{\dagger} \gamma_{-k}^{\dagger} + u_k v_{-k} \gamma_{-k} \gamma_k \right], \quad (8.52)$$

where the coefficients are determined in (5.83) with $g = \Omega(1-s)$ and $J = \Omega s$. This interaction connects the ground state of the reservoir only with $2^{n/2}$ of the overall 2^n reservoir states, see Fig. 8.3.

This is an example where the first order expectation value of this interaction in a thermal state does not vanish

$$\begin{aligned} \langle B \rangle_{\text{th}} &= \frac{\lambda}{\sqrt{n}} \left[n - 2 \sum_k |u_k|^2 \langle \gamma_k^{\dagger} \gamma_k \rangle_{\text{th}} + |v_k|^2 \langle \gamma_k \gamma_k^{\dagger} \rangle_{\text{th}} \right] \\ &= \frac{\lambda}{\sqrt{n}} \left[n - 2 \sum_k |u_k|^2 f(\epsilon_k) + |v_k|^2 [1 - f(\epsilon_k)] \right], \end{aligned} \quad (8.53)$$

where

$$f(\epsilon) = \frac{1}{e^{\beta\epsilon} + 1} \quad (8.54)$$

denotes the Fermi function at vanishing chemical potential. In the derivation of a master equation we do however assume that the first order expectation value of the reservoir coupling operator in the thermal state vanishes. We therefore rewrite system and interaction

$$H'_S = \frac{\omega_0}{2} \sigma_0^z + [\langle B \rangle_{\text{th}} - T] \sigma_0^x, \quad H'_I = \sigma_0^x \left[\frac{\lambda}{\sqrt{n}} \sum_{i=1}^n \sigma_i^x - \langle B \rangle_{\text{th}} \right] \equiv \sigma_0^x \otimes B', \quad (8.55)$$

such that $H'_S + H'_I = H_S + H_I$ and $\langle B' \rangle_{\text{th}} = 0$. We note that in the interaction picture, we have for the coupling operator

$$\begin{aligned} \mathbf{B}(\tau) &= \frac{\lambda}{\sqrt{n}} n \mathbf{1} - 2 \frac{\lambda}{\sqrt{n}} \sum_k \left[|u_k|^2 \gamma_k^\dagger \gamma_k + |v_{-k}|^2 \gamma_{-k} \gamma_{-k}^\dagger \right] \\ &\quad - 2 \frac{\lambda}{\sqrt{n}} \sum_k \left[+ u_k^* v_{-k}^* \gamma_k^\dagger \gamma_{-k}^\dagger e^{+2i\epsilon_k \tau} + u_k v_{-k} \gamma_{-k} \gamma_k e^{-2i\epsilon_k \tau} \right] \\ &\equiv B_0 + \mathbf{B}_1(\tau) \quad : \quad \langle \mathbf{B}(\tau) \rangle_{\text{th}} = \langle B \rangle_{\text{th}} = \langle B_0 \rangle_{\text{th}} \end{aligned} \quad (8.56)$$

Then, the correlation function becomes

$$\begin{aligned} C(\tau) &= \langle \mathbf{B}'(\tau) B' \rangle_{\text{th}} = \langle [B_0 - \langle B_0 \rangle + \mathbf{B}_1(\tau)] [B_0 - \langle B_0 \rangle + B_1] \rangle_{\text{th}} \\ &= \langle [B_0 - \langle B_0 \rangle]^2 \rangle + \langle \mathbf{B}_1(\tau) B_1 \rangle_{\text{th}} , \end{aligned} \quad (8.57)$$

were we have used that the expectation value of products of B_0 and B_1 vanishes. Even more, for large n we will have $\langle [B_0 - \langle B_0 \rangle]^2 \rangle \rightarrow 0$, such that we only need to consider the last term

$$\begin{aligned} C^+(\tau) &\rightarrow \frac{4\lambda^2}{n} \text{Tr} \left\{ \sum_k \left[u_k^* v_{-k}^* \gamma_k^\dagger \gamma_{-k}^\dagger e^{+2i\epsilon_k \tau} + u_k v_{-k} \gamma_{-k} \gamma_k e^{-2i\epsilon_k \tau} \right] \sum_q \left[u_q^* v_{-q}^* \gamma_q^\dagger \gamma_{-q}^\dagger + u_q v_{-q} \gamma_{-q} \gamma_q \right] \frac{e^{-\beta H_B^+}}{Z_B^+} \right\} \\ &= \frac{4\lambda^2}{n} \sum_{kq} \left[u_k^* v_{-k}^* u_q v_{-q} e^{+2i\epsilon_k \tau} \left\langle \gamma_k^\dagger \gamma_{-k}^\dagger \gamma_{-q} \gamma_q \right\rangle_{\text{th}} + u_k v_{-k} u_q^* v_{-q}^* e^{-2i\epsilon_k \tau} \left\langle \gamma_{-k} \gamma_k \gamma_q^\dagger \gamma_{-q}^\dagger \right\rangle_{\text{th}} \right] , \end{aligned} \quad (8.58)$$

where we have used that only few combinations of operators remain finite under the expectation value. The expectation value of quartic fermionic operators in a thermal state can now be separately evaluated (using that $\epsilon_k = \epsilon_{-k}$)

$$\begin{aligned} \left\langle \gamma_k^\dagger \gamma_{-k}^\dagger \gamma_{-q} \gamma_q \right\rangle_{\text{th}} &= f(\epsilon_k) f(\epsilon_{-k}) (\delta_{kq} - \delta_{k,-q}) = f^2(\epsilon_k) (\delta_{kq} - \delta_{q,-k}) , \\ \left\langle \gamma_{-k} \gamma_k \gamma_q^\dagger \gamma_{-q}^\dagger \right\rangle_{\text{th}} &= [1 - f(\epsilon_k)] [1 - f(\epsilon_{-k})] (\delta_{kq} - \delta_{k,-q}) = [1 - f(\epsilon_k)]^2 (\delta_{kq} - \delta_{q,-k}) , \end{aligned} \quad (8.59)$$

where we have used the fermionic anticommutation relations and where $f(\epsilon_k) = [e^{\beta\epsilon_k} + 1]^{-1}$ denotes the Fermi function at vanishing chemical potential. Using that $u_{-k} = u_{+k}$, $v_{-k} = -v_{+k}$, $\epsilon_{-k} = \epsilon_{+k}$, we can further write

$$C^+(\tau) = \frac{4\lambda^2}{n} \sum_k \left[2|u_k|^2 |v_k|^2 e^{+2i\epsilon_k \tau} f^2(\epsilon_k) + 2|u_k|^2 |v_k|^2 e^{-2i\epsilon_k \tau} [1 - f(\epsilon_k)]^2 \right] . \quad (8.60)$$

As a sanity check we see that $C(-\tau) = C^*(+\tau)$ and that the KMS relation $C(\tau) = C(-\tau - i\beta)$ is satisfied (compare lecture on quantum transport). For even n , the above summation over k runs over the half-integer values with $-(n-1)/2 \leq k \leq +(n-1)/2$ in integer steps, such that in the continuum limit $n \rightarrow \infty$ we may introduce $\kappa = 2\pi k/n$ and replace the summation above by an

integral

$$\begin{aligned}
C^+(\tau) &\rightarrow \frac{8\lambda^2}{2\pi} \int_{-\pi}^{\pi} d\kappa |u(\kappa)|^2 |v(\kappa)|^2 [e^{+2i\epsilon(\kappa)\tau} f^2(\epsilon(\kappa)) + e^{-2i\epsilon(\kappa)\tau} [1 - f(\epsilon(\kappa))]^2] \\
&= \frac{8\lambda^2}{\pi} \int_0^{\pi} d\kappa |u(\kappa)|^2 |v(\kappa)|^2 [e^{+2i\epsilon(\kappa)\tau} f^2(\epsilon(\kappa)) + e^{-2i\epsilon(\kappa)\tau} [1 - f(\epsilon(\kappa))]^2] \\
&= \frac{8\lambda^2}{\pi} \int_{2\Omega|1-2s|}^{2\Omega} \frac{d\epsilon}{\frac{d\epsilon}{d\kappa}} |u(\epsilon)|^2 |v(\epsilon)|^2 [e^{+2i\epsilon\tau} f^2(\epsilon) + e^{-2i\epsilon\tau} [1 - f(\epsilon)]^2] , \tag{8.61}
\end{aligned}$$

where we can deduce from Eq. (5.83)

$$\lim_{s \rightarrow 1/2} \frac{|u(\epsilon)|^2 |v(\epsilon)|^2}{\frac{d\epsilon}{d\kappa}} = \frac{\sqrt{4\Omega^2 - \epsilon^2}}{8\Omega^2} . \tag{8.62}$$

Thus, for a quantum-critical reservoir ($s = 1/2$ and continuum limit)

$$\begin{aligned}
C^+(\tau) &= \frac{8\lambda^2}{\pi} \int_0^{2\Omega} \frac{\sqrt{4\Omega^2 - \epsilon^2}}{8\Omega^2} [e^{+2i\epsilon\tau} f^2(\epsilon) + e^{-2i\epsilon\tau} [1 - f(\epsilon)]^2] \\
&= \frac{8\lambda^2}{\pi} \int_{-2\Omega}^{+2\Omega} \frac{\sqrt{4\Omega^2 - \epsilon^2}}{8\Omega^2} e^{-2i\epsilon\tau} [1 - f(\epsilon)]^2 d\epsilon \\
&= \frac{2\lambda^2}{\pi\Omega} \int_{-4\Omega}^{+4\Omega} \sqrt{1 - \frac{\omega^2}{16\Omega^2}} [1 - f(\omega/2)]^2 e^{-i\omega\tau} d\omega , \tag{8.63}
\end{aligned}$$

from which we can read off the Fourier transform

$$\gamma(\omega) = \frac{4\lambda^2}{\Omega} \sqrt{1 - \frac{\omega^2}{16\Omega^2}} [1 - f(\omega/2)]^2 \Theta(16\Omega^2 - \omega^2) . \tag{8.64}$$

This is all we need to write down the master equation (4.49) with the coupling operator $S = \sigma^x$. In particular, when $T = \langle B \rangle_{\text{th}}$, the renormalized system Hamiltonian is just $\omega_0/2\sigma_0^z$. This has the energy eigenbasis $\{|1\rangle, |0\rangle\}$, and the rate equation for the ground state occupation P_g and excited state occupation P_e assumes the form

$$\begin{aligned}
\dot{P}_e &= +\gamma(-\omega_0)P_g - \gamma(+\omega_0)P_e , \\
\dot{P}_g &= -\gamma(-\omega_0)P_g + \gamma(+\omega_0)P_e . \tag{8.65}
\end{aligned}$$

From $\gamma(-\omega_0)/\gamma(+\omega_0) = e^{-\beta\omega_0}$ we find that the system will just thermalize in the long-term limit.

8.2 Topological single-particle pumping

Chain models are suitable candidates to realize adiabatic pumping schemes. Here, the nature of the particles is typically not relevant as the pumping schemes rely only on the single-particle excitation spectra, which do not depend on the bosonic or fermionic character. Such a chain model exhibiting rich dynamics is the Aubry-Andre model

$$H = \Delta \sum_{n=1}^N [2 + \cos(2\pi nb + \phi)] c_n^\dagger c_n + T \sum_{n=1}^{N-1} [c_n^\dagger c_{n+1} + c_{n+1}^\dagger c_n] , \tag{8.66}$$

where T is a next-neighbour hopping amplitude, Δ defines the energy scale, n is the site index and b and ϕ are parameters. Specifically, b could in case of electrons be controlled by the magnetic field (compare solid state lecture). But also other means of implementing this Hamiltonian are conceivable. For example, the variation in the on-site energies can be achieved by using nearby gates with varying potentials.

When b is a rational number, the excitation spectrum of H exhibits a finite number of bands. For example, for $b = 1/2$, we find two bands (such a model can be mapped to a Su-Schrieffer-Heeger chain, compare lecture on solid state physics) and for $b = 1/3$ we find three bands. We will consider a chain of trimers $b = 1/3$ with $N_T = N/3 \in \mathbb{N}$ denoting the number of trimers. Some analytic understanding of the band structure can then be gained from analyzing the periodically closed version of the model

$$H_{\text{per}} = \Delta \sum_{n=1}^{3N_T} [2 + \cos(2\pi nb + \phi)] c_n^\dagger c_n + T \sum_{n=1}^{3N_T} [c_n^\dagger c_{n+1} + c_{n+1}^\dagger c_n], \quad (8.67)$$

with $c_{N+1} = c_1$. Using a DFT $c_n = \frac{1}{\sqrt{N}} \sum_{k=1}^N e^{2\pi i kn/N} d_k$ maps the Hamiltonian into one with decoupled trimers

$$H_{\text{per}} = \sum_{k=1}^{N_T} \left(d_k^\dagger, d_{k+N_T}^\dagger, d_{k+2N_T}^\dagger \right) \mathcal{H}_k \begin{pmatrix} d_k \\ d_{k+N_T} \\ d_{k+2N_T} \end{pmatrix},$$

$$\mathcal{H}_k = \Delta \begin{pmatrix} 2 & e^{-i\phi}/2 & e^{+i\phi}/2 \\ e^{+i\phi}/2 & 2 & e^{-i\phi}/2 \\ e^{-i\phi}/2 & e^{+i\phi}/2 & 2 \end{pmatrix} + 2T \begin{pmatrix} \cos\left(\frac{2\pi k}{3N_T}\right) & 0 & 0 \\ 0 & \cos\left(\frac{2\pi k}{3N_T} + \frac{2\pi}{3}\right) & 0 \\ 0 & 0 & \cos\left(\frac{2\pi k}{3N_T} + \frac{4\pi}{3}\right) \end{pmatrix}, \quad (8.68)$$

which can be analytically diagonalized individually. From this one finds that the periodically closed version of the model has three bands.

When we plot the single-particle excitation spectrum of the open chain model (8.66) for $b = 1/3$ as a function of ϕ , we see additionally to the bands also two regions where there are two isolated eigenvalues outside the bands, see Fig. 8.4. The points where these isolated levels come very close together (in fact, their splitting is exponentially small in the system size and can for $N = 81$ trimers hardly be numerically resolved, compare inset) can be understood from symmetry arguments: The trimers have the onsite-energies

$$\begin{aligned} \epsilon_A = \epsilon_1 &= \Delta \left[2 + \cos\left(\frac{2\pi}{3} + \phi\right) \right], \\ \epsilon_B = \epsilon_2 &= \Delta \left[2 + \cos\left(\frac{4\pi}{3} + \phi\right) \right], \\ \epsilon_C = \epsilon_3 &= \Delta \left[2 + \cos\left(\frac{6\pi}{3} + \phi\right) \right], \end{aligned} \quad (8.69)$$

which are periodically repeated along the chain. Now, when $\phi = 2\pi/3$ (the position of the first avoided crossing) we find that $\epsilon_A = \epsilon_C = \Delta \frac{3}{2}$ and $\epsilon_B = 3\Delta$, such that the chain has an inversion symmetry at this point. A similar thing happens at $\phi = 5\pi/3$ where $\epsilon_A = \epsilon_C = \Delta \frac{5}{2}$ and $\epsilon_B = \Delta$. If we look at the distribution of eigenstates across the sites, one can see that the isolated energy

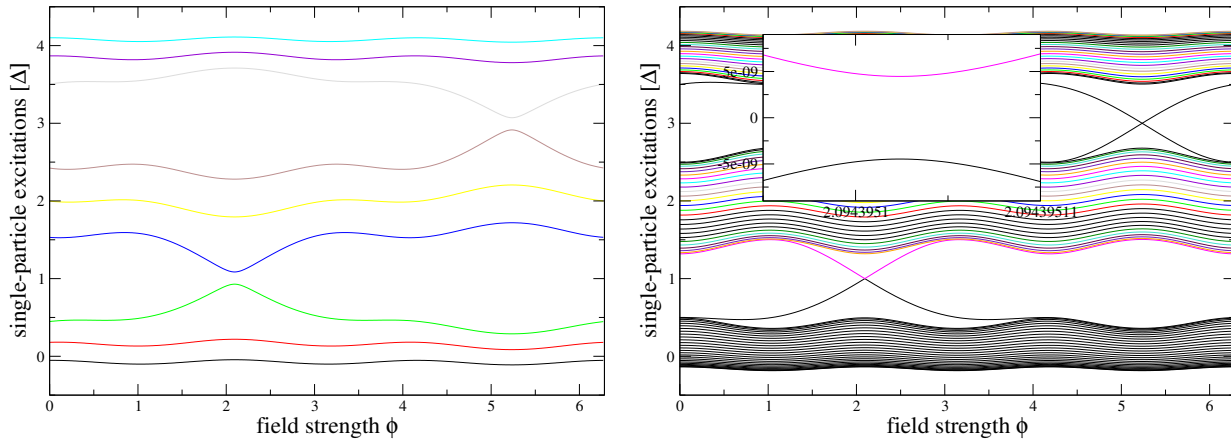


Figure 8.4: Single-particle spectrum of (8.66) with $b = 1/3$ for $N = 9$ (3 trimers, left) and $N = 81$ (27 trimers, right). As the trimer chain length grows, the bands are filled with eigenvalues, but additionally there are isolated levels that may become near-degenerate. Parameters: $T = \Delta$, $b = 1/3$.

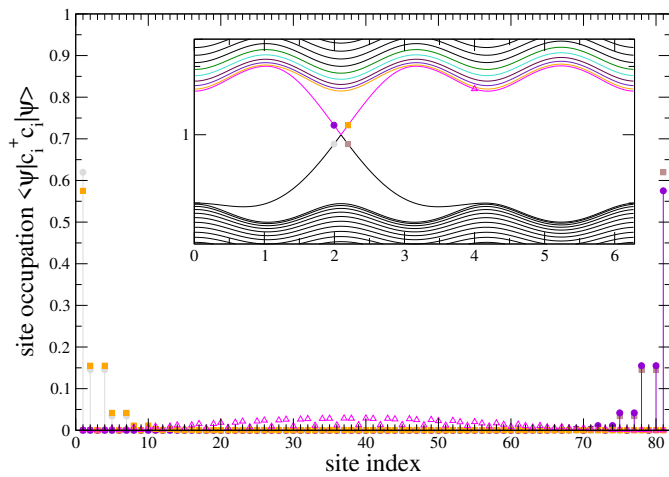


Figure 8.5: Distribution of selected eigenstates (symbols in inset) vs. the sites. Before the critical point, the lower eigenstate is left-dominated (grey circles), after the critical point it is right-dominated (brown squares). Starting from the state associated with the grey circle, by slowly increasing the ϕ parameter, one would non-adiabatically transfer to the orange state, and afterwards adiabatically move along the magenta curve (delocalized bulk states, triangle) to transfer to the right-dominated violet state, followed by a non-adiabatic transfer to the brown state, effectively teleporting a particle from left to right.

eigenstates are either left- or right dominated, see Fig. 8.5. At the avoided crossing (with exponentially small and numerically unresolvable energy gap), the nature of the lower energy eigenstate changes abruptly from left-dominated to right-dominated, such that an adiabatic transition (remaining in the lower eigenstate) is not possible. Writing the solution of the Schrödinger equation as

$$|\Psi(t_0 + \Delta t)\rangle = |\Psi(t_0)\rangle - i \int_{t_0}^{t_0 + \Delta t} H(t') |\Psi(t')\rangle dt', \quad (8.70)$$

one can see that a local Hamiltonian $H(t)$ can in short times Δt not generate a transition between a left-dominated state $|\Psi(t_0)\rangle$ and a right-dominated state. Therefore, the state will essentially remain the same at the avoided crossing (non-adiabatic transition), and after the avoided crossing all the amplitude is in the excited state. Afterwards, an adiabatic evolution is still possible (along the excited state) until $\Delta\phi = 2\pi$, where the excited state is again non-adiabatically transferred to the ground state – now right-dominated. Therefore, after $\Delta\phi = 2\pi$ and two non-adiabatic transitions, the particle is transferred from left to right.

This appears well reflected in the numerical solution of the time-dependent Schrödinger equation. In the single-particle subspace, we can use a short-hand notation

$$|n_{\text{pos}}\rangle = |0\rangle \otimes \dots \otimes |0\rangle \otimes \underbrace{|1\rangle}_{n\text{th pos.}} \otimes |0\rangle \otimes \dots \otimes |0\rangle. \quad (8.71)$$

Since the overall particle number is conserved by the Hamiltonian, it suffices to consider only the single-particle basis, and the spectrum in this subspace is just given by the previously considered single-particle energies. Initializing the system in a state where a single particle is localized on the left

$$|\Psi_0\rangle = |1_{\text{pos}}\rangle \langle 1_{\text{pos}}|, \quad (8.72)$$

we do not exactly prepare the system in an energy eigenstate. Nevertheless, this state has a large overlap with the left-dominated edge state. When we then solve the time-dependent Schrödinger equation subject to the time-dependent Hamiltonian with

$$\phi(t) = \frac{2\pi}{3} + 2\pi \frac{t}{T_{\text{rt}}} \quad : \quad 0 \leq t \leq T_{\text{rt}} \quad (8.73)$$

with a sufficiently large runtime T_{rt} , we may expect adiabatic evolution and hence will find the particle close to the right end of the chain at the end of the protocol, which is indeed what we observe for large runtimes T_{rt} in the numerical solution, see Fig. 8.6. This is not a conventional particle pumping scheme, as during the process, the wave function is completely delocalized. Rather, the particle is teleported from one end of the chain to the other. One may thereby wonder how robust this scheme is with respect to imperfections. These imperfections must however not destroy the inversion symmetry of the system. For example, the inversion symmetry is respected when we only perturb the intra-trimer couplings

$$\Delta H_1 = \sum_{n=1}^{N/3} r_n \left[c_{3n}^\dagger c_{3n+1} + c_{3n+1}^\dagger c_{3n} \right], \quad (8.74)$$

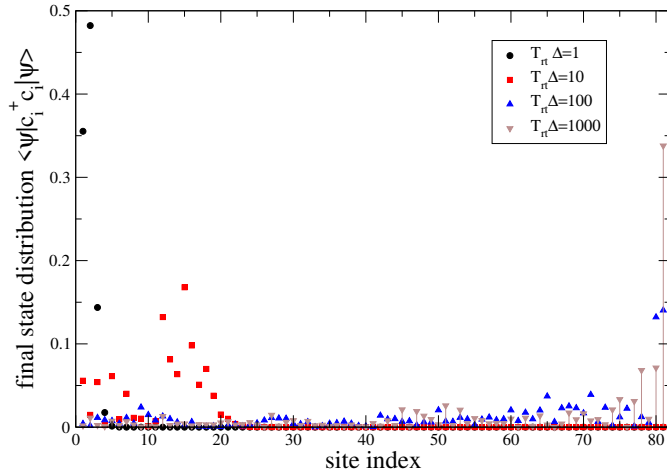


Figure 8.6: Final state amplitude distribution over the chain sites for $N = 81$ for an initial state (8.72). For slow evolution, the particle is transferred from left to right. Imperfections in state transfer result from a finite overlap of the initial state with an energy eigenstate. Other parameters: $T = \Delta$, $b = 1/3$.

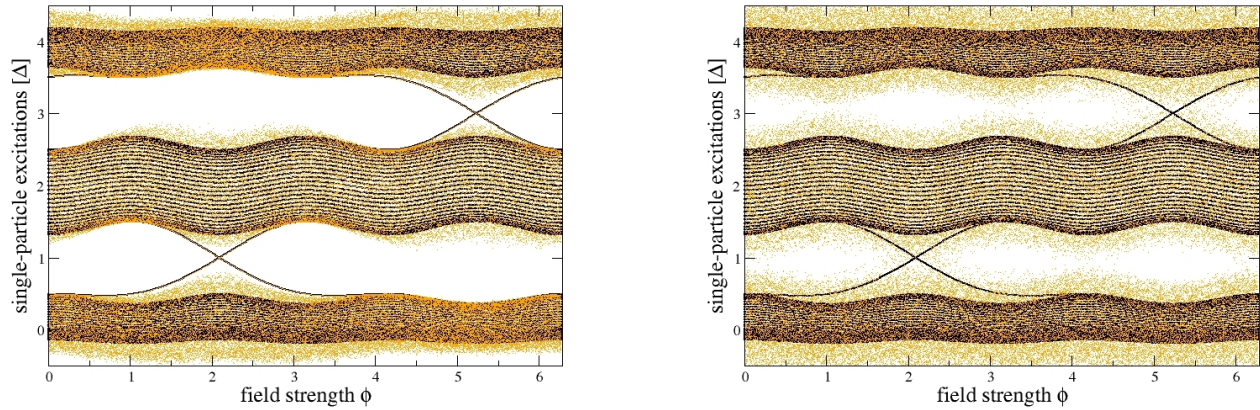


Figure 8.7: When random disorder in the tunneling amplitudes ($r_n \in \Delta[-1/2, +1/2]$ uniformly distributed) is added to the Hamiltonian, it will perturb all eigenvalues (orange dots vs. black curves). However, in case of intra-trimer disorder (8.74), the inversion symmetry is respected and so are the edge state eigenvalues (left). This is not the case when total disorder (8.75) is used (right).

it will not be respected when we perturb all tunnel couplings

$$\Delta H_2 = \sum_{n=1}^N r_n \left[c_n^\dagger c_{n+1} + c_{n+1}^\dagger c_n \right], \quad (8.75)$$

with random numbers r_n . This is clearly visible in the spectrum, see Fig. 8.7.

This robustness against disorder would then enable a teleportation protocol to work even through strongly disordered lattices.

Bibliography

- [1] Michael A. Nielsen and Isaac L. Chuang. *Quantum Computation and Quantum Information*. Cambridge University Press, Cambridge, 2000.
- [2] A. Einstein, B. Podolsky, and N. Rosen. Can quantum-mechanical description of physical reality be considered complete? *Phys. Rev.*, 47:777–780, May 1935.
- [3] John Stewart Bell. On the Einstein Podolsky Rosen paradox. *Physics*, 1(3):195, 1964.
- [4] Alain Aspect, Jean Dalibard, and Gérard Roger. Experimental test of Bell’s inequalities using time-varying analyzers. *Phys. Rev. Lett.*, 49:1804–1807, Dec 1982.
- [5] David Deutsch. Quantum theory, the Church-Turing principle and the universal quantum computer. *Proceedings of the Royal Society of London, Series A: Mathematical and Physical Sciences*, 400:97–117, 1985.
- [6] David Deutsch and Richard Jozsa. Rapid solution of problems by quantum computation. *Proceedings of the Royal Society of London, Series A: Mathematical and Physical Sciences*, 439:553, 1992.
- [7] William H. Press, Saul A. Teukolsky, William T. Vetterling, and Brian P. Flannery. *Numerical Recipes in C*. Cambridge University Press, 2nd edition, 1994.
- [8] D. Coppersmith. An approximate Fourier transform useful in quantum factoring. *Technical Report RC19642, IBM.*, page arXiv:0201067, 1994.
- [9] Peter W. Shor. Polynomial-time algorithms for prime factorization and discrete logarithms on a quantum computer. *SIAM Journal on Computing*, 26(5):1484–1509, 1997.
- [10] Lieven M. K. Vandersypen, Matthias Steffen, Gregory Breyta, Costantino S. Yannoni, Mark H. Sherwood, and Isaac L. Chuang. Experimental realization of Shor’s quantum factoring algorithm using nuclear magnetic resonance. *Nature*, 414:883–887, 2001.
- [11] Lov K. Grover. Quantum mechanics help in searching for a needle in a haystack. *Physical Review Letters*, 79(2):325–328, 1997.
- [12] H.-P. Breuer and F. Petruccione. *The Theory of Open Quantum Systems*. Oxford University Press, Oxford, 2002.
- [13] D. A. Lidar, Z. Bihary, and K. B. Whaley. From completely positive maps to the quantum Markovian semigroup master equation. *Chemical Physics*, 268:35–53, 2001.

- [14] V. Gorini, A. Kossakowski, and E. C. G. Sudarshan. Completely positive dynamical semigroups of n -level systems. *Journal of Mathematical Physics*, 17:821, 1976.
- [15] G. Lindblad. On the generators of quantum dynamical semigroups. *Communications in Mathematical Physics*, 48:119–130, 1976.
- [16] R. Dümcke and H. Spohn. The proper form of the generator in the weak coupling limit. *Zeitschrift für Physik B*, 34:419–422, 1979.
- [17] Tameem Albash, Sergio Boixo, Daniel A Lidar, and Paolo Zanardi. Quantum adiabatic Markovian master equations. *New Journal of Physics*, 14(12):123016, dec 2012.
- [18] Jérémie Roland and Nicolas J. Cerf. Quantum search by local adiabatic evolution. *Physical Review A*, 65:042308, Mar 2002.
- [19] R. Schützhold and G. Schaller. Adiabatic quantum algorithms as quantum phase transitions: First versus second order. *Physical Review A*, 74:060304(R), 2006.
- [20] Edward Farhi, Jeffrey Goldstone, Sam Gutmann, Joshua Lapan, Andrew Lundgren, and Daniel Preda. A quantum adiabatic evolution algorithm applied to random instances of an NP-complete problem. *Science*, 292:472–476, 2001.
- [21] G. Schaller and R. Schützhold. The role of symmetries in adiabatic quantum algorithms. *Quantum Information and Computation*, 10:0109–0140, 2010.
- [22] B. Altshuler, H. Krovi, and J. Roland. Anderson localization makes adiabatic quantum optimization fail. *PNAS*, 107:12446, 2010.
- [23] S. Sachdev. *Quantum Phase Transitions*. Cambridge University Press, 2000.
- [24] Jacek Dziarmaga. Dynamics of a quantum phase transition: Exact solution of the quantum Ising model. *Physical Review Letters*, 95:245701, 2005.
- [25] G. Schaller. Adiabatic preparation without quantum phase transitions. *Physical Review A*, 78:032328, 2008.
- [26] Tameem Albash and Daniel A. Lidar. Adiabatic quantum computation. *Review of Modern Physics*, 90:015002, 2018.
- [27] K Kraus. General state changes in quantum theory. *Annals of Physics*, 64(2):311 – 335, 1971.
- [28] Heinz-Peter Breuer. Foundations and measures of quantum non-Markovianity. *Journal of Physics B: Atomic, Molecular and Optical Physics*, 45:154001, 2012.
- [29] Göran Lindblad. Completely positive maps and entropy inequalities. *Communications in Mathematical Physics*, 40:147, 1975.
- [30] Herbert Spohn. Entropy production for quantum dynamical semigroups. *Journal of Mathematical Physics*, 19:1227, 1978.
- [31] G. Vidal, J. I. Latorre, E. Rico, and A. Kitaev. Entanglement in quantum critical phenomena. *Physical Review Letters*, 90:227902–1, 2003.

- [32] L. Cincio, J. Dziarmaga, M. M. Rams, and W. H. Zurek. Entropy of entanglement and correlations induced by a quench: Dynamics of a quantum phase transition in the quantum Ising model. *Physical Review A*, 75:052321, 2007.
- [33] J. Eisert, M. Cramer, and M. B. Plenio. Colloquium: Area laws for the entanglement entropy. *Rev. Mod. Phys.*, 82:277–306, Feb 2010.
- [34] M. Gross and S. Haroche. Superradiance: An essay on the theory of collective spontaneous emission. *Physics Reports*, 93:301–396, 1982.
- [35] Martin B. Plenio and S. Virmani. An introduction to entanglement measures. *Quant.Inf.Comput.*, 7:1–51, 2005.
- [36] William K. Wootters. Entanglement of formation of an arbitrary state of two qubits. *Physical Review Letters*, 80:2245–2248, Mar 1998.
- [37] A. Osterloh, L. Amico, G. Falci, and R. Fazio. Scaling of entanglement close to a quantum phase transition. *Nature*, 416:608, 2002.
- [38] T. J. Osborne and M. A. Nielsen. Entanglement in a simple quantum phase transition. *Physical Review A*, 66:032110, 2002.
- [39] Nan Li and Shunlong Luo. Total versus quantum correlations in quantum states. *Phys. Rev. A*, 76:032327, Sep 2007.
- [40] X. Wang and K. Mølmer. Pairwise entanglement in symmetric multi-qubit systems. *The European Physical Journal D*, 18:385, 2002.
- [41] R. H. Dicke. Coherence in spontaneous radiation processes. *Physical Review*, 93:99 – 110, 1954.
- [42] M. Esposito, K. Lindenberg, and C. Van den Broeck. Entropy production as correlation between system and reservoir. *New Journal of Physics*, 12:013013, 2010.
- [43] Gheorghe Nenciu. Independent electron model for open quantum systems: Landauer-Büttiker formula and strict positivity of the entropy production. *Journal of Mathematical Physics*, 48:033302, 2007.
- [44] R. Alicki. The quantum open system as a model of the heat engine. *Journal of Physics A: Mathematical and General*, 12:L103, 1979.
- [45] Ronnie Kosloff and Amikam Levy. Quantum heat engines and refrigerators: Continuous devices. *Annual Review of Physical Chemistry*, 65:365, 2014.
- [46] Johannes Roßnagel, Samuel T. Dawkins, Karl N. Tolazzi, Obinna Abah, Eric Lutz, Ferdinand Schmidt-Kaler, and Kilian Singer. A single-atom heat engine. *Science*, 352:325, 2016.
- [47] Michal Kloc, Pavel Cejnar, and Gernot Schaller. Collective performance of a finite-time quantum Otto cycle. *Phys. Rev. E*, 100:042126, Oct 2019.
- [48] David Gelbwaser-Klimovsky, Wassilij Kopylov, and Gernot Schaller. Cooperative efficiency boost for quantum heat engines. *Phys. Rev. A*, 99:022129, Feb 2019.

- [49] N. Linden, S. Popescu, A. J. Short, and A. Winter. Quantum mechanical evolution towards thermal equilibrium. *Physical Review E*, 79:061103, 2009.
- [50] Malte Vogl, Gernot Schaller, and Tobias Brandes. Criticality in transport through the quantum ising chain. *Physical Review Letters*, 109:240402, 2012.

Index

- 3-SAT problem, 71
- adiabaticity condition, 65
- ancilla qubits, 12
- Bell inequalities, 23
- Bell states, 19
- Berry phase, 64, 65
- bitflip parity, 78
- Bloch sphere representation, 13
- Bogoliubov transform, 81, 131
- Bogoliubov transformation, 81
- Born approximation, 55
- Born-Markov-secular master equation, 58
- Bose-Einstein distribution, 56

- Carnot efficiency, 124
- CHSH inequalities, 23
- circuit model of computation, 9
- classical fidelity, 96
- CNOT gate, 20
- coefficient of performance, 125
- computational basis, 13, 20
- concurrence, 106
- contractive, 94
- correlation entropy, 118

- decoherence, 53
- density matrix, 14
- density of states, 139
- Deutsch algorithm, 30
- Deutsch-Jozsa problem, 31
- Dicke states, 104, 133
- Discrete Fourier transform, 83
- discrete Fourier transform, 41, 81
- dual master equation, 135
- dynamical phase, 65

- EC-3, 72
- efficiency, 124
- entangled, 19
- entanglement entropy, 100
- entanglement of formation, 106
- entropy production, 117
- entropy production rate, 61
- exact master equation, 53
- exponential speedup, 31

- fermionic anticommutation relations, 79
- fidelity between states, 96
- first Markov approximation, 57

- gates, 9
- Gershgorin circle theorem, 140
- Gray code, 38
- Grover iterations, 46

- half-sided Fourier transform, 57

- Jordan-Wigner transform, 79

- Kolmogorov distance, 92
- Kraus map, 92
- Kronecker product, 20
- Kubo-Martin-Schwinger, 57
- Kullback-Leibler-divergence, 98

- ladder operators, 103
- Lindblad equation, 61
- Lindblad-Davies, 61
- LOCC operations, 106
- logic gate, 9

- maximally entangled state, 100
- mean-field approximation, 135
- metric, 92, 93
- mutual information, 99

- non-Markovian master equation, 56

- oracle, 45
- Otto cycle, 125

- partial trace, 27

Pauli master equation, 59
Pauli matrices, 8
polaron transformation, 51
positive semidefinite, 60
pure state, 14

quantum Fourier transform, 41
quantum Ising model in a transverse field, 77
quantum relative entropy, 98
qubit, 8, 13

Redfield-I equation, 57
Redfield-II equation, 57
reduced density matrix, 27
reference temperature, 136
reservoir correlation function, 56

Schmidt coefficients, 100
Schmidt decomposition, 100
Schrödinger equation, 7
second law of thermodynamics, 117
second Markov approximation, 57
secular approximation, 58
separable states, 105
Shannon entropy, 97
spectral coupling density, 56, 139
spectral density, 139
Spohn's inequality, 99
standard universal set of gates, 39
statistical operator, 14
superoperator, 61

tensor product, 18
thermal reference state, 136
time evolution operator, 7
time-averaged states, 138
Toffoli gate, 33
trace distance, 93

universal set of gates, 39

von-Neumann entropy, 97

wave function, 7
wires, 9